Microscopic Theory of Linear Response in Amorphous Materials

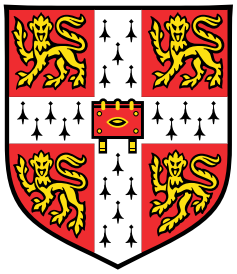

Bingyu Cui

Department of Physics
The Cavendish Laboratory
University of Cambridge

This dissertation is submitted for the degree of
Doctor of Philosophy

Gonville and Caius College June 2020

Declaration

This dissertation is the result of my own work and includes nothing which is the outcome of work done in collaboration except as declared in the Preface and specified in the text. It is not substantially the same as any that I have submitted, or, is being concurrently submitted for a degree or diploma or other qualification at the University of Cambridge or any other University or similar institution except as declared in the Preface and specified in the text. I further state that no substantial part of my dissertation has already been submitted, or, is being concurrently submitted for any such degree, diploma or other qualification at the University of Cambridge or any other University or similar institution except as declared in the Preface and specified in the text. It does not exceed the prescribed word limit of 60,000 words, including summary/abstract, tables, footnotes and appendices, but excluding table of contents, photographs, diagrams, figure captions, list of figures/diagrams, list of abbreviations/acronyms, bibliography and acknowledgements.

Some of my work reported in this thesis have been published in the following papers:

1. B. Cui and A. Zaccone. Analytical theory of enhanced logarithmic Rayleigh scattering in amorphous solids. Soft Matter 16, 7797 (2020).

2. B. Cui and E. Terentjev. Comparison of the Helmholtz, Gibbs, and Collective-modes methods to obtain nonaffine elastic constants. Journal of the Mechanics and Physics of Solids 140, 103954 (2020).

3. B. Cui, A. Zaccone, D. Rodney. Nonaffine lattice dynamics with the Ewald method reveals strongly nonaffine elasticity of α-quartz. Journal of Chemical Physics 151, 224509 (2019).

4. B. Cui, G. Ruocco, A. Zaccone. Theory of elastic constants of athermal amorphous solids with internal stresses. Granular Matter 21, 69 (2019).

5. B. Cui, Z. Evenson, B. Fan, M.-Z. Li, W.-H. Wang, A. Zaccone. Possible origin of beta relaxation in amorphous metal alloys from atomic-mass differences of the constituents. Physical Review B, 98, 144201 (2018).

6. B. Cui and A. Zaccone. Generalized Langevin Equation and fluctuation-dissipation theorem for particle-bath systems in external oscillating fields. Physical Review E 97, 060102(R) (2018).

7. B. Cui, J. Gebbia, J.-L. Tamarit, A. Zaccone. Disentangling alpha and beta relaxation in orientationally disordered crystals with theory and experiments. Physical Review E 97, 053001 (2018).

8. B. Cui, J. Yang, J. Qiao, M. Jiang, L. Dai, Y.-J. Wang, A. Zaccone. Atomic theory of viscoelastic response and memory effects in metallic glasses. Physical Review B 96, 094203 (2017).

9. B. Cui, R. Milkus, and A. Zaccone. Direct link between boson-peak modes and dielectric alpha-relaxation in glasses. Physical Review E 95, 022603 (2017).

I have contributed to all aspects of research in 1-9. Simulations in 5, 7, 8 and 9 were carried out by Beibei Fan, Jonathan Gebbia, Jie Yang and Rico Milkus respectively. Experimental parts in 5, 7 and 8 were performed by Zach Evenson, Jonathan Gebbia and Y.-J. Wang. Some work in 9 might be a part of the PhD thesis of Rico Milkus submitted to the University of Cambridge.

Bingyu Cui
June 2020

Microscopic Theory of Linear Response in Amorphous Materials

Bingyu Cui

This thesis provides an analytical and systematic framework from first-principles to study dielectric and mechanical properties of disordered materials, as well as non-centrosymmetric crystals. The Caldeira-Leggett Hamiltonian opens a route to the (both Markovian and non-Markovian) fluctuation-dissipation theorem (FDT) and gives rise to the generalised Langevin equation (GLE) in classical dynamics.

In the first place, I extend the GLE and the corresponding FDT for more general cases where both the tagged particle and bath oscillators respond to an external oscillatory field. This is the example of a charged or polarisable particle immersed in a bath of other particles that are also charged or polarisable, under an external AC electric field. Being linked to the vibrational density of states (VDOS), the dielectric function calculated based on the GLE is compared with experimental data for the paradigmatic case of molecular glasses: glycerol and Freons 112 & 113, around and above the glass transition temperature, T_g.

Moving to the mechanical aspect, the theory of nonaffine lattice dynamics is able to describe the various relaxation processes in the linear viscoelastic response of metallic glasses. In particular, to understand universal properties of relaxation, the VDOS obtained in simulations, or in experiments, is substituted into the model. The nonaffine contribution to elasticity is also important for the pre-stressed/stretched harmonic networks. In order to give an insight on nonaffinity, I compute static elastic constants of α-quartz, taking into account the long-range Coulomb interaction. The nonaffine (softening) correction is found very large, such that the overall elastic constants are at least 3-4 times smaller than the affine Born-Huang estimate.

Finally, I formulate the analytical expression of the dynamical structure factor by averaging over all quenched disorder along the acoustic branch, which stores the information of phonon transport in disordered materials. The Rayleigh scattering may be enhanced by a logarithmic factor in an intermediate range of wavenumber. I present a tensorial replica field-theoretic derivation based on heterogeneous or fluctuating elasticity, which suggests that long-range spatial correlations (in power-law decay) of elastic constants (or stress tensors) might be responsible for the logarithmic enhancement to Rayleigh scattering of phonons in amorphous solids.

I dedicate this dissertation to my academic advisors who guided me in this process.

Acknowledgements

I would like to extend my thanks to many people, in many countries, who generously contributed to the work presented in this thesis. Special mention goes to my enthusiastic mentor, Prof. Alessio Zaccone. My PhD has been an amazing experience and I thank him wholeheartedly, not only for his tremendous academic support, but also for giving me consistent guidance. Not many PhD candidates end up with over 10 publications within 3 years, not to mention taking regular visits to other research groups across the world.

Similar, profound gratitude goes to Prof. Eugene Terentjev, who has been a truly dedicated supervisor. I am particularly indebted to Eugene for sharing his taxonomic expertise so willingly, and for being so dedicated to his role as my principle supervisor after Alessio's leave.

Special mention goes to Rico Milkus, Jie Yang, Zhigang Hu, Chonghuan (Thomas) Zhang, Wei Li, Zhimian Hao, Yunhu Gao, Liwei Cao, Sushen Zhang, Harry Zhu, Yunfei Li Song, Ying Zhang, Yutong Han, for going far beyond the call of duty. To Cheng-Tai Lee, for his constructive suggestions. To Yanting Cao, for her consolation and encouragement. To Xinyi Kuang, for her sincere love, accompany and care during the COVID-19 pandemic lockdown in the UK. And to Prof. Hajime Tanaka and Prof. Yunjiang Wang, for hosting me in their labs.

Moreover, I hugely thanks CSC-Cambridge Scholarship. Without it, I was not able to carry out my PhD research at Cambridge. I also acknowledge the valuable comments from examiners who deeply read this thesis: Dr. Bartomeu Monserrat and Dr. Adrian Baule. Finally, but by no means least, thanks go to mum, dad for almost unbelievable support and love. They are the most important people in my life and I also dedicate this thesis to them.

Table of contents

List of figures

List of tables

Chapter 1

Preface

The theory of Brownian motion is so far the simplest approximation to the dynamics of nonequilibrium systems. The Langevin equation, and its equivalent counterpart, the Smoluchowski diffusion equation, describe the motion of a Brownian particle in an external force field and under the action of thermal agitation from the bath of solvent molecules, in which the Brownian particle is immersed. At steady-state, the thermal fluctuations that cause rapid changes in the particle velocity are dissipated by viscous drag.

This is a manifestation of the fluctuation-dissipation theorem (FDT), as was originally formulated in different contexts by Einstein and by Nyquist, and generalised by Onsager (1931) and by Callen and Welton (1951). Later, the theorem has been further elaborated in many different contexts (Akhiezer et al., 1967; Bernard and Callen, 1959; Blickle et al., 2006; Kubo, 1957; Landau and Lifshitz, 1960; Leontovich and Rytov, 1952; Pérez-Madrid et al., 2003; Rytov, 1953; Seifert and Speck, 2010). FDT stipulates that the response of a system in thermodynamic equilibrium to a small applied force is the same as its response to a spontaneous fluctuation, thus connecting the linear response relaxation of a system to equilibrium, from a prepared nonequilibrium state, with its statistical fluctuation properties in equilibrium. FDT applies to both classical and quantum mechanical systems (Ford, 2017; Hänggi and Ingold, 2005) and has been generalised to non-Markovian processes for classical systems (Zwanzig, 2002). In the latter case, the noise is no longer uncorrelated in time, and the time correlation of the stochastic force is dictated by the time correlation of the friction which plays the role of the memory function in the generalised Langevin equation (GLE). The non-Markovianity arises from the dynamical coupling of the tagged Brownian particle with many particles (harmonic oscillators) forming the heat bath. This coupling, which in physical systems may be provided by long-range molecular interactions, is thus responsible for both the thermal agitation and the damping experienced by the tagged particle.

All versions of the GLE, and of the associated FDT which can be derived from it, that have been considered in the past are limited to either systems in the absence of external time-dependent forces or, if an external time-dependent force is present, its action is restricted to the tagged Brownian particle, leaving the bath oscillators unaffected by the external field (Fisher and Zwerger, 1985; Kubo, 1957). Harada and Sasa considered time-dependent driving forces being exerted on the tagged particle and they found a violation of the fluctuation-response relation in driven nonequilibrium systems (Harada and Sasa, 2005, 2006). More recently, Maes and co-workers derived FDT for nonequilibrium systems by implementing mutual interactions between bath particles and also the effect of stochastic white-noise force on the bath particles dynamics (Maes, 2014, 2015). But none of the previous works takes into account the effect of external time-dependent fields on both the tagged particle and the bath particles dynamics. After introducing background theory used in this thesis in Chapter 2, important physical results (GLE and FDT) ignored due to the absence of external time-dependent forces acting on bath oscillators will be discussed in detail in Chapter 3.

The GLE elucidates microscopic system of its (linear) response to external fields. The α-relaxation, typically associated with collective and strong cooperative motions of a large number of entities rearranging in a long-range correlated way, is related to the slowest decay of density correlations and is widely observed in dielectric and mechanical responses. Within the energy landscape picture, the α-relaxation can be interpreted as the transition of the system from one meta-basin to another, by means of a collective thermally activated jump over a large energy barrier, a process that, for high-dimensional systems, can be well described by replica symmetry-breaking and related approaches (Yoshino, 2012; Yoshino and Mézard, 2010; Yoshino and Zamponi, 2014). While the calorimetric glass transition may be quite smooth, the vanishing of the low-frequency shear modulus near glass transition temperature T_g can be, instead, very dramatic, with a sudden drop by orders of magnitude that can be related to marginal stability (Liu et al., 2015; Zaccone and Terentjev, 2013). Developed by Fuchs et al. (1991), Mode-Coupling Theory (MCT) has provided a general interpretation of the α-peak in dielectric relaxation using a framework where the many-body microscopic dynamics of charges is treated statistically, in the same way as for an ensemble of classically interacting spherical particles (Goetze, 2008). The most striking success of MCT has been the first-principles derivation of the Kohlrausch stretched-exponential relaxation for α-relaxation in the liquid phase. While MCT has tremendous success in describing supercooled liquids at $T > T_g$, the situation is quite different at $T \simeq T_g$ or in the glass at $T < T_g$. For supercooled liquids, the empirical Kohlrausch stretched-exponential function $\sim \exp[-(t/\tau)^{\beta}]$ provides a good fit for the loss modulus of the α-relaxation, by taking the Fourier transform from time into frequency domain (Cardona et al., 2007; Williams and Watts,

1970). Although MCT provides a theoretical foundation for Kohlrausch stretched-exponential behaviour, direct comparisons with experimental data have not been possible due to the difficulty of calibrating various parameters in the theory. Other theories have focused on the mesoscopic-level description of nonlinear deformation such as the Shear-Transformation-Zone (STZ) (Argon, 1979; Falk and Langer, 1998; Langer, 2008). A recent theory based on coherent-potential approximation and on the continuum assumption of heterogeneously fluctuating modulus has achieved success in the comparison with experimental data of linear dynamic moduli of metallic glasses (MGs) (Schirmacher et al., 2015a), but does not provide microscopic atomic-scale insights and does not account for electronic effects. Presenting an alternative method that is microscopic, analytical and can be compared with experimental results constitutes the core topic in Chapter 3.

In addition to α-relaxation, an extra shoulder or wing also decorates the imaginary part of the modulus response, which is referred to as the β-relaxation, or as Johari-Goldstein or secondary relaxation. As discovered in Johari and Goldstein (1970) (JG) in glasses of rigid molecules and as described by the coupling model, the secondary relaxation involves the motion of the entire molecule. The Johari-Goldstein β-relaxation is the most well known amongst these, due to its ubiquity in all types of glasses (Johari and Goldstein, 1970; Ngai, 2000). Although the exact atomic-scale mechanism underlying the JG β-relaxation is still not clear, there appears to be a correlation to the α-relaxation, deformation and mechanical properties (Yu et al., 2014). In this regard, unraveling the atomic-scale dynamical features of the JG β-relaxation would represent considerable progress in our current understanding of its microscopic origin and its impact on the physical and materials properties of glasses (Ruta et al., 2017). Knowing the underlying mechanism of β-relaxation, is also of great importance for understanding many crucial unresolved issues in glassy physics and materials science and consequently for a wide potential application in technologies, ranging from glass transitions, deformation mechanisms, to diffusion and the breakdown of the Stokes-Einstein relations, physical aging, as well as the conductivity of ionic liquids and the stability of glassy pharmaceuticals and biomaterials. A key open question is about the role of different atomic/molecular constituents in the various relaxation processes, and in particular whether a relaxation process is controlled by the dynamics of a particular type of constituent(s). In the case of organic molecular glasses, it has been recently argued that all molecules seem to participate in the JG relaxation, although not all at the once (Cicerone and Tyagi, 2017). While many studies have examined both the structural and relaxational features of the JG β-relaxation in MGs (Evenson et al., 2014; Liu et al., 2014; Wang et al., 2015b; Yu et al., 2017), the connection to the atomic-scale vibrational properties remains to date greatly unexplored. The JG β-relaxation in MGs generally occurs on microsecond time scales, some

several orders of magnitude smaller than the α-relaxation of the glass (Liu et al., 2017; Yu et al., 2017). However, accessing the atomic-scale dynamics of MGs in this temporal regime is both experimentally and computationally challenging. Novel coherent X-ray scattering techniques probe collective atomic motion on time scales larger than about one second (Baldi et al., 2010; Wang et al., 2015b), while molecular dynamics (MD) simulations of the MG glassy-state dynamics have been only recently successfully tested up to 10 microseconds (Yu et al., 2017).

The main limitations for developing an atomic-scale theory of linear response in (dynamic) viscoelasticity are as follows: (i) the vibrational density of states (VDOS) which governs the atomic-scale dynamics is rich in low-energy soft modes (boson peak) whose physical origin has been elusive (Brink et al., 2016; Derlet et al., 2012), and only recently have been traced back to mesoscopic phonon scattering processes and the Ioffe-Regel crossover (Shintani and Tanaka, 2008), which are also in relation to the lack of centrosymmetry; (ii) there is currently no established understanding for the atomic-scale internal friction, which is crucial to deriving viscoelastic sum-rules, and is associated with memory effects which are known to be important for metallic glass (Luo et al., 2016); (iii) the atomic-scale dynamics of glasses under deformation is strongly nonaffine (Hufnagel et al., 2016; Zaccone and Scossa-Romano, 2011), meaning that additional displacements on top of the affine displacements prescribed by the strain tensor, are required to relax quenched neighbouring forces caused by the lack of centrosymmetry of the disordered lattice (Milkus and Zaccone, 2016); (iv) the interatomic interaction is strongly non-local, also due to the role of delocalised electrons which affect the interatomic interaction.

Lattice dynamics formulated through the pioneering work of Max Born and co-workers on the simplifying assumption that deformations are homogeneous, or in modern language, affine, is believed to resolve all issues above (Born and Huang, 1954). In practice, this implies that every atom is displaced under deformation by the macroscopic strain tensor operating on the original position vectors. This transformation defines the affine positions in the deformed lattice. Such a description assumes however that mechanical equilibrium is satisfied at the affine positions, which is certainly true for centrosymmetric lattices, where, owing to each atom being a local center of inversion symmetry, the forces transmitted by the neighbours cancel out by symmetry at the affine positions. The situation is however different for disordered systems like glasses and for non-centrosymmetric crystals as well as near crystalline defects like grain boundaries. In such cases, the atoms are not centers of symmetry and therefore receive forces from their neighbours, which sum up to a net force. The latter is released via an extra displacement, called nonaffine displacement or relaxation, which brings the atoms to final positions that do not coincide with the affine positions. Reformulating the

equations of motion by explicitly requiring that the atoms move along nonaffine pathways of mechanical equilibrium (where the net force on each atom is zero at all steps) leads to a negative (softening) correction to the elastic constants, which was first expressed analytically in Lemaitre and Maloney (2006) for systems of particles which interact through short-ranged pairwise potentials, although Born and Huang (BH) have actually discussed the nonaffine deformation case in great detail (but have not derived complete analytical expressions for nonaffine corrections) (Born and Huang, 1954). The resulting framework is known as the nonaffine response theory or nonaffine lattice dynamics and has recently been applied to various systems and materials, from packings where it recovers the $\sim (Z-2d)$ jamming scaling (Zaccone and Scossa-Romano, 2011), with Z the coordination number and d the spatial dimension, to polymers (Zaccone and Terentjev, 2013), and to analyse dissipation in high-frequency oscillatory rheology (Damart et al., 2017). The framework also provides quantitative predictions of dynamic viscoelastic moduli of coarse-grained (Kremer-Grest) glassy polymers (Palyulin et al., 2018). Especially, the nonaffine contribution to elastic constants can be prominent, which has been found in simulating a non-centrosymmetry lattice (Cui et al., 2019b). The detailed discussion of (static) nonaffinity is the theme of Chapter 4, while the application of nonaffine lattice dynamics to dynamical moduli in MGs is the topic of Chapter 5.

The framework of nonaffine lattice dynamics is essentially a mean field theory. Many features of sound wave propagating in the materials are stored in the dynamical structure factor (DSF), which can be directly measured in scattering experiments or calculated in numerical simulations. In particular, the width of the structural peaks in DSF is representative of the mechanical damping in the material. It is well known that, there is no sound attenuation in perfect crystals, upon the harmonic approximation, whereas in glasses, long-wavelength phonons are more damped than those in ordinary crystalline solids. A compilation of many experiments with X-ray and light scattering demonstrates that the wavenumber dependence of the longitudinal sound attenuation coefficient, $\Gamma_L(q)$ is in general divided into three regimes (Baldi et al., 2011, 2010, 2014, 2016; Carini et al., 1993; Masciovecchio et al., 2006; Monaco and Giordano, 2009; Monaco and Mossa, 2009; Rufflé et al., 2006): (1) $\Gamma_L(q) \sim q^2$ for low q; (2) $\Gamma_L(q) \sim q^4$ for an intermediate q regime; and (3) $\Gamma_L(q) \sim q^2$ for large q. Most computer studies address the sound attenuation problem at zero temperature in order to remove anharmonic effects and thus isolate the effect of disorder. It has been proven that the q^2 to q^4 transition for sound attenuation in large frequency regime is mainly harmonic (Schirmacher et al., 2007). To study the low vibrational modes, Schirmacher et al. (1998) constructed a cubic lattice of coupled classical harmonic oscillators with spatially fluctuating nearest neighbor force constants, and found the excess of a low-frequency peak in the scaled

density of states $D(\omega)$. Montagna et al. (1999) presented a mechanism reproducing q^2 dependence of the broadening of the Brillouin peaks. Yet there is no fully analytical approach to deal with the damping mechanism in the practically relevant range of low wavevectors. Accounting for the disorder via a Gaussian distribution of spring constant values in a perfectly ordered lattice makes it possible to carry out the analysis of DSF and the associated damping effects in a lattice with quenched random disorder. The sound (elastic) wave is replaced by lattice wave considered in the harmonic theory, which is valid for low wavevectors. The (observable) average DSF obtained in this way has a characteristic widening of structural peaks that lead to the analytical expression for the damping coefficient $\Gamma(q)$.

The $\Gamma(q) \sim q^{d+1}$ scaling law is known as Rayleigh scattering, whose validity has never been questioned in the last fifty years of studies of sound attenuation in amorphous materials (Strutt, 1871), although an additional logarithmic enhancement has been investigated in recent numerical simulations (Gelin et al., 2016; Mizuno and Ikeda, 2018). In particular, regardless of system size, a recent numerical study of 2D systems reveals that the logarithmic correction to the cubic scaling, $\Gamma_\lambda(q) \sim -q^3 \ln q$ ($\lambda = L, T$ stands for longitudinal and transverse) emerges in the boson peak (BP) regime, while it disappears as the wavenumber approaches the continuum limit, where $\Gamma_\lambda(q) \sim q^3$ is recovered (Mizuno and Ikeda, 2018). Gelin et al. (2016) even revisited data in experimental systems to confirm the damping coefficient indeed corresponds to the enhanced $-q^{d+1} \ln q$ law. To rationalise the observed logarithmic correction to the Rayleigh law, one interpretation is to invoke the existence of correlated inhomogeneities of the elastic constants within the framework of fluctuating or heterogeneous elasticity (HE), yet neither quantitative nor qualitative arguments have been presented (Marruzzo et al., 2013a,b; Mizuno and Mossa, 2019; Mizuno et al., 2013, 2014; Wang et al., 2019). Also, the possible relation between the logarithmic correction to the Rayleigh law and the long-range nature of elastic modulus has been questioned (Mizuno and Ikeda, 2018; Moriel et al., 2019). Simulation in Moriel et al. (2019) indicates that the log-enhancement to Rayleigh scattering does not correlate with fluctuations in the elastic constants, but appears, instead, to be strongly correlated with spatially heterogeneous internal stresses. Finally, a recent analysis in Caroli and Lemaître (2019) even argues that HE is unable to predict the logarithmic enhancement. With a fully tensorial replica field theory to athermal amorphous systems with power-law decay in elastic constant correlations, it becomes possible to make an attempt to reveal the origin of the enhanced phonon damping, especially where the logarithmic enhancement is prompted. The analytical theory shows that the logarithmic enhancement is either due to the long-range power-law correlations of elastic constants (John et al., 1983; John and Stephen, 1983; Maurer and Schirmacher, 2004) or to long-range power-law correlations of the internal stresses (with no fluctuations in the

elastic constants) (Maier et al., 2018; Wang et al., 2020), which is the key ingredient in the framework leading to the prediction of the logarithmic enhancement. Some previous works dealing with mean-field theory confirm the Rayleigh scattering law without the logarithmic factor. In those works, there is no power-law decay in correlations of elasticity (DeGiuli et al., 2014; Köhler et al., 2013; Maurer and Schirmacher, 2004; Shimada et al., 2020; Wyart, 2010). In Chapter 6, I will develop mean-field theories for disordered crystals and amorphous systems to elaborate the mechanism of phonon transport. In the last, conclusions and future insights will be presented in Chapter 7.

Chapter 2

Literature and background theory

This chapter provides the theroetical background serving as a starting point for the rest of the thesis. It starts with a textbook explanation of the lattice dynamics framework used to calculate the vibrational density of states that will be used throughout the thesis. It then goes on to introduce the standard Langevin equation describing the stochastic motion of a Brownian particle, and the non-Markovian extension to it that enables the inclusion of memory effects in the friction term. The non-Markovian (generalised) Lagenvin equation is essential to describe the dielectric (Chapter 3) and mechanic (Chapter 5) dynamic moduli of supercooled liquids, which consist of multistage relaxation processes that are then reviewed in the following section. In particular, a framework called nonaffine lattice dynamics witnesses its success in calculating static elastic constants (Chapter 4) and moduli (Chapter 5), only based on the information of microscopic structure of glasses. Reviews of some equivalent interpretations of this framework, i.e. the Lemaitre-Maloney formalism, the Born-Huang method and long-range collective motions of lattice, are presented in Section 2.4 - Section 2.6. The analysis of phonon transport in disordered solids, namely Chapter 6, is also an integral part of the thesis. Presenting the complete theory requires me to put details of Green's functions in the context of the present thesis, as well as an exposition of the dynamical structure factor for both crystalline and disordered systems, in the last two sections in this chapter.

Focusing on a tagged particle (e.g. a molecular subunit carrying a partial charge which reorients under the electric field), it is possible to describe its motion under the applied field using a particle-bath Hamiltonian of the Caldeira-Leggett type, in classical dynamics. The particle's Hamiltonian firstly studied in Zwanzig (1973) is bi-linearly coupled to a bath of harmonic oscillators which represent all other molecular degrees of freedom in the system. Any complex system of oscillators can be reduced to a set of independent oscillators by performing a suitable normal mode decomposition. This allows us to identify the spectrum

of eigenfrequencies of the system, i.e. the VDOS, as the spectrum of the set of harmonic oscillators forming the bath.

2.1 The vibrational density of states

Recall the theory of lattice dynamics leading to the definition of VDOS. In d-dimensional space, I expand the potential energy up to the 2nd order around an arbitrary surface for N particles occupying $\{\mathbf{R}_1, \mathbf{R}_2, ..., \mathbf{R}_N\}$ in space, which gives:

$$\mathscr{U}(\mathbf{R}_1, \mathbf{R}_2, ..., \mathbf{R}_N) = \mathscr{U}(\mathbf{R}_I^\circ) + \sum_I^N \sum_\mu^d s_I^\mu \left[\frac{\partial \mathscr{U}}{\partial R_I^\mu}\right]_{\mathbf{R}_I^\circ} + \frac{1}{2}\sum_{IJ}^N \sum_{\mu\nu}^d s_I^\mu s_J^\nu \left[\frac{\partial^2 \mathscr{U}}{\partial R_I^\mu \partial R_J^\nu}\right]_{\mathbf{R}_I^\circ}, \quad (2.1)$$

where μ, ν run over all Cartesian components and the starting configuration surface is denoted to be $\{\mathbf{R}_I^\circ\}$. The displacement of particle I along μ-axis is s_I^μ. I can define a d-vector with respect to $\mathbf{R}_I$ and a $d \times d$ matrix on $\mathbf{R}_I, \mathbf{R}_J$:

$$f_I^\mu = -\left[\frac{\partial \mathscr{U}}{\partial R_I^\mu}\right]_{\mathbf{R}_I^\circ}; \quad H_{IJ}^{\mu\nu} = \left[\frac{\partial^2 \mathscr{U}}{\partial R_I^\mu \partial R_J^\nu}\right]_{\mathbf{R}_I^\circ}. \quad (2.2)$$

Physically, f_I^μ is the force along the μ-axis on particle I in the reference configuration $\{\mathbf{R}_I^\circ\}$, while $-H_{IJ}^{\mu\nu}$ is the linear response coefficient of the μ-component of force acting on I due to the ν-component of the displacement of J. The total energy of N particles, each with mass M_I, can be written as

$$\mathscr{H} = \sum_{I=1}^N \sum_{\mu=1}^d \frac{M_I}{2}\left(\dot{s}_I^\mu\right)^2 + \mathscr{U}(\mathbf{R}_1, \mathbf{R}_2, ..., \mathbf{R}_N), \quad (2.3)$$

where the dot above s represents the 1st order derivative with respect to time. The classical equation of motion of the particle I (within the harmonic approximation) can be written as

$$M_I \ddot{s}_I^\mu = -\sum_{J\nu} H_{IJ}^{\mu\nu} s_J^\nu + f_I^\mu. \quad (2.4)$$

The right hand side represents the $\mu-$component of the force vector acting on I.
In lattice, every particle (I) lies in a (unit) cell (l). Because of the periodicity, I can write

$$f_I^\mu(l) = f_I^\mu; \quad H_{IJ}^{\mu\nu}(l, l') = H_{IJ}^{\mu\nu}(l - l', 0) \equiv H_{IJ}^{\mu\nu}(l - l'). \quad (2.5)$$

Following properties can be verified:

(1) Translation invariance: the potential remains unchanged if the system is displaced by an arbitrary vector **e**. Expanding the potential up to the 1st order, I have

$$\sum_{I\mu} f_I^\mu(l)e^\mu = 0 \Rightarrow \sum_I f_I^\mu(l) = 0, \tag{2.6}$$

which is equivalent to $\sum_I f_I^\mu = 0$.

(2) Homogeneous deformation about (l,I): after the deformation, the structure still remains as a perfect lattice. Thus,

$$\begin{aligned}&\sum_I \frac{\partial \mathscr{U}}{\partial s_I^\mu(l)} = 0 \Rightarrow \sum_I \{-f_I^\mu - \sum_{l'J\nu\xi} H_{IJ}^{\mu\nu}(l-l')s_{\nu\xi}R_{IJ}^\xi(l-l') + ...\} = 0 \\ &\Rightarrow \sum_{IJl'} H_{IJ}^{\mu\nu}(l-l')R_{IJ}^\xi(l-l') = 0.\end{aligned} \tag{2.7}$$

where $s_J^\mu(l') = \sum_\nu s_{\mu\nu}(R_J^\nu(l') - R_I^\nu(l)) \equiv \sum_\nu s_{\mu\nu}R_{JI}^\nu(l'-l)$ are displacements and $s_{\mu\nu} = \partial s^\mu/\partial R^\nu$ are known as deformation parameters.

(3) If all particles are displaced from the equilibrium configuration by the same vector $s_I^\mu(l) = e^\mu$, I get

$$\frac{\partial \mathscr{U}}{\partial s_I^\mu(l)} = -f_I^\mu + \sum_{l'J\nu} H_{IJ}^{\mu\nu}(l,l')e^\nu + \frac{1}{2}\sum_{l'l''Jk\nu\xi} K_{IJK}^{\mu\nu\xi}(ll'l'')e^\nu e^\xi + ... \tag{2.8}$$

where coefficients of all orders of e^μ are zero.

(4) If particles are displaced by $s_J^\nu(l') = \sum_\xi \omega_{\nu\xi}(R_J^\xi(l') - R_I^\xi(l)) = -\sum_\xi \omega_{\xi\nu}R_{JI}^\xi(l'-l)$, which is essentially a rotation, then

$$\frac{\partial \mathscr{U}}{\partial s_I^\mu(l)} = -f_I^\mu - \sum_{\xi l'J} H_{IJ}^{\mu\nu}(l-l')\omega_{\nu\xi}R_{IJ}^\xi(l-l') + ... \tag{2.9}$$

On the other hand, for a rigid rotation, $\partial\mathscr{U}/\partial s_I^\mu(l) = -\sum_\nu(\delta_{\mu\nu} + \omega_{\mu\nu})f_I^\nu(l) = -f_I^\mu - \sum_\nu \omega_{\mu\nu}f_I^\nu$, where $\delta_{\mu\nu}$ is the Kronecker delta function. Objects in the bracket after the first equality make the whole term behave as the μ-component of a vector, which corresponds to

the transformation matrix for rotation. Thus, by equating two expressions, I have

$$\sum_{\nu} \omega_{\mu\nu} f_I^{\nu} = \sum_{l'J\xi} H_{IJ}^{\mu\nu}(l-l')\omega_{\nu\xi} R_{IJ}^{\xi}(l-l') = \sum_{lJ\xi} H_{IJ}^{\mu\nu}(l)\omega_{\nu\xi} R_{IJ}^{\xi}(l) + \ldots \tag{2.10}$$

Differentiating both sides with respect to $\omega_{\mu\nu} = -\omega_{\nu\mu}$, I obtain

$$\delta_{\kappa\mu} f_I^{\nu} - \delta_{\kappa\nu} f_I^{\mu} = \sum_{lJ} \left\{ H_{IJ}^{\kappa\mu}(l) R_{IJ}^{\nu}(l) - H_{IJ}^{\kappa\nu}(l) R_{IJ}^{\mu}(l) \right\}. \tag{2.11}$$

Equilibrium conditions in lattice systems are in general twofold: (i) every particle is in mechanical equilibrium; (ii) the whole configuration corresponds to vanishing stresses (this condition could be relaxed, as will be shown in Chapter 4). Assuming the mechanical equilibrium condition, when the particle moves from $R_I^{\mu}(l)$ to $R_I^{\mu}(l) + s_I^{\mu}(l)$, it obeys the equation of motion

$$M_I \ddot{s}_I^{\mu}(l) = -\sum_{l'J\nu} H_{IJ}^{\mu\nu}(l,l') s_J^{\nu}(l'). \tag{2.12}$$

To solve Eq. (2.12), I take the ansatz $s_I^{\mu}(l) = e_I^{\mu} e^{i\mathbf{q}\cdot\mathbf{R}_I(l) - i\omega t}/\sqrt{M_I}$, where $\mathbf{q}$ is an arbitrary vector (wavevector) in the reciprocal space, i.e. $\mathbf{q} \in span\left\{ \frac{2\pi \mathbf{a}_2\times\mathbf{a}_3}{\mathbf{a}_1\cdot(\mathbf{a}_2\times\mathbf{a}_3)}, \frac{2\pi \mathbf{a}_3\times\mathbf{a}_1}{\mathbf{a}_1\cdot(\mathbf{a}_2\times\mathbf{a}_3)}, \frac{2\pi \mathbf{a}_1\times\mathbf{a}_2}{\mathbf{a}_1\cdot(\mathbf{a}_2\times\mathbf{a}_3)} \right\}$ where $\mathbf{a}_1, \mathbf{a}_2, \mathbf{a}_3$ are lattice vectors forming the periodic cell. The magnitude of $\mathbf{q}$ is the wavenumber. Substituting the ansatz into Eq. (2.12) gives

$$\omega^2(\mathbf{q},m) e_I^{\mu}(\mathbf{q},m) = \sum_{J\nu} D_{IJ}^{\mu\nu}(\mathbf{q}) e_J^{\nu}(\mathbf{q},m), \quad m = 1,2,\ldots,Nd, \tag{2.13}$$

with the dynamical matrix defined as

$$D_{IJ}^{\mu\nu}(\mathbf{q}) = \frac{1}{(M_I M_J)^{1/2}} \sum_{l'} H_{IJ}^{\mu\nu} e^{i\mathbf{q}\cdot\mathbf{R}_{JI}(l'-l)}. \tag{2.14}$$

This is the eigenvalue/eigenvector problem. There are Nd solutions for each wavevector $\mathbf{q}$. It is clear to see the symmetric properties of the dynamical matrix from its definition:

$$D_{IJ}^{\mu\nu}(\mathbf{q})^* = D_{JI}^{\nu\mu}(\mathbf{q}) = D_{IJ}^{\mu\nu}(-\mathbf{q}). \tag{2.15}$$

where * means the complex conjugate. In a nutshell, the spectrum of ω denotes the density of particles in frequency scale and is called the vibrational density of states (VDOS). The VDOS is an intrinsic property of the system and influence its response to external fields. For example, in the Lorentz dielectric model, displacements of all particles in the applied oscillating electric field have to be evaluated to obtain the polarisation. This requires a sum

over all degrees of freedom of all particles, which can be done by using the VDOS and integrating over the eigenfrequency. This protocol will be explained in detail in following sections.

2.2 The generalised Langevin equation

Markovian Langevin equation

In soft materials, the thermal energy k_BT available at room temperature is sufficient to induce deformation. The random motion of a small particle immersed in a fluid is called Brownian motion. The Brownian motion is the broad phenomenon investigated on nano- to micro-scale systems like pollen grains, dust particles, colloids etc. In the theory of Brownian motion, the "Brownian particle" is not necessarily a real particle, but could be some collective properties of a macroscopic system, which might be important for the instantaneous concentration of any component of a chemically reacting system in thermal equilibrium.

For a particle (mass M, position $\mathbf{x}$, velocity $\mathbf{v}$) suspended in a solvent (drag coefficient γ), its equation of motion reads (in 1d)

$$M\frac{dv}{dt} = F_{total}(t), \tag{2.16}$$

where $F_{total}(t)$ is the total instantaneous force induced by the multiple collisions from the surrounding solvent molecules to the particle at time t. In principle, if the position of the particle is known, as a function of time, then the form of force can be determined. In this sense, it is not random. For example, fluid dynamics tells us that this force is dominated by a drag force $-\gamma v$, proportional to the velocity of the Brownian particle. We can approximate the particle as a spherical object with radius r, then Stokes' law tells that $\gamma = 6\pi\eta r$, where η is the viscosity of the solvent. Replacing $F_{total}(t)$ by $-\gamma v$ and solving the linear 1st order differential equation gives

$$v(t) = v(0)e^{-\frac{\gamma t}{M}}. \tag{2.17}$$

This shows that, the velocity of the Brownian particle decays to zero at long time, which is not true because the mean squared velocity of the particle at thermal equilibrium should be $\langle v^2\rangle_{eq} = k_BT/M$ with k_B being the Boltzmann constant and T being the temperature. The assumption that $F_{total}(t)$ is dominated by the Stokes' drag force must be modified.

The drag force actually reflects the slow degrees of freedom associated with the overall motion of the particle. There are faster counterparts coupled to the motion of solvent. To describe this effect, we note that, over two successive time intervals τ, which are longer

than the inverse of the characteristic of rate of collisions from the solvent $\tau^{-1} \sim 10^{13} s^{-1}$, the motion of the particle is uncorrelated between the two successive timesteps. Over these timescales, we can add an additional "random" or "fluctuating" force $F_v(t)$ to the frictional force, so that the equation of motion becomes

$$M\frac{dv}{dt} = -\gamma v + F_v(t) \equiv F_{total}(t). \tag{2.18}$$

This is the Langevin equation for a Brownian particle, which was historically one of the first examples of a stochastic differential equation. In effect, the total force is split into a systematic part (friction) and a fluctuation part (noise), both come from the interaction of the Brownian particle with its surroundings. Note that, for each $F_v(t)$, there is a different trajectory $v(t)$. Thus, the physically interesting quantities will be average $\langle\cdot\rangle$ over different realisations of the random process $F_v(t)$. In an isotropic fluid, molecular collisions with the solvent do not have a preferential direction. This gives $\langle F_v(t)\rangle = 0$. Moreover, there should be no correlation between impacts in any distinct time, thus $\langle F_v(t)F_v(t')\rangle = B\delta(t-t')$, where B measures the strength of the fluctuating force.

The Langevin equation Eq. (2.18) can be solved to give

$$v(t) = v(0)e^{-\frac{\gamma t}{M}} + \int_0^\infty e^{-\frac{\gamma}{M}(t-t')}\frac{F_v(t')}{M}dt' \tag{2.19}$$

The integral on the RHS is a stochastic integral, i.e. it takes a different value for each realisation of the stochastic process $F_v(t)$. Examining averages over different realisations of $F_v(t)$, it is not hard to show that the mean squared velocity has the form

$$\langle v(t)^2\rangle = \frac{B}{2M\gamma}. \tag{2.20}$$

In the long time limit, the equipartition theorem fix the value of $\langle v^2\rangle \to k_BT/M$ (as $t \to \infty$). This constraint therefore determines the value of the constant $B = 2\gamma k_BT$. Consequently, the time correlation of noise F_v reads

$$\langle F_v(t)F_v(t')\rangle = 2k_BT\gamma\delta(t-t'). \tag{2.21}$$

This result is known as the fluctuation-dissipation theorem (FDT). It relates the strength B of the fluctuation of a particle to the dissipation drag γ that the same particle experiences when it is actively moved through a fluid. It expresses the balance between friction, which tends to drive any system to a "dead" state, and noise, which tends to keep the system "alive", which is required to have a thermal equilibrium state at long times (Zwanzig, 2002).

The velocity correlation function might also find its connection with the self-diffusion coefficient D. The 1d diffusion equation of the concentration $P(x,t)$ (i.e. probability) of a tagged particle on space and time reads

$$\frac{\partial P(x,t)}{\partial t} = D\frac{\partial^2 P(x,t)}{\partial x^2}. \tag{2.22}$$

The mean square displacement at time t can be found by multiplying the diffusion equation by x^2 and integrating over x:

$$\frac{\partial \langle x^2 \rangle}{\partial t} = \int x^2 \frac{\partial P(x,t)}{\partial t} dx = D\int x^2 \frac{\partial^2 P(x,t)}{\partial x^2} dx = 2D\int P(x,t)dx = 2D. \tag{2.23}$$

The last line holds since the concentration is normalised to unity. Upon integrating over time, the result is the well-known Einstein formula for diffusion in 1d, which is $\langle x^2 \rangle = 2Dt$. Meanwhile, from Eq. (2.19) one can also find the equivalent form of time correlation of displacement, which gives us (Zwanzig, 2002)

$$D = \int_0^\infty \langle v(0)v(t)\rangle dt = \frac{k_B T}{\gamma}. \tag{2.24}$$

The generalisation of the Langevin equation

There are in general two generalisions of the Langevin equation: nonlinear Langevin equations and non-Markovian Langevin equations. I only review the latter. The Langevin equation considered up to now is called "Markovian", since it indicates the friction at time t is proportional to velocity at the same time, and that the noise is delta-function correlated. However, real problems are often not Markovian. The friction at time t might depend on the history of the velocity $v(t')$ for time t' earlier than t. In this regard, the drag (friction) is replaced by a memory function $\nu(t)$ (note the symbolic difference from velocity), so that the friction force at time t becomes

$$-\gamma v(t) \to -\int_{-\infty}^{t} \nu(t-t')\frac{dx(t')}{dt'}dt'. \tag{2.25}$$

Problems of this kind are called non-Markovian and the corresponding Langevin equation is named as the generalised Langevin equation (GLE). Likewise, the diffusion equation, Eq. (2.22), would also be modified in a similar way in the non-Markovian case, which is

$$\frac{\partial P(x,t)}{\partial t} = -\mathrm{div}J \quad \to \quad \frac{\partial P(x,t)}{\partial t} = -\int_{-\infty}^{t} \nu'(t-t')\left(-k_B T\frac{\partial P}{\partial x}\right)dt', \tag{2.26}$$

where $J(x,t)$ is the flux and $\nu'(t-t') \sim 1/\gamma$ is the mobility kernel. Thus, the non-Markovian version of diffusion constant becomes $D = k_B T \nu'(t-t')$. This means, if a system approaches to equilibrium at long times, the FDT must be modified and the noise is no longer white (the Fourier transform of the correlation function of the noise is independent of frequency).

To give a simple illustration of how non-Markovian behaviour can arise, I start from Markovian Langevin equations:

$$\frac{dx}{dt} = \frac{P}{M}; \quad \frac{dP}{dt} = -M\omega^2 x - \gamma\frac{P}{M} + F_P(t) \tag{2.27}$$

where $P(t) = Mv(t)$ is the momentum vanishing in the infinite past, $P(-\infty) = 0$. I solve the second equation for $P(t)$ by integrating from $-\infty$ to t:

$$P(t) = \int_{-\infty}^{t} e^{-\frac{\gamma(t-t')}{M}}(-M\omega^2 x(t') + F_P(t'))dt' \tag{2.28}$$

Putting this back to the equation of dx/dt, I obtain

$$\frac{dx(t)}{dt} = -\int_0^\infty \nu(t')x(t-t')dt' + F_x(t), \tag{2.29}$$

where the memory function $\nu(t)$ and the new fluctuating force $F_x(t)$ are

$$\nu(t) = \omega^2 e^{-\frac{\gamma|t|}{M}}; \quad F_x(t) = \frac{1}{M}\int_0^\infty e^{-\frac{\gamma t'}{M}} F_p(t-t')dt'. \tag{2.30}$$

The second momentum of x at equilibrium is $\langle x^2\rangle_{eq} = k_B T/(M\omega^2)$, so after some algebra, the correlation of $F_x(t)$ is (Zwanzig, 2002)

$$\langle F_x(t)F_x(t')\rangle = \langle x^2\rangle_{eq}\nu(|t-t'|). \tag{2.31}$$

This is a non-Markovian version of the FDT. The correlation function of the new noise is proportional to the memory function for the new friction. If the friction is very large, or if we are concerned with times much longer than M/γ, then the memory function $\nu(t)$ can be approximated by a delta function,

$$\nu(t) \approx 2\frac{M\omega^2}{\gamma}\delta(t), \tag{2.32}$$

corresponding to the Markovian friction. Then, Eq. (2.29) is approximately the (Markovian) Langevin equation for the position $x(t)$.

2.3 Multi-stage relaxation processes in supercooled liquids

Supercooled liquids and the glass transition

Unlike crystalline solids and disordered liquids, the ordinary structural glass (SG) formers represent an intermediate state of matter without long-range structural order. In general, a liquid enters into a supercooled regime, i.e. its viscosity becomes too large to stop flowing on any practical time scale, when it is rapidly cooled to below its melting point. Supercooled liquids exhibit a complex response function on vibrational excitations (Angell et al., 2000; Dean, 1972; Donth, 2001; Martinez and Angell, 2001). Many experiments and computer simulations have shown that the structural and thermodynamic properties of supercooled liquids only exhibit weak dependence on temperature. Because of different characteristic temperatures in various materials (e.g. melting point), it is useful to analyse temperature (T) dependence of viscosity or relaxation time (τ) using a reduced temperature scale. The glass transition temperature (T_g) is defined as the temperature at which the viscosity exceeds 10^{12} Pa.s or the (structural) relaxation time exceeds 100 seconds. To quantitatively characterise the difference in the growth of relaxation time (or viscosity) as a function of (inverse of) T from one material to another, one can further define the kinetic fragility index as $m = (\partial \log \tau / \partial (T_g/T))\big|_{T=T_g}$, ranging between ≈ 16 (strong glasses) and 200 (fragile glasses) (Angell, 1988; Böhmer et al., 1993). Fragility is an important quantity with profound physical significance. For example, silica are strong glass formers whose viscosity satisfies an Arrhenius-type growth, i.e. $\tau = \tau_0 \exp(E_\alpha / k_B T)$ where the activation energy, E_α, is temperature independent (for strong glass), upon cooling. On the other hand, fragile materials have a viscosity increasing faster than an Arrhenius law (super-Arrhenius behavior). Although there is no theory to date has been able to predict a material's degree of fragility from the sole knowledge of its microscopic structure, it has been widely believed that a thorough understanding of the mechanisms underlying fragility will be the key to achieving a universal description of the glass transition (Kob, 2003).

In addition to the structural glasses, orientational glasses (OGs) can be obtained from orientationally disordered (OD) phases that are high-symmetry lattices in which weakly interacting molecules are orientationally disordered (Brand et al., 2002; Ramos et al., 1997; Suga and Seki, 1974; Tamarit et al., 1997). On cooling, some OD phases exhibit the same features as structural (canonical) glass formers. With respect to the fragility index, OGs are usually strong whereas for SGs a wide range of fragility values are found: the most fragile being the cis- or trans-decahydronaphthalene ($m \approx 147$) (Kalyan and Richert, 2002). The most fragile OGs known to date are Freon 112 (CCl_2F-CCl_2F, hereinafter F112) with $m = 68$

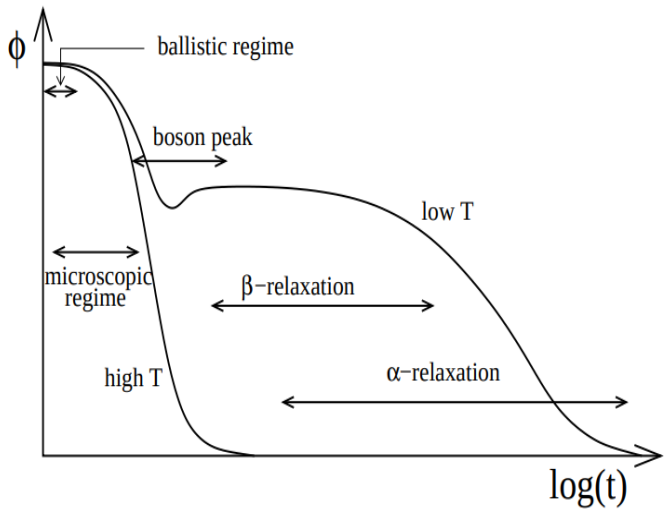

Fig. 2.1 Time dependence of a typical time correlation function $\Phi(t)$. Left curve corresponds to relatively high T while the curve on the right represents the typical glassy system in low temperature (Kob, 2003).

(Pardo et al., 2006). For Freon 113 (CCl_2F-$CClF_2$, hereinafter F113), $m = 127$ (Vispa et al., 2017).

Relaxations in time and frequency

I only discuss the temperature dependence of macroscopic quantities, such as viscosity or characteristic time, in the last subsection. Many experiments like dynamic light scattering, dielectric measurements, ect., give also direct access to the time dependence of microscopic correlation functions, e.g. the density-density correlator. Correlation functions contain more information than the mentioned macroscopic quantities since the latter can be expressed as the time integral over such correlation functions. For example, viscosity is related to the integral over the stress-stress correlation function (Balucani and Zoppi, 1994; Hansen and McDonald, 2008).

Figure 2.1 shows a schematic way the time dependency of a typical correlation function (e.g. the intermediate scattering function $F(q,t)$ discussed in Chapter 5). At high temperature, the system is in its normal liquid state, and the relaxation is relatively simple: At very short times, $\Phi(t)$ is quadratic in t, which follows directly from the Taylor expansion of the Newton's equations for particles (Balucani and Zoppi, 1994; Hansen and McDonald, 2008). This time window is often called "ballistic regime". When t becomes larger, $\Phi(t)$ is governed by the interactions between particles and it is called the "microscopic regime". For even longer

times, the t-dependence of $\Phi(t)$ can be approximated by an exponential function, i.e. the system shows a Debye relaxation (the form of dielectric relaxation is shown in Chapter 3).

On the other hand, $\Phi(t)$ exhibits a more complex time dependence at low temperature. The ballistic regime again emerges at short times. In contrast to the correlator at high T, $\Phi(t)$ shows a plateau at intermediate times. The corresponding time window is called the "β-relaxation". For much longer time, the correlation function decays to zero. The time interval where the correlator drops below the plateau is known as the "α-relaxation". The early part of the α-relaxation might coincide with the late part of β-relaxation. At low T, each particle is surrounded by neighbouring particles forming a temporary cage. At very short times, the particles move ballistically and reflect t^2 dependence in the correlation function. At somewhat longer times, the particles start to interact with their neighbours and the correlator enters into the microscopic regime. For intermediate time range, particles are trapped by their neighbours and hence the correlation function is almost constant. Only for much larger times they are able to escape from trappings and hence the correlation function starts to decay to zero. The physical mechanism behind the plateau is understood as "cage effect".

The correlation function exhibiting dependence on time has its counterpart in the frequency domain. As a result of linear response theory, calculating the time-Fourier transform of a correlation function and multiplies its imaginary part with $\omega/(2k_BT)$ gives a frequency dependent susceptibility $\chi''(\omega)$ (Balucani and Zoppi, 1994; Hansen and McDonald, 2008). There is a particular concern to the evolution of the main relaxation (α-process), its susceptibility has derivations at high frequencies, which fills the gap between the slow relaxation dynamics (α-peak) and fast dynamics ($\nu > 1$GHz) (Davidson and Cole, 1951; Dixon et al., 1990; Kudlik et al., 1995; Schönhals et al., 1993). The interplay of fast and slow dynamics usually leads to a minimum in susceptibility $\chi''(\omega)$. Here, it is important to note that, the secondary relaxation process, i.e. β-process, which is faster than the α-process, is still significantly slower than the fast relaxation. Fast dynamics is described in some cases by assuming thermally activated transitions in asymmetric double well potentials (ADWPs), e.g. within the Gilroy and Philips approach (GP) (Gilroy and Phillips, 1981; Tielbürger et al., 1992). Light scattering (LS) study presented the first survey of fast dynamics well below T_g extending down to $\nu \approx 1$GHz. Also, in contrast to the α-relaxation, the β-relaxation is not necessarily found in all glass formers and the relaxation strength varies significantly among the different systems (Wiedersich et al., 1999).

So far, three distinguished relaxation processes have been reviewed: (i) fast dynamics (ii) β-process and (iii) some kind of background noise being reminiscent of the high frequency-wing of the α-relaxation. In addition to structural and dynamical observables,

other thermodynamics quantities, such as the pressure, specific heat, enthalpy, entropy etc., show a smooth and relatively mild T-dependence. Reviews on these properties can be found in Kob (2003); Nielsen (1999); Scheidler et al. (2001); Stillinger (1988); Wolfgardt et al. (1996); Zaccone (2020). Further, most of the system discussed here are liquids in supercooled state. However, a slow relaxation dynamics is not necessarily related to the supercooled state. In other words, in order to understand the physics for the slow relaxation of a system, its supercooled state cannot be a relevant factor. Thus, one sometimes also uses "glassy liquids" to describe a liquid whose relaxation time is already much larger than the typical microscopic timescale. In this thesis, I will only use "supercooled liquids" or "glass".

2.4 Nonaffine lattice dynamics

Aiming at deriving a suitable equation of motion for a tagged atom (or ion) in a glass in response of applied strain, I extend the Zwanzig-Caldeira-Leggett (ZCL) approach to atomic dynamics in disordered materials by taking into account the disordered environment as well as the dissipation. In the construction of this approach, it is well known that one cannot consider anharmonicity, as illustrated in Weiss (2012). However, anharmonicity is indirectly taken into account in the framework through the VDOS and the emergent friction kernel.

In the ZCL approach, the Hamiltonian of a tagged atom (mass M, position Q and momentum P) coupled to all other atoms (treated as harmonic oscillators with mass M_m, position Q_m and momentum P_m) in the material has expression in 1d as (Zwanzig, 2002)

$$\mathscr{H} = \frac{P^2}{2M} + \mathscr{U}(Q) + \frac{1}{2}\sum_m \left[\frac{P_m^2}{M_m} + M_m\omega_m^2\left(X_m - \frac{F_m(Q)}{M_m\omega_m^2}\right)^2\right]. \tag{2.33}$$

The extension of the ZCL formalism to the presence of external field is shown in Chapter 3. The coupling force between the tagged particle and the mth-oscillator is defined as $F_m(Q)$. Introducing the mass-scaled tagged-particle displacement $s = Q\sqrt{M}$, the resulting equation of motion for the tagged particle becomes

$$\ddot{s} = -\mathscr{U}'(s) - \int_{-\infty}^{t} \nu(t-t')\frac{ds}{dt'}dt' + F_p(t), \tag{2.34}$$

where $F_p(t)$ is the noise. Upon focusing on the athermal limit of the dynamics for $T < T_g$, the noise term $F_p(t)$ that amounts to assuming low thermal noise and frozen-in atomic positions can be ignored, which is a meaningful approximation below T_g. Also, for dynamical response to an oscillatory strain, one can average the dynamical equation over many cycles, which

amounts to a time-average. Since the noise F_p is shown to have zero-mean, an average over many cycles could be effectively similar to an ensemble average thus leaving $\langle F_p \rangle = 0$ in the above equation. According to Damart et al. (2017), when the system is non-ergodic below T_g, nothing guarantees this is true a priori, but there is initial evidence that this approximation might be reasonable in the linear regime where the response converges to a reproducible noise-free average stress.

Nonaffine deformations

Nonaffine lattice dynamics has been studied systematically in work of Lemaitre and Maloney (LM), which is applicable to both amorphous materials and ordered crystals (Lemaitre and Maloney, 2006). In this formalism, the response directly to external strain is called affine if particles' displacements are just the old positions transformed by the macroscopic strain tensor. In a disordered, or a non-centrosymmetric lattice where local inversion symmetry is absent, the situation becomes different since forces from the surrounding environment acting on every particle no longer cancel by symmetry. However, they have to be relaxed with additional displacements of particles, such that the whole system remains in mechanical equilibrium at every step in the deformation (Milkus and Zaccone, 2016). These additional atomic displacements are called nonaffine displacements. The nonaffine deformation mechanism is depicted in the cartoon in Fig. 2.2.

In the language of elasticity, particles (atoms) are assumed to lie in a unit cell described by three Bravais vectors $\underline{\underline{h}} = (\mathbf{a}, \mathbf{b}, \mathbf{c})$. Thus, the interaction potential depends on both R_I^μ and $\underline{\underline{h}}$, $\mathscr{U} = \mathscr{U}(R_I^\mu, \underline{\underline{h}})$ and any vector $\mathbf{R}$ is mapped onto a reference cell: $\mathbf{R} = \underline{\underline{h}}\mathbf{w}, w^\nu \in [-0.5, 0.5]$. We can call the unit cell before deformation the reference frame $\mathring{\underline{\underline{h}}}$, and denote the deformed cell by the new set $\underline{\underline{h}}$. When a given particle undergoes a displacement to the position R_I^μ, the process can be interpreted in two steps: initially, we have $\mathbf{R}_I = \underline{\underline{F}}\mathring{\mathbf{R}}_I$ where $\underline{\underline{F}} = \underline{\underline{h}}\mathring{\underline{\underline{h}}}^{-1}$ is the deformation gradient tensor. In other words, $\underline{\underline{F}}$ describes an affine transformation of the unit cell, whereas $\mathring{\mathbf{R}}_I$ remains unchanged. The deformation tensor $\underline{\underline{F}}$ is related to the (generalised) Cauchy-Green strain tensor as $\underline{\underline{\eta}} = (\underline{\underline{F}}^T\underline{\underline{F}} - \underline{\underline{I}})/2$ describing even nonlinear deformations (Ray, 1983; Ray et al., 1985; Ray and Rahman, 1984). The potential energy can be written either in the reference frame, or in the deformed frame, $\mathring{\mathscr{U}}(\{\mathring{R}_I^\mu\}, \underline{\underline{\eta}}) \equiv \mathscr{U}(\{R_I^\mu\}, \underline{\underline{F}})$. In the second step of the process, particles perform nonaffine displacements by relaxing to their nearest equilibrium position $\{R_I^\mu\}$, while the shape of the cell, $\underline{\underline{h}}$ (and hence the tensor $\underline{\underline{F}}$), remains unchanged. Thus, in the reference frame $\{\mathring{R}_I^\mu\}$, changing $\underline{\underline{\eta}}$ means the response to affine strain of the whole system, while the change in the reference configuration $\{\mathring{R}_I^\mu\}$ corresponds to additional nonaffine displacements. Those new coordinates are generally

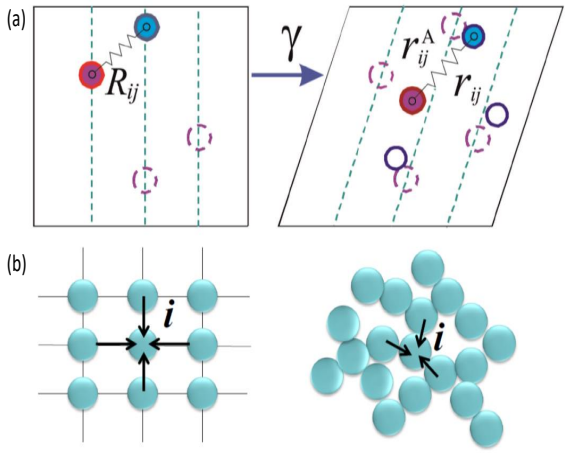

Fig. 2.2 Panel (a) shows the nonaffine displacements for two bonded atoms: if the displacements were purely affine, which is the case in a centrosymmetric crystal, the atoms would still lie in the deformed (sheared) configuration. In contrast in glasses, they are to be found away from the affine (deformed) positions. The nonaffine displacements are defined as the distance between the actual end position (away from the dashed line) and the affine position (on the dashed line). The interatomic distance at rest is indicated as R_{ij}, whereas that in affine positions is labeled as r_{ij}^{A}. The bottom cartoon, or panel (b), depicts a comparison of the force-balance in the affine position (prescribed by a strain tensor) in a centrosymmetric crystal (left) and in a glass (right). In the former case, all forces from nearest neighbours cancel by symmetry and the atom i is in mechanical equilibrium, i.e. $\mathbf{f}_i = \mathbf{0}$, no further (nonaffine) displacement is needed. In glasses, the forces do not cancel due to the lack of inversion symmetry, hence for each tagged particle, a net non-zero force remains in the affine position, which has to be relaxed through an additional displacement. For a fixed strain γ, the net force is related to affine force field $\boldsymbol{\Xi}$ as $\mathbf{f}_i = \boldsymbol{\Xi}_i \gamma$ (Zaccone, 2020).

different from the affine positions derived by the reference coordinates, $\{\mathbf{R}_I\} \neq \{\underline{\underline{F}}\mathring{\mathbf{R}}_I\}$. For small deformations, the nonaffine equilibrium positions of the particles are a continuous function of $\underline{\underline{h}}$: $\{R_I^\mu\} = \{R_I^\mu(\underline{\underline{h}})\}$.

Static elastic constant

When the linear strain is applied slow enough, the deformation can be regarded as static, and mechanical equilibrium is valid at any stage. I can expand the force acting on an individual particle I, $f_I^\mu = -\partial\mathring{\mathscr{U}}/\partial\mathring{R}_I^\mu$ (share the same meaning of force as defined before), in terms of the components of the strain tensor $\underline{\underline{\eta}}$ and $\{\mathbf{R}_I\}$ (Lemaitre and Maloney, 2006; Zaccone and Scossa-Romano, 2011):

$$\delta f_I^\mu = \sum_{J\nu} \frac{\partial^2\mathring{\mathscr{U}}}{\partial\mathring{R}_I^\mu\partial\mathring{R}_J^\nu}\delta\mathring{R}_J^\nu + \frac{\partial^2\mathring{\mathscr{U}}}{\partial R_I^\mu\partial\eta_{\xi\iota}}\delta\eta_{\xi\iota} = 0. \tag{2.35}$$

This is equivalent to the Nd linear system of equations for the nonaffine displacements $\delta\mathring{R}_I^\mu$:

$$\sum_{J\nu} H_{IJ}^{\mu\nu}\delta\mathring{R}_J^\nu = \Xi_{I,\xi\iota}^\mu\delta\eta_{\xi\iota}, \tag{2.36}$$

where the Hessian matrix $H_{IJ}^{\mu\nu}$ defined earlier and the affine force field $\Xi_{I,\xi\iota}^\mu$ is:

$$\Xi_{I,\xi\iota}^\mu = -\frac{\partial^2\mathring{\mathscr{U}}}{\partial\mathring{R}_I^\mu\partial\eta_{\xi\iota}}, \quad \text{with} \quad H_{IJ}^{\mu\nu} = \frac{\partial^2\mathring{\mathscr{U}}}{\partial\mathring{R}_I^\mu\partial\mathring{R}_J^\nu}. \tag{2.37}$$

Assuming pairwise interaction, it is easy to see the Hessian matrix is real and symmetric. Hence, it can be diagonalised as $\underline{\underline{H}} = \underline{\underline{P\Lambda P^T}}$ where $\underline{\underline{\Lambda}}$ is the diagonal matrix consisting of eigenvalues of $\underline{\underline{H}}$, and $\underline{\underline{P}}$ is the orthogonal matrix (with $\underline{\underline{PP^T}} = \underline{\underline{P}}^T\underline{\underline{P}} = \underline{\underline{I}}$) whose columns are made of corresponding normalised eigenvectors. Denoting $\delta\vec{\mathring{R}} \equiv \underline{\underline{P}}^T\delta\vec{\hat{R}}$, I have, from transforming Eq. (2.36),

$$\underline{\underline{\Lambda}}\delta\vec{\hat{R}} = \underline{\underline{P}}^T\vec{\Xi}_{\xi\iota}\delta\eta_{\xi\iota} \tag{2.38}$$

for fixed $\xi\iota$. Here, vectors originally written in d-dimensional space are transformed to Nd-vectors labeled by an arrow above the symbol. Because of translation invariance, the Hessian matrix contains d zero eigenvalues, so $\Lambda = diag\{0,...,0,\lambda_{d+1},...,\lambda_{Nd}\}$ where I assume the (increasing) order in eigenvalues without loss of generality. This means, only

$\delta\hat{R}_m, m = d+1, ..., Nd$ can be solved:

$$\begin{pmatrix} \delta\hat{R}_{d+1} \\ . \\ . \\ . \\ \delta\hat{R}_{Nd} \end{pmatrix} = \begin{pmatrix} \frac{\vec{e}_{d+1}\cdot\vec{\Xi}_{\xi\iota}}{\lambda_{d+1}} \\ . \\ . \\ . \\ \frac{\vec{e}_{Nd}\cdot\vec{\Xi}_{\xi\iota}}{\lambda_{Nd}} \end{pmatrix} \tag{2.39}$$

where $\vec{e}_m, m = 1, ..., Nd$ are orthonormal eigenvectors of the Hessian matrix. Transferring back to $\delta\mathring{R}_m$, I obtain

$$\frac{\delta\mathring{R}_m}{\delta\eta_{\xi\iota}} = \sum_{n=1}^{d} e_{nm}\delta\hat{R}_n + \sum_{n=d+1}^{Nd} \frac{(\vec{e}_n\cdot\vec{\Xi}_{\xi\iota})e_{nm}}{\lambda_n}. \tag{2.40}$$

Here, e_{nm} is the (n,m)-entry of P and $\delta\hat{R}_n, n = 1, ..., d$ are unknown. The elastic constant is defined as the second derivative of potential energy $\mathring{\mathscr{U}}$ with respect to the strain tensor per unit volume: $C_{\mu\nu\xi\iota} = (\mathscr{D}^2\mathring{\mathscr{U}}/\mathscr{D}\eta_{\mu\nu}\mathscr{D}\eta_{\xi\iota})/\mathring{V}$. The material derivative is denoted as $\mathscr{D}\mathring{\mathscr{U}}/\mathscr{D}\underline{\underline{\eta}} = \sum_{I\mu}(\partial\mathring{\mathscr{U}}/\partial\mathring{R}_I^\mu)(\partial\mathring{R}_I^\mu/\partial\underline{\underline{\eta}}) + \partial\mathring{\mathscr{U}}/\partial\underline{\underline{\eta}}$. Because of mechanical equilibrium, $f_I^\mu = 0$ for all I, μ, it is easy to have $\mathscr{D}\mathring{\mathscr{U}}/\mathscr{D}\underline{\underline{\eta}} = \partial\mathring{\mathscr{U}}/\partial\underline{\underline{\eta}}$. Then the elastic modulus is calculated as

$$\begin{aligned} C_{\mu\nu\xi\iota} &= \frac{1}{\mathring{V}}\frac{\mathscr{D}^2\mathring{\mathscr{U}}}{\mathscr{D}\eta_{\mu\nu}\mathscr{D}\eta_{\xi\iota}} = \frac{1}{\mathring{V}}\left(\frac{\partial^2\mathring{\mathscr{U}}}{\partial\eta_{\mu\nu}\partial\eta_{\xi\iota}} + \sum_{I\kappa}\frac{\partial^2\mathring{\mathscr{U}}}{\partial\mathring{R}_I^\kappa\partial\eta_{\mu\nu}}\cdot\frac{\mathscr{D}\mathring{R}_I^\kappa}{\mathscr{D}\eta_{\xi\iota}}\right) \\ &= \frac{1}{\mathring{V}}\frac{\partial^2\mathring{\mathscr{U}}}{\partial\eta_{\mu\nu}\partial\eta_{\xi\iota}} - \frac{1}{\mathring{V}}\sum_{I\kappa}\Xi_{I,\mu\nu}^\kappa\frac{\mathscr{D}\mathring{R}_I^\kappa}{\mathscr{D}\eta_{\xi\iota}} \\ &\equiv C_{\mu\nu\xi\iota}^A + C_{\mu\nu\xi\iota}^{NA}. \end{aligned} \tag{2.41}$$

The affine moduli, $C_{\mu\nu\xi\iota}^A$, is also called high-frequency moduli that an external constraint (or perturbation) is rapidly transmitted affinely to the system before the relaxational response of the system has a chance to relax fully. The isothermal elasticity tensor is derived in Tadmor and Miller (2011), which reduces to the same form as given in Lemaitre and Maloney (2006) at $T = 0K$. In experiments, the calculated affine moduli is relevant in the high-frequency limit of standard rheological measurements, e.g. shear modulus of glassy polymers in high-frequency oscillatory context (Wittmer et al., 2015; Zaccone and Terentjev, 2013). Wallace (1970) compares the bewildering different forms the affine moduli may take if different strain definitions (transformations) are used. This matters especially if external stresses are present. This is the case in virtually all soft matter systems and glasses and also in all systems with

internal and external surfaces (surface tension). These stresses contribute linearly to the experimentally relevant small-strain elasticity tensor (Birch, 1938) and drop out if the energy or free energy is differentiated insisting on a Lagrangian or Eulerian strain. Using the affine terms presented here, a shear modulus of a liquid at a finite pressure would not vanish. This can also be verified using the standard stress-fluctuation formalism (Wittmer et al., 2013). At finite pressure, the presented affine terms are not consistent with the well-known compressed modulus of a standard liquid, according to the Rowlinson relation (Allen and Tildesley, 2017).

Using Eq. (2.40), I can explicitly write the nonaffine elasticity, $C^{NA}_{\mu\nu\xi\iota}$, as

$$\begin{aligned} C^{NA}_{\mu\nu\xi\iota} &= -\frac{1}{\mathring{V}}\sum_{m=1}^{Nd}\Xi_{m,\mu\nu}\frac{\delta\mathring{R}_m}{\delta\eta_{\xi\iota}} = -\frac{1}{\mathring{V}}\sum_{m=1}^{Nd}\Xi_{m,\mu\nu}\left(\sum_{n=1}^{d}e_{nm}\delta\hat{R}_n + \sum_{n=d+1}^{Nd}e_{nm}\frac{\vec{e}_n\cdot\vec{\Xi}_{\xi\iota}}{\lambda_n}\right) \\ &= -\frac{1}{\mathring{V}}\sum_{n=1}^{d}(\vec{e}_n\cdot\vec{\Xi}_{\mu\nu})\delta\hat{R}_n - \frac{1}{\mathring{V}}\sum_{n=d+1}^{Nd}\frac{(\vec{e}_n\cdot\vec{\Xi}_{\mu\nu})(\vec{e}_n\cdot\vec{\Xi}_{\xi\iota})}{\lambda_n} \end{aligned} \tag{2.42}$$

As for the inner product in the 1st term on the RHS, since the corresponding eigenvalues of eigenvectors $\vec{e}_n, n = 1,...,d$, are all zero, forms of eigenvectors are $e_{nm} = 1/\sqrt{N}$ if m is a multiply of n and $e_{nm} = 0$ otherwise, for $n = 1,...,Nd$. Therefore, $\vec{e}_n\cdot\vec{\Xi}_{\mu\nu} \propto \sum_I \Xi^n_{I,\mu\nu}$. In this thesis, I only consider pairwise interaction in harmonic approximation, so the affine force field $\Xi^\kappa_{I,\mu\nu}$ can be expressed as follows (Lemaitre and Maloney, 2006)

$$\begin{aligned} \Xi^\kappa_{I,\mu\nu} &= -\sum_J \frac{\partial^2\mathring{\mathscr{U}}}{\partial\mathring{R}^\kappa_{IJ}\partial\mathring{R}^\kappa_{IJ}}\frac{\partial\mathring{R}^\kappa_{IJ}}{\partial\eta_{\mu\nu}} = -\sum_J\left[(\mathring{R}_{IJ}s_{IJ}-t_{IJ})n^\kappa_{IJ}n^\mu_{IJ}n^\nu_{IJ} + \frac{1}{2}t_{IJ}(\delta_{\kappa\mu}n^\nu_{IJ}+\delta_{\kappa\nu}n^\mu_{IJ})\right] \\ &= -\sum_J(\mathring{R}_{IJ}s_{IJ}-t_{IJ})n^\kappa_{IJ}n^\mu_{IJ}n^\nu_{IJ}, \end{aligned} \tag{2.43}$$

with the orientation unit vector n^μ, tension of a bond t_{IJ} and stiffness of the bond s_{IJ} defined as

$$n^\mu_{IJ} = \frac{\mathring{R}^\mu_{IJ}}{\mathring{R}_{IJ}}, \quad t_{IJ} = \frac{\partial\mathring{\mathscr{U}}}{\partial\mathring{R}_{IJ}}, \quad s_{IJ} = \frac{\partial^2\mathscr{U}}{\partial\mathring{R}^2_{IJ}}. \tag{2.44}$$

Here, by $\mathring{R}^\mu_{IJ}$, I mean $\mathring{R}^\mu_{IJ} = \mathring{R}^\mu_J - \mathring{R}^\mu_I$. To get the 2nd equality in Eq. (2.43), I used the identity $\partial\mathring{R}^\kappa_{IJ}/\partial\eta_{\mu\nu} = (\delta_{\kappa\mu}\mathring{R}^\nu_{IJ} + \delta_{\kappa\nu}\mathring{R}^\mu_{IJ})$. The 2nd term in square bracket vanishes because of the

mechanical equilibrium condition. Likewise, the Hessian matrix is expressed as:

$$H_{IJ}^{\mu\nu} = \begin{cases} -(s_{IJ} - \frac{t_{IJ}}{R_{IJ}}) n_{IJ}^{\mu} n_{IJ}^{\nu} - \frac{t_{IJ}}{R_{IJ}} \delta_{\mu\nu}, & I \neq J \\ \sum_{K \neq I} (s_{IK} - \frac{t_{IK}}{R_{IK}}) n_{IK}^{\mu} n_{IK}^{\nu} + \frac{t_{IK}}{R_{IK}} \delta_{\mu\nu}, & I = J. \end{cases} \tag{2.45}$$

Now it is clear that the first term in Eq. (2.42) vanishes due to the inversion symmetry of $\mathbf{n}_{IJ}$, i.e. $\mathbf{n}_{IJ} = -\mathbf{n}_{JI}$. Thus, the remaining (negative) nonaffine elastic constant can be written as

$$C_{\mu\nu\xi\iota}^{NA} = -\frac{1}{\mathring{V}} \sum_{n=d+1}^{Nd} \frac{(\vec{e}_n \cdot \vec{\Xi}_{\mu\nu})(\vec{e}_n \cdot \vec{\Xi}_{\xi\iota})}{\lambda_n} < 0 \tag{2.46}$$

where contributions from zero eigenvalues are excluded in the summation. Although this derivation and argument are different from original LM's formalism, the final result, Eq. (2.46), reproduces the key LM result.

Accounting for the thermal effect, the Strasbourrg theory shows this affine moduli corrected by nonaffine contribution may be obtained more generally, by averaging different ensembles (Wittmer et al., 2015, 2013). One can use the integral by parts to reduce the fluctuation of an intensive variable in an ensemble where the average intensive variable is imposed, to a simple average. Imposing a vanishing or finite average intensive variable, one may switch off or on Birch coefficients. Then using the Lebowitz-Percus-Verlet (LPV) transformation between different conjugated ensembles, one can see the complete modulus is given by the affine modulus minus a correction term. As is already shown in Lutsko (1988), the argument holds in the zero-temperature limit.

Viscoelastic modulus

I rewrite the Eq. (2.34) for a tagged atom in d dimension, which moves with an affine velocity prescribed by the deformation gradient tensor $\underline{\underline{\dot{F}}}$:

$$\ddot{R}_I^{\mu} = f_I^{\mu} - \int_{-\infty}^{t} \nu(t-t') \left(\dot{R}_I^{\mu} - u^{\mu} \right) dt' \tag{2.47}$$

where $f_I^{\mu} = -\partial \mathscr{U} / \partial R_I^{\mu}$ generalises the $-\mathscr{U}'(s)$ to the tagged atom. Furthermore, I used the Galilean transformations to express the particle velocity in the moving frame: $\dot{\mathbf{R}}_I = \underline{\underline{F}} \dot{\mathring{\mathbf{R}}}_I + \mathbf{u}$ where $\mathbf{u} = \underline{\underline{\dot{F}}} \mathring{\mathbf{R}}_I$ represents the local velocity of the moving frame. This is consistent with the use of the circle on the variables to signify that they are measured with respect to the reference rest frame. In terms of the original rest frame $\{\mathring{\mathbf{R}}_I\}$, the equation of motion can be

written as

$$\underline{\underline{F}}\ddot{\mathring{\mathbf{R}}}_I = \mathbf{f}_I - \int_{-\infty}^{t} \nu(t-t') \cdot \frac{\underline{\underline{F}} d\mathring{\mathbf{R}}_I}{dt'} dt' - 2\dot{\underline{\underline{F}}} \frac{d\mathring{\mathbf{R}}_I}{dt}. \tag{2.48}$$

Terms $\ddot{\underline{\underline{F}}}\mathring{\mathbf{R}}_I$ and $\int_{-\infty}^{t} \nu(t-t')\dot{\underline{\underline{F}}} \cdot \mathring{\mathbf{R}}_I dt'$ are not allowed into the equation of motion because they depend on the position of the particle, and therefore have to vanish for a system with translation invariance, already noted by Andersen (1980) and by Ray and Rahman (1984).

I work in the linear regime of small strain $\| \underline{\underline{F}} - \underline{\underline{1}} \| \ll 1$ by making a perturbative expansion in terms of the small displacement $\{\mathbf{s}_I(t) = \mathring{\mathbf{R}}_I(t) - \mathring{\mathbf{R}}_I\}$ around a known rest frame $\mathring{\mathbf{R}}_I$. That is, I take $\underline{\underline{F}} = \underline{\underline{1}} + \delta\underline{\underline{F}} + ...$ where $\delta\underline{\underline{F}} \approx \underline{\underline{F}} - \underline{\underline{1}}$ is the small parameter. For the term $\delta\mathbf{f}_I$, considering mechanical equilibrium again, which is $\mathbf{f}_I = 0$. I can write Eq. (2.48) in linear order:

$$\frac{d^2\mathbf{s}_I}{dt^2} + \int_{-\infty}^{t} \nu(t-t') \frac{d\mathbf{s}_I}{dt'} dt' + \underline{\underline{H}}_{IJ}\mathbf{s}_J = \mathbf{\Xi}_{I,\kappa\chi}\eta_{\kappa\chi}, \tag{2.49}$$

which can be solved by performing the Fourier transformation followed by taking the normal mode decomposition. If I specialise on time-dependent uniaxial strain $\eta_{xx}(t)$, the vector $\mathbf{\Xi}_{I,xx}$ represents the force per unit strain acting on particle I due to the motion of its nearest-neighbors which are moving towards their respective affine positions (see e.g. Lemaitre and Maloney (2006) for a more detailed discussion). In metallic glasses, it also includes electronic effects empirically via the embedded-atom model (EAM) (see Appendix A for explicit formulas).

Now I extend all matrices and vectors to be $Nd \times Nd$ and Nd-dimensional, respectively. After taking the Fourier transformation of Eq. (2.49), I have

$$-\omega^2\vec{\tilde{s}} + i\tilde{\nu}(\omega)\omega\vec{\tilde{s}} + \underline{\underline{H}}\vec{\tilde{s}} = \vec{\Xi}_{\kappa\chi}\tilde{\eta}_{\kappa\chi}. \tag{2.50}$$

where $\tilde{\nu}(\omega)$ is the Fourier transform of $\nu(t)$. Next, I take the normal mode decomposition. This is equivalent to diagonalising the Hessian matrix $\underline{\underline{H}}$. Same as the static case, I have, the m-th mode of displacement written as:

$$-\omega^2\hat{\tilde{s}}_m(\omega) + i\tilde{\nu}(\omega)\omega\hat{\tilde{s}}_m(\omega) + \omega_m^2\hat{\tilde{s}}_m(\omega) = \hat{\Xi}_{m,\kappa\chi}(\omega)\tilde{\eta}_{\kappa\chi}, \tag{2.51}$$

It was shown in previous work of Lemaitre and Maloney (2006) that $\hat{\Xi}_{m,\kappa\chi} = \vec{e}_m \cdot \vec{\Xi}_{\kappa\chi}$ is self-averaging, and one might introduce the smooth correlator function $\Gamma_{\mu\nu\kappa\chi}(\omega) = \langle \hat{\Xi}_{m,\mu\nu}\hat{\Xi}_{m,\kappa\chi} \rangle_{\omega_m \in \{\omega, \omega+\delta\omega\}}$ on frequency shells. Following the general procedure of Lemaitre and Maloney (2006) to find the oscillatory stress for a dynamic nonaffine deformation, the

stress is obtained to first order in strain amplitude as a function of ω:

$$\begin{aligned}\tilde{\sigma}_{\mu\nu}(\omega) &= \sum_{\kappa\chi} C^{A}_{\mu\nu\kappa\chi}\tilde{\eta}_{\kappa\chi}(\omega) - \frac{1}{\mathring{V}}\sum_{m\kappa\chi}\hat{\Xi}_{m,\mu\nu}\hat{\tilde{s}}_{m}(\omega) \\ &= \sum_{\kappa\chi} C^{A}_{\mu\nu\kappa\chi}\tilde{\eta}_{\kappa\chi}(\omega) + \frac{1}{\mathring{V}}\sum_{m\kappa\chi}\frac{\hat{\Xi}_{m,\mu\nu}\hat{\Xi}_{m,\kappa\chi}}{\omega^2-\omega_m^2-i\tilde{\nu}(\omega)\omega}\tilde{\eta}_{\kappa\chi}(\omega) \\ &\equiv \sum_{\kappa\chi} C_{\mu\nu\kappa\chi}(\omega)\tilde{\eta}_{\kappa\chi}(\omega). \end{aligned} \tag{2.52}$$

In the thermodynamic limit with continuous spectrum, I replace the discrete sum over Nd degrees of freedom in Eq. (2.52) with an integral over vibrational frequencies up to the Debye (cut-off) frequency ω_D, and the complex elastic constant defined on the last line can be written as:

$$C(\omega)_{\mu\nu\kappa\chi} = C^{A}_{\mu\nu\kappa\chi} - \rho d\int_0^{\omega_D}\frac{D(\omega_p)\Gamma(\omega_p)_{\mu\nu\kappa\chi}}{\omega_p^2-\omega^2+i\tilde{\nu}(\omega)\omega}d\omega_p, \tag{2.53}$$

where $\rho = N/\mathring{V}$ denotes the atomic density of the solid. This is a crucial result, which differs from a previous result obtained in Lemaitre and Maloney (2006) because the friction coefficient is non-Markovian, hence frequency-dependent, whereas in Lemaitre and Maloney (2006) it is just a constant, corresponding to Markovian dynamics. This turns out to be a fundamental difference, because as I will show later, SGs data cannot be described by a friction coefficient which is constant with frequency. Furthermore, this result is derived from a microscopic (ZCL) Hamiltonian.

In the numerical simulations, the VDOS is actually not a continuous function, but discrete. Thus, in Eq. (2.53) I replace the VDOS with its spectral representation given by a sum of delta-functions and rewrite $C(\omega)$ as a sum over a discrete distribution of ω_m from the molecular dynamics (MD) simulation of VDOS, $C(\omega) = C'(\omega) + iC''(\omega)$:

$$C'(\omega) = C^{A} - A\sum_m \frac{\Gamma(\omega_m)(\omega_m^2-\omega^2+\tilde{\nu}_2\omega)}{(\omega_m^2-\omega^2+\tilde{\nu}_2\omega)^2+(\omega\tilde{\nu}_1)^2} \tag{2.54}$$

$$C''(\omega) = B\sum_m \frac{\Gamma(\omega_m)(\omega\tilde{\nu}_1)}{(\omega_m^2-\omega^2+\tilde{\nu}_2\omega)^2+(\omega\tilde{\nu}_1)^2} \tag{2.55}$$

where C^A, A, and B are rescaling constants; $\tilde{\nu}_1$ and $\tilde{\nu}_2$ are the real and (minus) imaginary parts of $\tilde{\nu}(\omega)$, respectively. I have dropped Cartesian indices.

Apart from ZCL Hamiltonian, the Nose-Hoover method developed by Hoover (1985) also provides a route towards estimating the time-dependent non-Markovian friction. It has been verified by my colleagues (Jie Yang et al.) that, after carrying out numerical simulations for

the model system below T_g, one obtains a simple-exponential decay of the friction coefficient, with which, however, one cannot reproduce the experimentally-measured curves of C' and C'', over any interval in frequency. This problem might be due to the limitations of using the Nose-Hoover method for nonequilibrium systems (Cui et al., 2017b).

2.5 The Born-Huang method to obtain static elasticity

This section and the following one reproduce the BH analysis (Born and Huang, 1954). In non-ionic crystals, only the short-range pairwise interaction is considered. The long-range Coulombic effect which usually causes divergence will be ignored here, although there exist ways to tackle the issue of divergence (see Chapter 4 for details). In continuum media, the deformation in a small neighborhood of $\mathbf{R}^\circ$ can be expressed as:

$$s^\mu(\mathbf{R}^\circ+\delta\mathbf{R}) = s^\mu(\mathbf{R}^\circ)+\sum_\nu \frac{\partial s^\mu}{\partial R^\nu}\delta R^\nu \tag{2.56}$$

The first term on the RHS represents the translation of the small region as a whole, while the last term is the elastic deformation. Making analogue to a lattice, since particle (atom) I lies in cell l has displacement $s_I^\mu(l)$, Eq. (2.56) is equivalent to

$$s_I^\mu(l) = s_I^\mu+\sum_\nu \frac{\partial s^\mu}{\partial R^\nu}R_I^\nu(l) \tag{2.57}$$

where s_I^μ is the nonaffine displacement all particles of each type has in response to elastic deformation. From this, setting $l=0$ as the reference cell, I have $s_J^\mu(l')-s_I^\mu(0) = s_J^\mu - s_I^\mu+\sum_\nu(\partial s^\mu/\partial R^\nu)R_{JI}^\nu(l')$. In this section, by $R_{JI}^\nu(l')$, I mean the relative displacement $R_J^\nu(l')-R_I^\nu(0)$. To make it convenient for calculation, I assume the potential depends on the square of interparticle distance, $\mathscr{U}(\mathbf{R}_I(l),\mathbf{R}_J(l')) = \mathscr{U}(|\mathbf{R}_I(l)-\mathbf{R}_J(l')|^2)$. The total energy is $\mathscr{U} = \sum_{IJll'}\mathscr{U}(\mathbf{R}_I(l),\mathbf{R}_J(l'))/2$. In the BH method, there is no internal tension and the temperature is zero, so that the system will stay in mechanical equilibrium. Due to the deformation, the change of square of separation between $\mathbf{R}_J(l')$ and $\mathbf{R}_I(0)$ is

$$\begin{aligned}|\mathbf{R}_J(l')+\mathbf{s}_J(l')-\mathbf{R}_I(0)-\mathbf{s}_I(0)|^2-|\mathbf{R}_J(l')-\mathbf{R}_I(0)|^2 &= \sum_\mu\left(s_J^\mu-s_I^\mu+\sum_\nu s_{\mu\nu}R_{JI}^\nu(l')\right)^2\\ +2\sum_\mu R_{JI}^\mu(l')\left(s_J^\mu-s_I^\mu+\sum_\nu s_{\mu\nu}R_{JI}^\nu(l')\right).&\end{aligned} \tag{2.58}$$

The corresponding change in $\mathscr{U}(\mathbf{R}_I(0),\mathbf{R}_J(l'))$ is the difference of $\mathscr{U}$ with arguments in (2.58) and the original $\mathscr{U}(\mathbf{R}_I(0),\mathbf{R}_J(l'))$. Then, up to the 2nd order, this change is:

$$\mathscr{U}'(|\mathbf{R}_{JI}(l')|^2)\left[\sum_\mu\left(s_J^\mu-s_I^\mu+\sum_\nu s_{\mu\nu}R_{JI}^\nu(l')\right)^2+2\sum_\mu R_{JI}^\mu(l')\left(s_J^\mu-s_I^\mu+\sum_\nu s_{\mu\nu}R_{JI}^\nu(l')\right)\right]$$
$$+2\mathscr{U}''(|\mathbf{R}_{JI}(l')|^2)\left[\sum_\mu R_{JI}^\mu(l')\left(s_J^\mu-s_I^\mu+\sum_\nu s_{\mu\nu}R_{JI}^\nu(l')\right)\right]^2 \tag{2.59}$$

Summing these increments of pairwise energy over the unit cell, I have:

$$Uv_a=-2\sum_{I\mu}\left(s_I^\mu+\sum_\nu s_I^\nu s_{\nu\mu}\right)\sum_{l'J}[\mathscr{U}'R^\mu]_{\mathbf{R}_{JI}(l')}+\sum_{\mu\nu}\left(s_{\mu\nu}+\frac{1}{2}\sum_\xi s_{\xi\mu}s_{\xi\nu}\right)\sum_{l'IJ}[\mathscr{U}'R^\mu R^\nu]_{\mathbf{R}_{JI}(l')}$$
$$+\sum_{IJ\mu\nu}s_I^\mu s_J^\nu\times\left(\delta_{JI}\delta_{\mu\nu}\sum_{l'K}[\mathscr{U}']_{\mathbf{R}_{KI}(l')}-\delta_{\mu\nu}\sum_{l'}[\mathscr{U}']_{\mathbf{R}_{IJ}(l')}+2\delta_{IJ}\sum_{l'K}[\mathscr{U}''R^\mu R^\nu]_{\mathbf{R}_{KI}(l')}\right.$$
$$\left.-2\sum_{l'}[\mathscr{U}''R^\mu R^\nu]_{\mathbf{R}_{JI}(l')}\right)-4\sum_{I\mu\nu\xi}s_I^\mu s_{\nu\xi}\sum_{l'J}[\mathscr{U}''R^\mu R^\nu R^\xi]_{\mathbf{R}_{JI}(l')}+\sum_{\mu\nu\xi\iota}s_{\mu\xi}s_{\nu\iota}\sum_{l'JI}[\mathscr{U}''R^\mu R^\nu R^\xi R^\iota]_{\mathbf{R}_{JI}(l')}, \tag{2.60}$$

where v_a is the volume of the unit cell and U is the energy density. This calculation is reproducing the BH analysis. Equilibrium conditions require terms linear in s_I^μ and $s_{\mu\nu}$ to vanish, which gives

$$\sum_{l'J}[\mathscr{U}'R^\mu]_{\mathbf{R}_{JI}(l')}=0;\quad\sum_{l'JI}[\mathscr{U}'R^\mu R^\nu]_{\mathbf{R}_{JI}(l')}=0 \tag{2.61}$$

Eliminating these linear terms, U is rewritten as

$$U = \frac{1}{2}\sum_{IJ\mu\nu}\begin{Bmatrix} I & J \\ \mu & \nu \end{Bmatrix} s_I^\mu s_J^\nu + \sum_{I\mu\nu\xi}\begin{Bmatrix} I & \nu\xi \\ \mu & \end{Bmatrix} s_I^\mu \frac{\partial s^\nu}{\partial R^\xi} + \frac{1}{2}\sum_{\mu\nu\xi\iota}\{\mu\nu\xi\iota\}\frac{\partial s^\mu}{\partial R^\nu}\frac{\partial s^\xi}{\partial R^\iota}, \quad \text{where}$$

$$\begin{Bmatrix} I & J \\ \mu & \nu \end{Bmatrix} = \frac{2}{v_a}\Bigg\{\delta_{IJ}\delta_{\mu\nu}\sum_{l'K}[\mathscr{U}']_{\mathbf{R}_{KI}(l')} - \delta_{\mu\nu}\sum_{l'}[\mathscr{U}']_{\mathbf{R}_{JI}(l')} + 2\delta_{IJ}\sum_{l'K}[\mathscr{U}''R^\mu R^\nu]_{\mathbf{R}_{KI}(l')}$$
$$-2\sum_{l'}[\mathscr{U}''R^\mu R^\nu]_{\mathbf{R}_{JI}(l')}\Bigg\};$$

$$\begin{Bmatrix} I & \nu\xi \\ \mu & \end{Bmatrix} = -\frac{4}{v_a}\sum_{l'J}[\mathscr{U}''R^\mu R^\nu R^\xi]_{\mathbf{R}_{JI}(l')};$$

$$\{\mu\nu\xi\iota\} = \frac{2}{v_a}\sum_{l'JI}[\mathscr{U}''R^\mu R^\nu R^\xi R^\iota]_{\mathbf{R}_{JI}(l')}. \tag{2.62}$$

Denoting the symmetric (external) strain $\underline{\underline{\eta}}$ by

$$\eta_{\mu\nu} = \eta_{\nu\mu} = \frac{1}{2}\left(\frac{\partial s^\mu}{\partial R^\nu} + \frac{\partial s^\nu}{\partial R^\mu}\right), \tag{2.63}$$

the energy density U is rewritten as

$$U = \frac{1}{2}\sum_{IJ\mu\nu}\begin{Bmatrix} I & J \\ \mu & \nu \end{Bmatrix} s_I^\mu s_J^\nu + \sum_{I\mu\nu\xi}\begin{Bmatrix} I & \nu\xi \\ \mu & \end{Bmatrix} s_I^\mu \eta_{\nu\xi} + \frac{1}{2}\sum_{\mu\nu\xi\iota}\{\mu\nu\xi\iota\}\eta_{\mu\nu}\eta_{\xi\iota} \tag{2.64}$$

Note that the symmetric strain $\underline{\underline{\eta}}$ defined here is the linear version of the general Cauchy-Green strain tensor defined in Section 2.4. Thus, I use the same convention. Physically, the internal nonaffine displacements s_I^μ adjust themselves such that the energy density becomes minimum, for the given external elastic strain components $\eta_{\mu\nu}$. That is,

$$0 = \frac{\partial U}{\partial s_I^\mu} = \sum_{J\nu}\begin{Bmatrix} I & J \\ \mu & \nu \end{Bmatrix} s_J^\nu + \sum_{\nu\xi}\begin{Bmatrix} I & \nu\xi \\ \mu & \end{Bmatrix}\eta_{\nu\xi}, \tag{2.65}$$

which gives $(N-1)d$ independent equations. The solutions $s_I^\mu(\underline{\underline{\eta}})$ of these mechanical equilibrium conditions are, in fact, the nonaffine displacements. Because of the free translation, without loss of generality, I can let $\mathbf{s}_1 = \mathbf{0}$. When the internal displacements are eliminated as independent variables, the energy density becomes a quadratic expression in $\underline{\underline{\eta}}$, whose coefficients matrix, $\{\mu\nu\xi\iota\}$, will receive a correction after solving for $\mathbf{s}_I$, which I denote as $\{\mu\nu\xi\iota\}'$. The detailed analysis of the resultant correction to elastic constant will be shown

in Section 4.3. Since the stress tensor is defined as

$$\sigma_{\mu\nu} = \sum_{\xi\iota} C_{\mu\nu\xi\iota}\eta_{\xi\iota} \equiv \sum_{\xi\iota} \{\mu\nu\xi\iota\}'\eta_{\xi\iota}, \tag{2.66}$$

which represents the μ-component of the force exerted on the medium which is on the negative of a unit surface normal to the ν-direction, its divergence is the local force per unit volume. The local equation of motion is then expressed as,

$$\rho\ddot{s}^{\mu} = \sum_{\nu\xi} \frac{\partial\sigma_{\mu\nu}}{\partial R^{\xi}} = \sum_{\nu\xi\iota} C_{\mu\nu\xi\iota} \frac{\partial^2 s^{\nu}}{\partial R^{\xi}\partial R^{\iota}}, \tag{2.67}$$

where ρ is the density. To solve this, I express the elastic wave with an amplitude vector $e^{\mu}(\mathbf{q})$:

$$s^{\mu}(\mathbf{R},t) = e^{\mu}(\mathbf{q})e^{i\mathbf{q}\cdot\mathbf{R}-i\omega t} \quad \Rightarrow \quad \rho\omega^2 e^{\mu}(\mathbf{q}) = \sum_{\nu}\left(\sum_{\xi\iota} C_{\mu\nu\xi\iota}q^{\xi}q^{\iota}\right)e^{\nu}(\mathbf{q}). \tag{2.68}$$

This is the equation for the (global) elastic waves in solids.

2.6 Long-range acoustic waves from collective modes

Firstly I recall collective modes derived in Section 2.1, the equation due to lattice vibration is

$$\begin{aligned} &\omega^2(\mathbf{q},m)e_I^{\mu}(\mathbf{q},m) = \sum_{J\nu} D_{IJ}^{\mu\nu}(\mathbf{q})e_J^{\nu}(\mathbf{q},m), m = 1,2,...,Nd, \\ \text{with} \quad &D_{IJ}^{\mu\nu}(\mathbf{q}) = \frac{1}{(M_I M_J)^{1/2}}\sum_{l'} H_{IJ}^{\mu\nu} e^{i\mathbf{q}\cdot\mathbf{R}_{JI}(l'-l)}. \end{aligned} \tag{2.69}$$

I consider the perturbation in the wavevector from $q = 0$ along one of acoustic branches. Using a small number ε to track the order of magnitude of small vector $\mathbf{q}$, I have:

$$D_{IJ}^{\mu\nu}(\varepsilon\mathbf{q}) = [D_{IJ}^{\mu\nu}]^{(0)} + i\varepsilon\sum_{\xi}[D_{IJ}^{\mu\nu,\xi}]^{(1)}q^{\xi} + \frac{\varepsilon^2}{2}\sum_{\xi\iota}[D_{IJ}^{\mu\nu,\xi\iota}]^{(2)}q^{\xi}q^{\iota} + ...; \tag{2.70}$$

$$\omega(\varepsilon\mathbf{q},m) = \varepsilon\omega^{(1)}(\mathbf{0},m) + \frac{\varepsilon^2}{2}\omega^{(2)}(\mathbf{0},m) + ...; \tag{2.71}$$

$$e_I^{\mu}(\varepsilon\mathbf{q},m) = [e_I^{\mu}(\mathbf{0},m)]^{(0)} + i\varepsilon e_I^{\mu}(\mathbf{0},m)]^{(1)} + \frac{\varepsilon^2}{2}[e_I^{\mu}(\mathbf{0},m)]^{(2)} + ... \tag{2.72}$$

Note that I use ε to highlight that the perturbation means the expansion in terms of a small amplitude of $\mathbf{q}$. The perturbation on $D_{IJ}^{\mu\nu}(\varepsilon\mathbf{q})$ reads:

$$[D_{IJ}^{\mu\nu}]^{(0)} = \frac{1}{\sqrt{M_I M_J}} \sum_l H_{IJ}^{\mu\nu}(l) = [D_{JI}^{\nu\mu}]^{(0)}; \tag{2.73}$$

$$[D_{IJ}^{\mu\nu,\xi}]^{(1)} = \frac{-1}{\sqrt{M_I M_J}} \sum_l H_{IJ}^{\mu\nu}(l) R_{IJ}^{\xi}(l) = -[D_{JI}^{\nu\mu,\xi}]^{(1)}; \tag{2.74}$$

$$[D_{IJ}^{\mu\nu,\xi\iota}]^{(2)} = \frac{-1}{\sqrt{M_I M_J}} \sum_l H_{IJ}^{\mu\nu}(l) R_{IJ}^{\xi}(l) R_{IJ}^{\iota}(l) = [D_{JI}^{\nu\mu,\xi\iota}]^{(2)} = [D_{JI}^{\mu\nu,\iota\xi}]^{(2)}. \tag{2.75}$$

Using Eqs. (2.6, 2.7, 2.8, 2.11), it can be verified that the following properties hold:

$$\sum_J \sqrt{M_J}[D_{IJ}^{\mu\nu}]^{(0)} = \sum_J \sqrt{M_J}[D_{JI}^{\nu\mu}]^{(0)} = 0; \tag{2.76}$$

$$\sum_J \sqrt{M_J}[D_{IJ}^{\mu\nu,\xi}]^{(1)} = \sum_J \sqrt{M_J}[D_{IJ}^{\mu\xi,\nu}]^{(1)}; \tag{2.77}$$

$$\sum_{IJ} \sqrt{M_I M_J}[D_{IJ}^{\mu\nu,\xi}]^{(1)} = 0. \tag{2.78}$$

Substituting Eqs. (2.70,2.71,2.72) into Eq. (2.69), for each order in ε, I have

$$\varepsilon^0 : 0 = \sum_{J\nu} [D_{IJ}^{\mu\nu}]^{(0)} [e_J^{\nu}(\mathbf{0},m)]^{(0)}; \tag{2.79}$$

$$\varepsilon^1 : 0 = \sum_{J\nu\xi} [D_{IJ}^{\mu\nu,\xi}]^{(1)} q^{\xi} [e_J^{\nu}(\mathbf{0},m)]^{(0)} + \sum_{J\nu} [D_{IJ}^{\mu\nu}]^{(0)} [e_J^{\nu}(\mathbf{0},m)]^{(1)}; \tag{2.80}$$

$$\begin{aligned}\varepsilon^2 : [\omega^{(1)}(\mathbf{0},m)]^2 [e_I^{\mu}(\mathbf{0},m)]^{(0)} &= \frac{1}{2} \sum_{J\nu\xi\iota} [D_{IJ}^{\mu\nu\xi\iota}]^{(2)} q^{\xi} q^{\iota} [e_J^{\nu}(\mathbf{0},m)]^{(0)} \\ &- \sum_{J\nu\xi} [D_{IJ}^{\mu\nu,\xi}]^{(1)} q^{\xi} [e_J^{\nu}(\mathbf{0},m)]^{(1)} + \frac{1}{2} \sum_{J\nu} [D_{IJ}^{\mu\nu}]^{(0)} [e_J^{\nu}(\mathbf{0},m)]^{(2)}.\end{aligned} \tag{2.81}$$

The LHS in equations of ε^0 and ε^1 are set to zero because the acoustic mode vanishes at zero frequency. For the 0th order, the solution is obvious because of the specific symmetry properties of matrix $D_{IJ}^{\mu\nu}$, i.e. Eq. (2.73). Then, I have $[e_I^{\mu}(\mathbf{0},m)]^{(0)} = \sqrt{M_I} u^{\mu}(m)$ for arbitrary $u^{\mu}(m)$. The linear order equation of ε^1 can be written as

$$\sum_{J\nu} [D_{IJ}^{\mu\nu}]^{(0)} [e_J^{\nu}(\mathbf{0},m)]^{(1)} = -\sum_{J\nu\xi} [D_{IJ}^{\mu\nu,\xi}]^{(1)} q^{\xi} [e_J^{\nu}(\mathbf{0},m)]^{(0)}. \tag{2.82}$$

Also using these properties, the LHS vanishes by multiplying $\sum_I \sqrt{M_I}$ on both sides, which reduces to $(N-1)d$ independent equations for unknown $[e_J^{\nu}(\mathbf{0},m)]^{(0)}$. In this case, the

symmetric matrix $[D_{IJ}^{\mu\nu}]^{(0)}$ is $(N-1)d \times (N-1)d$ and its inverse $\Gamma_{IJ}^{\mu\nu}$ is also symmetric. Without loss of generality, I can let $[e_0^{\mu}(\mathbf{0},m)] = 0, \mu = 1,...,d$ and extend $\Gamma_{IJ}^{\mu\nu}, I,J \neq 0$ to $Nd \times Nd$ by letting $\Gamma_{IJ}^{\mu\nu} = 0$ if I or $J = 0$. Then,

$$\begin{aligned}[e_K^{\mu}(\mathbf{0},m)]^{(1)} &= -\sum_{I=1}^{N-1}\sum_{\alpha}\Gamma_{KI}^{\mu\alpha}\sum_{J=0}^{N-1}\sum_{\nu\xi}\sqrt{M_J}[D_{IJ}^{\alpha\nu,\xi}]^{(1)}q^{\xi}u^{\nu}(m) \\ &= -\sum_{I\alpha}\Gamma_{KI}^{\mu\alpha}\sum_{J\nu\xi}\sqrt{M_I}[D_{IJ}^{\alpha\nu,\xi}]^{(1)}q^{\xi}u^{\nu}(m). \end{aligned} \tag{2.83}$$

Given solutions of the 0th and the 1st order, the 2nd order in ε^2 can be written as:

$$\begin{aligned}&\frac{1}{2}\sum_{J\nu}[D_{IJ}^{\mu\nu}]^{(0)}[e_J^{\nu}(\mathbf{0},m)]^{(2)} = [\omega^{(1)}(\mathbf{0},m)]^2\sqrt{M_I}u^{\mu}(m) - \frac{1}{2}\sum_{J\nu\xi\iota}\sqrt{M_J}[D_{IJ}^{\mu\nu,\xi\iota}]^{(2)}q^{\xi}q^{\iota}u^{\nu}(m) \\ &-\sum_{J\alpha\xi}[D_{IJ}^{\mu\nu,\xi}]^{(1)}q^{\xi}\sum_{K\beta}\Gamma_{JK}^{\nu\beta}\sum_{L\xi\iota}[D_{KL}^{\beta\xi,\iota}]^{(1)}\sqrt{M_L}q^{\iota}u^{\xi}(m). \end{aligned} \tag{2.84}$$

I can still use the properties of the matrix $D_{IJ}^{\mu\nu}$ as before, so that after multiplying $\sum_I \sqrt{M_I}$ on both sides, the LHS vanishes. After this operation, I am left with (divided by the volume of unit cell v_a):

$$\left(\frac{\sum_I M_I}{v_a}\right)[\omega^{(1)}(\mathbf{0},m)]^2u^{\mu}(m) = \sum_{\nu}\left\{\sum_{\xi\iota}[\mu\nu,\xi\iota]q^{\xi}q^{\iota} + \sum_{\xi\iota}(\mu\xi,\nu\iota)q^{\xi}q^{\iota}\right\}u^{\nu}(m), \tag{2.85}$$

where the matrix coefficients in the RHS are

$$\begin{aligned}&[\mu\nu,\xi\iota] = \frac{1}{2v_a}\sum_{IJ}\sqrt{M_IM_J}[D_{IJ}^{\mu\nu,\xi\iota}]^{(2)} = [\nu\mu,\xi\iota] = [\mu\nu,\iota\xi]; \\ &(\mu\xi,\nu\iota) = \frac{-1}{v_a}\sum_{IJ\alpha\beta}\Gamma_{IJ}^{\alpha\beta}\left(\sum_K[D_{IK}^{\alpha\mu,\xi}]^{(1)}\sqrt{M_K}\right)\left(\sum_L[D_{JL}^{\beta\nu,\iota}]^{(1)}\sqrt{M_L}\right) = (\xi\mu,\nu\iota) = (\nu\iota,\xi\mu). \end{aligned} \tag{2.86}$$

Comparing Eqs. (2.68) and (2.85), I obtain the relations defining the matrix elements of the elastic coefficients:

$$\begin{aligned}&\sum_{\xi\iota}C_{\mu\nu\xi\iota}q^{\xi}q^{\iota} = \sum_{\xi\iota}\{[\mu\nu,\xi\iota] + (\mu\xi,\nu\iota)\}q^{\xi}q^{\iota} \\ \Rightarrow\quad &C_{\mu\nu\xi\iota} + C_{\mu\nu\iota\xi} = 2[\mu\nu,\xi\iota] + (\mu\xi,\nu\iota) + (\mu\iota,\nu\xi) \end{aligned} \tag{2.87}$$

Equation (2.87) connects the dynamical matrix and the elastic constants. In other words, Eq. (2.87) obtained in BH framework, provides two paths to elastic constants: lattice vibrations (RHS) or stress-strain relation (LHS). As will be shown later, the result would be exactly the same as that of the LM formalism. However, the formula of $C_{\mu\nu\xi\iota}$ is not derived in BH framework. Thus, the way to write down full elastic constant from LHS is not feasible until I report my findings in Section 4.1.

2.7 The Green's functions

The notation of the Green's function is very useful to solve ordinary differential equations. Given the equation

$$\hat{L}(\mathbf{r})f(\mathbf{r}) = g(\mathbf{r}) \tag{2.88}$$

for some unknown function f, where $\hat{L}$ is a time independent, linear, Hermitian operator and the source term $g(\mathbf{r})$ is known. Let $G(\mathbf{r},\mathbf{r}')$ be some functions such that

$$\hat{L}(\mathbf{r})G(\mathbf{r},\mathbf{r}') = \delta(\mathbf{r}-\mathbf{r}'), \tag{2.89}$$

one can easily verify that $f(\mathbf{r}) = \int_V g(\mathbf{r})G(\mathbf{r},\mathbf{r}')d^d r'$ in domain V where $G(\mathbf{r},\mathbf{r}')$ is subject to some boundary conditions (BCs). Thus, it suffices to solve $\hat{L}(\mathbf{r})G(\mathbf{r},\mathbf{r}') = \delta(\mathbf{r}-\mathbf{r}')$. Consider the equation in form of a damped harmonic oscillator (DHO):

$$\ddot{x}+\Gamma\dot{x}+\Omega^2 x = F(t). \tag{2.90}$$

Choosing $F(t) = \delta(t)$, the solution is $x(t) = \sin(\Omega t)e^{-\Gamma t/2}H(t)/\Omega$, where $H(t)$ is the Heaviside step function. In general, the arbitrary function $F(t)$, $t \in \mathscr{R}$ is real, can be expressed as

$$F(t) = \int_{t'=-\infty}^{\infty} F(t')\delta(t-t')dt', \tag{2.91}$$

Then, we can write $x(t) = \int_{t'=-\infty}^{\infty} G(t,t')F(t')dt'$ where $G(t,t') = \sin(\Omega(t-t'))e^{-\Gamma(t-t')/2}H(t-t')/\Omega$ is the Green's function of the DHO. Note that, we require $G(t,t') = 0$ for $t < t'$. Write $\hat{L}(\mathbf{r}) \equiv z - \hat{l}(\mathbf{r})$ such that $(z-\hat{l}(\mathbf{r}))G(\mathbf{r},\mathbf{r}',z) = \delta(\mathbf{r}-\mathbf{r}')$, where z is a complex variable. For $\hat{l}(\mathbf{r})$, I look for eigenfunctions:

$$\hat{l}(\mathbf{r})e_n(\mathbf{r}) = \lambda_n e_n(\mathbf{r}), n = 1,2,3..., \tag{2.92}$$

where $\{e_n(\mathbf{r})\}$ satisfy the same BCs as $G(\mathbf{r},\mathbf{r}',z)$. Since $\hat{L}(\mathbf{r})$ is Hermitian, so is $\hat{l}(\mathbf{r})$. Without loss of generality, $\{e_n(\mathbf{r})\}$ can be chosen to be orthonormal, i.e.

$$\int_V e_n^*(\mathbf{r})e_m(\mathbf{r})d^d r = \delta_{nm}, \tag{2.93}$$

where $e_m^*(\mathbf{r})$ is the conjugate of $e_m(\mathbf{r})$. It can be verified that $\{e_n(\mathbf{r})\}$ is complete (Economou, 2006). Therefore, any well-behaved function $E(\mathbf{r})$ defined on V and satisfying proper BCs can be written as a linear combination of $e_m(\mathbf{r})$:

$$E(\mathbf{r}) = \sum_n c_n e_n(\mathbf{r}); \quad c_n = \int_V e_n^*(\mathbf{r})E(\mathbf{r})d^d r, \tag{2.94}$$

which gives

$$E(\mathbf{r}) = \sum_n \int_V e_n^*(\mathbf{r}')e_n(\mathbf{r})E(\mathbf{r}')d^d r'. \tag{2.95}$$

Thus, I have

$$\sum_n e_n(\mathbf{r})e_n^*(\mathbf{r}') = \delta(\mathbf{r}-\mathbf{r}'). \tag{2.96}$$

Using the definition of the Green's function, I write

$$\begin{aligned} \left[z-\hat{l}(\mathbf{r})\right] G(\mathbf{r},\mathbf{r}',z) &= \sum_n e_n(\mathbf{r})e_n^*(\mathbf{r}') \\ G(\mathbf{r},\mathbf{r}',z) &= \left[z-\hat{l}(\mathbf{r})\right]^{-1} \sum_n e_n(\mathbf{r})e_n^*(\mathbf{r}') \end{aligned} \tag{2.97}$$

Because $e_n(\mathbf{r}) = \left[z-\hat{l}(\mathbf{r})\right]^{-1}\left[z-\hat{l}(\mathbf{r})\right] e_n(\mathbf{r}) = (z-\lambda_n)\left[z-\hat{l}(\mathbf{r})\right]^{-1} e_n(\mathbf{r})$, I can write $G(\mathbf{r},\mathbf{r}',z)$ as

$$G(\mathbf{r},\mathbf{r}',z) = \sum_n \frac{e_n(\mathbf{r})e_n^*(\mathbf{r}')}{z-\lambda_n} \tag{2.98}$$

$G(\mathbf{r},\mathbf{r}',z)$ is not well defined when z lies in the spectrum of eigenvalues. This can be resolved by replacing z with $z+i\varepsilon$ and letting $\varepsilon \to 0$:

$$G(\mathbf{r},\mathbf{r}',z) = \lim_{\varepsilon\to 0^+} \sum_n \frac{\phi_n(\mathbf{r})\phi_n^*(\mathbf{r}')}{z+i\varepsilon-\lambda_n}. \tag{2.99}$$

By using the fact

$$\lim_{\varepsilon\to 0^+} \frac{1}{x+i\varepsilon} = \mathscr{P}\left(\frac{1}{x}\right) \mp i\pi\delta(x), \tag{2.100}$$

where the first term on the RHS means taking the principal value, I have

$$\begin{aligned}
&\int \mathrm{Im}\,[G(\mathbf{r},\mathbf{r},z)]\,d^d r = \int \mathrm{Im}\left[\lim_{\varepsilon\to 0^+}\sum_n \frac{\phi_n(\mathbf{r})\phi_n^*(\mathbf{r})}{z+i\varepsilon-\lambda_n}\right] d^d r \\
&= \mathrm{Im}\left[\lim_{\varepsilon\to 0^+}\sum_n \frac{1}{z+i\varepsilon-\lambda_n}\right] = -\pi\sum_n \delta(z-\lambda_n) \\
&\equiv -\pi D(z),
\end{aligned} \tag{2.101}$$

where $D(z)$ is called the density of states.

the lattice Green's function

In lattice dynamics, upon assuming the same mass M for all particles, the matrix form of the lattice Green's function is

$$[M\omega^2 I - H]G_L = I \tag{2.102}$$

where the Hessian matrix H and dynamical matrix D are related as $H = MD$. In component form, I have

$$\sum_{l''}[M\omega^2\delta_{ll''} - H(l,l'')]G_L(l'',l',\omega) = \delta_{ll'}, \tag{2.103}$$

where l, l'' refer to lattice sites. Since matrix $H(l,l')$ has its eigenvalues and eigenvectors:

$$\sum_{l'} H(l,l')e_{l'}^m = M\omega_m^2 e_l^m, \tag{2.104}$$

I have

$$\sum_{l''}[M\omega^2\delta_{ll''} - H(l,l'')]e_{l''}^m = M\omega^2 e_l^m - M\omega_m^2 e_l^m = M(\omega^2-\omega_m^2)e_l^m. \tag{2.105}$$

To find $G_L(l,l',\omega)$, I try the following

$$\begin{aligned}
&\sum_{l''}[M\omega^2\delta_{ll''} - H(l,l'')]\sum_m e_{l''}^m\,(e_{l'}^m)^*\,\frac{1}{N(M\omega^2 - M\omega_m^2)} \\
&= \frac{1}{N}\sum_m [M\omega^2 - M\omega_m^2]e_l^m\,(e_{l'}^m)^*\,\frac{1}{(M\omega^2 - M\omega_m^2)} \\
&= \frac{\delta_{ll'}}{N}\sum_m [M\omega^2 - M\omega_m^2]\frac{1}{(M\omega^2 - M\omega_m^2)} = \delta_{ll'}
\end{aligned} \tag{2.106}$$

To get the 2nd equality, I use the fact that eigenvectors e_l^m are orthonormal. This implies

$$G_L(l,l',\omega) = \sum_m e_l^m \left(e_{l'}^m\right)^* \frac{1}{NM(\omega^2-\omega_m^2)}. \tag{2.107}$$

To identify $G_L(q,\omega)$, I can take the spatial Fourier transform of $G_L(l,l',\omega)$:

$$G_L(q,\omega) \equiv \sum_{l,l'} G(l,l',\omega) e^{iq(l-l')} = \sum_m \frac{\left|\sum_l e_l^m e^{iql}\right|^2}{NM(\omega^2-\omega_m^2)}. \tag{2.108}$$

When the system is subject to some perturbations (say V), the new Green's function can be obtained in terms of the unperturbed one (H):

$$G_L' = (\omega^2 I - H - V)^{-1} = G_L(I - G_L V)^{-1}. \tag{2.109}$$

Writing $V = \Omega + i\Gamma$, the perturbed Green's function is expressed in terms of Ω and Γ:

$$G_L' = \frac{\omega^2 I - H - \Omega + i\Gamma}{(\omega^2 I - H - \Omega)^2 + \Gamma^2}. \tag{2.110}$$

By analogue to 1D DHO equation, Eq. (2.90), it can be understood that Γ is the "damping coefficient" in the perturbed (lattice) Green's function.

the elastic Green's function

The elastic wave should contain information about local elastic properties (Gelin et al., 2016). In a continuum, deformations cause a time-dependent displacement field $\mathbf{u}(\mathring{\mathbf{r}},t) = \mathbf{r}(\mathring{\mathbf{r}},t) - \mathring{\mathbf{r}}$, where the former is the current location at time t, while the latter is the initial position of any material point. Ignoring the body force and assuming the uniform mass density ρ, the elastic wave function writes as

$$\rho \frac{\partial^2 u^\mu(\mathring{\mathbf{r}})}{\partial t^2} = \sum_{\nu\kappa\chi} \frac{\partial}{\partial \mathring{\mathbf{r}}^\nu} \left[S_{\mu\nu\kappa\chi}(\mathring{\mathbf{r}}) \frac{\partial u^\kappa(\mathring{\mathbf{r}})}{\partial \mathring{r}^\chi} \right], \tag{2.111}$$

with $S_{\mu\nu\kappa\chi}(\mathring{\mathbf{r}}) = C_{\mu\nu\kappa\chi}(\mathring{\mathbf{r}}) + \delta_{\mu\kappa}\sigma_{\nu\chi}(\mathring{\mathbf{r}})$, where $C_{\mu\nu\kappa\chi}(\mathring{\mathbf{r}})$ and $\sigma_{\nu\chi}(\mathring{\mathbf{r}})$ are the elastic constants and the Cauchy stress in the reference configuration, respectively. The corresponding equation of motion for the elastic Green's function of waves then reads

$$\sum_\eta \left[\rho \frac{\partial^2 u^\mu(\mathbf{r})}{\partial t^2} \delta_{\mu\eta} - \sum_{\nu\kappa\chi} \nabla_\nu S_{\mu\nu\kappa\chi}(\mathbf{r}) \nabla_\kappa \right] G_E^{\chi\eta}(\mathbf{r},\mathbf{r}',t) = \delta_{\mu\eta}\delta(\mathbf{r}-\mathbf{r}'), \tag{2.112}$$

where I have dropped $^\circ$ for convenience. The solution of the elastic Green's function will be explored in Chapter 6.

2.8 Dynamical structure factor

I will derive the dynamical structure factor in both lattice and disordered systems.

Quantum theory of Neutron scattering in lattice

The classical theory of diffraction fails to describe the temperature dependence of the scattering and ignores the effect of zero-point motion. A fully quantum calculation is called to address these concerns (Ashcroft and Mermin, 1976; Van Hove, 1954). Imagine the scattering takes place in a region with volume V. The initial (final) state of the neutron-ion system is given by $\Psi_{i(f)} = \phi_{i(f)}\psi_{i(f)}$ with the energy $\varepsilon_{i(f)} = E_{i(f)} + \hbar\omega_{i(f)}, \hbar\omega_{i(f)} = k^2_{i(f)}/(2M)$, where the wave function of the incident (transmitted) neutron is $\psi_{i(f)} = e^{i(\mathbf{k}_{i(f)}\cdot\mathbf{r} - \omega_{i(f)}t)}/\sqrt{V}$. I take the full neutron-lattice interaction to be

$$\begin{aligned}\mathscr{U}(\mathbf{r}) &= \sum_{lI}\mathscr{U}(\mathbf{r}-\mathbf{r}_I(l)) = \sum_{lI}\mathscr{U}_I(l)\delta(\mathbf{r}-\mathbf{r}_I(l)) \\ &= \sum_{lI}\frac{\mathscr{U}_I(l)}{V}\int d^3q e^{i\mathbf{q}\cdot(\mathbf{r}-\mathbf{r}_I(l))} = \frac{2\pi\hbar^2 a}{MV}\sum_{lI}\int d^3q e^{i\mathbf{q}\cdot(\mathbf{r}-\mathbf{r}_I(l))}\end{aligned} \tag{2.113}$$

On the last line, I choose $\mathscr{U}_I(l) = 2\pi\hbar^2 a/M$ such that the total cross section calculated below is $\sigma = 4\pi a^2$, where a is the scattering length (Ashcroft and Mermin, 1976). Using Fermi's golden rule for time dependent perturbation theory (equivalent to the lowest-order Born approximation), the probability per unit time for a neutron to scatter from state $\mathbf{k}_i$ to $\mathbf{k}_f$ is

$$\begin{aligned}Pr &= \frac{2\pi}{\hbar}\sum_f \delta(\varepsilon_i - \varepsilon_f)\left|\left\langle\Psi_f|\mathscr{U}(\mathbf{r})|\Psi_i\right\rangle\right|^2 \\ &= \frac{2\pi}{\hbar}\sum_f \delta(E_i + \hbar\omega_i - E_f - \hbar\omega_f)\left|\frac{1}{V}\int d^3r e^{i(\mathbf{k_i}-\mathbf{k_f})\cdot\mathbf{r}}\left\langle\phi_f|\mathscr{U}(\mathbf{r})|\phi_i\right\rangle\right|^2 \\ &= a^2\frac{(2\pi\hbar)^3}{(MV)^2}\sum_f \delta(E_i - E_f + \hbar\omega)\left|\sum_{lI}\left\langle\phi_f|e^{i\mathbf{K}\cdot\mathbf{r}_I(l)}|\phi_i\right\rangle\right|^2\end{aligned} \tag{2.114}$$

The inelastic scattering takes place with momentum and energy transfer from neutron to the lattice being $\mathbf{K} = \mathbf{k}_i - \mathbf{k}_f$ and $\hbar\omega = \hbar(\omega_i - \omega_f)$, respectively. Note that a differential volume element of momentum space d^3k_f contains $Vd^3k_f/(2\pi\hbar)^3$ neutron states (Ashcroft

and Mermin, 1976). The incident neutron flux of states (velocity times density) is

$$\mathbf{j} = \frac{\hbar \mathbf{k}_i}{M} |\psi_i|^2 = \frac{\hbar \mathbf{k}_i}{MV}. \tag{2.115}$$

Since the number of neutrons is conserved, I have

$$\begin{aligned} j d\sigma &= j \frac{d\sigma}{dE d\Omega} dE d\Omega = \frac{\hbar k_i}{MV} \frac{d\sigma}{dE d\Omega} dE d\Omega \\ &= Pr \cdot V \frac{d^3 k_f}{(2\pi\hbar)^3} = Pr \cdot V \frac{k_f^2 dk_f d\Omega}{(2\pi\hbar)^3} = Pr \cdot V \frac{k_f M dE d\Omega}{(2\pi\hbar)^3}. \end{aligned} \tag{2.116}$$

where $d\Omega$ is the differential of solid angle. The last equality holds since $E = k_f^2/2M$ for thermal (non-relativistic) neutrons. Using the result of Pr, I obtain

$$\frac{d\sigma}{dE d\Omega} = \frac{a^2 k_f}{k_i} \sum_f \delta(E_i - E_f + \hbar\omega) \left| \sum_{lI} \langle \phi_f | e^{i\mathbf{K}\cdot\mathbf{r}_I(l)} | \phi_i \rangle \right|^2 \equiv \frac{a^2 N k_f}{\hbar k_i} S(\mathbf{K}, \omega) \tag{2.117}$$

where

$$\begin{aligned} S(\mathbf{K}, \omega) &= \frac{\hbar}{N} \sum_f \delta(E_i - E_f + \hbar\omega) \left| \sum_{lI} \langle \phi_f | e^{i\mathbf{K}\cdot\mathbf{r}_I(l)} | \phi_i \rangle \right|^2 \\ &= \frac{1}{N} \sum_f \int_{-\infty}^{\infty} \frac{dt}{2\pi} e^{-i[(E_i - E_f)/\hbar + \omega]t} \sum_{ll''IJ} \langle \phi_i | \left(e^{i\mathbf{K}\cdot\mathbf{r}_J(l'')} \right)^* | \phi_f \rangle \langle \phi_f | e^{i\mathbf{K}\cdot\mathbf{r}_I(l)} | \phi_i \rangle \end{aligned} \tag{2.118}$$

is the dynamic structure factor. I let the normalisation factor, N, be the number of particles in the scattered region. Note that, any operators A, B obey relation $e^{i(E_f - E_i)t/\hbar}(\phi_f, A\phi_i) = (\phi_f, e^{iHt/\hbar} A e^{-iHt/\hbar} \phi_i)$ and $\sum_f (\phi_i, A\phi_f)(\phi_f, B\phi_i) = (\phi_i, AB\phi_i)$. I can write $S(\mathbf{K}, \omega)$ as

$$\begin{aligned} S(\mathbf{K}, \omega) &= \frac{1}{N} \sum_f \int_{-\infty}^{\infty} \frac{dt}{2\pi} e^{-i\omega t} \sum_{ll''IJ} \langle \phi_i | \left(e^{i\mathbf{K}\cdot\mathbf{r}_{l'',J}} \right)^* | \phi_f \rangle \langle \phi_f | e^{i\mathbf{K}\cdot\mathbf{r}_{l,I}(t)} | \phi_i \rangle \\ &= \frac{1}{N} \int_{-\infty}^{\infty} \frac{dt}{2\pi} e^{-i\omega t} \sum_{ll''IJ} \langle \phi_i | \left(e^{i\mathbf{K}\cdot\mathbf{r}_{l'',J}} \right)^* e^{i\mathbf{K}\cdot\mathbf{r}_{l,I}(t)} | \phi_i \rangle \end{aligned} \tag{2.119}$$

in Heisenberg representation. Writing the lattice position from its equilibrium position $\mathbf{r}_{l,I}(t) = \mathbf{R}_{l,I} + \mathbf{s}_{l,I}(t)$, I have

$$S(\mathbf{K}, \omega) = \frac{1}{N} \sum_{ll''IJ} \int_{-\infty}^{\infty} \frac{dt}{2\pi} e^{i[\mathbf{K}\cdot(\mathbf{R}_{l,I} - \mathbf{R}_{l'',J}) - \omega t]} \langle \phi_0 | e^{i\mathbf{K}\cdot\mathbf{s}_{l,I}(t)} \left(e^{-i\mathbf{K}\cdot\mathbf{s}_{l'',J}} \right) | \phi_0 \rangle \tag{2.120}$$

This is correct at zero temperature. To account for effects of finite temperature, we need to take the thermal average over all states:

$$\langle\phi_i|A|\phi_i\rangle \to \langle A\rangle = \frac{\sum_i e^{-E_i/(k_BT)}\langle\phi_i|A|\phi_i\rangle}{\sum_i e^{-E_i/(k_BT)}}. \tag{2.121}$$

Thus, the dynamical structure factor is expressed as

$$S(\mathbf{K},\omega) = \frac{1}{N}\sum_{ll''IJ}\int_{-\infty}^{\infty}\frac{dt}{2\pi}e^{i[\mathbf{K}\cdot(\mathbf{R}_{l,I}-\mathbf{R}_{l'',J})-\omega t]}\left\langle e^{i\mathbf{K}\cdot\mathbf{s}_{l,I}(t)}\left(e^{i\mathbf{K}\cdot\mathbf{s}_{l'',J}}\right)^*\right\rangle \tag{2.122}$$

Recall in lattice dynamics (in d-dimension), the lattice displacement $\mathbf{s}_{l,I}(t)$ can be decomposed in terms of vibrational modes:

$$\mathbf{s}_{l,I}(t) = \int d^dq\sum_m \frac{1}{\sqrt{M_I}}\mathbf{e}_I^m e^{i(\mathbf{q}\cdot\mathbf{R}_l-\omega_m(\mathbf{q})t)}. \tag{2.123}$$

I express $\mathbf{s}_{l,I}(t)$ in terms of creation and annihilation operators:

$$\mathbf{s}_{l,I}(t) = \frac{1}{\sqrt{M_IN_c}}\int d^dq\sum_m\sqrt{\frac{\hbar}{2\omega_m(\mathbf{q})}}\mathbf{e}_I^m(\mathbf{q})(a_m(\mathbf{q},t)+a_m^\dagger(-\mathbf{q},t))e^{i\mathbf{q}\cdot\mathbf{R}_l}, \tag{2.124}$$

which consists of positive and negative-frequency parts. Here, N_c is the number of unit cells (locating at $\mathbf{R}_l$) in the scattered region. In the Heisenberg representation, we have

$$\begin{aligned}
a_m(\mathbf{q},t) &= e^{i\mathscr{H}t/\hbar}a_m(\mathbf{q})e^{-i\mathscr{H}t/\hbar}\\
&= e^{i\omega_m(\mathbf{q})ta_m^\dagger(\mathbf{q})a_m(\mathbf{q})}a_m(\mathbf{q})e^{-i\omega_m(\mathbf{q})ta_m^\dagger(\mathbf{q})a_m(\mathbf{q})}\\
&= a_m(\mathbf{q})e^{i[\omega_m(\mathbf{q})ta_m^\dagger(\mathbf{q})a_m(\mathbf{q})-1]}e^{-i\omega_m(\mathbf{q})ta_m^\dagger(\mathbf{q})a_m(\mathbf{q})}\\
&= a_m(\mathbf{q})e^{-i\omega_m(\mathbf{q})t}
\end{aligned} \tag{2.125}$$

by rules in commutators. Similarly, $a_m^\dagger(\mathbf{q},t) = a_m^\dagger(\mathbf{q})e^{i\omega_m(\mathbf{q})t}$. Therefore,

$$\mathbf{s}_{l,I}(t) = \frac{1}{\sqrt{M_IN_c}}\int d^dq\sum_m\sqrt{\frac{\hbar}{2\omega_m(\mathbf{q})}}\mathbf{e}_I^m(\mathbf{q})\left(a_m(\mathbf{q})e^{-i\omega_m(\mathbf{q})t}+a_m^\dagger(-\mathbf{q})e^{i\omega_m(\mathbf{q})t}\right)e^{i\mathbf{q}\cdot\mathbf{R}_l} \tag{2.126}$$

One can easily verify that $\langle\mathbf{s}_{l,I}(t)\rangle = \langle\mathbf{s}_{l,I}\rangle = 0$. Let operators $A = i\mathbf{K}\cdot\mathbf{s}_{l,I}(t)$ and $B = (i\mathbf{K}\cdot\mathbf{s}_{l'',J}(0))^*$, since they are linear in $a^\dagger$ and a of a harmonic crystal, then (Ashcroft and

Mermin, 1976)

$$\begin{aligned}\langle e^A e^B\rangle &= \left\langle \left(1+A+\frac{1}{2}A^2+...\right)\left(1+B+\frac{1}{2}B^2+...\right)\right\rangle \\ &= \left\langle 1+A+B+AB+\frac{1}{2}A^2+\frac{1}{2}B^2+...\right\rangle \\ &= 1+\frac{1}{2}\left\langle 2AB+A^2+B^2\right\rangle+... \\ &= e^{\frac{1}{2}\langle 2AB+A^2+B^2\rangle}. \end{aligned} \tag{2.127}$$

Thus,

$$\left\langle e^{i\mathbf{K}\cdot\mathbf{s}_{l,I}(t)}\left(e^{i\mathbf{K}\cdot\mathbf{s}_{l'',J}}\right)^*\right\rangle = \langle e^{i\mathbf{K}\cdot\mathbf{s}_{l,I}(t)}e^{-i\mathbf{K}\cdot\mathbf{s}^*_{l'',J}}\rangle = e^{-\frac{1}{2}\langle(\mathbf{K}\cdot\mathbf{s}_{l,I}(t))^2\rangle}e^{-\frac{1}{2}\langle(\mathbf{K}\cdot\mathbf{s}^*_{l'',J})^2\rangle}e^{\langle\mathbf{K}\cdot\mathbf{s}_{l,I}(t)\mathbf{K}\cdot\mathbf{s}^*_{l'',J}\rangle} \tag{2.128}$$

For the first two terms on the RHS, I note

$$\begin{aligned}&\langle(\mathbf{K}\cdot\mathbf{s}_{l,I}(t))^2\rangle = \frac{1}{M_I N_c}\int d^3q d^3p \sum_{mn}\frac{\hbar}{2\sqrt{\omega_m(\mathbf{q})\omega_n(\mathbf{p})}}\mathbf{K}\cdot\mathbf{e}^m_I(\mathbf{q})\mathbf{K}\cdot\mathbf{e}^n_I(\mathbf{p})e^{i\mathbf{q}\cdot\mathbf{R}_l}e^{i\mathbf{p}\cdot\mathbf{R}_l}. \\ &\langle[a_m(\mathbf{q})e^{-i\omega_m(\mathbf{q})t}+a^\dagger_m(-\mathbf{q})e^{i\omega_m(\mathbf{q})t}][a_n(\mathbf{p})e^{-i\omega_n(\mathbf{p})t}+a^\dagger_n(-\mathbf{p})e^{i\omega_n(\mathbf{p})t}]\rangle \\ &= \frac{1}{M_I N_c}\sum_m\int d^3q\frac{\hbar}{2\sqrt{\omega_m(\mathbf{q})\omega_m(-\mathbf{q})}}\mathbf{K}\cdot\mathbf{e}^m_I(\mathbf{q})\mathbf{K}\cdot\mathbf{e}^m_I(-\mathbf{q})e^{i\mathbf{q}\cdot\mathbf{R}_l}e^{i(-\mathbf{q})\cdot\mathbf{R}_l}. \\ &\langle[a_m(\mathbf{q})e^{-i\omega_m(\mathbf{q})t}+a^\dagger_m(-\mathbf{q})e^{i\omega_m(\mathbf{q})t}][a_m(-\mathbf{q})e^{-i\omega_m(-\mathbf{q})t}+a^\dagger_m(\mathbf{q})e^{i\omega_m(-\mathbf{q})t}]\rangle \\ &= \frac{1}{M_I N_c}\sum_m\int d^dq\frac{\hbar}{2\omega_m(\mathbf{q})}\mathbf{K}\cdot\mathbf{e}^m_I(\mathbf{q})\mathbf{K}\cdot\mathbf{e}^m_I(-\mathbf{q})\langle[a_m(\mathbf{q})a^\dagger_m(\mathbf{q})+a^\dagger_m(-\mathbf{q})a_m(-\mathbf{q})]\rangle \\ &= \langle(\mathbf{K}\cdot\mathbf{s}_{l,I})^2\rangle \\ &= \langle(\mathbf{K}\cdot\mathbf{s}^*_{l,I})^2\rangle \\ &\equiv W_I \end{aligned} \tag{2.129}$$

where the second equality holds because only when $\mathbf{q}=-\mathbf{p}$ and $m=n$ can relevant terms survive. The elastic and inelastic process can be distinguished by expanding the exponential, $e^{\langle\mathbf{K}\cdot\mathbf{s}_{l,I}(t)\mathbf{K}\cdot\mathbf{s}^*_{l'',J}\rangle}=\sum_r(\langle\mathbf{K}\cdot\mathbf{s}_{l,I}(t)\mathbf{K}\cdot\mathbf{s}^*_{l'',J}\rangle)^r/(r!)$ and one-phonon inelastic scattering

corresponds to case $r = 1$, which involves either the absorption or creation of a phonon:

$$\begin{aligned}
S_1(\mathbf{K},\omega) &= \frac{1}{N}\sum_{ll''IJ} e^{\frac{-(W_I+W_J)}{2}} \int_{-\infty}^{\infty} \frac{dt}{2\pi} e^{i[\mathbf{K}\cdot(\mathbf{R}_{l,I}-\mathbf{R}_{l'',J})-\omega t]} \langle \mathbf{K}\cdot\mathbf{s}_{l,I}(t)\mathbf{K}\cdot\mathbf{s}^*_{l'',J}\rangle \\
&= \frac{1}{N}\sum_{ll''IJ} e^{\frac{-(W_I+W_J)}{2}} \int_{-\infty}^{\infty} \frac{dt}{2\pi} e^{i[\mathbf{K}\cdot(\mathbf{R}_{l,I}-\mathbf{R}_{l'',I}+\mathbf{R}_{l'',I}-\mathbf{R}_{l'',J})-\omega t]} \langle \mathbf{K}\cdot\mathbf{s}_{l,I}(t)\mathbf{K}\cdot\mathbf{s}^*_{l'',J}\rangle \\
&= \frac{1}{N_p}\sum_{IJ} e^{\frac{-(W_I+W_J)}{2}} \int_{-\infty}^{\infty} \frac{dt}{2\pi} e^{-i\omega t} \int d^3q \sum_m \frac{\hbar(\mathbf{K}\cdot\mathbf{e}_I^m(\mathbf{K})\mathbf{K}\cdot\mathbf{e}_J^m(\mathbf{K}))}{2\omega_m(\mathbf{q})\sqrt{M_I M_J}} e^{i\mathbf{K}\cdot(\mathbf{R}_I-\mathbf{R}_J)}\cdot \\
&\delta(\mathbf{K}+\mathbf{q}-\mathbf{G})\left[e^{-i\omega_m(\mathbf{q})t}\langle a_m(\mathbf{K})a_m^\dagger(\mathbf{K})\rangle + e^{i\omega_m(\mathbf{q})t}\langle a_m^\dagger(-\mathbf{K})a_m(-\mathbf{K})\rangle\right]
\end{aligned} \tag{2.130}$$

where I have used the fact that

$$\sum_l e^{i\mathbf{K}\cdot\mathbf{R}_l} = \begin{cases} 0, \mathbf{K} = \mathbf{G}; \\ N_c, \mathbf{K} \neq \mathbf{G}. \end{cases} \tag{2.131}$$

for $\mathbf{G}$ being a multiply of the reciprocal vectors. The total number of particles within the unit cell is N_p. It can be verified that $\vec{e}_m(\mathbf{G}-\mathbf{k}) = \vec{e}_m(-\mathbf{k}) = [\vec{e}_m(\mathbf{k})]^*, \omega_m(\mathbf{G}-\mathbf{k}) = \omega_m(\mathbf{k})$ and the occupancy of each mode $n_m(\mathbf{q}) = a_m^\dagger(\mathbf{q})a_m(\mathbf{q})$ satisfies the Bose-Einstein distribution $\langle n_m(\mathbf{q})\rangle = 1/e^{(\hbar\omega_m(\mathbf{q})/k_BT)} - 1)$ (see Ashcroft and Mermin (1976) for details), finally I have

$$\begin{aligned}
S_1(\mathbf{K},\omega) =& \frac{1}{N_p}\sum_{IJm} e^{\frac{-(W_I+W_J)}{2}} \frac{\hbar(\mathbf{K}\cdot\mathbf{e}_I^m(\mathbf{K})\mathbf{K}\cdot\mathbf{e}_J^m(\mathbf{K}))}{2\omega_m(\mathbf{K})\sqrt{M_I M_J}} e^{i\mathbf{K}\cdot(\mathbf{R}_I-\mathbf{R}_J)}\cdot \\
& [n_m(\mathbf{K})\delta(\omega-\omega_m(\mathbf{K})) + (1+n_m(\mathbf{K}))\delta(\omega+\omega_m(\mathbf{K}))]
\end{aligned} \tag{2.132}$$

Term $\delta(\omega-\omega_m(\mathbf{K}))$ means we only get a contribution when $\omega = \omega_m(\mathbf{K})$, i.e. $\omega_i - \omega_f = \omega_m(\mathbf{K})$, namely the final energy of the neutron is smaller than the initial energy. The energy is lost in emitting a phonon, which can happen at any temperature since $n_m(\mathbf{K}) \neq 0$ at any T. In the classical limit, $\hbar \to 0$, then Eq. (2.132) reduces to

$$\begin{aligned}
S_1(\mathbf{K},\omega) &= \frac{1}{N_p}\sum_{IJm} \frac{k_BT(\mathbf{K}\cdot\mathbf{e}_I^m(\mathbf{K})\mathbf{K}\cdot\mathbf{e}_J^m(\mathbf{K}))}{2\omega_m^2(\mathbf{K})\sqrt{M_I M_J}} e^{i\mathbf{K}\cdot(\mathbf{R}_I-\mathbf{R}_J)} (\delta(\omega-\omega_m(\mathbf{K})) + \delta(\omega+\omega_m(\mathbf{K}))) \\
&= \frac{k_BT}{2N_p}\sum_m \left|\sum_I \frac{\mathbf{K}\cdot\mathbf{e}_I^m(\mathbf{K})}{\omega_m(\mathbf{K})\sqrt{M_I}} e^{i\mathbf{K}\cdot\mathbf{r}_I}\right|^2 (\delta(\omega-\omega_m(\mathbf{K})) + \delta(\omega+\omega_m(\mathbf{K})))
\end{aligned} \tag{2.133}$$

To take a consistent convention, I will write $S(\mathbf{q},\omega)$.

Disordered systems

There is no boundary periodicity in disordered materials. Imposing harmonic approximation, the displacement of particle I from its equilibrium position writes as

$$\mathbf{s}_I(t) = \sum_m \sqrt{\frac{\hbar}{2M_I\omega_m}}\mathbf{e}_I^m(a_m^\dagger e^{i\omega_m t} + a_m e^{-i\omega_m t}), \tag{2.134}$$

in terms of creation and annihilation operators. I can use the Bloch theorem valid for harmonic approximation, $\langle e^Q\rangle = e^{\langle Q^2\rangle/2}$, ($Q$ is any linear combination of harmonic-oscillator coordinates and angular brackets denote thermal average over an ensemble of harmonic-oscillator eigenstates) to simplify $S(\mathbf{q},\omega)$:

$$S(\mathbf{q},\omega) = \frac{1}{N}\sum_{I,J}\exp\left[-i\mathbf{q}\cdot(\mathbf{R}_I-\mathbf{R}_J)\right]e^{\frac{-(W_I+W_J)}{2}}\int_{-\infty}^{\infty} e^{\left(\frac{\hbar}{2\sqrt{M_IM_J}}\sum_m(\mathbf{q}\cdot\mathbf{e}_I^m)(\mathbf{q}\cdot\mathbf{e}_J^m)g(\omega_m,t)\right)}e^{-i\omega t}\frac{dt}{2\pi}, \tag{2.135}$$

where $W_I = \langle(\mathbf{q}\cdot\mathbf{s}_I)^2\rangle$ is Debye-Waller factor reflecting the influence of the atomic thermal motions; $g(\omega_m,t) = [(n_m+1)e^{-i\omega_m t} + n_m e^{i\omega_m t}]/\omega_m$; $n_m = (e^{\beta\hbar\omega_m}-1)^{-1}, \beta = 1/(k_BT)$ is the average number of phonons of energy $\hbar\omega_m$ for the mth normal mode at temperature T (Kim and Nelkin, 1973). In the classical limit, W_I and $g(\omega_m,t)$ reduce to:

$$W_I = \frac{1}{M_I\beta}\sum_m\frac{|\mathbf{q}\cdot\mathbf{e}_I^m|^2}{\omega_m^2}, \quad g(\omega_m,t) = \frac{2\cos(\omega_m t)}{\beta\hbar\omega_m^2} \tag{2.136}$$

For the third term in Eq. (2.135), I expand the exponential again:

$$e^{\left(\frac{\hbar}{2\sqrt{M_IM_J}}\sum_m(\mathbf{q}\cdot\mathbf{e}_I^m)(\mathbf{q}\cdot\mathbf{e}_J^\gamma)g(\omega_m,t)\right)} = \sum_{r=0}^{\infty}\frac{1}{r!}\left[\frac{\hbar}{2\sqrt{M_IM_J}}\sum_m(\mathbf{q}\cdot\mathbf{e}_I^m)(\mathbf{q}\cdot\mathbf{e}_J^m)g(\omega_m,t)\right]^r \tag{2.137}$$

Term of $r=0$ corresponds to the Bragg diffraction, while $r=1$ means the scattering process involves one phonon only. For $r>1$, those terms only contribute to the background scattering in a neutron scattering measurement (Ashcroft and Mermin, 1976). Taking one phonon excitation approximation, I have:

$$\frac{\hbar}{2\sqrt{M_IM_J}}\sum_m(\mathbf{q}\cdot\mathbf{e}_I^m)(\mathbf{q}\cdot\mathbf{e}_J^m)g(\omega_m,t) = \frac{k_BT}{\sqrt{M_IM_J}}\sum_m(\mathbf{q}\cdot\mathbf{e}_I^m)(\mathbf{q}\cdot\mathbf{e}_J^m)\frac{\cos(\omega_m t)}{\omega_m^2} \tag{2.138}$$

In the low temperature limit, $\beta \to \infty$, so $W_I \to 0$. The DSF reduces to

$$
\begin{aligned}
S(\mathbf{q},\omega) &= N^{-1}\sum_{I,J}\exp\left[-i\mathbf{q}\cdot(\mathbf{R}_I-\mathbf{R}_J)\right]\int_{-\infty}^{\infty}\frac{k_BT}{\sqrt{M_IM_J}}\sum_m(\mathbf{q}\cdot\mathbf{e}_I^m)(\mathbf{q}\cdot\mathbf{e}_J^m)\frac{\cos(\omega_m t)}{\omega_m^2}e^{-i\omega t}\frac{dt}{2\pi} \\
&= \sum_{I,J}\frac{k_BT}{2N\sqrt{M_IM_J}}\exp\left[-i\mathbf{q}\cdot(\mathbf{R}_I-\mathbf{R}_J)\right]\sum_m\frac{(\mathbf{q}\cdot\mathbf{e}_I^m)(\mathbf{q}\cdot\mathbf{e}_J^m)}{\omega_m^2}(\delta(\omega-\omega_m)+\delta(\omega+\omega_m)) \\
&= \frac{k_BTq^2}{2N}\sum_m\left|\sum_I\frac{1}{\sqrt{M_I}\omega_m}[\hat{\mathbf{q}}\cdot\mathbf{e}_I^m]\exp(-i\mathbf{q}\cdot\mathbf{R}_I)\right|^2(\delta(\omega-\omega_m)+\delta(\omega+\omega_m)) \qquad (2.139)
\end{aligned}
$$

This form is the same as Eq. (2.133) except that the eigenvectors/eigenvalues are independent of wavevector because there is only one "cell" and the reciprocal space is not defined in amorphous systems.

Chapter 3

Dielectric relaxation in glasses

Materials exhibit a temporary delay in their dielectric constants, which is known as dielectric relaxation. The dielectric relaxation is usually caused by the delay in polarisation of charges in a dielectric medium exposed in a varying external electric field. In general, relaxation is a linear delay response or lag, and therefore dielectric relaxation is measured relative to the expected linear steady state (equilibrium) dielectric values. In physics, dielectric relaxation refers to the relaxation response of a dielectric medium to an external, oscillating electric field. This relaxation is often described in terms of permittivity in frequency domain. Debye derived an formula of the complex permittivity for an ideal, noninteracting population of dipoles to an alternating external electric field (Debye, 1929): $\varepsilon(\omega) = \varepsilon_\infty + (\varepsilon_0 - \varepsilon_\infty)/(1 + i\omega\tau)$ where ε_0 and ε_∞ are the permittivity at initial and high (infinity) frequency ; τ is known as characteristic relaxation time categorising (each) relaxation process (see the discussion in Section 2.3).

Glycerol $[C_3H_5(OH)_3]$ is a hydrogen-bonded material that can be easily supercooled and has been theoretically investigated in numerous attempts to test models of glass transition, yet no microscopic theory has been used to describe the dielectric response of this material apart from empirical models (e.g. Havriliak-Negami), which has no physics behind. It has melting temperature $T_m \approx 291$K with glass transition temperature around 100K lower, $T_g \approx 185$K (Lunkenheimer et al., 1996). Starting from the first principle assumption that the microscopic Hamiltonian can be modeled using a classical particle-bath coupling of the Caldeira-Leggett type, a simple and explicit relation between the dielectric relaxation function and the VDOS of glassy system presents to be a potential theoretical interpretation of the α-peak and Kohlrausch stretched-exponential relaxation (Cui et al., 2017a).

For Freon 112 and Freon 113, previous study on thermal conductivities reveals the existence of quasilocalised low-energy vibrational modes at energy lower than the values of the maximum of the boson peak (see Section 3.1 for clear definition) compared with other

OGs, which results in an increase of VDOS (Vdovichenko et al., 2015). It was thought that the high value of kinetic fragility of F113 is produced by strong orientational correlations, which is evidenced by low values of the stretching exponent in Kohlrausch stretched-exponential function close to T_g, where only α-relaxation is observed with no sign of the β-relaxation. In contrast, in dielectric spectra of F112 from T_g to above, β-relaxation becomes evident as temperature drops to T_g. These experimental facts are the origin of my interest in applying a microscopic theoretical model to orientationally disordered crystals. In particular, Freons F112 and F113 are chemically and molecularly similar compounds displaying glassy states (they both belong to the series $C_2X_{(6-n)}Y_n$, with X, Y=Cl, F, Br, and $n = 0, ..., 6$), but with completely different dynamics and relaxation. This provides a unique opportunity to explain, from a microscopic point of view, the physical origin of secondary β-relaxation (Zaccone, 2020).

3.1 Methods to obtain the vibrational density of states

VDOS from random network: a simple model

The vibrational density of states (VDOS) obtained from numerical diagonalisation of the simulation is expressed in terms of dimensionless eigenfrequencies ω_m. To configure the simulation system, the total interaction is modeled by the sum of the truncated Lenard-Jones (LJ) potential $\mathscr{U}(R) = (1/R^{12} - 2/R^6 + 0.031)H(2-R)$ depending only on the distance between two particles. 4000 particles are initially placed randomly in an orthogonal box imposed with periodic boundary conditions, and the whole system is brought to a metastable low energy state by a Monte Carlo energy-relaxation algorithm (Binder and Heermann, 2001). Bonds are formed only between nearest neighbours and the bond length is distributed around the mean value $R_0 = 0.94$. The density is kept constant ($\rho = N/V = 1.467$). In random networks model, the VDOS also depends on the coordination number Z, i.e. the number of nearest neighbours for each particle, whose value can be reduced by randomly cutting bonds from the initial configuration with average value being $Z = 9$, while keeping a narrow distribution. In the final step, the LJ interactions between nearest neighbours are all replaced by harmonic springs with pair potential $\mathscr{U}(R) = (k/2)(R-R_0)^2$, where k is the spring constant. The numerical procedure was performed by my colleagues (Milkus and Zaccone, 2016). Generally, the eigenfrequency ω_m obtained from the numerical calculation and the eigenfrequency ω'_m of the *real* experimental systems are related via $\omega'_m \approx \sqrt{k/M}\omega_m$ where M is the effective mass (of the charged particle), under the normalisation condition on VDOS $D(\omega_p)$ that $\int_0^{\omega'_D} D'(\omega'_p)d\omega'_p = \int_0^{\omega_D} D(\omega_p)d\omega_p$, with $D(\omega_p) \sim \sum_m \delta(\omega_p - \omega_m)$. I

use the constant $C = \sqrt{k/M}$ as a fitting parameter. k and M are both equal to unity in the numerical simulation, whereas their values are of course different for different experimental systems.

Due to the disorder in the lattice, and in particular, due to the absence of local inversion symmetry (Milkus and Zaccone, 2016), the low-frequency part of the VDOS is dominated by an excess of soft modes (vibrational normal modes with the largest displacement in the lowest frequency) over the Debye ω_p^2 law valid for crystals. This excess of soft modes in the VDOS is universally known in the literature on glassy physics and disordered systems as the "boson peak" (Schirmacher et al., 2007). In the following, I use this terminology and refer to the broad ensemble of all these excess soft modes over the Debye ω_p^2 law as the boson peak. The boson peak frequency drifts towards lower values of ω_p according to the scaling $\omega_p^{BP} \sim (Z-6)$ (see Fig. 3.1). It is important to note that, in the sub-field of dielectric spectroscopy of glasses, the terminology "boson peak" is sometimes used to designate an isolated peak in the THz frequency regime of the dielectric loss modulus ε'', which is different from the peak, for example, in the onset of the normalised VDOS in Fig. 3.1. In this thesis, I will never refer to or consider this THz-frequency peak in the loss modulus, so there is no ambiguity in my terminology and the term "boson peak" is used exclusively to designate the ensemble of excess non-Debye modes in the low-ω_p part of the VDOS.

In all experimental systems measuring the T-dependent material response, the temperature is varied at constant pressure, which implies that thermal expansion is important. That is, Z is the crucial control parameter of the relaxation process in a real molecular glass changing with T. Therefore, in order to use numerical VDOS data in the evaluation of the dielectric function, we need to find a physically meaningful relation between Z and T at the glass transition. Within this picture, Z represents the effective number of intermolecular contacts, which increases the number of positive charges to which a negative charge is bounded in the material. Following previous work, I thus employ thermal expansion ideas in Zaccone and Terentjev (2013) to relate Z and T. Upon introducing the thermal expansion coefficient $\alpha_T = (\partial V/\partial T)/V$ and replacing the total volume V of the sample via the volume fraction $\phi = vN/V$ occupied by the particles (v is the volume of one molecule), I obtain $\ln(1/\phi) = \alpha_T T + const$ upon integration. Approximating $Z \sim \phi$ locally, I get $Z = Z_0 e^{-\alpha_T T}$. Although this approximation is not true in strictly speaking jamming systems, in general disordered systems such as liquids (recall that my model contains a harmonic attractive part of interaction), Z and ϕ are related as $Z = 24\phi \int_1^r r^2 g(r) dr$ where $g(r)$ is the radial distribution function (Hansen and McDonald, 2008; Zaccone and Del Gado, 2010). Imposing that $Z_0 = 12$, as for FCC crystals at $T = 0$ in accordance with Nernst principle determines

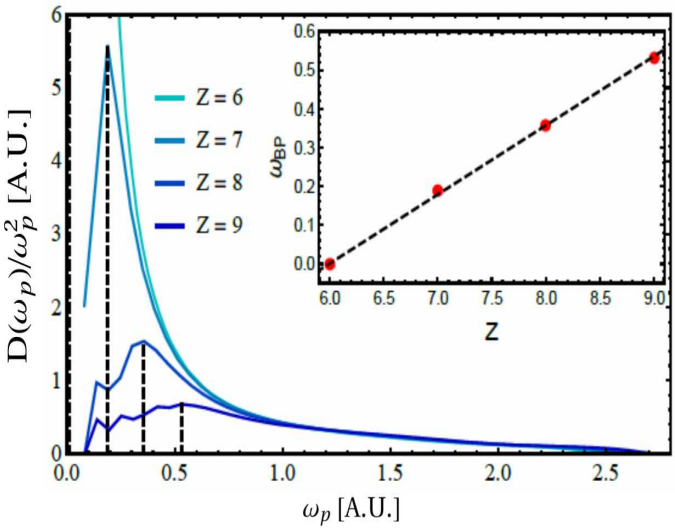

Fig. 3.1 The VDOS normalised by Debye's ω_p^2 law, for (from bottom to top): $Z = 9, Z = 8, Z = 7, Z = 6$, which gives evidence of the boson peak at low ω_p. The eigenfrequency of the boson peak scales as $\omega_p^{BP} \sim (Z-6)$ as known from work for disordered systems with central-force interactions (Cui et al., 2017a).

the relation between Z and T. For glycerol, $Z \approx 6.02$ when $T = 184K$ close to the reported T_g (Lunkenheimer et al., 1996).

It is seen in Fig. 3.1 and in Fig. 3.2 that for the case $Z = 6.1$, i.e. very close to the solid-liquid (glass) transition that occurs at $Z = 6$, a strong and broad boson peak is present in the VDOS. Upon increasing Z towards higher values, the boson peak is still present but its amplitude decreases markedly. At $Z = 6.1$, the continuum Debye regime $\sim \omega_p^2$ is not visible or absent, whereas a very small gap between $\omega_p = 0$ and the lowest vibrational frequency exists. Hence, under conditions close to the glass transition where the system loses its (shear) rigidity, the vibrational spectrum is dominated by a large and broad excess of soft modes with respect to Debye $\sim \omega_p^2$ law at low frequency (Cui et al., 2019a; Milkus and Zaccone, 2016).

VDOS obatined from inelastic neutron scattering

The essential experimental VDOS $D(\omega)$ is usually measured by means of inelastic neutron scattering (INS) using the direct spectrometer MARI of the ISIS facility. In Fig. 3.3, the VDOS of F113 clearly exhibits a much more significant excess of low-frequency (boson-peak) modes, with respect to F112, in the range $2-5$ meV. In a multi-component system with predominantly coherent scatters, a generalised, neutron-weighted VDOS can be obtained

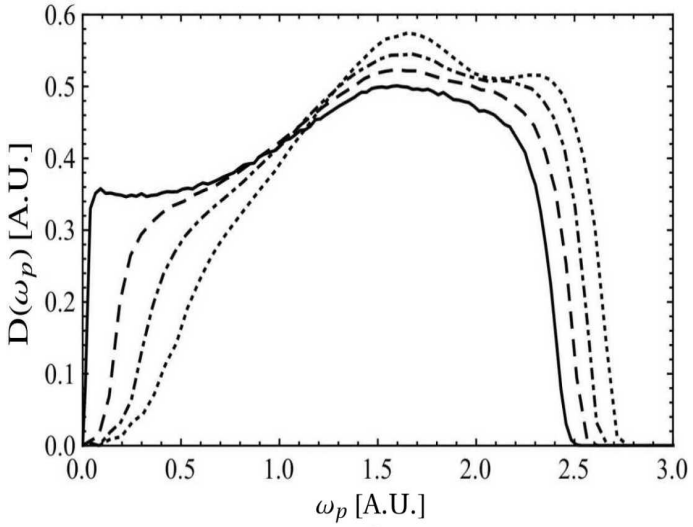

Fig. 3.2 VDOS with respect to eigenfrequency ω_p at $Z = 6.1$ (solid line), i.e. close to the marginal stability limit $Z = 6$ that I identify here as the solid-liquid (glass) transition; plots of the VDOS at $Z = 7, Z = 8, Z = 9$ are also shown, and are marked as dashed, dot dashed and dotted lines, respectively (Cui et al., 2017a).

under the incoherent one-phonon approximation, where the measured dynamical structure factor $S(q,\omega)$, integrated over the accessible q-range (q is the wavenumber), is proportional to $D(\omega)/\omega^2$ (Meyer et al., 1996). The INS experiments were performed by my collaborators (Cui et al., 2018b).

3.2 Deriving the generalised Langevin equation in AC field

The limitation that previous work ignored the dielectric effect on bath oscillators is obviously artificial and not realistic. Further, as is shown in Appendix B, bath oscillators actually carry charges and hence are subjected to the external AC field. Thus, such limitation clearly leaves out a number of important physical problems, where not only the tagged particle is subjected to the AC field, but also the particles that constitute the heat bath are subjected to it. This situation is clearly encountered in dielectric matter under a uniform AC electric field $E(t)$. In this case, every building block (atom, molecule, ion) is polarisable or charged such that it is subjected to a force from the electric field. Hence, if the bath is constituted by polarisable or charged particles, these will also respond to the AC field and it is nonphysical to neglect the effect of the AC field on the dynamics of the bath oscillators. This situation is schematically depicted in Fig. 3.4.

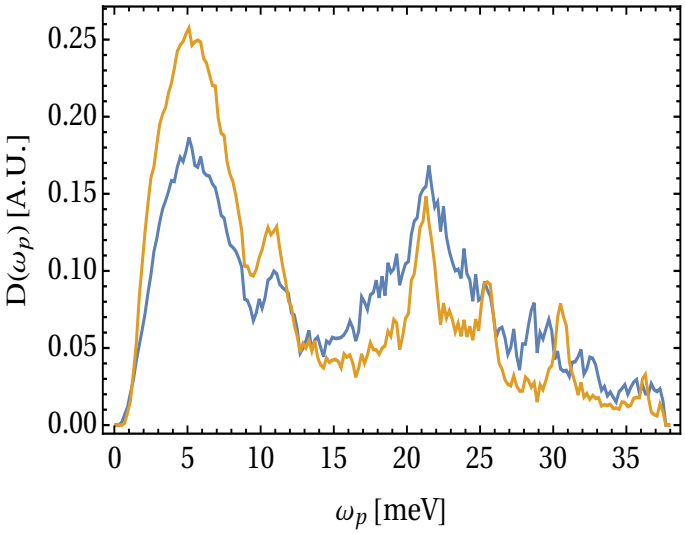

Fig. 3.3 Experimental VDOS for Freon 112 (blue) and Freon 113 (yellow). The data for Freon 112 were published in Sharapova et al. (2010), while the data for Freon 113 were taken from Vispa et al. (2017).

In this contribution, I provide a solution to this problem by formulating a Caldeira-Leggett particle-bath Hamiltonian, where both the particle and the bath oscillators are subjected to the external AC field, which is explicitly accounted for in both the Hamiltonian of the particle and the Hamiltonian of the bath (Caldeira, 2014). The two Hamiltonians are then connected via a bi-linear coupling as is standard in this type of models. I analytically solve the coupled Hamiltonian for the tagged particle to find a new generalised Langevin equation, which, for the first time, accounts for the effect of the polarisation of the bath under the AC field on the dynamics of the tagged particle. This is a more general GLE than any of those proposed so far, and only in certain limits can it reduce to the known forms of the GLE with external time-dependent field.

Harmonic oscillation heat bath

In condensed matter physics, the Zwanzig-Caldeira-Leggett (ZCL) system-bath model is widely applied to low-temperature quantum physics problems, especially in quantum tunnelling in superconductors and in chemical reaction rate theory. I study the classical version of the Caldeira-Leggett coupling between the tagged particle and a bath of harmonic oscillators, which was already proposed by Zwanzig (1973), and add a new term, $\mathscr{H}_E$, which contains the force due to the applied AC electric field acting on both the tagged particle and the harmonic oscillators:

$$\mathscr{H} = \mathscr{H}_S + \mathscr{H}_B + \mathscr{H}_E, \tag{3.1}$$

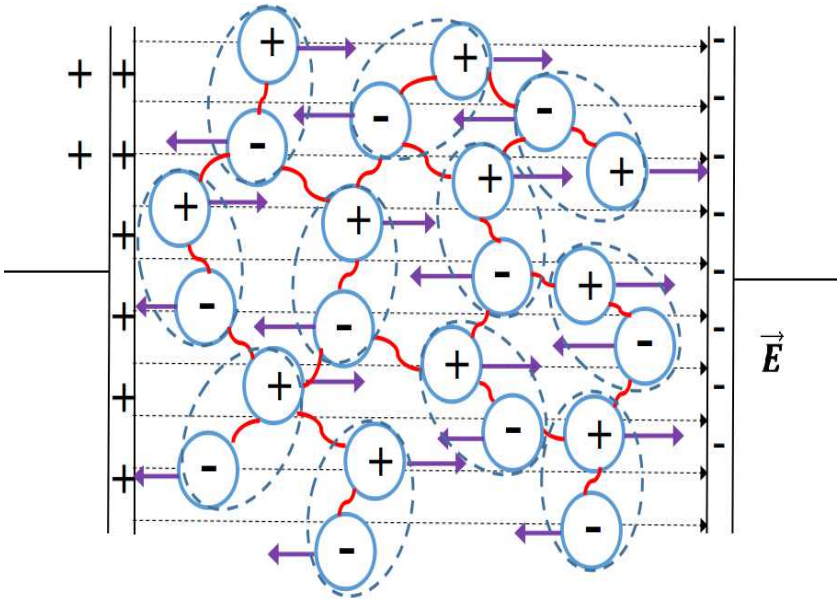

Fig. 3.4 Schematic example of system of charged (solid circles) or polarisable (dashed lines) molecules. In the former case the particles could be ions in a plasma or ions and electrons in a liquid metal. In the latter case, the negatively and positively charged particles represent the electron cloud and the molecular ion of a polarised neutral molecule as in e.g. dielectric relaxation of molecular liquids. A particle-bath Hamiltonian like Eq. (3.1) can be applied to these systems where a tagged particle (positively or negatively charged) interacts with the local environment via an interaction potential $\mathscr{U}(Q)$, which may represent the interaction with neighbours, and also with all other degrees of freedom in the system which can be effectively represented as a bath of harmonic oscillators to which the tagged particle is coupled via a set of coupling constants c_m, where m runs over all other bath oscillators in the system. In traditional models of bath-oscillator dynamics, only the tagged particle is subjected to the external AC field, whereas the other particles are not. In the proposed model, both the tagged particle and also all the other particles (forming the bath) are responding to the AC electric field, which provides an opportunity to better represent the properties of physical systems in the model and this allows for better insight into the physics in these systems.

where $\mathscr{H}_S = P^2/2M + \mathscr{U}(Q)$ is the Hamiltonian of the tagged particle (P is momentum and Q is position) without external field. The second term on the RHS is the standard Hamiltonian of the bath of harmonic oscillators that are coupled to the tagged particle, $\mathscr{H}_B = \sum_{m=1}^{N} \left[P_m^2/M_m + M_m \omega_m^2 \left(X_m - F_m(Q)/\omega_m^2 \right)^2 \right]/2$, consisting of the standard harmonic oscillator expression for each bath oscillator m, and of the coupling term between the tagged particle and the m-th bath oscillator, which contains the coupling function $F_m(Q)$. The new term

$$\mathscr{H}_E = -z\Phi(Q,t) - \sum_m z_m \Phi(X_m,t) = -E_0 \sin(\omega t) \left(zQ + \sum_m z_m X_m \right) \tag{3.2}$$

represents the influence of electric field on both the tagged particle (first term in the bracket) and the bath oscillators (second term in the bracket). Here, z is the total charge of tagged particle, where e.g. $z = \pm 1e$ for monovalent ions/electrons in a plasma or $z = -1e$ for the case of molecular dielectrics where a molecule polarises into a negatively charged electron cloud which oscillates about a positively charged molecular ion; z_m is the net charge of bath particle subjected to the same polarisation. Here, I only consider the movement along the direction of the AC field, $E(t) = E_0 \sin(\omega t)$, and Φ is the electric potential.

In the Caldeira-Leggett model, the classical friction force can be modeled by a linear coupling to a proper distribution of harmonic oscillators, the coupling function is hence taken to be $F_m(Q) = c_m Q$, where c_m is known as the strength of coupling between the tagged particle and the oscillator m. The original coupling is expected to be large for nearby particles and small for particles far away in the materials and hence c_m is different for all the different oscillators (at their own frequencies) the tagged particle is interacting with. See Appendix B for more discussion about the linear coupling.

This Hamiltonian leads in a straightforward manner to the following system of differential equations:

$$\begin{aligned} \frac{dQ}{dt} &= \frac{P}{M}; \quad \frac{dP}{dt} = -\mathscr{U}'(Q) + \sum_m M_m c_m \left(X_m - \frac{c_m Q}{\omega_m^2} \right) + zE_0 \sin(\omega t) \\ \frac{dX_m}{dt} &= \frac{P_m}{M_m}; \quad \frac{dP_m}{dt} = -M_m \omega_m^2 X_m + M_m c_m Q + z_m E_0 \sin(\omega t) \end{aligned} \tag{3.3}$$

From the second line, upon solving the second-order inhomogeneous ODE with the Green's function method, I get

$$X_m(t) = X_m(0)\cos(\omega_m t) + \frac{P_m(0)\sin(\omega_m t)}{M_m\omega_m} + \int_0^t \left[c_m Q(t') + \frac{z_m}{M_m}E_0\sin(\omega t')\right]\frac{\sin(\omega_m(t-t'))}{\omega_m}dt' \tag{3.4}$$

The integral $\int_0^t c_m Q(t')\sin(\omega_m(t-t'))/\omega_m dt'$ can be evaluated via integration by parts. Upon further denoting $E_m(t) = \int_0^t z_m E_0\sin(\omega t')\sin(\omega_m(t-t'))/\omega_m dt'$, I obtain

$$\begin{aligned} X_m(t) - \frac{c_m Q(t)}{\omega_m^2} &= \left(X_m(0) - \frac{c_m Q(0)}{\omega_m^2}\right)\cos(\omega_m t) \\ &+ P_m(0)\frac{\sin(\omega_m t)}{M_m\omega_m} - \int_0^t \frac{c_m P(t')\cos(\omega_m(t-t'))}{M\omega_m^2}dt' + \frac{E_m(t)}{M_m} \end{aligned} \tag{3.5}$$

Substituting Eq. (3.5) into the equation for $P(t)$ in Eq. (3.3), I derive the following GLE with AC electric field acting on the tagged particle:

$$\begin{aligned} \frac{dP}{dt} &= -\mathscr{U}'(Q(t)) - \sum_m \int_0^t \frac{M_m\cos(\omega_m(t-t'))}{M\omega_m^2}c_m^2 P(t')dt' + zE_0\sin(\omega t) \\ &+ \sum_m \left\{M_m c_m\left[X_m(0) - \frac{c_m Q(0)}{\omega_m^2}\right]\cos(\omega_m t) + c_m P_m(0)\frac{\sin(\omega_m t)}{\omega_m} + c_m E_m(t)\right\} \\ &= -\mathscr{U}'(Q(t)) - \int_0^t \nu(t')\frac{M_m P(t-t')}{M}dt' + zE_0\sin(\omega t) + F_P(t). \end{aligned} \tag{3.6}$$

I have introduced the noise or stochastic force $F_P(t)$ which is equal to the second line in Eq. (3.6):

$$F_p(t) = \sum_m \left\{M_m c_m\left[X_m(0) - \frac{c_m Q(0)}{\omega_m^2}\right]\cos(\omega_m t) + c_m P_m(0)\frac{\sin(\omega_m t)}{\omega_m} + c_m E_m(t)\right\}. \tag{3.7}$$

Note that this expression for the stochastic force is identical with the one derived in Zwanzig (2002) for a particle-bath system without external field, except for the important term $c_m E_m(t)$, which is new and contains the effect of the external AC field on the bath oscillators dynamics. This is a crucial point because the dynamical response of the bath oscillators to the external AC field in turn produces a modification of spectral properties of the bath fluctuations, and thus leads to a new form of the stochastic force which is different from those studied in previous works.

The memory function for the friction $\nu(t) = \sum_m M_m c_m^2 \cos(\omega_m t)/(M\omega_m^2)$ is identical to the memory function of systems without external time-dependent forces such as the one derived by Zwanzig (1973, 2002).

The fluctuation-dissipation theorem

The integral in the function $E_m(t) = \int_0^t z_m E_0 \sin(\omega t') \sin(\omega_m(t-t'))/\omega_m dt'$, can be evaluated using trigonometric identities, which leads to

$$E_m(t) = \frac{z_m E_0(\omega \sin(\omega_m t) - \omega_m \sin(\omega t))}{\omega_m(\omega^2 - \omega_m^2)}. \tag{3.8}$$

For the case without external time-dependent fields, $F_P(t)$ is defined in terms of initial positions and momenta of bath oscillators, but here it now also depends on the sinusoidal electric field at time t. Note that, by shifting the time origin, it can be easily verified that the statistical average is stationary. Following Zwanzig (2002), I assume the initial conditions for the bath oscillators can be taken to be Boltzmann-distributed $\sim \exp(-\mathscr{H}_B/k_B T)$, where the bath is in thermal equilibrium with respect to a frozen or constrained system coordinate $X(0)$.

Then for the averaged X and P, I obtain:

$$\left\langle X_m(0) - \frac{c_m Q(0)}{\omega_m^2} \right\rangle = 0, \quad \langle P_m(0) \rangle = 0. \tag{3.9}$$

The second moments are

$$\left\langle \left(X_m(0) - \frac{c_m Q(0)}{\omega_m^2} \right)^2 \right\rangle = \frac{k_B T}{M_m \omega_m^2}, \quad \langle P_m(0)^2 \rangle = M_m k_B T. \tag{3.10}$$

Both these results are consistent with what one finds for systems without external time-dependent fields, since obviously they descend directly from the assumption of Boltzmann-distributed degrees of freedom at the initial time.

As for $\sum_m c_m E_m(t)$, I first notice there is no divergence when $\omega_m \to \omega$ and $\omega_m \to 0$:

$$\begin{aligned} \lim_{\omega_m \to \omega} \frac{\omega \sin(\omega_m t) - \omega_m \sin(\omega t)}{\omega_m(\omega^2 - \omega_m^2)} &= -\frac{\omega t \cos(\omega t) - \sin(\omega t)}{2\omega^2}; \\ \lim_{\omega_m \to 0} \frac{\omega \sin(\omega_\alpha t) - \omega_m \sin(\omega t)}{\omega_m(\omega^2 - \omega_m^2)} &= \frac{\omega t - \sin(\omega t)}{\omega^2}. \end{aligned} \tag{3.11}$$

Focusing on ions, atoms or molecules, ω_m is at least in the THz regime or higher, which is many orders of magnitude larger than the frequency of the applied field ω (this assumption of course may not hold for THz spectroscopy, which deserves a separate treatment in future work). Hence, the first term in the numerator on the RHS of Eq. (3.8) can be neglected, and the electric effect on bath oscillators to the tagged particle can be approximated as follows:

$$\sum_m c_m E_m(t) \approx \sum_m \frac{c_m z_m}{\omega_m^2} E_0 \sin(\omega t) \propto E(t). \tag{3.12}$$

I now take the Boltzmann average of the stochastic force, Eq. (3.7), and find:

$$\langle F_P(t) \rangle = \zeta E(t), \tag{3.13}$$

for some constant ζ in unit of charge.

Now, by direct calculation, using Eqs. (3.9) and (3.10) and standard trigonometric identities, I can get the fluctuation-dissipation theorem (FDT) for the particle-bath Hamiltonian under a uniform AC field:

$$\begin{aligned}
&\langle F_P(t) F_P(t') \rangle = \frac{1}{Z_N} \int F_P(t) F_P(t') \exp\left(-\frac{\mathscr{H}_B}{k_B T}\right) d\vec{X}(0) d\vec{P}(0) \\
&= \sum_m \left(M_m c_m^2 \frac{k_B T}{\omega_m^2} \cos(\omega_m t) \cos(\omega_m t') + M_m c_m^2 \frac{k_B T}{\omega_m^2} \sin(\omega_m t) \sin(\omega_m t') \right) + (\zeta)^2 E(t) E(t') \\
&= k_B T \sum_m \frac{M_m c_m^2}{\omega_m^2} \cos(\omega_m (t - t')) + (\zeta)^2 E(t) E(t') \\
&= M k_B T \nu(t - t') + (\zeta)^2 E(t) E(t'),
\end{aligned} \tag{3.14}$$

where Z_N is the canonical partition function

$$Z_N = \int \exp\left(-\frac{\mathscr{H}_B}{k_B T}\right) d\vec{X}(0) d\vec{P}(0), \tag{3.15}$$

and $\vec{X}(0) = \{X_1(0), X_2(0), ...\}$, $\vec{P}(0) = \{P_1(0), P_2(0), ...\}$.

Compared with FDT without the presence of external field, namely Eq. (2.31), the 2nd term on the RHS of Eq. (3.14) is the additional effect from the field on the fluctuating force. I remark that this term has a deterministic component (via the correlation of the electric field), in the sense that couplings between the tagged particle and bath oscillators are also related to the distribution of bath oscillators, so ζ is not random. The noise intensity, defined as the covariance of the noise, is still proportional to T. In contrast, from the perspective of

the tagged particle, the influence from the electric field on bath oscillators is a part of noise on its motion, and the effect of the additional coupling is merely to renormalise the constant z in the equation of motion of the tagged particle, as can be seen in Eq. (3.6) and Eq. (3.13). Equation (3.14) is one of the key results I have found and is the FDT associated with the GLE given by Eq. (3.6). This is a remarkable result which shows that in the presence of an external AC field which affects the microscopic dynamics of both the tagged particle and the bath oscillators, the strength of the noise is no longer proportional to thermal energy only, but also has an important deterministic contribution proportional to the AC field amplitude squared.

The memory kernel

Let the spectrum be continuous and c_m be a function of eigenfrequency ω_p, which leads to the following expression for the friction kernel:

$$\nu(t) = \int_0^\infty \frac{M_p \gamma^2(\omega_p)}{M\omega_p^2} \cos(\omega_p t) D(\omega_p) d\omega_p. \tag{3.16}$$

For any given (well behaved) VDOS function $D(\omega_p)$, the existence of a well-behaved function $\gamma(\omega_p)$ that satisfies Eq. (3.16) is guaranteed by the fact that one can always decompose $\nu(t)$ into a basis of $\{\cos(\omega_p t)\}$ functions, by taking a cosine transform. The inverse cosine transform in turn gives the spectrum of coupling constants $\gamma(\omega_p)$ as a function of the memory kernel:

$$\gamma^2(\omega_p) = \frac{2\omega_p^2}{\pi D(\omega_p)} \int_0^\infty \nu(t) \cos(\omega_p t) dt. \tag{3.17}$$

This coupling function contains information on how strongly the particle's motion is coupled to the motion of other particles in a mode with vibrational frequency ω_p. This is an important information, because it tells us about the degree of long-range anharmonic couplings in the motion of the molecules.

Looking at Eq. (3.16) again, it is evident that the ZCL Hamiltonian does not provide any prescription to the form of the memory function $\nu(t)$, which can take any form depending on the values of the coefficients c_m, as is shown in Zwanzig (1973). Hence, a shortcoming of CL-type models, including ZCL, is that the functional form of $\nu(t)$ cannot be derived a priori for a given system, because, while the VDOS is certainly an easily accessible quantity from simulations of a physical system, the spectrum of coupling constants $\{c_m\}$ is basically a phenomenological parameter.

In general, the determination of the memory kernel is an open problem for which several approaches have been proposed very recently, most of which have been tested only on model systems so far, some examples can be found in Izvekov (2017); Jung et al. (2017); Li et al. (2016, 2017); Meyer et al. (2017). However, for a supercooled liquid, the time-dependent friction, which is dominated by slow collective dynamics, has been famously derived within kinetic theory (Boltzmann equation) using a mode-coupling type approximation by Sjogren and Sjolander (1979), and is given by the following elegant expressions:

$$\nu(t) = \frac{\rho k_B T}{6\pi^2 M} \int_0^\infty dq q^4 F_s(q,t)[c(q)]^2 F(q,t) \tag{3.18}$$

where $c(q)$ is the direct correlation function of liquid-state theory, $F_s(q,t)$ is the self-part of the intermediate scattering function (ISF), $F(q,t)$, and ρ is the density. All of these quantities are functions of the wavenumber q. Clearly, the integral over q leaves a time-dependence of $\nu(t)$ which is controlled by the product $F_s(q,t)F(q,t)$. For a chemically homogeneous system, $F_s(q,t)F(q,t) \sim F(q,t)^2$, especially in the long-time regime. From theory and simulations in supercooled liquids, Hansen and McDonald (2008) found $F(q,t) \sim \exp\left[-(t/\tau)^\xi\right]$. Hence, when I fit experimental data, I will take

$$\nu(t) = \nu_0 \sum_i \nu_i e^{-(t/\tau_i)^{b_i}}, \tag{3.19}$$

where τ_i is the characteristic time and ν_0 is a constant pre-factor. Here, $b_i > 0$ is positive, and $0 < \nu_i \leq 1$ indicate weights for each stretched exponential. A number of stretched exponentials are summed, which will be justified in detail when I apply this approach to specific examples. It will be shown that conceptually this approach is a great improvement on direct phenomenological fitting. It is possible to use other phenomenological fits for the memory function. However, improving the memory kernel goes beyond the scope of this thesis and I leave it for future work.

3.3 Deriving the dielectric permittivity from ZCL model

As is standard for normal mode analysis, I introduce the mass-scaled tagged-particle displacement $s = Q\sqrt{M}$ in the Hamiltonian, such that the resulting equation of motion, which is Eq. (3.6), under the mass-scaled coordinates, becomes

$$\ddot{s} = -\mathscr{U}'(s) - \int_0^t \nu(t-t')\frac{ds}{dt'}dt' + F_p(t) + zE(t). \tag{3.20}$$

Compared to Eq. (2.34), the last term on the RHS is an additional term relating to the system's response to external electric field, where the charge z has been redefined to be the mass-scaled charge. In order to determine the dependence of the polarisation and of the dielectric function on the frequency of the field in d-dimensional space, I have to describe the displacement $\mathbf{s}$ of each molecule from its own equilibrium position under the applied field $\mathbf{E}$. Upon treating the dynamics classically, the equation of motion for a charge I under forces coming from interactions with other charges and from the applied electric field is given by

$$\ddot{s}_I^\mu = -\sum_{J\nu} H_{IJ}^{\mu\nu} s_J^\nu - \int_0^t \nu(t-t') \frac{ds_I^\mu}{dt'} dt' + F_I^\mu(t) + z_I E^\mu(t). \tag{3.21}$$

where the pairwise interaction is assumed.

To solve this equation, the first step is to take the Fourier transform, $s_I^\mu(t) \to \tilde{s}_I^\mu(\omega)$, leading to the equation

$$-\omega^2 \vec{\tilde{s}} + i\omega\tilde{\nu}(\omega)\vec{\tilde{s}} + H\vec{\tilde{s}}_J = \vec{\tilde{F}}_I + z_I \vec{\tilde{E}} \tag{3.22}$$

where the tilde is used to denote Fourier-transformed variables. Hence, $\tilde{\nu}(\omega)$ is the Fourier transform of $\nu(t)$. Since the Hessian matrix is real and symmetric, I can implement normal-mode decomposition: $\hat{\tilde{s}}_m(\omega) = \sum_n \tilde{s}_n(\omega) e_{nm}$, where the hat is used to denote the coefficient of the projected quantity, e_{mn} consists of orthonormal eigenvectors of the Hessian matrix and m, n run from 1 to Nd. Then, I obtain

$$-\omega^2 \hat{\tilde{s}}_m + i\omega\tilde{\nu}(\omega)\hat{\tilde{s}}_m + \omega_m^2 \hat{\tilde{s}}_m = \hat{\tilde{F}}_m + (z\hat{\tilde{E}})_m. \tag{3.23}$$

The equation is solved by

$$\hat{\tilde{s}}_m(\omega) = -\frac{\hat{\tilde{F}}_m + (z\hat{\tilde{E}})_m}{\omega^2 - i\omega\tilde{\nu}(\omega) - \omega_m^2} \tag{3.24}$$

Transforming back to a vector equation for the Fourier-transformed displacement of charge I, I have:

$$\tilde{s}_I^\mu(\omega) = \sum_m -\frac{e_{mn}\left[\hat{\tilde{F}}_m + (z\hat{\tilde{E}})_m\right]}{\omega^2 - i\omega\tilde{\nu}(\omega) - \omega_m^2} \tag{3.25}$$

Here, indices n and (I, μ) are mutually related in an implicit way. Each particle contributes to the polarisation a moment $\mathbf{p}_I = z_I \mathbf{s}_I$. In order to evaluate the macroscopic polarisation, I need to add together the averaged contributions from all microscopic degrees of freedom in the system, $\mathbf{P} = \sum_I \mathbf{p}_I$. In order to do this analytically, I use Eqs. (3.13) and (3.25) to

obtain the averaged polarisation before performing the standard procedure of replacing the discrete sum over the total degrees of freedom of the solid with the continuous integral over the eigenfrequencies $\omega_m, \sum_m ... \rightarrow \int D(\omega_p)...d\omega_p$, which gives the following sum rule in integral form for the polarisation in glasses:

$$\tilde{\mathbf{P}}(\omega) = -\left[\int_0^{\omega_D} \frac{D(\omega_p)\Gamma'(\omega_p)}{\omega^2 - i\omega\tilde{\nu}(\omega) - \omega_p^2} d\omega_p\right] \tilde{\mathbf{E}}(\omega) \tag{3.26}$$

Here, ω_D is the cutoff Debye frequency arising from the normalisation of the VDOS (i.e. the highest eigenfrequency in the VDOS spectrum). The smooth correlator function $\Gamma'(\omega) \equiv \langle \hat{z}_m^2 + \zeta \hat{z}_m \rangle_{\omega_m \in \{\omega, \omega+\delta\omega\}}, \hat{z}_m = \vec{z} \cdot \vec{e}_m$ with $\vec{z}$ generalised to be an Nd-vector, is defined in a similar way in mechanical case (see Section 2.4 for details). Note that, I have also taken the ensemble average over the system. The complex dielectric permittivity ε is defined as $\varepsilon = 1 + 4\pi\chi_e$, where χ_e is the dielectric susceptibility which connects the polarisation and electric field as $\mathbf{P} = \chi_e \mathbf{E}$ (Born and Wolf, 1999). Within the extended Lorentz model, the dielectric function is finally expressed as a frequency integral as

$$\begin{aligned} \varepsilon(\omega) &= 1 - \int_0^{\omega_D} \frac{AD(\omega_p)}{\omega^2 - i\omega\tilde{\nu}(\omega) - \omega_p^2} d\omega_p, \\ \text{with} \quad A &\equiv 4\pi\Gamma'(\omega_p). \end{aligned} \tag{3.27}$$

In general, A will depend on the material chemistry since it depends on intermolecular forces through Γ'. However, in real experiments, the dielectric permittivity usually takes arbitrary units. Thus, A will be the free fitting parameter when I use Eq. (3.27) in practice. Clearly, if $D(\omega_p)$ were given by a Dirac delta, one would recover the standard simple-exponential (Debye) relaxation for small ω. Note that, this approach can be extended to deal with molecules that have stronger inner polarisability by replacing the external field field $\mathbf{E}$ with the local electric field $\mathbf{E}_{loc}$, which has been studied in Froehlich (1958). In condensed matter systems, the electric field that effectively acts on a molecule locally is equal to the external field only in the limit of vanishing polarisability of the molecule. This is a well-known effect whereby the field in the medium is affected (diminished) by the local alignment of the polarised molecules. The simple Lorentz cavity model works well in materials where the building blocks are not pathologically shaped or anisotropic, and is applicable to random isotropic distribution of the building blocks. Without loss of generality, I present an analysis for the case of Markovian friction $\nu = const$. The derivation of the local field or Lorentz

field can be found in many textbooks,

$$\mathbf{E}_{loc} = \mathbf{E} + \frac{4\pi}{3}\mathbf{P}. \tag{3.28}$$

As a consequence, replacing $\mathbf{E}$ with $\mathbf{E}_{loc}$, I write the equation of motion as (noise excluded)

$$\tilde{\mathbf{s}}_I'(\omega) = -\frac{z_I}{\omega^2 - i\omega\nu - \omega_m^2}\left(\tilde{\mathbf{E}}(\omega) + \frac{4\pi}{3}\tilde{\mathbf{P}}(\omega)\right). \tag{3.29}$$

Combining the above relations together and summing over all contributions from all the building blocks, I obtain

$$\begin{aligned}
&\mathbf{P} = \left(\sum_I z_I \mathbf{s}_I' + c\mathbf{E}_{loc}\right); \quad \varepsilon(\omega) = 1 - \frac{\chi(\omega) - 4\pi c}{1 + \frac{1}{3}\chi(\omega) + 4\pi c};\\
&\chi(\omega) = \int_0^{\omega_D} \frac{AD(\omega_p)}{\omega^2 - \omega_p^2 + i\omega\nu} d\omega_p,
\end{aligned} \tag{3.30}$$

where the total polarisation comes from the additional effect from the local electric field and c is the microscopic electronic polarisability and I used $\mathbf{D} = \varepsilon\mathbf{E} = \mathbf{E} + 4\pi\mathbf{P}$. I have checked that accounting for the Lorentz field and using Eq. (3.30) for the fitting produces very similar results and will not alter the fitting of the dielectric relaxation data qualitatively.

If I use a VDOS obtained numerically from a system with a finite number of particles in simulations, for example, the random networks in Section 3.1, then it is important to correctly take care of finite size effects in Eq. (3.27). Recall if a finite number of particles is used in such simulations, the VDOS $D(\omega_p)$ is not a continuous function, but discrete, which is $D(\omega_p) \sim \sum_m \delta(\omega_p - \omega_m)$. Thus, I rewrite Eq. (3.27) as a sum rule over a discrete distribution of ω_m:

$$\varepsilon(\omega) = 1 - \sum_m \frac{A}{\omega^2 - i\omega\tilde{\nu}(\omega) - \omega_m^2} \tag{3.31}$$

where A has absorbed the scaling constant. Since the dielectric function is a complex quantity, I split it into its real and imaginary parts, i.e. $\varepsilon(\omega) = \varepsilon'(\omega) - i\varepsilon''(\omega)$:

$$\varepsilon'(\omega) = \varepsilon_\infty' + \sum_m \frac{A_1(C^2\omega_m^2 - \omega^2 + \tilde{\nu}_2(\omega)\omega)}{(C^2\omega_m^2 - \omega^2 + \omega\tilde{\nu}_2(\omega))^2 + (\omega\tilde{\nu}_1(\omega))^2}, \tag{3.32}$$

$$\varepsilon''(\omega) = \sum_m \frac{A_2(\omega\tilde{\nu}_1(\omega))}{(C^2\omega_m^2 - \omega^2 + \omega\tilde{\nu}_2(\omega))^2 + (\omega\tilde{\nu}_1(\omega))^2}. \tag{3.33}$$

Recall that parameter C relates vibrational frequencies between realistic systems and simulations; $\tilde{\nu}_1$ and $\tilde{\nu}_2$ are real and (minus) imaginary parts of $\tilde{\nu}(\omega)$ in Fourier space, $\tilde{\nu}(\omega) =$

$\tilde{\nu}_1(\omega) - i\tilde{\nu}_2(\omega)$. The Markovian friction case is retrieved by simply setting $\tilde{\nu} = \tilde{\nu}_1 = const$ in the above expressions. $A_1, A_2, \varepsilon'_\infty$ are re-scaling constants that need to be calibrated in the comparison with experimental data. It is important to note that the experimental data of dielectric permittivity and dielectric loss are not necessarily given in the same units and there is, in general, no coherence between the offsets in the plots of the ε' and ε'' curves. For this reason, values of A_1 and A_2 do not necessarily coincide.

The linear behaviour of ε'' when $\omega \to 0$

Observed in all numerical calculations of the VDOS in the vicinity of the mechanical stability point of disordered solids, there exists a lowest non-zero eigenfrequency $\omega_{min} \ll 1$, and a vanishingly small gap between $\omega_0 = 0$ and ω_{min}. Recent studies, e.g. Lerner et al. (2016); Schwartzman-Nowik et al. (2019), have pointed out that a scaling $D(\omega_p) \sim \omega_p^4$, is possibly related to soft anharmonic modes. I perform an asymptotic analysis of the limiting behaviour of $D(\omega_p)$ at $\omega_p \to 0$ in the context of the dielectric response, which clearly shows that only asymptotic scalings $D(\omega_p) \sim \omega_p^n$, with $n > 3$ can lead to meaningful behaviour of $\varepsilon''(\omega)$.

I specialise on the Markovian case $\nu = const$ and take the limit $\omega \to 0$ in Eq. (3.27):

$$\lim_{\omega\to 0} \varepsilon(\omega) = \lim_{\omega\to 0} \left(1 - \int_0^{\omega_D} \frac{AD(\omega_p)}{\omega^2 - i\omega\nu - \omega_p^2} d\omega_p \right) = 1 - A \lim_{\omega\to 0} \int_0^{\omega_D} \frac{D(\omega_p)}{\omega^2 - i\omega\nu - \omega_p^2} d\omega_p. \tag{3.34}$$

I can expand $D(\omega_p)$ around $\omega_p = 0$:

$$D(\omega_p) = D(0) + D'(0)\omega_p + \frac{D''(0)}{2}\omega_p^2 + \frac{D^{(3)}(0)}{6}\omega_p^3 + ... \tag{3.35}$$

Thus, after substituting Eq. (3.35) into Eq. (3.34), I have

$$\begin{aligned}
&\lim_{\omega\to 0}\varepsilon(\omega) = 1 - A\lim_{\omega\to 0}\int_0^{\omega_D}\frac{D(0)+D'(0)\omega_p+\frac{D''(0)}{2}\omega_p^2+\frac{D^{(3)}(0)}{6}\omega_p^3+\ldots}{\omega^2-i\nu\omega-\omega_p^2}d\omega_p\\
&= 1 - A\lim_{\omega\to 0}\int_0^{\omega_D}\frac{\left[D(0)+D'(0)\omega_p+\frac{D''(0)}{2}\omega_p^2+\frac{D^{(3)}(0)}{6}\omega_p^3+\ldots\right](\omega^2+i\nu\omega-\omega_p^2)}{\omega^4-2\omega^2\omega_p^2+\omega_p^4+\omega^2\nu^2}d\omega_p\\
&= 1 - A\lim_{\omega\to 0}\int_0^{\omega_D}\frac{W_0(\omega)+W_1(\omega)\omega_p+W_2(\omega)\omega_p^2+W_3(\omega)\omega_p^3+\ldots}{\omega^4-2\omega^2\omega_p^2+\omega_p^4+\omega^2\nu^2}d\omega_p
\end{aligned}$$

where I denote:

$$\begin{aligned}
&W_0(\omega) = D(0)(\omega^2+i\nu\omega), \quad W_1(\omega) = D(0)'(\omega^2+i\nu\omega),\\
&W_2(\omega) = -D(0)+\frac{D(0)''}{2}(\omega^2+i\omega), W_3(\omega) = \frac{(\omega^2+i\nu\omega)D^{(3)}(0)}{6}-D'(0).
\end{aligned} \tag{3.36}$$

In order to let the integrand be continuous for both real and imaginary parts, I require $(\omega,\omega_p)\in\mathscr{R}^+\cup\{0\}\times\mathscr{R}^+\cup\{0\}$, such that it makes sense to change the order of integration/limit at $(0,0)$, so $D(\omega_p)\to 0, D'(\omega_p)\to 0, D''(\omega_p)\to 0, D^{(3)}(\omega_p)\to 0$ as $\omega_p\to 0$. There is no restriction for $D^{(4)}(\omega_p)$ or higher order. Hence, we must have $D(\omega_p)\sim\omega_p^n$ for $n>3$. As for the scaling of ε'' for small ω, which will be shown shortly, I set $D(\omega_p)\sim\omega_p^4$ to study the behavior of

$$\lim_{\omega\to 0}\int_0^{\omega_D}\frac{\omega_p^4}{\omega^2-i\nu\omega-\omega_p^2}d\omega_p. \tag{3.37}$$

To give a trivial example for the asymptotic analysis, I take $\omega_D = v = 1$, and the integral can be evaluated analytically to the following expression

$$\varepsilon''(\omega) = \int_0^1\frac{\omega\omega_p^4}{(\omega_p^2-\omega^2)^2+\omega^2}d\omega_p \tag{3.38}$$

$$= \omega+\frac{1}{2}\left((\omega^2+i\omega)^{3/2}\arctan\left[\frac{i}{\sqrt{\omega^2+i\omega}}\right]-(\omega^2-i\omega)^{3/2}\arctan\left[\frac{i}{\sqrt{\omega^2-i\omega}}\right]\right) \tag{3.39}$$

from which I obtain

$$\varepsilon''(\omega)\approx\omega+\frac{\pi}{4}((\omega^2+i\omega)^{3/2}-(\omega^2-i\omega)^{3/2}) \tag{3.40}$$

and hence $\varepsilon''(\omega)\sim\omega$ in the limit of small frequency. This finding lends further support to this form of the VDOS in the zero frequency limit, and I therefore use this scaling in the finite-size gap between $\omega_0 = 0$ and ω_{min}, which results in a linear behaviour of the left flank

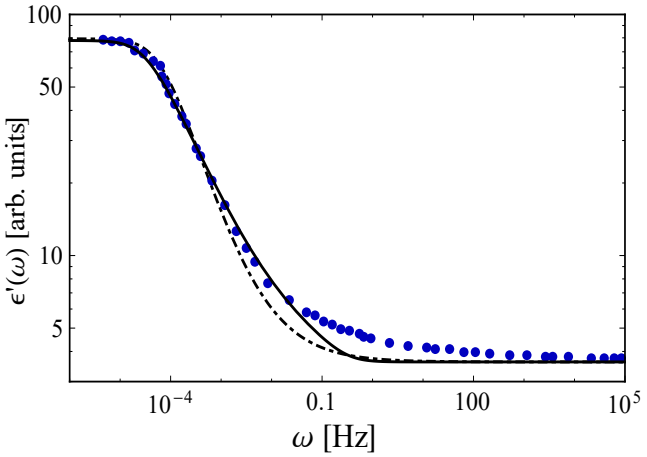

Fig. 3.5 Real part of the dielectric function as a function of the frequency of the applied field. Symbols are experimental data of the real part of the dielectric function of glycerol at $T = 184$K from Lunkenheimer et al. (2000). The solid line is the theoretical calculation for the Markovian friction case, i.e. $\nu = const$ in Eq. (3.32). The dot-dashed line is the real part of the Fourier transform when I consider the best-fitting (empirical) stretched-exponential function with $\beta = 0.65$ and $\tau = 6555$. I have taken $C = 10, \nu = 1620$ and $A_1 = 0.039$. Rescaling constants are used to adjust the height of the curves.

of the α-peak in $\varepsilon''(\omega)$ in perfect agreement with experimental data, which will be shown in the next section.

It is important to emphasise that in Eq. (3.27), low-frequency soft modes which present in $D(\omega_p)$ necessarily play an important role also at low field frequencies ω, because of the ω^2 term in the denominator. As we will see, this fact in the theory implies a direct role of the boson peak on the low-frequency part of the dielectric relaxation, and in particular on the α-relaxation process.

3.4 α-relaxation in dielectric response of glassy glycerol

I firstly present theoretical fittings of experimental data (Lunkenheimer et al., 1996, 2000) on glycerol at $T \approx T_g$ using Eqs. (3.32,3.33), also in comparison with the empirical best-fitting using Kohlrausch stretched-exponential relaxation, namely $\varepsilon(t) \sim \exp[-(t/\tau)^\beta]$.

In Fig. 3.5, I plot the comparisons for $\varepsilon'(\omega)$ at $T = 184\,K$, i.e. slightly below T_g, obtained by implementing the numerical VDOS of Fig. 3.2 for $Z = 6.1$ in Eq. (3.32). In this case, it is clear that the theoretical model performs significantly better than the Kohlrausch best-fitting (that is optimised for the joint fitting of dielectric loss below). This suggests that excess soft modes are important for the fitting of the dielectric response at the glass transition.

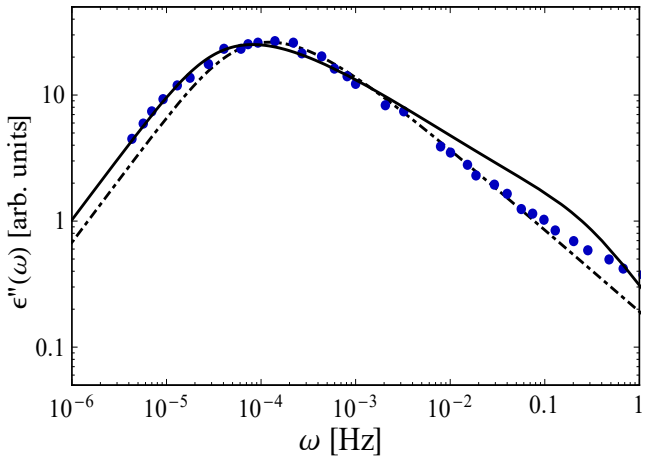

Fig. 3.6 Dielectric loss modulus as a function of the frequency of the applied field. Symbols are experimental data of the imaginary part of dielectric function of glycerol at $T = 184$K from Lunkenheimer et al. (2000). The solid line is the theoretical calculation for the Markovian friction case, i.e. $\nu = const$ in Eq. (3.33). The dot-dashed line is the imaginary part of the Fourier transform when I consider the best-fitting (empirical) stretched exponential (Kohlrausch) function with $\beta = 0.65$ and $\tau = 6555$. In the calculation, I have taken $C = 10, \nu = 1620$ and $A_2 = 0.0437$. Rescaling constants are used to adjust the height of the curves.

In Fig. 3.6, I present fittings of the dielectric loss, $\varepsilon''(\omega)$ for the Markovian case $\tilde{\nu} = \tilde{\nu}_1 = const$ in Eq. (3.33). In this case, it is seen that the framework, even in its Markovian-friction version, provides a reasonably good fitting of the α-peak on both the left-hand and the right-hand side of the peak, and the overall quality of the fitting is comparable to one of the Kohlrausch best empirical fittings. The theoretical model provides the crucial connection between the salient features of the VDOS near T_g and the corresponding features of the response. Of course, at the higher-frequency end of the α-wing, other effects may as well be important which are not described by the model: in particular, the existence of Johari-Goldstein β-relaxation-type contributions to the loss modulus in this regime has been shown for a variety of systems (Blochowicz and Rössler, 2004; Döß et al., 2002; Mattsson et al., 2003; Paluch et al., 2001; Schneider et al., 2000).

On the left-hand ascending side of the peak, the scaling $D(\omega_p) \sim \omega_p^4$ leads to the linear behaviour $\sim \omega^1$, as being analysed in the last section, for the ascending part of the peak. On the high-ω side of the peak, where the dynamics is dominated by the soft boson-peak modes and the VDOS is approximately flat as a function of ω_p in Fig. 3.2, the model, reproduces, remarkably, the asymmetric α-wing behaviour, still in good agreement with the experimental data.

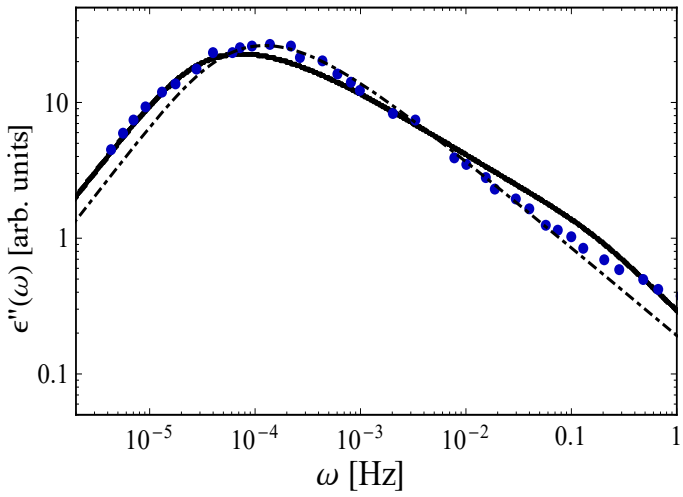

Fig. 3.7 Dielectric loss modulus as a function of the frequency of the applied field. Symbols are experimental data of the imaginary part of dielectric function of glycerol at $T = 184$K from Lunkenheimer et al. (2000). The solid line is the theoretical description presented in this work for the non-Markovian friction case, i.e. $\tilde{\nu}(\omega)$ in Eq. (3.33) is the Fourier transform of $\nu(t) = \nu_0 \exp(-4t^b)$. The dot-dashed line is the imaginary part of the Fourier transform when I consider the best-fitting (empirical) Kohlrausch relaxation function $\varepsilon(t) \sim \exp[-(t/\tau)^\beta]$ with $\beta = 0.65$ and $\tau = 6555$. In the calculation, I have taken $C = 10$, $A_2 = 0.0437$ and $b = 0.3$. Rescaling constants are used to adjust the height of the curves.

In Fig. 3.7, I present the same fitting, but now with a non-Markovian friction given by $\nu(t) = \nu_0 \exp(-4t^b)$ used in Eq. (3.33), with $b = 0.3$ suggested by previous studies on glassy dynamics (Hansen and McDonald, 2008). Overall, the non-Markovian friction provides a better fitting, especially on the large frequency regime, which suggests that memory effects in the atomic dynamics are non-negligible. However, the memory kernel due to non-Markovian friction does not appear to be essential to generate and reproduce the α-wing asymmetry, which emerges in Fig. 3.6.

This comparative analysis therefore demonstrates quite clearly that while memory effects are important, the main cause for the α-wing asymmetry is the excess of soft vibrational modes in the VDOS, which is a very important outcome of my study.

3.5 Dielectric relaxation in the time domain

It is also interesting to have the dielectric response in the time domain. In order to keep the derivation amenable to analytical treatment, I focus on the case of Markovian friction, $\nu = const$. The time dependent dielectric function $\varepsilon(t)$ and complex dielectric function $\varepsilon(\omega)$

are related as:

$$\frac{d\varepsilon(t)}{dt} = \frac{1}{2\pi}\int_{-\infty}^{\infty}(\varepsilon(\omega)-\varepsilon_{\infty})e^{i\omega t}d\omega; \quad \varepsilon(\omega) = \varepsilon_{\infty} - \int_{0}^{\infty}\frac{d\varepsilon(t)}{dt}e^{-i\omega t}dt. \tag{3.41}$$

Recall that the Fourier transform of a function $f(t)$, in this thesis, is defined as:

$$\tilde{f}(\omega) = \int_{-\infty}^{\infty} f(t)e^{-i\omega t}dt \tag{3.42}$$

while the inverse Fourier transform is

$$f(t) = \frac{1}{2\pi}\int_{-\infty}^{\infty}\tilde{f}(\omega)e^{i\omega t}d\omega. \tag{3.43}$$

I firstly need to find the time derivative of $\varepsilon(t)$:

$$\begin{aligned}\frac{d\varepsilon(t)}{dt} &= -\frac{1}{2\pi}\int_{0}^{\infty}\int_{0}^{\omega_D}\frac{AD(\omega_p)e^{i\omega t}}{\omega^2-(C\omega_p)^2-i\omega\nu}d\omega_p d\omega \\ &= \int_{0}^{\omega_D}AD(\omega_p)\int_{0}^{\infty}-\frac{1}{2\pi}\frac{e^{i\omega t}}{\omega^2-(C\omega_p)^2-i\omega\nu}d\omega d\omega_p.\end{aligned} \tag{3.44}$$

Note that, for the inner integration, $\int_0^{\infty} -e^{i\omega t}/(\omega^2-(C\omega_p)^2-i\omega\nu)d\omega$, one could make an analytic continuation of ω to the complex plane and use contour integration to evaluate the Bromwich integral. However, I can achieve the same result via a simpler route just using the Fourier inversion theorem (Folland, 1992), where the uniqueness of the inverse Fourier transform is ensured. If we can find a function of time, whose Fourier transformation gives back the complex dielectric function $\varepsilon(\omega)$, then this function would be the time derivative of the dielectric relaxation $\varepsilon(t)$. I use the following ansatz

$$\frac{e^{-\xi t}\sin(\iota t)}{\iota}H(t) \tag{3.45}$$

where $\xi = \nu/(2M)$ and $\iota = [\nu^2/(4m^2)-(C\omega_p)^2]^{1/2}$, whose Fourier transformation is expressed as $1/(\omega^2 - i\nu\omega - (C\omega_p)^2)$.

However, we need to put care in taking $\nu \gg 2mC\omega_D$, which amounts to restricting our analysis to the high-friction overdamped dynamical regime. In this way, I finally obtain, upon integrating over t,

$$\varepsilon(t) = B + \int_{0}^{\omega_D}\frac{AD(\omega_p)}{2\iota}\left(\frac{e^{(\iota-\nu/2m)t}}{\iota-\nu/2m}+\frac{e^{-(\iota+\nu/2m)t}}{\iota+\nu/2m}\right)d\omega_p, \tag{3.46}$$

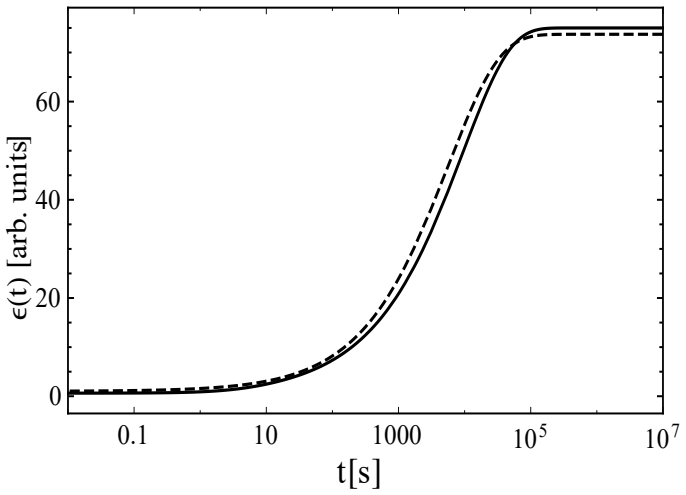

Fig. 3.8 Time-dependent dielectric response. The solid line is calculated using Eq. (3.46) with physical parameters calibrated in the fitting of Fig. 3.5. The dashed line represents the stretched-exponential Kohlrausch function that more closely approximates our prediction, calculated using the parameters $\beta = 0.56$ and $\tau = 5655$. Rescaling constants are used to adjust the height of the curves.

where B is a re-scaling constant. This equation is a key result: it provides a direct and quantitative relation between the macroscopic relaxation function of the material and the VDOS. The presence of a boson peak in $D(\omega_p)$ directly causes stretched-exponential decay in $\varepsilon(t)$ via Eq. (3.46).

In Fig. 3.8, I plot predictions of Eq. (3.46) with the parameters calibrated in the glycerol data fitting for the case $\nu = const$, along with the Kohlrausch function (Montroll and Bendler, 1984), for the relaxation in the time domain. It is seen that the description based on soft modes is able to perfectly recover stretched-exponential relaxation, with stretching-exponent $\beta = 0.56$, over many decades in frequency. Without the boson-peak modes in the VDOS, I have checked that stretched-exponential relaxation cannot be recovered, and the decay is simple-exponential. Hence, Eq. (3.46) provides the long-sought cause-effect relationship between soft modes and stretched-exponential relaxation, even for the simple case of Markovian friction where the response is clearly dominated by the VDOS.

3.6 Secondary dielectric relaxation in glassy Freons

Compared with glycerol whose experimental data of VDOS is absent, for two Freons, I instead utilise the VDOS measured in experiments at $T = 10$K. For F113, I use only one

Temperature	91K	115K	131K
b_1	0.45	0.625	0.7
τ_1 (seconds)	0.558	$3.12 \cdot 10^{-7}$	$6.99 \cdot 10^{-9}$
b_2	0.2	0.56	
τ_2 (seconds)	$1.55 \cdot 10^{-2}$	$5.48 \cdot 10^{-8}$	
ν_0	$4 \cdot 10^6$	$3.9 \cdot 10^6$	$6.3 \cdot 10^6$

Table 3.1 Parameters of the memory function for Freon 112.

Temperature	72K	74K	76K
b	0.26	0.3	0.35
τ (seconds)	7.133	0.326	$2.38 \cdot 10^{-2}$
ν_0	$8.28 \cdot 10^6$	$7.28 \cdot 10^6$	$6.28 \cdot 10^6$

Table 3.2 Parameters of the memory function for Freon 113.

stretched exponential term in the memory $\nu(t)$. For F112, if a secondary (β) relaxation is investigated, then $\nu(t)$ is the sum of two terms, both of which are in forms of stretched exponential. The first term represents mainly the α-process although it also affects the β-relaxation (while the second term describes only β-relaxation). Thus, the time-scale of β-relaxation is not directly related to the time-scale of the second stretched exponential parameter, τ_2. This amounts to the fact that β-relaxation is a process which is cooperative and at the same time quasilocalised. That is, on one hand β-relaxation is known to be related to jumps across local wells within the same metabasin. On the other hand, my analysis will show that there is a memory function related to β-relaxation, which is a stretched exponential. This stretched exponential may arise from the distribution of these jumping rates (possibly related to the coupling spectrum) but this would be ascertained in future work. The link between α-relaxation time and stretched exponential relaxation is well known empirically from modeling of experimental data, and this has been shown many times on many different glass forming systems (Ngai, 2011). My model puts this fact within a first-principle theoretical framework of GLE, which has not been done before. For the β-relaxation, the memory function with two stretched exponentials comes directly from the fitting of the experimental data with the GLE. To my knowledge, it has not been possible to fit the experimental data with different forms, so this provides the underpinning for the form of memory function, which is the first attempt to model dielectric relaxation with GLE semi-analytical approach. Fitting parameters for F112 and F113 at different temperatures are listed in Table 3.1 & 3.2 and resulting fittings of dielectric loss are displayed in Fig. 3.9.

For the fitting procedure, I have assumed that $D(\omega_p)$ and the overall scaling for the height of curve, A, are temperature-independent. To physically understand the difference between F112 and F113, their dynamical coupling parameters, which is Eq. (3.17), have

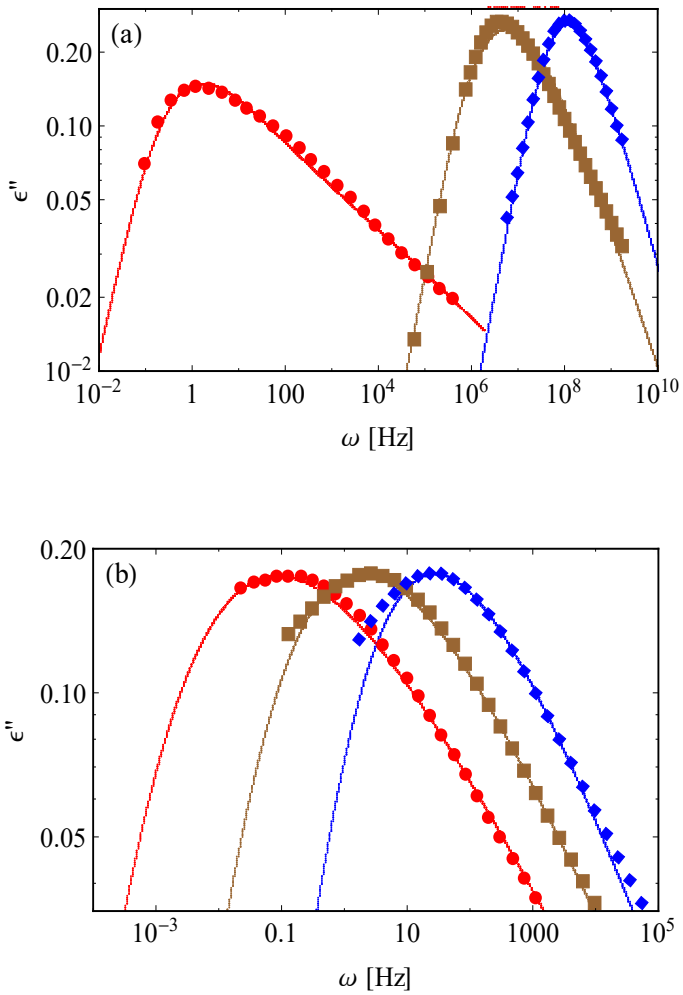

Fig. 3.9 Fitting of experimental data using the proposed theoretical model for Freon 112 (top) at 91 K (red circles), 115 K (brown squares) and 131 K (blue diamonds) and for Freon 113 (bottom) at 72 K (red circles), 74 K (brown squares) and 76 K (blue diamonds). Solid lines are the theoretical model presented here. A rescaling constant was used to adjust the height of the curves since the data are in arbitrary units. Experimental data for Freon 112 were taken from Pardo et al. (2006), while data for Freon 113 were taken from Vispa et al. (2017).

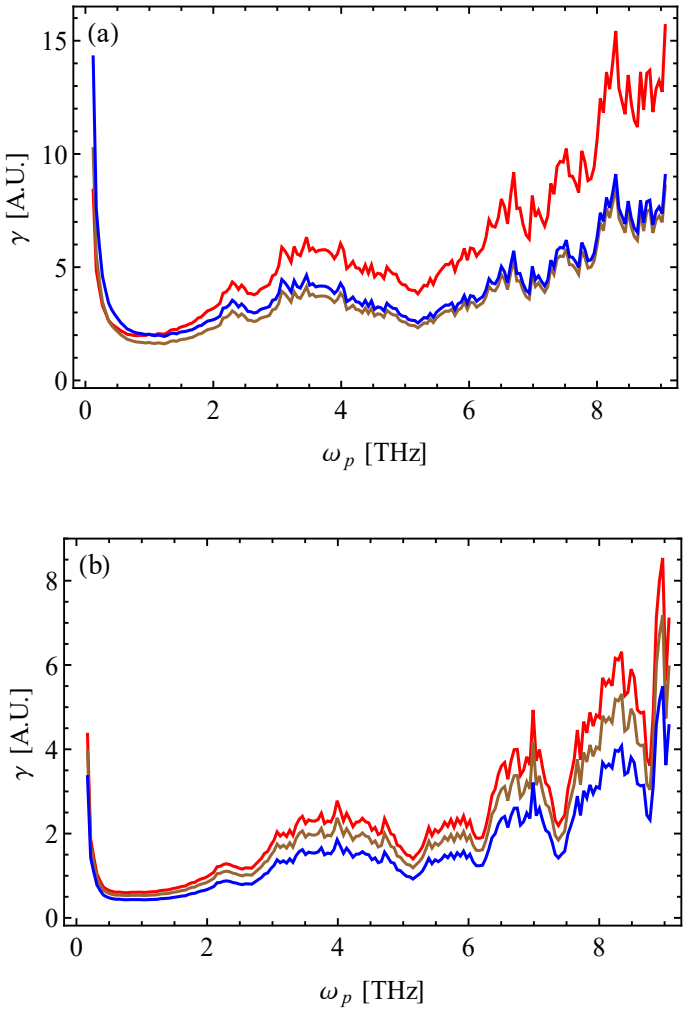

Fig. 3.10 Spectrum of coupling constants of Freon 112 (top) and Freon 113 (bottom) as a function of the vibrational eigenfrequency computed according to Eq. (3.17) using the phenomenological memory functions $\nu(t)$ used in the fitting of dielectric response in Fig. 3.9, with same colour settings for the different temperatures.

been analysed, as is shown in Fig. 3.10. In general, the coupling spectrum decays from the highest Debye cut-off frequency of short-range high-frequency in-cage motions, down to the low eigenfrequency part where the coupling goes up with decreasing ω_p towards zero, due to phonons or phonon-like excitations, which are collective and long-wavelength and hence result in a larger value of γ.

There is a substantial difference between F112 and F113, especially in the middle part of the coupling spectrum where F112 shows much stronger coupling, which corresponds to medium-range correlated motions. This means that motions are strongly coupled also in the intermediate eigenfrequency domain, where modes are typically quasilocalised, which corresponds to mesoscopic string-like motions typically associated with β-relaxation. In addition, the F113 spectrum is overall comparatively much lower in that energy regime, which clearly indicates that, for F113, the intermediate part of the coupling spectrum, i.e. the one of mesoscopic and string-like motions, is scarcely populated and one has a steep decay from the short-range high-frequency in-cage motions to the long-wavelength phonon-like excitations, with not much in between in the mesoscopic range. Hence in F113, the anharmonicity is much less prominent and intermediate excitations are not important. This origin of the secondary relaxation aligns with the simulation results of Cohen et al. (2012); Widmer-Cooper et al. (2008), which point at the cooperative, though localised or quasilocalised, nature of secondary relaxation. This also gives insights into the difference in the form of the memory function used for the fittings of the two Freons. Upon focusing on the integration in Eq. (3.17): the integral of $\nu(t)$ from 0 to ∞ increases from high ω_p (short-range and fast vibration) to low ω_p (long-range and slow vibration), because for slow collective vibration there is clearly much more extended friction due to contact between many particles all moving at the same time. Thus, the integral factor definitely contributes to the coupling being overall stronger for F112 than for F113. However, also the boson peak contributes to the coupling of F112 being larger than that of F113 (via the VDOS in the denominator of Eq. (3.17)) in the specific frequency range that corresponds to the boson peak). The boson peak maximum (in $D(\omega_p)/\omega_p^2$, not shown) for both materials is of the order of $2-3$ meV, i.e., $\approx 0.5-0.7$ THz, which corresponds virtually to the lowest minimum in the coupling function (see Fig. 3.10) where, in addition, the minimum value is much lower for F113 (with larger boson peak) than for F112. That means that in such region not only there are larger dynamical couplings for F112 due to stronger medium-range correlations/anahrmonicity, in general, but also for the additional effect of boson peak (soft weakly-coupled modes, see Fig. 3.3) being smaller for F112 in that regime of vibrations.

As far as temperature effects on the coupling strength are concerned, I need to point out first that, due to the fragility difference between the two Freons, the temperature range in

which fittings were performed are noticeably different. For F113 ($T_g = 71$ K) experimental dielectric functions are available at the highest reduced temperature of $T_r = 76/71 = 1.07$, whereas for F112 ($T_g = 90$ K) the highest value is around $T_r = 131/90 = 1.46$. Bearing this in mind, it can be noticed that upon increasing temperature, the "going up" tail at decreasing ω_p towards zero becomes smaller, which means less phonon-like modes. In general, absolute coupling values shift down (lower coupling) with the increase of temperature, as expected, and the decay of correlated motions from high ω_p to low ω_p becomes also somewhat steeper with increasing T (Cui et al., 2018b).

The stronger coupling between collective and individual motions for F112 could be a physical explanation of why in the dielectric study of F112 in Pardo et al. (2006), the authors described so many problems to discern α- from β-relaxation. For F112 collective vibrations, medium-ranged and slow motions are much more important than for F113, in such a way that individual molecular motions (β-relaxation) should correlate, i.e. are much more coupled, with motions of surrounding molecules (collective motions associated with the α-relaxation) for F112 than for F113. And, even more, if slow vibrations are more important and more heterogeneous in F112, this should mean stronger couplings between collective and individual motions, so then, much more phonon scattering for F112 and, as a consequence, lower thermal conductivity for F112 than for F113, as it has been experimentally shown. For example, see Fig. 5 in Vdovichenko et al. (2015). In addition, it should be emphasised that the higher thermal conductivity for F113, analysed in terms of the soft-potential model, was also attributed to the low coupling strength between sound waves and the soft quasilocalised modes. Moreover, the dynamical coupling function γ extends over a frequency range much broader than that of the boson peak, and thus the role of the boson peak is confined to a specific frequency range which is around the minimum in the coupling spectrum. The fact that boson peak is stronger for F113 leads to a lower coupling in that region and contributes to the already lower coupling of F113 compared to F112 in that region. Because the boson peak is associated with soft modes, which "break" the coherence of phonons (hence more phonon scattering), it leads to even lower coupling in the boson peak frequency range for F113 compared to F112.

Summary

Starting from the same presumption of Goetze (2008) that dielectric relaxation emerges from many-body dynamics in a statistical way, transcending the details of charge transport, I have built up a model for the dielectric response of simple glass-formers. The model effectively

accounts for the medium and long-range anharmonic coupling among molecular degrees of freedom and allows one to disentangle α- and β-relaxation on the basis of the extent of dynamical coupling in different eigenfrequency sectors of the vibrational spectrum.

Chapter 4

Nonaffinity in non-centrosymmetric medium

In both glasses and athermal granular solids, and unlike ordinary solids (e.g. crystals), the elasticity, mechanical stability and deformation behaviour are strongly affected by internal stresses, and by the local stress transmission, in the form of force-chains or central-force random networks (Geng et al., 2003; Kondic et al., 2012; Majmudar and Behringer, 2005). Indeed, glasses can be described as emerging from the liquid through a mechanism of vitrification that can rationalise history-dependence and frozen stresses (Ballauff et al., 2013; Fuchs and Cates, 2002). In order to elucidate the elasticity of amorphous solids in a unifying framework, the two most studied paradigms of amorphous solids are given by random networks, which is a model for biological filaments such as the cytoskeleton, and other polymer-based materials and random sphere packings, a model for granular materials and jammed matter (Levine and Lubensky, 2000; O'Hern et al., 2003) .

While numerical simulations have substantially confirmed the picture emerging from experimental characterisation of force transmission in granular and disordered materials, theory has somehow been left behind, with few exceptions (Blumenfeld, 2004). The central problem is that it is very difficult to incorporate stress-transmission in theoretical models, such as lattice theories. As remarked in Cates et al. (1998), the reason is that "In such a medium the displacement field is not single valued, and the solution of the elastic problem, though possible in principle, requires the whole construction history to be taken into account". The latter task is clearly challenging for theory. As a consequence, all analytical theories of the elasticity and rigidity of amorphous solids proposed so far have specialised to the case of packings near the jamming point, where all forces vanish (Mizuno et al., 2016).

In this contribution, I attempt a step forward in the direction of incorporating internal stresses into the lattice dynamical theory of amorphous solids. The starting point, which

allows us to proceed in this direction, is the formulation of an appropriate ansatz for the eigenvectors of amorphous solids which contains the effect of disorder as a random perturbation to wave-like components (Mazzacurati, V. et al., 1996). Using this form for the eigenvectors, we are able to evaluate the lattice dynamics for nonaffine deformations and we can consider the effect of internal stress in a mean-field way, in the two opposite limits of stretched bonds and compressed bonds.

Although the effects of nonaffinity have been intensively investigated in glassy materials, the same is not true for crystals. Here I will also show that nonaffine effects are very strong in a prototypical non-centrosymmetric crystal: α-quartz, for which the non-centrosymmetry is also the root cause of piezoelectricity (Kholkin et al., 2008). Interatomic interactions are modeled using a classical BKS potential proposed by van Beest et al. (1990), which includes both a short-ranged potential and long-ranged Coulomb interactions between partial charges on silicon and oxygen atoms. In disordered glasses, these interactions can be treated with a truncation and can therefore be handled using the original LM approach (Carré et al., 2007; Damart et al., 2017; Fennell and Gezelter, 2006; Wolf et al., 1999). By way of contrast, in an ordered crystal like α-quartz, Coulomb interactions are conditionally convergent and must be treated accordingly using the Ewald method (Ewald, 1921; Lee and Cai, 2009). I will show later in this chapter that the corresponding long-ranged many-body contribution can be also treated analytically and incorporated in the nonaffine response theory to predict the elastic constants of α-quartz.

4.1 A new way to obtain nonaffine elasticity

In Chapter 2, I have shown equivalent roles of the LM formalism and the BH method to obtain static elastic constants. In general, it is cumbersome to apply the BH method directly because one has to express potential energy in terms of Helmholtz displacements that consist of affine and nonaffine parts. The affine displacements are related to the external strain, whereas the nonaffine displacements must be solved via Eq. (2.65), given that one is able to express the total potential in terms of Helmholtz displacement. However, I note that, in the BH method, objects like

$$\{\mu\nu\xi\iota\};\begin{Bmatrix} I & J \\ \mu & \nu \end{Bmatrix};\begin{Bmatrix} I & \nu\xi \\ \mu & \end{Bmatrix},$$

are mathematically equivalent to affine elastic constant $C^A_{\mu\nu\xi\iota}$, the Hessian matrix $H^{\mu\nu}_{IJ}$ and affine force field $\Xi^{\mu}_{I,\nu\xi}$, respectively. Therefore, when I take a derivative of Eq. (2.65) with respect to the strain $\underline{\underline{\eta}}$, I do recover Eq. (2.36). Since the Hessian matrix always has d

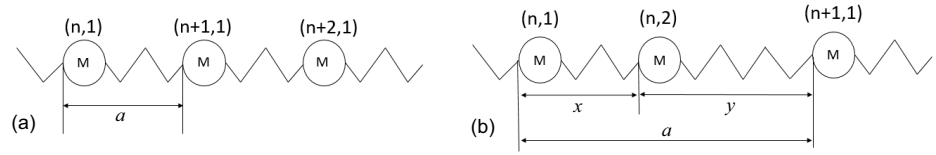

Fig. 4.1 Sketch for the lattice examples studied here: (a) 1D linear chain with one mass in each unit cell; (b) 1D linear chain with two masses in a unit cell of size a.

zero eigenvalues and is non-invertible, rather than taking normal mode decomposing and simply ignore zero eigenmodes, one could instead introduce a reduced tensor $\tilde{H}_{IJ}^{\mu\nu}$ and the corresponding local force $\tilde{\Xi}_{I,\xi\iota}^{\mu}$, by deleting the first d rows and columns in $H_{IJ}^{\mu\nu}$ and first d elements in $\Xi_{I,\xi\iota}^{\mu}$, respectively. This is because the system has translation invariance, s_1^{μ} can be set to zero without loss of generality. Then the first d rows and columns in $H_{IJ}^{\mu\nu}$ actually contribute nothing in the first term of RHS in Eq. (2.64). The reduced $\tilde{H}_{IJ}^{\mu\nu}$ is symmetric and now invertible because for $\tilde{H}_{IJ}^{\mu\nu}$, since the interaction between pairs are uncorrelated in pairwise potential, for each I, columns (rows) in $\tilde{H}_{IJ}^{\mu\nu}$ are linearly independent for J,μ,ν. As a result, $\tilde{H}_{IJ}^{\mu\nu}$ does not have zero eigenvalues. Thus, the energy density becomes

$$U = \frac{1}{2}\sum_{IJ\mu\nu}\tilde{H}_{IJ}^{\mu\nu}s_I^{\mu}s_J^{\nu} + \sum_{I\mu\nu\xi}\tilde{\Xi}_{I,\nu\xi}^{\mu}s_I^{\mu}\eta_{\nu\xi} + \frac{1}{2}C_{\mu\nu\xi\iota}^{A}\eta_{\mu\nu}\eta_{\xi\iota}. \tag{4.1}$$

Likewise, the minimisation condition requires $s_I^{\mu} = \sum_{J\nu\xi\iota}(\tilde{H}_{IJ}^{\mu\nu})^{-1}\tilde{\Xi}_{J,\xi\iota}^{\mu}\eta_{\xi\iota}$. Solving the minimisation condition for nonaffine displacements s_J^{ν}, and substituting back to Eq. (4.1) gives the nonaffine BH correction to affine elastic constant:

$$C_{\mu\nu\xi\iota} = C_{\mu\nu\xi\iota}^{A} - C_{\mu\nu\xi\iota}^{NA} \equiv \frac{1}{\mathring{V}}\frac{\partial^2\mathscr{U}}{\partial\eta_{\mu\nu}\partial\eta_{\xi\iota}} - \frac{1}{\mathring{V}}\sum_{IJ\kappa\chi}\tilde{\Xi}_{I,\mu\nu}^{\kappa}(\tilde{H}_{IJ}^{\kappa\chi})^{-1}\tilde{\Xi}_{J,\xi\iota}^{\chi} \tag{4.2}$$

Comparing C^{NA} with the nonaffine correction in the LM method, Eq. (2.46), I remark that these two objects will produce the same results, as long as one takes normal mode decomposition of full Hessian matrix properly. Perhaps this is not surprising in retrospect. I name the way to get elastic constants via the reduced Hessian matrix and the reduced affine force field leading to Eq. (4.2) as "the method of reduced fields".

I will now test all these methods to obtain static elastic constants discussed in previous sections for several specific mechanical models. First of all, consider the simplest elastic system, the 1D linear chains of equal masses M connected by springs k, as is shown in Fig. 4.1(a). In this case, the potential energy of a deformed string is $\mathscr{U} = \sum_n(R(n+1) -$

$R(n))^2(1+\eta)^2k/2$, with the Hessian being simply a number: $H = 2k$. If we want to preserve the lattice periodicity in the disordered state, then there cannot be any nonaffine displacements. The elastic modulus, in all three methods, is $C = ak$.

1D linear chain with two masses in a cell

I take a 1D linear chain with two masses connected via springs, with the same spring constant k but different original lengths (see Fig. 4.1(b)). The size of each cell is a, within which the original length of spring between masses M_1, while M_2 is x and $y = a - x$ is the original length of the spring across cells. I firstly refer to the BH method in Section 2.5. After the deformation with a homogeneous strain η, positions of masses move from $R_I(n)$ to $R_I(n) + \eta R_I(n) + s_I, I = 1,2$ where s_I are the additional nonaffine displacements each mass has, in response to elastic deformation. The potential energy then takes the form of a sum over cells: $\mathscr{U} = \sum_n \mathscr{U}_n$ with

$$\begin{aligned}\mathscr{U}_n = &\frac{k}{2}((1+\eta)(R_2(n) - R_1(n)) + s_2 - s_1 - x)^2 \\ &+ \frac{k}{2}((1+\eta)(R_1(n+1) - R_2(n)) + s_1 - s_2 - y)^2\end{aligned} \tag{4.3}$$

Note that the spring potentials in $\mathscr{U}_n$ reflect the external strain η applied. The internal displacements $s_{1,2}$ are such that the change of potential energy becomes minimal. Taking $s_1 = 0$, this minimisation gives

$$s_2 = \frac{1}{2}\left[(1+\eta)(R_1(n) + R_1(n+1) - 2R_2(n)) + x - y\right]. \tag{4.4}$$

Substituting $s_{1,2}$ back to $\mathscr{U}_n$ and extracting the quadratic term in η, I obtain

$$\frac{k}{8}\left[(R_1(n+1) - R_1(n))^2 + (R_1(n+1) - R_1(n))^2\right]\eta^2. \tag{4.5}$$

Since a is the size of repeated cell and $R_1(n+1) - R_1(n) = a$, the elastic constant from this method is equal to $C = ak/2$.

To check the approach via collective modes, I write the total potential energy as $\mathscr{U} = k\sum_n[(s_1(n) - s_2(n))^2 + (s_2(n) - s_1(n+1))^2]/2$, where initial mechanical equilibrium condition has been assumed and the external strain is not imposed. The equation of motion for

each mass takes the form

$$M_1\ddot{s}_1(n) = -2k\left[s_1(n) - \frac{s_2(n)+s_2(n-1)}{2}\right];$$
$$M_2\ddot{s}_2(n) = -2k\left[s_2(n) - \frac{s_1(n)+s_1(n-1)}{2}\right]. \tag{4.6}$$

There are two different ansatz for the solution and I check the results separately:
(1). I assume

$$s_1(n) = \frac{1}{\sqrt{M_1}}e_1(q)e^{i(qna-\omega t)}; \quad s_2(n) = \frac{1}{\sqrt{M_2}}e_2(q)e^{i(qna-\omega t)}, \tag{4.7}$$

and put them into the coupled equations of motion to get

$$\sqrt{M_1}\omega^2 e_1 = 2k\left[\frac{e_1}{\sqrt{M_1}} - \frac{1+e^{-iqa}}{2\sqrt{M_2}}e_2\right];$$
$$\sqrt{M_2}\omega^2 e_2 = 2k\left[\frac{e_2}{\sqrt{M_2}} - \frac{1+e^{iqa}}{2\sqrt{M_1}}e_1\right], \tag{4.8}$$

which is equivalent to

$$(D(q)-\omega^2 I)(e_1 \quad e_2)^T = 0,$$
$$D(q) = \begin{pmatrix} \frac{2k}{M_1} & -\frac{k}{\sqrt{M_1M_2}}(1+e^{-iqa}) \\ -\frac{k}{\sqrt{M_1M_2}}(1+e^{iqa}) & \frac{2k}{M_2} \end{pmatrix} \tag{4.9}$$

For convenience, I let $M \equiv M_1 = M_2$ and from Eq. (2.85), the coefficient of generic solution $u(m)$ is

$$\left(\frac{\sum_{I=1,2}M}{a}\right)[\omega^{(1)}(0,m)]^2 = \frac{ak}{2}q^2 \tag{4.10}$$

and the elastic constant is $C = ak/2$.

(2). If I instead assume the form of solution to be

$$s_1(n) = \frac{1}{\sqrt{M_1}}e_1(q)e^{i(qna-\omega t)}; \quad s_2(n) = \frac{1}{\sqrt{M_2}}e_2(q)e^{i(qna+qx-\omega t)}. \tag{4.11}$$

The dynamical matrix becomes

$$D(q) = \begin{pmatrix} \frac{2k}{M_1} & -\frac{k}{\sqrt{M_1 M_2}}(1+e^{-iqa})e^{iqx} \\ -\frac{k}{\sqrt{M_1 M_2}}(1+e^{iqa})e^{-iqx} & \frac{2k}{M_2} \end{pmatrix} \tag{4.12}$$

Defining $\tilde{e}_2 = e_2 e^{iqx}$, we can readily identify same solutions in (1), so is the dispersion relation:

$$\omega^2(q) = k\left(\frac{1}{M_1}+\frac{1}{M_2}\right) \pm k\sqrt{\left(\frac{1}{M_1}+\frac{1}{M_2}\right)^2 - \frac{4}{M_1 M_2}\sin^2\left(\frac{qa}{2}\right)}, \tag{4.13}$$

which is independent of x.

Again let $M \equiv M_1 = M_2$ and use Eq. (2.85) by expanding vibrational frequency to the 2nd order of wavenumber, the elastic constant is computed to be $C = ak/2$.

To test the LM formalism in Section 2.4, I write potential energy as $\mathscr{U} = \sum_n \mathscr{U}_n = k\sum_n[(R_2(n)-R_1(n)-x)^2 + (R_1(n+1)-R_2(n)-y)^2]/2$. The energy after putting the (affine) strain η,

$$\mathscr{U}_n(\eta) = \frac{k}{2}[(1+\eta)(R_2(n)-R_1(n))-x]^2 + \frac{k}{2}[(1+\eta)(R_1(n+1)-R_2(n))-y]^2 \tag{4.14}$$

and

$$\begin{aligned} C^A &= \frac{1}{a}\frac{\partial^2 \mathscr{U}_n(\eta)}{\partial \eta^2} = \frac{k}{a}(x^2+y^2) \\ F_{R_1(n)}(\eta) &= -\frac{\partial \mathscr{U}_n(\eta)}{\partial R_1(n)} = k[(1+\eta)(R_2(n)-R_1(n))-x] \\ &\quad -k[(1+\eta)(R_1(n)-R_2(n-1))-y] \\ \Xi_{R_1(n)} &= \frac{\partial}{\partial \eta}F_{R_1(n)}(\eta) = k(x-y) \end{aligned} \tag{4.15}$$

where $\Xi_{R_1(n)}$ reflects the affine force acting on each particle. And similarly,

$$\begin{aligned} F_{R_2(n)} &= k[(1+\eta)(R_2(n)-R_1(n)-x)] \\ &\quad +k[(1+\eta)(R_1(n+1)-R_2(n)-y)] \\ \Xi_{R_2(n)} &= k(y-x) \end{aligned} \tag{4.16}$$

Initial equilibrium condition requires $F_{R_{n,1}}(0)$ and $F_{R_{n,2}}(0)$ to be zero, so $R_2(n)-R_1(n)=x, R_1(n)-R_2(n-1)=y$. The Hessian matrix is

$$H = k\begin{pmatrix} 2 & -2 \\ -2 & 2 \end{pmatrix}, \tag{4.17}$$

whose eigenvalues are $\lambda_1 = 0, \lambda_2 = 4k$, with the eigenvectors corresponding to $\vec{e}_1 = 1/\sqrt{2}(1,1)$, $\vec{e}_2 = 1/\sqrt{2}(1,-1)$. I have

$$C = C^A - \frac{1}{a}\frac{(\vec{\Xi}\cdot\vec{e}_2)^2}{\lambda_2} = \frac{ak}{2}, \tag{4.18}$$

where the nonaffine correction is reflected via the $\vec{\Xi}$. This is consistent with the BH result.

Last, I check the newly proposed way to find C^{NA}, namely if the reduced Hessian and affine force field, as discussed in Eq. (4.2), can reproduce the correct elastic constant. Deleting the first row and column in H of Eq. (4.17) and the first element in $\vec{\Xi}$, I obtain $\tilde{H} = 2k, \tilde{\Xi} = k(y-x)$. The nonaffine correction of Eq. (4.2) now reads

$$\frac{1}{a}\tilde{\Xi}\tilde{H}^{-1}\tilde{\Xi} = \frac{k(y-x)^2}{2a}. \tag{4.19}$$

With $C^A = (k/a)(x^2+y^2)$, this again gives the correct the elastic constant: $C = ak/2$, but in a faster and more convenient way compared to the original BH method.

4.2 Sinusoidal wave approximation of eigenmodes

I have already defined the Hessian matrix, affine force field, affine and nonaffine elastic constants. In an approximation (supported by simulations) suggested in Mazzacurati, V. et al. (1996), one can model the (normalised) eigenvectors as sinusoidal waves with wavenumber $q_m = \omega_m/v$ plus a random component, $\varepsilon_I(m)$, with zero average, and with variance $\sigma^2 = \langle\varepsilon_I^2(m)\rangle$ independent of normal mode $m \in \{1,2,...,Nd\}$, i.e.

$$e_I^\mu(m) = \hat{n}^\mu \frac{1}{\sqrt{Nd}}\left[\sqrt{2(1-\sigma^2)}\sin(\mathbf{q}_m\cdot\mathbf{R}_I) + \varepsilon_I(m)\right] \tag{4.20}$$

where $\hat{n}^\mu$ is the polarisation unit vector such that $\hat{n}^\mu\hat{n}^\nu = \delta_{\mu\nu}$.

I define the angular average as:

$$\sum_{I=1}^{N} \sin^i(\mathbf{q}_m \cdot \mathbf{R}_I)\varepsilon_I^j(m) = N\langle \sin^i(\mathbf{q}_m \cdot \mathbf{R}_I)\rangle \langle \varepsilon_I^j(m)\rangle \tag{4.21}$$

where i, j are non-negative integers.

For the case $i = 2$, which is of interest for the normalisation of the eigenvectors, the average can be evaluated as follows. Assuming translation invariance (which is justified for a uniform amorphous system at least in the low-q limit), there is complete freedom in choosing or shifting the origin of the reference frame, i.e. $\mathbf{R} \to \mathbf{R} + \mathbf{R}'$, where $\mathbf{R}'$ is an arbitrary shift. Hence, $\langle \sin^2(\mathbf{q}\cdot\mathbf{R})\rangle = \langle \sin^2(\mathbf{q}\cdot(\mathbf{R}+\mathbf{R}'))\rangle = \langle \sin^2(\mathbf{q}\cdot\mathbf{R} + \mathbf{q}\cdot\mathbf{R}')\rangle$. Next I define $\vartheta \equiv \mathbf{q}\cdot\mathbf{R}'$, from which I get $\langle \sin^2(\mathbf{q}\cdot\mathbf{R})\rangle = \langle \sin^2(\mathbf{q}\cdot\mathbf{R} + \vartheta)\rangle$. Since ϑ is an arbitrary scalar, I can choose $\vartheta = \pi/2$, without loss of generality, the identity must hold for any values of ϑ. Then, clearly $\langle \sin^2(\mathbf{q}\cdot\mathbf{R})\rangle = \langle \cos^2(\mathbf{q}\cdot\mathbf{R})\rangle$, which implies

$$\langle \sin^2(\mathbf{q}\cdot\mathbf{R})\rangle = \frac{1}{2}. \tag{4.22}$$

Using this result, it is easy to check that e_I^μ is normalised,

$$\begin{aligned}
&\sum_{I\mu}[e_I^\mu(m)]^2 = \sum_I \frac{d}{Nd}\left[2(1-\sigma^2)\sin^2(\mathbf{q}_m\cdot\mathbf{R}_I) + 2\sqrt{2(1-\sigma^2)}\sin(\mathbf{q}_m\cdot\mathbf{R}_I)\varepsilon_I(m) + \varepsilon_I^2(m)\right] \\
&= \frac{1}{N}\left[2(1-\sigma^2)\cdot\frac{N}{2} + N\sigma^2\right] = 1.
\end{aligned}$$

I want to find the form of the eigenvalue λ of an eigenvector $\vec{e}$, i.e. $H\vec{e} = \lambda\vec{e}$, that is

$$\begin{aligned}
[H\vec{e}]_I^\mu &= \sum_{J\nu} H_{IJ}^{\mu\nu} e_J^\nu = \sum_{J\neq I}\sum_\nu H_{IJ}^{\mu\nu} e_J^\nu + \sum_\nu H_{II}^{\mu\nu} e_I^\nu \\
&= \sum_{J\neq I}\sum_\nu \left[(s_{IJ} - \frac{t_{IJ}}{R_{IJ}})n_{IJ}^\mu n_{IJ}^\nu + \frac{t_{IJ}}{R_{IJ}}\delta_{\mu\nu}\right](e_I^\nu - e_J^\nu)
\end{aligned} \tag{4.23}$$

where I used Eq. (2.45) for the expression of Hessian matrix. According to Zaccone and Scossa-Romano (2011), the orientational-dependent factors $n_{IJ}^\mu n_{IJ}^\nu$ for a large system with uncorrelated isotropic disorder can be replaced with its isotropic (angular) average, i.e.

$n_{IJ}^{\mu} n_{IJ}^{\nu} \to \delta_{\mu\nu}/d$, this gives

$$\begin{aligned}
[H\vec{e}]_I^{\mu} &= \sum_{J\neq I}\sum_{\mu}\left(s_{IJ} - \frac{t_{IJ}}{R_{IJ}}\right) n_{IJ}^{\mu} n_{IJ}^{\nu}(e_I^{\nu} - e_J^{\nu}) + \sum_{J\neq I}\frac{t_{IJ}}{R_{IJ}}(e_I^{\mu} - e_J^{\mu}) \\
&= \sum_{J\neq I}\frac{1}{d}\left(s_{IJ} - \frac{t_{IJ}}{R_{IJ}} + d\frac{t_{IJ}}{R_{IJ}}\right)(e_I^{\mu} - e_J^{\mu}) = \frac{1}{d}\sum_{J\neq I}\left[s_{IJ} + (d-1)\frac{t_{IJ}}{R_{IJ}}\right] e_I^{\mu} \\
&\equiv \lambda e_I^{\mu}
\end{aligned} \tag{4.24}$$

Terms proportional to e_J^{μ} vanish because the definition of eigenvector requires the final result must be independent of e_J^{μ}.

With these approximations, I am able to write $(\vec{\Xi}_{\kappa\chi}\cdot\vec{e}(m))(\vec{\Xi}_{\iota\xi}\cdot\vec{e}(m))$ in analytical form:

$$\begin{aligned}
(\vec{\Xi}_{\kappa\chi}\cdot\vec{e}(m))(\vec{\Xi}_{\iota\xi}\cdot\vec{e}(m)) &= \sum_{II'}^{N}\sum_{\mu\nu}^{d}\Xi_{I,\kappa\chi}^{\mu} e_I^{\mu}\,\Xi_{I',\iota\xi}^{\nu} e_{I'}^{\nu} \\
&= \frac{1}{Nd}\sum_{II'JJ'}^{N}\sum_{\mu\nu}^{d}(R_{IJ}s_{IJ} - t_{IJ})(R_{I'J'}s_{I'J'} - t_{I'J'}) n_{IJ}^{\mu} n_{IJ}^{\kappa} n_{IJ}^{\chi} n_{I'J'}^{\nu} n_{I'J'}^{\iota} n_{I'J'}^{\xi} \hat{n}^{\mu}\hat{n}^{\nu}\cdot \\
&\quad \left[\sqrt{2(1-\sigma^2)}\sin(\mathbf{q}_m\cdot\mathbf{R}_I) + \varepsilon_I\right]\left[\sqrt{2(1-\sigma^2)}\sin(\mathbf{q}_m\cdot\mathbf{R}_{I'}) + \varepsilon_{I'}\right].
\end{aligned} \tag{4.25}$$

Here, upon taking an isotropic average, the term $n_{IJ}^{\mu} n_{IJ}^{\kappa} n_{IJ}^{\chi} n_{I'J'}^{\mu} n_{I'J'}^{\iota} n_{I'J'}^{\xi}$ may be replaced with $(\delta_{II'}\delta_{JJ'} - \delta_{IJ'}\delta_{I'J})B_{\mu,\kappa\chi\iota\xi}$, where $B_{\mu,\kappa\chi\iota\xi}$ are geometric coefficients resulting from the angular average and are tabulated in Zaccone and Scossa-Romano (2011), I simplify

$$\begin{aligned}
&(\vec{\Xi}_{\kappa\chi}\cdot\vec{e}(m))(\vec{\Xi}_{\iota\xi}\cdot\vec{e}(m)) = \frac{1}{Nd}\sum_{\mu}^{d} B_{\mu,\kappa\chi\iota\xi}\sum_{II'JJ'}(\delta_{II'}\delta_{JJ'} - \delta_{IJ'}\delta_{I'J})(R_{IJ}s_{IJ} - t_{IJ})(R_{I'J'}s_{I'J'} - t_{I'J'})\cdot \\
&\left[2(1-\sigma^2)\sin(\mathbf{q}_m\cdot\mathbf{R}_I)\sin(\mathbf{q}_m\cdot\mathbf{R}_{I'}) + \varepsilon_I\sqrt{2(1-\sigma^2)}\sin(\mathbf{q}_m\cdot\mathbf{R}_{I'}) + \varepsilon_{I'}\sqrt{2(1-\sigma^2)}\sin(\mathbf{q}_m\cdot\mathbf{R}_I) + \varepsilon_I\varepsilon_{I'}\right] \\
&= \frac{1}{Nd}\sum_{\mu}^{d} B_{\mu,\kappa\chi\iota\xi}\sum_{IJ}^{N}(R_{IJ}s_{IJ} - t_{IJ})^2\left[2(1-\sigma^2)\sin^2(\mathbf{q}_m\cdot\mathbf{R}_I) + 2\varepsilon_I\sqrt{2(1-\sigma^2)}\sin(\mathbf{q}_m\cdot\mathbf{R}_{I'}) + \varepsilon_I^2\right. \\
&\left.-2(1-\sigma^2)\sin(\mathbf{q}_m\cdot\mathbf{R}_I)\sin(\mathbf{q}_m\cdot\mathbf{R}_J) - \varepsilon_I\sqrt{2(1-\sigma^2)}\sin(\mathbf{q}_m\cdot\mathbf{R}_J) - \varepsilon_J\sqrt{2(1-\sigma^2)}\sin(\mathbf{q}_m\cdot\mathbf{R}_I) - \varepsilon_I\varepsilon_J\right] \\
&= \frac{Z}{d}\sum_{\mu}^{d} B_{\mu,\kappa\chi\iota\xi}\langle(R_{IJ}s_{IJ} - t_{IJ})^2\rangle.
\end{aligned} \tag{4.26}$$

Recall, in the last line, Z is the coordinate number labeling the number of nearest neighborhoods of a tagged particle. Assuming disorder is spatially uncorrelated, the angular and radial average have been taken separately.

4.3 Elastic modulus in random network

Unstressed random network

I first take the case of a random network of central-force springs, with no internal stress. The interaction potential is a harmonic potential $\mathscr{U}(R_{IJ}) = (R_{IJ} - R_0^2)/2$. Also, $k \equiv s_{IJ}$ is the spring constant and R_0 is the distance between two particles in contact in the reference frame. The reference state is unstressed, i.e, all springs are relaxed in the minimum of the harmonic well. Hence, $t_{IJ} \equiv 0$ and $R_{IJ} \equiv R_0$.

For the nonaffine part of the elastic stiffness tensor, recalling Eq. (2.46), I have

$$C^{NA}_{\kappa\chi\iota\xi} = \frac{1}{V} \cdot dN \cdot \frac{ZR_0^2k^2 \sum_\mu B_{\mu,\kappa\chi\iota\xi}}{d \cdot \frac{1}{d}Zk} = \frac{dNR_0^2k}{V} \sum_\mu B_{\mu,\kappa\chi\iota\xi}. \tag{4.27}$$

The eigenvalue λ is actually independent of normal modes. Likewise, the affine term can be expressed as

$$C^{A}_{\kappa\chi\iota\xi} = \frac{NZR_0^2k}{2V} \langle n^\kappa_{IJ} n^\chi_{IJ} n^\iota_{IJ} n^\xi_{IJ} \rangle. \tag{4.28}$$

Here $\langle n^\kappa_{IJ} n^\chi_{IJ} n^\iota_{IJ} n^\xi_{IJ} \rangle = \sum_\mu^d B_{\mu,\kappa\chi\iota\xi}$, and I write the elastic constant tensor as

$$C_{\kappa\chi\iota\xi} = C^{A}_{\kappa\chi\iota\xi} - C^{NA}_{\kappa\chi\iota\xi} = \frac{NR_0^2k}{2V} \sum_{\mu=1}^{d} B_{\mu,\kappa\chi\iota\xi}(Z-2d) \tag{4.29}$$

For the shear modulus, $\sum_\mu^d B_{\mu,xyxy} = 1/15$ and Eq. (4.29) recovers the same analytical results in Zaccone and Scossa-Romano (2011), without any fitting parameters. The prefactor has been compared with the simulations in $d = 3$ of random frictionless packings near jamming interacting via harmonic potential in O'Hern et al. (2003), and an excellent quantitative agreement was found, even for the prefactor $NR_0^2k/(30V)$. For example, see Fig. 1 in Zaccone and Scossa-Romano (2011).

One should note that the prediction for the bulk modulus does not describe what is found in jammed packings, where $K \sim Z$, instead of $K \sim (Z-2d)$. The reason was explained in Ellenbroek et al. (2009) and has to do with the short-range particle correlations in the packing,

which alters the affine force balance on the particle and reduce the nonaffinity. Upon duly accounting for these correlations, the correct scaling can be recovered within the present framework, as shown in Schlegel et al. (2016); Zaccone and Terentjev (2014).

Random network with internal stresses

Now I relax the condition that the interparticle distance R_0 coincides with the minimum of the harmonic potential, by introducing a distribution of interparticle distances peaked at an average value $R_e \neq R_0$. On average, I let $R_{IJ} \equiv R_e$. The fact that the actual distance between two particles in contact deviates from the minimum of the interaction automatically implies the existence of a bond-tension or stress. In other words, the spring is either compressed, $R_e < R_0$, or stretched, $R_e > R_0$.

It was pointed out by S. Alexander with the famous metaphor of the violin strings, that internal stresses, which cause bonds to stretch, can make underconstrained lattices (i.e. with $Z < 2d$) fully rigid, which otherwise would be floppy (Alexander, 1998). From numerical simulations it is also known that, in disordered elastic networks, internal stresses have a profound effect on mechanical response, and can indeed make underconstrained lattices rigid (Huisman and Lubensky, 2011).

With these model assumptions, I get

$$C^{A}_{\kappa\chi\iota\xi} = \frac{NZR_0R_ek}{2V}\langle n^{\kappa}_{IJ}n^{\chi}_{IJ}n^{\iota}_{IJ}n^{\xi}_{IJ}\rangle = \frac{NZR_0R_ek}{2V}\sum_{\mu}^{d}B_{\mu,\kappa\chi\iota\xi} \tag{4.30}$$

To evaluate the nonaffine contribution to elastic constants $C^{NA}_{\kappa\chi\iota\xi}$, I have

$$(\vec{\Xi}_{\kappa\chi}\cdot\vec{e}(m))(\vec{\Xi}_{\iota\xi}\cdot\vec{e}(m)) = \frac{1}{Nd}\sum_{\mu}^{d}B_{\mu,\kappa\chi\iota\xi}\cdot NZ\cdot(kR_0)^2 = \frac{Zk^2R_0^2}{d}\sum_{\mu}^{d}B_{\mu,\kappa\chi\iota\xi} \tag{4.31}$$

$$\lambda = \frac{1}{d}\sum_{J\neq I}\left[s_{IJ}+(d-1)\frac{t_{IJ}}{R_{IJ}}\right] = \frac{Z}{d}\left[k+k(d-1)\left(1-\frac{R_0}{R_e}\right)\right] \tag{4.32}$$

$$\begin{aligned} C^{NA}_{\kappa\chi\iota\xi} &= \frac{1}{V}\cdot Nd\cdot\frac{dZk^2R_0^2}{dZ\left[k+k(d-1)\left(1-\frac{R_0}{R_e}\right)\right]}\sum_{\mu}^{d}B_{\mu,\kappa\chi\iota\xi} \\ &= \frac{NdkR_0^2}{V\left[1+(d-1)\left(1-\frac{R_0}{R_e}\right)\right]}\sum_{\mu}^{d}B_{\mu,\kappa\chi\iota\xi}, \end{aligned} \tag{4.33}$$

where I used $t_{IJ} = k(R_e - R_0)$. Finally, the elastic constants for the network with internal stress may be expressed as

$$C_{\kappa\chi\iota\xi} = C^{A}_{\kappa\chi\iota\xi} - C^{NA}_{\kappa\chi\iota\xi} = \frac{NkR_0R_e}{2V}\left[Z - \frac{2d\frac{R_0}{R_e}}{1+(d-1)\left(1-\frac{R_0}{R_e}\right)}\right]\sum_{\mu}^{d} B_{\mu,\kappa\chi\iota\xi} \tag{4.34}$$

Obviously, if $R_e = R_0$, then I recover Eq. (4.29).

Thus, I have found that with internal stresses, the elastic constants (including the shear modulus C_{xyxy}) are given by:

$$C_{\kappa\chi\iota\xi} \sim (Z - 2df), \quad f = \frac{R_0/R_e}{1+(d-1)\left(1-\frac{R_0}{R_e}\right)}. \tag{4.35}$$

If $R_e < R_0$, then $f > 1$; if $R_e > R_0$, then $f < 1$. Fig. 4.2 shows, when $d = 2$, how the ratio R_e/R_0 affects the dependence of $C_{\kappa\chi\iota\xi}$ on Z.

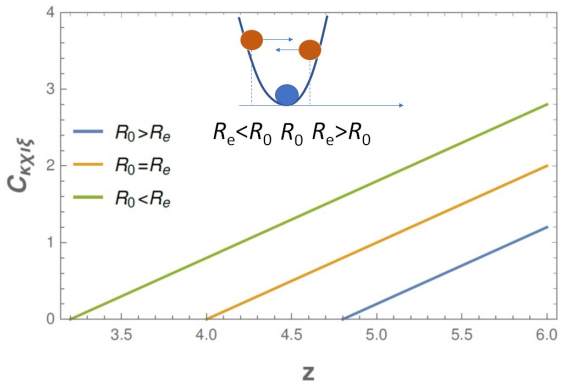

Fig. 4.2 Sketch of the dependence of the elastic constant $C_{\kappa\chi\iota\xi}$ as a function of coordination Z for different values of the internal stress parameter R_e/R_0 which indicates the initial particle displacement from the interaction minimum. Results are obtained in the 2-dimensional system.

From a physical point of view, the behavior seen in Fig. 4.2, means that when the internal strain is raised due to initially stretched network bonds, then larger elastic constants are required to "pull back" particles to equilibrium positions. On the other hand, if the bonds are initially compressed, the elastic constants become smaller. The fact that pre-stretched bonds lead to a larger elastic modulus confirms an earlier intuition of Alexander (1998).

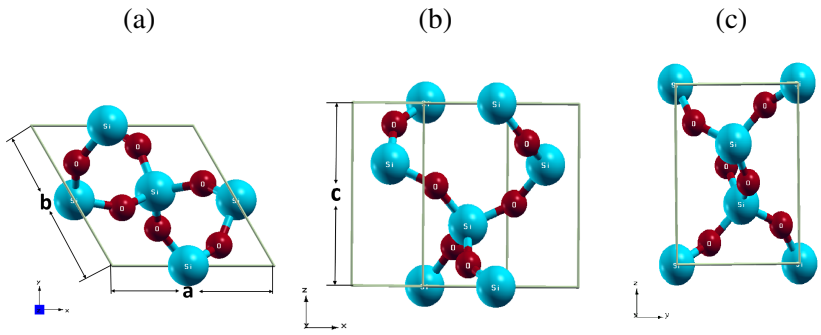

Fig. 4.3 Unit cell of α-quartz from different perspectives: (a) top view (b) left view (c) front view. Si atoms are in cyan, O atoms in red.

4.4 Generating the relaxed structure of α-quartz

Lattice structure

X-ray and neutron crystallography have been applied to many materials to determine the crystal structure and atomic positions, including α-quartz. It has been shown that crystals of α-quartz have a trigonal Bravais lattice composed of SiO_4 tetrahedra that are linked together at their corners to form a 3-dimensional network (Sutter and Yavas, 2017). The conventional unit cell, shown in Fig. 4.3, is hexagonal and contains three molecules of SiO_2. Its c-axis is a threefold screw axis; that is, the lattice remains unchanged after a rotation of 120° about this axis followed by a translation of $+c/3$ along the same axis. Along the negative c direction, the screw axis is left-handed if the 120° rotation appears clockwise while if the rotation appears counterclockwise, the screw axis is right-handed. α-quartz may exist in either of these forms, which are enantiomorphs (mirror images). α-quartz crystals rotate the polarization of light propagating parallel to the c-axis, which is therefore also called the optical axis, in the same sense as the screw. Perpendicular to the c-axis, are three twofold axes that are separated from one another by angles of 120° and intercept the c-axis at intervals of $c/3$. The absence of an inversion center allows α-quartz to exhibit piezoelectricity when pressed along one of the twofold axes that are therefore often named electrical axes (Sutter and Yavas, 2017).

Two space groups, $P3_121$ or $P3_221$, can be used to label the α-quartz, depending on whether the c-axis is left- or right-handed. Here, I initially used the consistent results of lattice constants from Bragg and Gibbs (1925), Wyckoff (1963) and Kihara (1990), with lattices parameters a and c at 298K equal to 4.9137Å and 5.4047Å respectively. The atomic positions of left-handed α-quartz are given in the right-handed hexagonal coordinate systems in Table 4.1.

Atom	x	y	z
Si	0.4697	0	0
Si	0	0.4697	2/3
Si	0.5303	0.5303	1/3
O	0.4133	0.2672	0.1188
O	0.2672	0.4133	0.5479
O	0.7328	0.1461	0.7855
O	0.5867	0.8539	0.2145
O	0.8539	0.5867	0.4521
O	0.1461	0.7328	0.8812

Table 4.1 Fractional coordinates of atoms of left-handed α-quartz given in the scaled unit at 298K at ambient pressure (Kihara, 1990).

Empirical potential

In the present work, the cohesion of α-quartz is modeled with the classical BKS potential, which is based on a short-range Buckingham potential and long-range Coulombic interactions between partial charges on Si and O atoms. Different parametrisations of this potential exist in Mantisi et al. (2012); van Beest et al. (1990). I have used the original parameters from van Beest et al. (1990), which do not include any direct Si-Si longer-range interaction, because they provide the best agreement with experimental measurements of elastic constants of α-quartz (Carré et al., 2008). The short-range potential between atoms I and J is expressed as:

$$\Phi^{sh}(R_{IJ}) = \left\{ A_{IJ} e^{-\frac{R_{IJ}}{\rho_{IJ}}} - \frac{C_{IJ}}{R_{IJ}^6} - \left[A_{IJ} e^{-\frac{R_{c,sh}}{\rho_{IJ}}} - \frac{C_{IJ}}{R_{c,sh}^6} \right] \right\} H(R_{c,sh} - R_{IJ}). \tag{4.36}$$

The parameters of the potential are given in Table 4.2. The best agreement with experimental data is obtained for $R_{c,sh} = 10$Å (Carré et al., 2008).

In order to treat the Coulombic interactions analytically, I used the classical Ewald method (Born and Huang, 1954; Ewald, 1921; Lee and Cai, 2009; Toukmaji and Board, 1996). In this approach, the point charge distribution, which is described by delta functions, is transformed by adding and subtracting Gaussian distributions. The total electrostatic energy is then re-written as the sum of a short-range term (difference between point and Gaussian charge distributions) in real space, a long-range term (Gaussian charge distribution) in Fourier space plus a self-interaction constant:

	A_{IJ}(eV)	$\rho_{IJ}(\mathring{A})$	C_{IJ}(eV$\mathring{A}^6$)
O-O	1388.773	0.3623	175.0
Si-O	18003.7572	0.2052	133.5381

Table 4.2 Parameters of the empirical potential used to model α-quartz.

$$E \equiv E_{SR} + E_{LR} + E_{SI}$$
$$= \frac{1}{4\pi\varepsilon_0}\frac{1}{2}\sum_{I\neq J}\frac{z_I z_J}{R_{IJ}}\mathrm{erfc}\left(\frac{r_{IJ}}{\sqrt{2}\sigma}\right) + \frac{1}{2V\varepsilon_0}\sum_{\mathbf{G}\neq\mathbf{0}}\frac{\exp(-\sigma^2G^2/2)}{G^2}|S(\mathbf{G})|^2 - \frac{1}{4\pi\varepsilon_0}\frac{1}{\sqrt{2\pi}\sigma}\sum_I q_I^2, \tag{4.37}$$

where z_I is the charge on atom I, erfc(r) $= 1 - 2/\sqrt{\pi}\int_0^r \exp(t^2)dt$ is the complementary error function, $\mathbf{G} = 2\pi[n_x/L_x, n_y/L_y, n_z/L_z]$ refers to reciprocal lattice vectors and $S(\mathbf{G}) = \sum_J z_J \exp(i\mathbf{G}\cdot\mathbf{R}_J)$ is the structure factor. Here, L_x, L_y, L_z are the dimensions of the simulation cell, which is assumed periodic and orthogonal. The parameter σ is the standard deviation of the Gaussian distribution. It sets the cross-over between the real and reciprocal terms, which both converge absolutely and rapidly. In the literature, one may also find the use of a parameter $\alpha = 1/(\sqrt{2}\sigma)$. It is recommended for accurate calculations to use a cut-off radius for the real space potential $R_{cut} = 3.12/\alpha$ and a summation in reciprocal space up to $n_{\kappa,max} = \alpha L_\kappa$. I used $R_{cut} = 10$Å, which is a trade-off between the computing times of the short-ranged term, E_{SR}, and of the long-range summation in Fourier space, E_{LR}.

In the following, the short-range and self-interaction terms will be included in the short-range BKS term of Eq. (4.36). This term can be treated with the original LM approach in Section 2.4. Hence, only E_{LR} requires a special treatment because of its many-body nature.

Simulation procedure

Since I consider the properties of a perfect crystal, the system can in principle be limited to a single unit cell. In practice, I used a small but finite system, containing 1350 atoms in a periodic orthogonal cell. I started from the lattice positions in Table 4.1 and the experimental lattice constants, under ambient condition, where random velocity was assigned to consume the thermal energy (Bragg and Gibbs, 1925; Kihara, 1990; Wyckoff, 1963). The full empirical potential energy was chosen to be the sum of Eq. (4.36) and Eq. (4.37), where parameters of BKS part are shown in Table 4.2. The structure was cooled down to $\sim$ 0K within 100ns, with NPT ensemble being carried out. The timestep was set to be 1ps. I then relaxed the simulation cell via energy minimisation reached by the steepest-descent method, adapting

the cell dimensions with a barostat to impose zero internal stresses. The simulation was performed with LAMMPS package (Plimpton, 1995). The equilibrium lattice constants thus obtained are $a = 4.94$ and $c = 5.44$ Å, corresponding to a density of 2.60 g/cm^3, close to the experimental value of 2.65 g/cm^3 (Heyliger et al., 2003; Wang et al., 2015a).

To validate the analytical expressions of the elastic constants, I computed numerically their values by straining the crystal in small increments (1e-5) and computing the slope of the resulting stress-strain curves. To obtain the affine constants, no relaxation was allowed between affine deformation steps, i.e. the atoms remained at their affine positions, while the nonaffine constants were computed by relaxing the atomic positions at fixed cell shape between each strain increment.

4.5 Nonaffine lattice dynamics with the Ewald method

Ewald sum contribution

I now consider the contribution of the long-ranged term E_{LR} in Eq. (4.37) to the affine and nonaffine elastic constants. The expressions in elastic constants remain valid, but I need to express the contribution of E_{LR} to the dynamical matrix, the affine elastic constants and the nonaffine forces.

Forces and dynamical matrix

The long-range energy E_{LR} produces atomic forces due to the dependence of the structure factor, $S(\mathbf{G})$, on atomic positions. The expression of the resulting force is (Lee and Cai, 2009; Toukmaji and Board, 1996):

$$\begin{aligned}
\mathbf{f}_I &= -\frac{\partial E_{LR}}{\partial \mathbf{R}_I} \\
&= -\frac{1}{2V\varepsilon_0}\sum_{\mathbf{G}\neq\mathbf{0}}\frac{\exp(-\sigma^2G^2/2)}{G^2}[S(\mathbf{G})(-i\mathbf{G})z_I\exp[-i\mathbf{G}\cdot\mathbf{R}_I]+S(-\mathbf{G})z_I(i\mathbf{G})\exp[i\mathbf{G}\cdot\mathbf{R}_I])] \\
&= -\frac{1}{V\varepsilon_0}\sum_{\mathbf{G}\neq\mathbf{0}}\frac{\exp(-\sigma^2G^2/2)}{G^2}\mathbf{G}z_I\mathrm{Im}[S(\mathbf{G})\exp[-i\mathbf{G}\cdot\mathbf{R}_I]] \\
&= \frac{z_I}{V\varepsilon_0}\sum_{\mathbf{G}\neq\mathbf{0}}\frac{\exp(-\sigma^2G^2/2)}{G^2}\mathbf{G}\sum_J z_J\sin(\mathbf{G}\cdot\mathbf{R}_{IJ}).
\end{aligned} \tag{4.38}$$

In the following, I simplify the notations by noting $T(u) = \exp(-\sigma^2 u/2)/u$, such that the contribution of the Ewald long-range term to the atomic force is written as:

$$\mathbf{f}_I = \frac{z_I}{V\varepsilon_0} \sum_{\mathbf{G}\neq\mathbf{0}} T(G^2)\mathbf{G} \sum_J z_J \sin(\mathbf{G}\cdot\mathbf{R}_{IJ}) \tag{4.39}$$

The long-range contribution to the Hessian matrix elements can be computed similarly:

1. $I \neq J$:

$$H_{IJ}^{\mu\nu} = \frac{\partial^2 E_{LR}}{\partial R_I^\mu \partial R_J^\nu} = \frac{z_I z_J}{V\varepsilon_0} \sum_{\mathbf{G}\neq\mathbf{0}} T(G^2) G^\mu G^\nu \cos(\mathbf{G}\cdot\mathbf{R}_{IJ}) \tag{4.40}$$

2. $I = J$:

$$H_{IJ}^{\mu\nu} = -\frac{z_I}{V\varepsilon_0} \sum_{\mathbf{G}\neq\mathbf{0}} T(G^2) G^\mu G^\nu \sum_{J\neq I} z_J \cos(\mathbf{G}\cdot\mathbf{R}_{IJ}) = -\sum_{J\neq I} H_{IJ}^{\mu\nu}$$

Tensile deformation

To find the long-range effect on the nonaffine forces, I need to express the variation of the atomic force in Eq. (4.39) when an incremental affine strain is applied to the system. I consider first a uniaxial strain η along direction x. The dependence on η is due to the dependence of three terms:

- the volume, $V \to V(1+\eta)$
- the reciprocal vectors, which in an orthogonal box become $\mathbf{G} \to 2\pi[n_X/L_X(1+\eta), n_Y/L_Y, n_Z/L_Z]$
- the atom-to-atom vectors, $\mathbf{R}_{IJ} \to [R_{IJ}^x(1+\eta), R_{IJ}^y, R_{IJ}^z]$

I note that with these transformations, $\mathbf{G}\cdot\mathbf{R}_{IJ}$ is unchanged and so that the structure factor $S(\mathbf{G})$ is constant. Taking the derivative of $\mathbf{f}_I$ in Eq. (4.39) with respect to η and I obtain:

$$\Xi_{I,xx} = -\frac{z_I}{V\varepsilon_0} \sum_{\mathbf{G}\neq\mathbf{0}} T(G^2) \left(\sigma^2 + \frac{2}{G^2}\right) G_x^2 \mathbf{G} \sum_J z_J \sin(\mathbf{G}\cdot\mathbf{R}_{IJ}). \tag{4.41}$$

Taking the first and second derivatives of E_{LR} with respect to η, I obtain the tensile stress and affine elastic constants for the tensile strain:

$$\sigma_{xx} = \frac{1}{V}\frac{\partial E_{LR}}{\partial \eta} = \frac{1}{2V^2\varepsilon_0}\sum_{\mathbf{G}\neq\mathbf{0}} T(G^2)|S(\mathbf{G})|^2\Big(\left[\sigma^2+\frac{2}{G^2}\right]G_x^2 - 1\Big) \tag{4.42}$$

and

$$C^A_{xxxx} = \frac{1}{V}\frac{\partial^2 E_{LR}}{\partial \eta^2} = \frac{1}{V^2\varepsilon_0}\sum_{\mathbf{G}\neq\mathbf{0}} T(G^2)|S(\mathbf{G})|^2\left(1-\frac{5}{2}\left[\sigma^2+\frac{2}{G^2}\right]G_x^2+\left[\frac{4}{G^4}+2\frac{\sigma^2}{G^2}+\frac{\sigma^4}{2}\right]G_x^4\right). \tag{4.43}$$

Similar expressions are obtained for tensile deformations along y and z. Finally, the cross-terms are expressed as:

$$C^A_{\mu\mu\nu\nu} = \frac{1}{V^2\varepsilon_0}\sum_{\mathbf{G}\neq\mathbf{0}} T(G^2)|S(\mathbf{G})|^2\left(\frac{1}{2}-\left[\sigma^2+\frac{2}{G^2}\right]\frac{G_\mu^2+G_\nu^2}{2}+\left[\frac{4}{G^4}+2\frac{\sigma^2}{G^2}+\frac{\sigma^4}{2}\right]G_\mu^2G_\nu^2\right). \tag{4.44}$$

Shear deformation

I now consider the case of an affine shear strain parallel to the y planes with displacements along the x direction. The applied strain is noted $\gamma_{xy}\equiv\gamma$. Under this strain, axes of the box become: $\mathbf{a}'_1 = (L_x,0,0) = \mathbf{a}_1, \mathbf{a}'_2 = (L_x\gamma, L_y, 0), \mathbf{a}'_3 = (0,0,L_z) = \mathbf{a}_3$ while the reciprocal vectors become: $\mathbf{G}' = 2\pi(n_x/L_x, n_y/L_y - n_x\gamma/L_x, n_z/L_z)$ and the atom-to-atom vectors become: $\mathbf{R}'_{ij} = (R^x_{IJ}+R^y_{IJ}\gamma, R^y_{IJ}, R^z_{IJ})$. One can check that again $\mathbf{G}\cdot\mathbf{R}_{IJ}$ is unchanged during the transformation. After taking the derivative of the long-range force in Eq. (4.39) with respect to γ, I obtain:

$$\mathbf{\Xi}_{I,xy} = -\frac{z_I}{V\varepsilon_0}\sum_{\mathbf{G}\neq\mathbf{0}} T(G^2)\left(\sigma^2+\frac{2}{G^2}\right)G_xG_y\mathbf{G}\sum_J z_J\sin(\mathbf{G}\cdot\mathbf{R}_{IJ}). \tag{4.45}$$

Similarly, the shear stress is expressed as:

$$\sigma_{xy} = \frac{1}{2V^2\varepsilon_0} \sum_{\mathbf{G}\neq\mathbf{0}} T(G^2)|S(\mathbf{G})|^2 \left(\sigma^2 + \frac{2}{G^2}\right) G_x G_y \tag{4.46}$$

and the affine elastic constant:

$$C^A_{xyxy} = \frac{\partial\sigma_{xy}}{\partial\gamma} = \frac{1}{2V^2\varepsilon_0} \sum_{\mathbf{G}\neq\mathbf{0}} T(G^2)|S(\mathbf{G})|^2 \left(\sigma^4 + 4\frac{\sigma^2}{G^2} + \frac{8}{G^4}\right) G_x^2 G_y^2 \tag{4.47}$$

Some other affine elastic constants from E_{LR}

Recall the formula of affine approximation hold for a generic strain tensor, Eq. (2.41):

$$C^A_{\mu\nu\kappa\chi} = \frac{1}{V}\frac{\partial^2 E_{LR}}{\partial\eta_{\mu\nu}\partial\eta_{\kappa\chi}} \tag{4.48}$$

For $C_{16} = C_{xxxy}$, $C_{14} = C_{xxyz}$ and $C_{56} = C_{xyxz}$, I have respectively,

$$\begin{aligned}
C_{xxxy} &= \frac{1}{2V^2\varepsilon_0} \sum_{\mathbf{G}\neq\mathbf{0}} T(G^2)|S(\mathbf{G})|^2 \left[\left(\sigma^4 + \frac{4\sigma^2}{G^2} + \frac{4}{G^4}\right) G_x^2 - \left(\sigma^2 + \frac{2}{G^2}\right)\right] G_x G_y \\
&\quad + \frac{1}{2V^2\varepsilon_0} \sum_{\mathbf{G}\neq\mathbf{0}} T(G^2)|S(\mathbf{G})|^2 \frac{2G_x^2}{G^4} 2G_x G_y \\
&= \frac{1}{2V^2\varepsilon_0} \sum_{\mathbf{G}\neq\mathbf{0}} T(G^2)|S(\mathbf{G})|^2 \left[\left(\sigma^4 + \frac{4\sigma^2}{G^2} + \frac{8}{G^4}\right) G_x^2 - \sigma^2 - \frac{2}{G^2}\right] G_x G_y
\end{aligned} \tag{4.49}$$

$$C_{xxyz} = \frac{1}{2V^2\varepsilon_0} \sum_{\mathbf{G}\neq\mathbf{0}} T(G^2)|S(\mathbf{G})|^2 \left[\left(\sigma^4 + \frac{4\sigma^2}{G^2} + \frac{8}{G^4}\right) G_x^2 - \sigma^2 - \frac{2}{G^2}\right] G_y G_z \tag{4.50}$$

$$\begin{aligned}
C_{xyxz} &= \frac{1}{2V^2\varepsilon_0} \sum_{\mathbf{G}\neq\mathbf{0}} T(G^2)|S(\mathbf{G})|^2 \left(\sigma^4 + \frac{4}{G^4} + \frac{4\sigma^2}{G^2}\right) G_x G_y G_x G_z \\
&\quad + \frac{1}{2V^2\varepsilon_0} \sum_{\mathbf{G}\neq\mathbf{0}} T(G^2)|S(\mathbf{G})|^2 \frac{4}{G^4} G_x G_y G_x G_z \\
&= \frac{1}{2V^2\varepsilon_0} \sum_{\mathbf{G}\neq\mathbf{0}} T(G^2)|S(\mathbf{G})|^2 \left(\sigma^4 + \frac{8}{G^4} + \frac{4\sigma^2}{G^2}\right) G_x G_y G_x G_z
\end{aligned} \tag{4.51}$$

4.6 Comparison with experimental data for α-quartz

I first use Eq. (4.40) to compute the dynamical matrix of the present atomic-scale model of α-quartz and, after diagonalisation, obtain the VDOS. The result is shown in Fig. (4.4)(a),

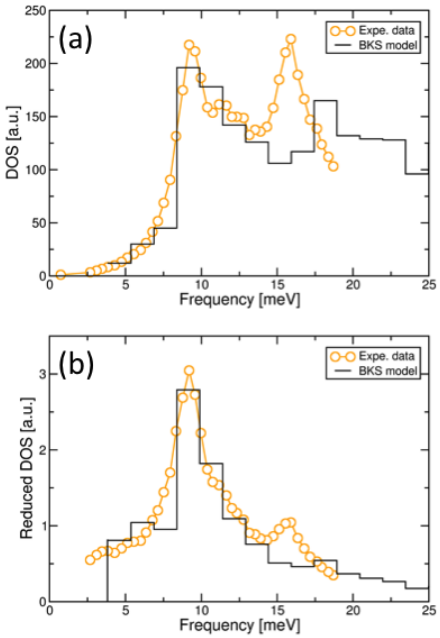

Fig. 4.4 Comparison of the VDOS (a) and reduced VDOS (normalised by the frequency squared) (b) obtained numerically with the BKS model and experimentally with inelastic X-ray scattering (Chumakov et al., 2014).

with a comparison to the experimental data obtained by Chumakov et al. (2014). The present implementation of the BKS model predicts accurately the first peak of the VDOS, which occurs at about 10 meV. The second peak is reproduced only qualitatively, being located at a slightly higher frequency (18 instead of 16 meV) and with a slightly lower amplitude. Normalising the VDOS by Debye law $\sim \omega^2$ in Fig. (4.4)(b), we see that the numerical model reproduces well the boson peak reported experimentally. Note that the piecewise nature of the BKS model arises from setting the large bin for the discrete vibrational frequency of a system with finite size. I can conclude that the present model reproduces satisfactorily the VDOS and boson peak of α-quartz.

Second, I use Eq. (2.41) with the short- and long-ranged terms presented above to compute both the affine and total elastic constants of α-quartz. The result is given in Table 4.3 with a comparison to experimental data. I checked by direct numerical calculations that the analytical expressions described in the last section predict faithfully the elastic constants. I chose the same parametrisation of the BKS potential and Ewald summation as Carré et al. (2008), because they yield a very good agreement with experimental data, as seen in Table 4.3, when both the affine and nonaffine contributions are included. On the other hand, when only the affine deformation is allowed, the elastic constants are largely overestimated, by a factor 3 to 4 for C_{11}, C_{33}, C_{44}, C_{66}, and up to a factor of 15 for C_{12} and C_{13}. Said in other

words, the nonaffine correction decreases the affine elastic constants by about 70 % for C_{11}, C_{33},C_{44}, C_{66} and up to 90 % for C_{12} and C_{13}. I also list several elastic moduli calculated from the method of reduced fields in section 4.1, namely Eq. (4.2). It is clear that, results are exactly same between the LM formalism and the method of reduced fields.

Elast. Const. (GPa)	C_{11}	C_{33}	C_{44}	C_{66}	C_{12}	C_{13}
Affine+Nonaffine	90.5	107.0	50.2	41.1	8.1	15.2
Affine only	375.6	329.6	189.2	125.4	125.2	189.1
Exp. Will et al. (1988)	86.8	105.8	58.2	39.9	7.0	19.1
Exp. Heyliger et al. (2003)	87.3	105.8	57.2	40.4	6.57	12.0
Exp. Wang et al. (2015a)	86.6	106.4	58		6.74	12.4
Affine+Nonaffine(reduced fields)	90.5	107.0		41.1		

Table 4.3 Comparison between experimental measurements of the elastic constants of α-quartz and the present numerical calculations, including both affine and nonaffine contributions or only the affine part. The last row is presented, where results are calculated via method of reduced fields(in section 4.1).

The nonaffine relaxations originate from the lack of symmetry of the α-quartz crystal (Damart et al., 2017; Milkus and Zaccone, 2016). This is evident for the short-ranged pair potential part of the interatomic potential since the nonaffine force vector, $\mathbf{\Xi}_I$, which drives the nonaffine relaxations, is written as a sum over neighbors of terms of the type $D_{IJ}^{\mu\nu} R_{IJ}^{\kappa}$ that add up to zero in a centrosymmetric environment. The same is true for the long-range terms in Eqs. (4.41) and (4.45), which depend on $\sum_J z_J \sin(\mathbf{G}\cdot\mathbf{R}_{IJ})$, which is also zero if atom I is a center of centrosymmetry. In α-quartz, neither Si nor O atoms are centers of symmetry, which may explain why nonaffine relaxations are so important in this crystal. However, Si atoms are surrounded by close-to-perfect tetrahedra of O atoms as explained before, while O atoms are in clearly asymmetrical environments since the Si-O-Si bonds are not straight, but make an angle close to 148^o. The higher symmetry of the environment of the Si atoms implies more limited nonaffine relaxations for these atoms. The latter depend on the imposed deformation, but I have checked that the nonaffine displacements of the Si atoms is systematically at least a factor of 2 smaller than that of the O atoms.

It was suggested in a recent work Milkus and Zaccone (2016) that the lack of centrosymmetry is responsible not only for the nonaffinity of the elastic constants, but also for the boson peak that shows up in the VDOS of glasses and non-centrosymmetric crystals. In Milkus and Zaccone (2016), model systems were studied numerically, which included random spring networks derived from glasses, and crystals with random bond-depletion. A universal correlation was found between the boson peak amplitude and a new order parameter for centrosymmetry (but importantly, *not* with the standard bond-orientational order parameter),

which allowed for the collapse of data from systems with very different lattice topologies (i.e. random networks and defective crystals).

Summary

I proposed a new simplified way to obtain static elastic constants, based on the BH method. A fully analytical derivation of the elastic constants of athermal disordered solids within the framework of nonaffine lattice dynamics was presented. When the particles are initially away from the minimum, initial stresses are present. Two opposite limits of bonds being on average stretched and bonds being on average compressed have been considered.

Nonaffine contributions are not small corrections to the elastic constants: they are substantial (negative) contributions, which can make the resulting elastic constants up to many times smaller than the affine estimates. This important fact has been overlooked in previous studies on α-quartz lattice dynamics (Bosak et al., 2012).

Chapter 5

Viscoelastic response in metallic glasses

Compared with traditional disordered materials, metallic glasses (MGs) exhibit extraordinary physical properties, in terms of their ability to sustain large loads prior to yielding and their ductility (Spaepen and Turnbull, 1984). They are solid metallic materials, usually an alloy, with disordered structure in atomic level. Although previous atomic-scale theories based on defect physics and lattice dynamics, like Nabarro and de Villiers (1995), have provided a good understanding of mechanical relaxation and internal friction in crystalline metals, revealing from the same microscopic scale the relation between viscoelasticity and dynamical heterogeneity for MGs has been a long-term challenge.

With the advent of MGs as the next-generation metallic materials for technological applications, extensive experimental investigations like stress relaxation technique have brought a wealth of observations about the viscoelasticty and anelasticity of these materials. A lot of research, like Qiao et al. (2015); Wang et al. (2014), has been taken on the stress relaxation of various MGs, which claims that localised plastic flow could be activated during viscoelastic and plastic deformation. Like the situation in dielectric relaxation, the whole relaxation spectrum of viscoelastic materials is usually fitted by the empirical Kohlrausch (stretched exponential) function which does not arise from any physical mechanism.

Here I provide an answer to all these issues in a unifying way, by using a nonaffine atomic-scale theory of viscoelastic response and relaxation of metallic glasses, in a bottom-up way starting from a microscopic Hamiltonian. Similar as dielectric case, I use the ZCL system-bath Hamiltonian to derive an average equation of motion for a tagged atom (or ion), which turns out to be a GLE, with a non-Markovian atomic-scale friction (memory kernel). Zwanzig (2002) and Weiss (2012) show that the latter memory kernel arises from integrating out the fast degrees of freedom of the atomic motion. Although it is currently not possible to specify the functional form of the time-dependence of the friction within ZCL models,

approximated stretched-exponential forms for the microscopic friction in supercooled liquids derived by Sjogren and Sjolander (1979) based on many-body kinetic theory are utilised.

5.1 Set-up for $Cu_{50}Zr_{50}$

In order to test the theory I firstly use stress-relaxation experiments on $Cu_{50}Zr_{50}$ glassy system. The VDOS is needed as an input to calculate the viscoelastic response. To this aim, I used numerical simulations of the same MGs, which takes also electronic structure effects into account at the level of the embedded atom method (EAM).

Experiments

Thanks to the thermal stability of CuZr- based metallic glass. MG ribbons made up of $Cu_{50}Zr_{50}$ with length over 7 mm were processed by the melt-spinning technique in an inert argon atmosphere. Differential scanning calorimetry (DSC) was used to determine the thermal properties of the samples that has a glass transition temperature T_g at 670 K at a heating rate of 20 K/min. The tensile stress relaxation experiments were performed by my colleagues with dynamical mechanical analysis (DMA) experiments using a TA Q800 dynamic mechanical analyzer. To eliminate any influences from initial states, the MG ribbons were heated above T_g before the measurements. The tensile stress relaxation, carried out at a constant strain of 0.4% was loaded on the model alloy for 24 hours after an initial 3 minutes equilibrium (Cui et al., 2017b). The resultant stress relaxation in a form of time dependency that is fitted by the Kohlrausch function $\sigma(t) = \sigma_0 \exp[-(t/\tau)^\beta]$ with σ_0 being stress relaxation at $t = 0$, which is shown in Fig. 5.1, under three different temperatures T_g(670 K), 0.9 T_g(603 K) and 0.8 T_g (536 K). Note that, the stress at large sufficient time, σ_∞, which is $\sigma(t)$ at $t = \infty$, has been estimated to be zero for the three temperatures.

In Fig. 5.1 the fitting is excellent apart from deviations which are due to processes other than the α-relaxation (e.g. other long-time or low-frequency relaxation processes). For $Cu_{50}Zr_{50}$, I only focus on a theory of α-relaxation and its associated viscoelastic response, without considering other processes. In the following, I will use the fitted Kohlrausch function to obtain the dynamic moduli E' and E'' in the frequency domain. In this way, I will be targeting the α-relaxation only, and consistently focus our attention on the comparison between the theory and data extracted from experiments where effects other than α-relaxation have been removed.

MD simulations with EAM potentials

In molecular dynamics (MD) simulations, my collaborators utilised the Finnis-Sinclair type EAM potentials optimised for realistic amorphous Cu-Zr structures, whose expression is shown in Eq. (A.1) in Appendix A (Mendelev et al., 2009). Seven independent $Cu_{50}Zr_{50}$ MG models were obtained by quenching the system at cooling rate 10^{10} K/s from a liquid state equilibrated at 2000 K with different initial positions and velocity distributions, to targeted temperatures. The energy of system was then minimised using the conjugate gradient (CG) algorithm, before the snapshot was taken to extract information of coordinates of atoms. Each model was composed of 8192 atoms and external pressure was held at zero during the quenching process using Parrinello and Rahman (1981) barostat. Periodic boundary conditions were imposed automatically. The resulting VDOSs averaged from seven independent glassy models are shown in Fig. 5.2. It can be easily seen that the eigenfrequency spectrum is not sensitive to T because in the VDOS calculated for the CuZr- system, the system finds itself in the inherent structure of the glassy state, which is only weakly sensitive to temperatures below T_g. This holds at harmonic level where particles locate in a basin of the deep minimum in the energy landscape. In simulations, although there are different temperatures, the internal coordinates of atoms are quite similar except for the thermal expansion in the simulation box, thus giving rise to very similar VDOSs. However, looking at the inset panel that shows the simulated VDOS at the three different temperatures scaled by Debye law, without adjusting the scale of the curves, one can find differences near the boson peak between the three temperatures (Cui et al., 2017b).

Since under each temperature, we have seven simulated samples with different configurations for position and velocity to calculate the VDOS, I take the same fitting parameters for each sample and found that they all generate the same results. Hence, in Fig. 5.3 and 5.4, I simply show results from one out of these seven simulated systems. The VDOS is calculated by diagonalising the Hessian matrix for the interaction energy of an atom in CuZr alloys in mass-rescaled coordinates, which is also used to calculate the $\boldsymbol{\Xi}_I$ vectors and hence $\Gamma(\omega_p)$. Analytical expressions for the Hessian and for $\boldsymbol{\Xi}_I$ as a function of the EAM interaction have been derived in the Appendix A.

Again, I have chosen the ansatz of $\nu(t) = \nu_0 \exp(-rt^b)$ motivated by Sjogren and Sjolander (1979), where $b = 0.3$ was found to work well for glycerol in Chapter 3. Here, a larger value of b appears appropriate for MG (Baldi et al., 2010).

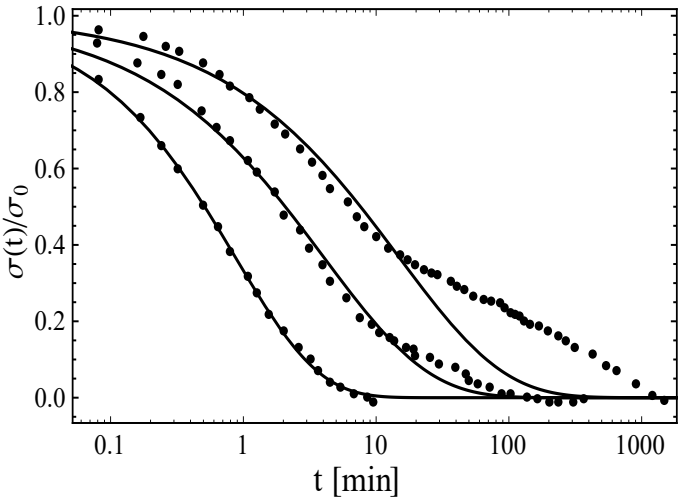

Fig. 5.1 Kohlrausch empirical fits (solid lines) of experimental data (symbols). Top to bottom corresponds to temperatures in the following order: 536 K, 603 K, 670 K(T_g). Solid curves are Kohlrausch $\sigma(t) \sim \exp[-(t/\tau)^{\beta}]$ empirical fittings used to calibrate results, where the two parameters β and τ were chosen to be 0.69, 0.87 (mins); 0.55, 4.03 (mins); 0.55, 14.87 (mins) for T_g, 0.9 T_g and 0.8 T_g respectively.

5.2 α-relaxation in Young's modulus of $Cu_{50}Zr_{50}$

Before presenting a comparison between the theory and the empirical best-fitting Kohlrausch stretched-exponential relaxation fitting of experimental data on $Cu_{50}Zr_{50}$, I firstly convert the linear response of the material to applied stress from time-dependent compliance to the frequency-dependent dynamic moduli, for a uniaxial strain of amplitude η_0:

$$E'(\omega) = \frac{\sigma_\infty}{\eta_0} + \frac{\sigma_0 \omega}{\eta_0} \int_0^\infty e^{-(t/\tau)^\beta} \sin(\omega t) dt, \tag{5.1}$$

$$E''(\omega) = \frac{\sigma_0 \omega}{\eta_0} \int_0^\infty e^{-(t/\tau)^\beta} \cos(\omega t) dt. \tag{5.2}$$

A detailed derivation of this result is reported in Appendix C.

In Fig. 5.3, I plot the comparisons for $E'(\omega)$ at $T_g = 670$ K, i.e. exactly at T_g, from Eq. (2.54) and Eq. (5.1). In this case, it is clear that the theoretical model is in excellent agreement with the transformed experimental data, and is also very close to the Kohlrausch function. This shows how crucial soft modes are, as well as the memory effects embodied in the non-Markovian friction, for the understanding of the viscoelastic response and of α-relaxation below the glass transition. In Fig. 5.4, I present fittings of the loss modulus, $E''(\omega)$. Also in this case, it is seen that the theory, given by Eq. (2.55), provides an excellent description of the experimental data. Note that, for clarity of presentation, I have changed

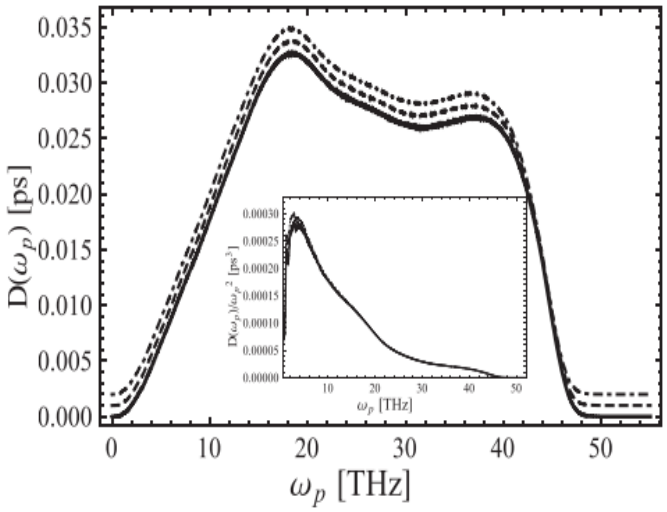

Fig. 5.2 VDOS from simulated $Cu_{50}Zr_{50}$ system. Solid, dashed and dotted lines correspond to VDOS at 670 K, 603 K and 536 K, respectively. The curves have been lifted upward in order to be distinguishable for the reader. The inset shows the VDOS normalised by the Debye law $\sim \omega_p^2$ which shows clear evidence of a strong boson peak.

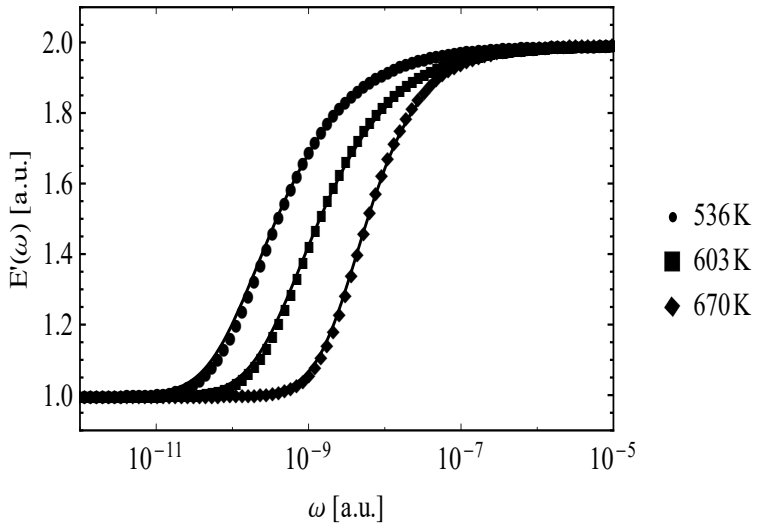

Fig. 5.3 Real part of the complex viscoelastic modulus. From right to left solid lines represent E' for T_g, 0.9 T_g and 0.8 T_g respectively, from the Kohlrausch best fitting of the experimental data. Symbols are calculated based on the theory. For T_g, 0.9 T_g and 0.8 T_g, b was chosen to be 0.72, 0.58 and 0.58; r was taken to be 1.2×10^{-6}, 7×10^{-6} and 3.4×10^{-6}. ν_0=0.137 was same for all temperatures. Rescaling constants have been taken to adjust the height.

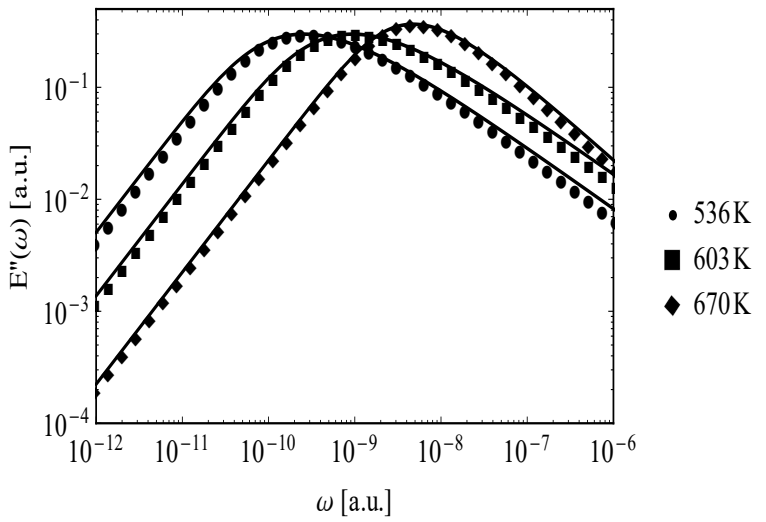

Fig. 5.4 Imaginary part of the complex viscoelastic modulus. From right to left solid lines represent E'' for T_g, 0.9 T_g and 0.8 T_g respectively, from empirical Kohlrausch fittings of the experimental data. Symbols are calculated from the theory. For T_g, 0.9 T_g and 0.8 T_g, b in the memory-kernel of our theory was chosen to be 0.72, 0.58 and 0.58; r was taken to be $1.2 \times 10^{-6}, 7 \times 10^{-6}$ and 3.4×10^{-6}. ν_0=0.137 was same for all temperatures. Rescaling constants have been taken to adjust the height.

the unit of time to shift curves horizontally. This means we have arbitrary units on abscissa and ordinate.

Remarkably, the theoretical model provides the long-sought crucial and direct connection between the excess of low-energy (boson-peak) modes of the VDOS at T_g, the memory effects in the dynamics, and the corresponding features of the response such as the α-wing asymmetry in $E''(\omega)$. It is in fact impossible to achieve a fitting of the data using a Debye model for the VDOS which has no excess of soft modes.

Even more crucially, in contrast with previous approaches, the theory shows that memory effects are as important as the boson peak modes in order to describe the experimental data. I have indeed checked that using a constant (Markovian) friction $\nu = \text{const}$, or even a simple-exponential time-dependence for $\nu(t)$, is not possible to describe the experimental data. Only a stretched-exponential form of $\nu(t)$ with a value of the stretching exponent in the range $0.58 - 0.72$, which decreases upon decreasing T further down from T_g, allows us to describe the data. Since ν in the theory physically represents the spectrum of dynamic coupling between an atom and all other atoms in the material, this result implies that every atom is long-ranged coupled to many other atoms beyond the nearest-neighbour shell, which

is the result of the anharmonicity of the interaction and of the non-locality of the electronic contributions to the interatomic interaction.

Also, this theoretical analysis shows that the time-scale over which atoms retain memory of their previous collision history, $\tau \equiv r^{-1/b}$ in the model, also increases upon decreasing the temperature, by more than a factor two overall, even though this increase appears to be somewhat non-monotonic, from $\tau \approx 1.14$ at $T = T_g$, to $\tau \approx 3.1$ at $T = 0.9T_g$, to $\tau \approx 2.0$ at $T = 0.8T_g$. The variation of τ on T could be elaborated in future, when more experimental data is available.

5.3 Set-up for another type of metallic glasses, $La_{60}Ni_{15}Al_{25}$

Here, I combine experimental and simulation investigations with the microscopic theoretical framework of viscoelastic response and relaxation of MGs. With this novel approach, I will be able to unveil the atomic-scale dynamics in MGs on time-scales as many as 12 orders of magnitude, thus providing necessary, complementary information for advanced simulation and experimental studies.

Considering the success of the work linking the low-energy boson peak with α-relaxation and dynamical heterogeneity in $Cu_{50}Zr_{50}$, results presented in the remaining sections in this chapter give a new insight into the atomic-scale dynamical facets of the JG β-relaxation in MGs. In particular, I will show the strong evidence that the JG β-relaxation is controlled by the smallest (lightest) atomic scale species present in the MG, and that the existence of two relaxation modes (α and JG β) can be traced down to the large differences in atomic mass of the metallic elements that comprise the MG.

Dynamical mechanical analysis and inelastic neutron scattering

My collaborators carried out DMA experiments according to the procedure outlined in Zhu et al. (2014), using a TAQ800 dynamical mechanical analyzer. Fully amorphous cylindrical samples of $La_{60}Ni_{15}Al_{25}$ with a diameter of 2 mm were tested using the single-cantilever bending method in an isothermal mode with a strain amplitude of 5 μm, temperature step of 3 K and discrete testing frequencies of 1, 2, 4, 8, and 16 Hz. The complex viscoelastic shear modulus is obtained as $G(\omega,T) = G'(\omega,T) + iG''(\omega,T)$ as a function of test frequency ω and temperature T, with mechanical relaxations appearing peaks in the loss modulus $G''(\omega,T)$ (Cui et al., 2018a).

Glassy ribbons of $La_{60}Ni_{15}Al_{25}$ were produced by melt spinning at the Institute for Physics, Chinese Academy of Sciences in Beijing. About 12 m of ribbons with a cross-section of 2.5×0.06 mm^2 were placed in a thin-walled aluminum hollow cylinder (height 51 mm, diameter 20 mm, thickness 0.55 mm) for the INS experiments at the time-of-flight spectrometer TOFTOF in Garching. An incident wavelength of $\lambda = 2.8$ Å resulted in an accessible momentum transfer range of $0.8 \leq q \leq 4.2$ Å^{-1} at zero-energy transfer. The raw data were normalised to a vanadium standard, corrected for empty container scattering and sample shelf-absorption, and interpolated to constant q in order to obtain the dynamic structure factor. The background was corrected by separate measurements of the cryostat with an empty sample holder. As the scattering probability of the ribbons was calculated to be around 8 %, multiple scattering effects were neglected.

In order to access the largest energy transfer range available, only the data located on the neutron energy gain side of the spectrometer were analysed. In a multi-component system with predominantly coherent scatterers, a generalised, neutron-weighted VDOS, $D(\omega_p)$, can be obtained under the incoherent one-phonon approximation. The neutron-weighted VDOS was obtained in an iterative procedure using the FRIDA-1 software (Wuttke, 2013; Wuttke et al., 1993).

Molecular Dynamics simulations

My colleagues specialised in numerical simulations performed classical MD simulations for the $La_{60}Ni_{15}Al_{25}$ metallic alloy system using the LAMMPS package (Plimpton, 1995). The interatomic interactions were described by the EAM potential (Sheng et al., 2008). To obtain the VDOS of the system at various temperatures, the direct diagonalisation method was adopted, in which the steepest-descent method is carried out for the final configuration.

The structure model contains 10,000 atoms in a cubic box with periodic boundary conditions applied in three dimensions. It was first fully equilibrated at $T = 2000$K for 1 ns in the NPT (isobaric and isothermal) ensemble, then cooled down to 300 K with a cooling rate of 10^{12} K/s. In the cooling process, the box size was adjusted to give zero pressure. At 300 K, the structure was then relaxed for 2 ns in the NPT ensemble. To obtain the atomic structures at 330, 360, 390, and 410 K, the structure at 300 K was then heated with a heating rate of 10^{10} K/s, and then relaxed for 2 ns in NPT ensemble at each temperature of interest. The MD timestep was set to be 2 fs (Cui et al., 2018a).

The VDOS can be calculated by directly diagonalising the dynamical matrix as

$$D(\omega_p) = \frac{1}{3N-3} \sum_m \delta(\omega_p - \omega_m), \tag{5.3}$$

where ω_m is the eigenfrequency of the dynamical matrix and modes with zero vibrational frequency due to free translation are excluded.

5.4 Secondary relaxation in shear modulus of $La_{60}Ni_{15}Al_{25}$

Qualitative arguments for the form of friction kernel in $La_{60}Ni_{15}Al_{25}$

As has been shown before in the context of Eq. (2.51), assuming $\underline{\underline{P}}^T \tilde{\nu} \underline{\underline{P}}$ to be a diagonal matrix, i.e. the damping is not correlated across different eigenvalues, the friction that the m-th mode feels is approximated by $i\omega \sum_n (P_{nm})^2 \tilde{\nu}_n$ (Cui et al., 2018a). In terms of the different atomic species forming the alloy, I write:

$$\begin{aligned}\sum_n (P_{nm})^2 \tilde{\nu}_n = &\left[\sum_{Al}^{25}(P_{nm})^2 \sum_\alpha \frac{m_\alpha}{m_{Al}} \frac{c^2_{\alpha,Al}}{\omega^2_\alpha} + \sum_{La}^{60}(P_{nm})^2 \sum_\alpha \frac{m_\alpha}{m_{La}} \frac{c^2_{\alpha,La}}{\omega^2_\alpha} + \sum_{Ni}^{15}(P_{nm})^2 \sum_\alpha \frac{m_\alpha}{m_{Ni}} \frac{c^2_{\alpha,Ni}}{\omega^2_\alpha}\right] \cdot \\ &\frac{\pi}{2}[\delta(\omega-\omega_\alpha)] \\ = &\sum_\alpha \left[\sum_{Al}^{25}(P_{nm})^2 \frac{m_\alpha}{m_{Al}} \frac{c^2_{\alpha,Al}}{\omega^2_\alpha} + \sum_{La}^{60}(P_{nm})^2 \frac{m_\alpha}{m_{La}} \frac{c^2_{\alpha,La}}{\omega^2_\alpha} + \sum_{Ni}^{15}(P_{nm})^2 \frac{m_\alpha}{m_{Ni}} \frac{c^2_{\alpha,Ni}}{\omega^2_\alpha}\right] \cdot \\ &\frac{\pi}{2}[\delta(\omega-\omega_\alpha)]. \end{aligned} \tag{5.4}$$

The role of P_{nm} is to give a weight to each $\tilde{\nu}_n$ contribution in the sum. All these sums could be written also as integrals upon replacing the discrete variable ω_α with the continuous eigenfrequency ω_p and introducing the VDOS as a factor in the integral over ω_p. Here, one can find that each term is inversely proportional to the mass of the atomic species in question. I note that the atomic mass of La (138.9 u) is more than twice as large as the mass of Ni (58.7 u) and five times larger than the mass of Al (26.98 u), which gives a much larger weight in the sum to the Al and Ni terms. Hence, taking also stoichiometry into account, the two terms relative to Ni and Al considered together are about three times larger than the contribution of the La term.

In order to strengthen this claim, I also consider the role of the unknown dynamical coupling coefficients c_α appearing in Eq. (5.4). While the values of these coefficients cannot be determined from first principles, I can still obtain valuable indications about the probable magnitude by considering quantities like the partial correlation $g(R)$ functions in the system. Since these coefficients are associated with medium-range (or generically, beyond-short-range) dynamics, features in the $g(R)$ may give an indication about relative magnitude of dynamical coupling between different species in the alloy.

Also, while $g(R)$ is a static structural quantity, it is also true that it is directly related to dynamics via the Boltzmann inversion relation which yields the potential of mean force (V_{mfp}) as $V_{mfp}/k_BT = -\ln g(R)$. In turn, the potential of mean force represents the interaction energy between two atoms mediated by the presence of all other atoms in the system, hence it also contains many-body effects. Therefore, $g(R)$ is directly related to the potential of mean force which in turn influences the correlated motions (hence the dynamics) of the atoms and establishes (e.g. through long-range attractions) the dynamic coupling.

Consideration of the pair correlation function obtained from simulations as shown in Fig. 5.5 indicates that there is a clear broad peak for Al-Al in the regime of the medium-range order. This supports the claim that the JG β-relaxation is due to medium-range correlations and coupling between Al atoms. This broad peak of Al-Al with respect to the short-range order peak stands out in comparison with the other contributions in the medium-range regime.

Finally, not only the pre-factor of the memory function of La will be smaller compared to the other two atomic species, for the reason above, but also the characteristic time-scale of memory decay associated with La (which would be τ_3, since La would contribute a third term to memory function) is comparatively larger, as the relaxation time is typically inversely proportional to the mass (or at least inversely proportional to square root of the mass). Hence, the contribution of La to memory and, hence, to the ISF would be at a somewhat longer time-scale compared to Ni. Additionally, this contribution would be probably hybridised or obscured by Ni, which has a larger prefactor and would explain why I result in only two decays in the model for the ISF and memory function.

These arguments, which indicate that the La-term in the form of the memory function given by Eq. (5.4) may be negligible, can be summarised as follows: (i) the mass-factor in the denominator makes the contribution of La about three times smaller than the two contributions of Ni and Al taken together; (ii) the main medium-range contributions to the features of the $g(R)$ emanate from Al, which corroborates the hypothesis that the c_α coefficients are larger for Al and justify dominance of Al dynamics in the JG β-relaxation; (iii) if modeled as a third stretched exponential function, the contribution of La would have a larger characteristic time-scale of decay and would show up at longer times, probably masked or hybridised with the Ni contribution. Based on this approximation, the form of memory function for the interatomic friction in Eq. (5.4) reduces to

$$\begin{aligned}\sum_n (P_{nm})^2 \nu_n(t) &= \sum_\alpha \sum_{Ni}^{15} (P_{nm})^2 \frac{m_\alpha}{m_{Ni}} \frac{c^2_{\alpha,Ni}}{\omega^2_\alpha} \cos(\omega_\alpha t) + \sum_\alpha \sum_{Al}^{25} (P_{nm})^2 \frac{m_\alpha}{m_{Al}} \frac{c^2_{\alpha,Al}}{\omega^2_\alpha} \cos(\omega_\alpha t) \\ &= \nu_1(t) + \nu_2(t). \end{aligned} \tag{5.5}$$

where $\nu_1(t)$ and $\nu_2(t)$ are two generic functions of time.

Radial distribution function and partials thereof

From the MD simulations, the partial pair correlation functions $g(R)$ can be obtained for all atomic pairs, which are shown in Fig. 5.5. The partial functions shown in Fig. 5.5(b) clearly indicate that, in the regime of the medium-range order (between $r = 4$ Å and $r = 7$ Å), there are broad peaks for Ni-Ni and Al-Al, which are either much larger or comparable in magnitude to the primary peak associated with the short-range order (up to $r \sim 3$ Å). In contrast to the La-pairs, in which the short-range order peak appears to be the most dominant (Fig. 5.5a), the more active Ni-Ni and Al-Al pair-interactions at the length-scale of the medium-range order would also indicate a stronger dynamical coupling in this spatial regime.

The vibrational density of states for $La_{60}Ni_{15}Al_{25}$

The filled gray circles in Fig. 5.6 represent the total $D(\omega_p)$ as obtained from MD simulations introduction in Section 5.3. A more detailed look at the VDOS can be seen through the respective contributions of the La, Ni and Al atoms. It is clear that the initial maximum of the total $D(\omega_p)$ at around 8 meV is attributed to low-energy vibrations involving the heavy La atoms, while vibrations of the Ni atoms occur around 15 meV and are responsible for an apparent shoulder on the high-energy side of the main vibrational band. The vibrational dynamics of the light Al atoms are, in contrast, well separated from that of the other elements and exhibit a double-band structure at around 25 and 35 meV. The $D(\omega_p)$ as obtained in INS experiments is shown alongside the simulation data. It is important to note here that the experimental $D(\omega_p)$ is additionally weighted by the isotope-specific neutron scattering cross-sections of the constituent elements, of which Ni-Ni and Ni-La atomic pairs will dominate. Hence, the experimental $D(\omega_p)$ should be taken only to represent a generalised, neutron-weighted VDOS. In any case, it is apparent that the predominant contribution to the high-frequency side of both VDOS of this MG stems from the vibrations of the Al atoms.

Dynamic mechanical analysis and comparison with theory

In Fig. 5.7, I show a master curve of the experimentally measured $G''(\omega)$ obtained from Zhu et al. (2014) for $La_{60}Ni_{15}Al_{25}$ at a reference temperature of 453 K, together with a theoretical fitting provided by Eq. (2.55). The α-relaxation appears as the main loss peak situated around 1 Hz. A distinct feature of this system is the prominent and well separated loss peak on the high-frequency side around 10^6Hz and is attributed to the JG β-relaxation.

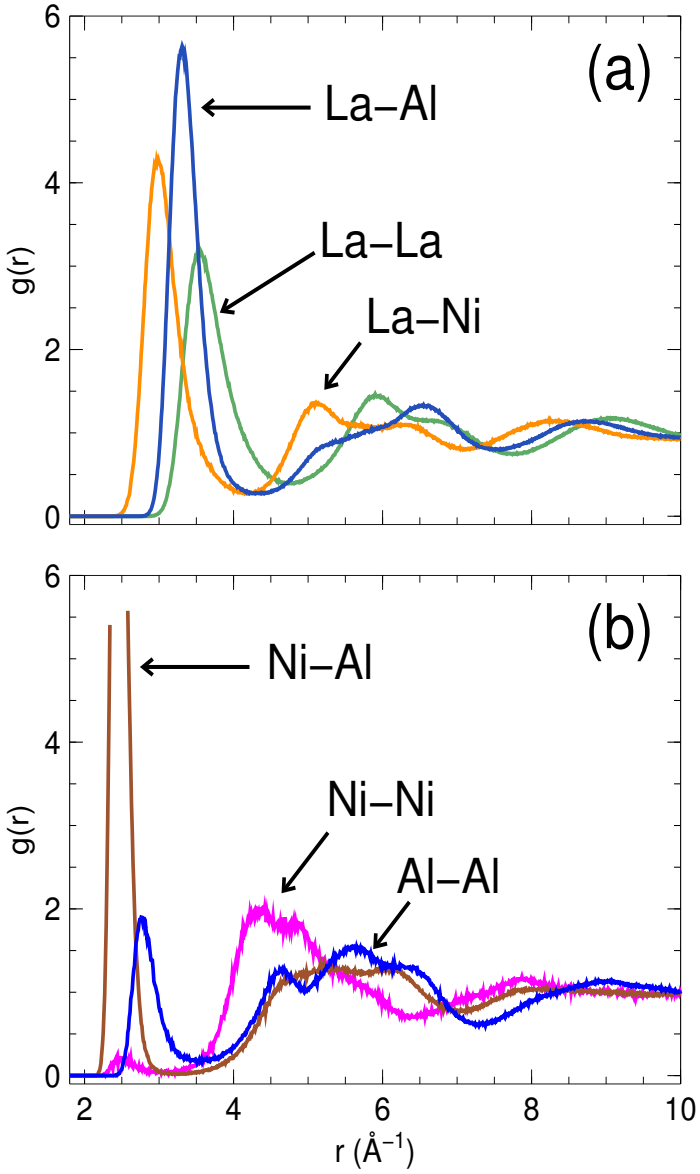

Fig. 5.5 Partial contributions to the radial distribution function $g(R)$, as calculated from MD simulations for $La_{60}Ni_{15}Al_{25}$ at $T = 300$ K. The large maximum of the Ni-Al partial in (b) occurs at $g(R_{max}) = 12$, which falls out of the range of the vertical axis of the plot.

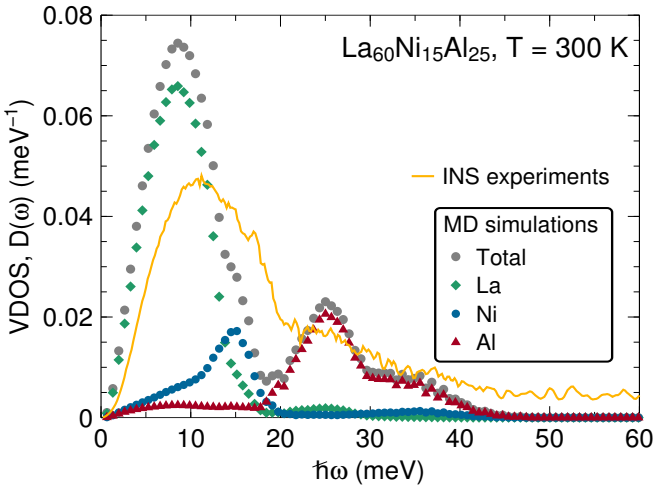

Fig. 5.6 VDOS of $La_{60}Ni_{15}Al_{25}$ at $T = 300$ K as determined in INS experiments (solid line) and MD simulations (symbols).

The nonaffine lattice dynamics theory of viscoelasticity of glasses outlined above allows us to quantitatively link the macroscopic features of the JG β-relaxation with the atomic-scale vibrational properties of this MG. Within this framework, it is possible to rationalise the average friction in the atomic motion of a tagged atom in the glass in terms of the respective contributions of the atomic components, for which the friction coefficient of the I-th atom, ν_I, is proportional to the reciprocal of the atomic mass of atom I (Cui et al., 2017b; Zwanzig, 2002). Thus, when summing over all tagged atoms in $i\omega\sum_n (P_{nm})^2\tilde{\nu}_n$, the contributions to the friction coefficient coming from the heaviest atoms, i.e. La, turn out to be smaller by at least a factor of $1/3$ in comparison with the contributions of Al and Ni (taken together). For the case of $La_{60}Ni_{15}Al_{25}$, I thus find that the contribution of La can be neglected, given the comparatively very large mass of La, which leaves the average friction as the sum of two contributions, those of Ni and Al, respectively, which carry widely different relaxation time scales, by virtue of the different atomic masses.

As derived before, in the sum over n only terms corresponding to Ni and Al atoms survive, which are well separated in magnitude given the difference in mass between Ni and Al. I then divide the sum into two groups, for Ni and Al, respectively, and then average each group separately. The final result is that the average friction memory function consists of two distinct contributions, according to Eq. (5.5), both of which will decay in time but with two different and well-separated relaxation times, τ_1 and τ_2, respectively. The shorter relaxation time τ_2 (associated with the JG β-relaxation) is related to the atomic dynamics of the lighter

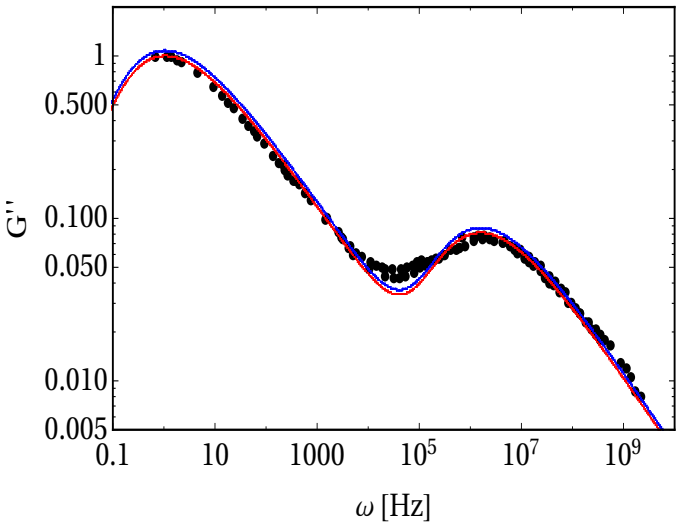

Fig. 5.7 Master curve of the imaginary part of the complex viscoelastic modulus, $G''(\omega)$, at a reference temperature $T = 453$ K. The red and blue curves are fitting results to the theoretical model using the experimental and simulated VDOS, respectively, as input.

element, Al, whereas the other term has a longer relaxation time τ_1, dominated by the atomic dynamics of the heavier element, Ni, which contributes to the α-relaxation time.

With an appropriate ansatz for $\nu(t)$, I obtain the ISF via $\nu(t) \sim F(q,t)^2$ (Bagchi, 2012; Sjogren and Sjolander, 1979). It is known that in supercooled liquids $F(q,t) \sim \exp[(-t/\tau)^b]$ for the α-relaxation, where the stretching exponent b has value between $b = 0.5 - 0.7$ (Hansen and McDonald, 2008). When both α- and β-relaxations are present, $F(q,t)$ has a two-step decay, with a first decay at shorter times due to the β-relaxation, and a second decay at much longer times due to the α-relaxation. On the basis of this evidence, I take the time dependence of each of the two terms in the memory function to be stretched-exponential with different values of τ and b,

$$\nu(t) \sim \exp[-(t/\tau_1)^{b_1}] + \nu_2 \exp[-(t/\tau_2)^{b_2}], \tag{5.6}$$

where ν_2 is a constant.

The curves in Fig. 5.7 are fits to experimental data using the VDOS obtained in both INS experiments (red) and MD simulations (blue). It is apparent that the theoretical model excellently captures both peaks in the loss spectrum over a frequency range of some 10 orders of magnitude with the resulting parameters: $\tau_1 = 0.67$s, $b_1 = 0.45$, $\tau_2 = 4.04 \cdot 10^{-7}$s, $b_2 = 0.47$ and $\nu_2 = 0.07$. I note here that the two-component ansatz is the simplest model with the smallest number of free parameters that completely describes the experimental G''

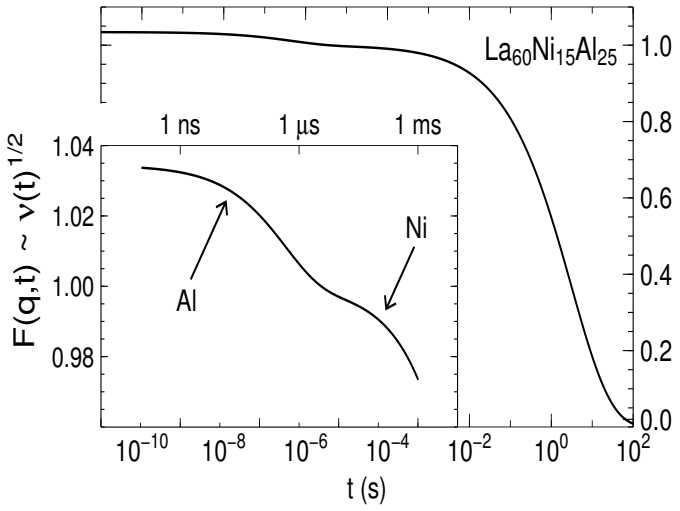

Fig. 5.8 Time decay of the square-root of total memory function for the friction $\nu(t)$, exhibiting two decays corresponding to α- and β- decay in the intermediate scattering function $F(q,t)$, respectively, according to the relation $F(q,t) \sim \sqrt{\nu(t)}$ that follows from Eq. (3.18)

data, which is congruent with the theoretical result derived in previous sections, where $\nu(t)$ reduces to a sum of two terms. Surprisingly, I obtain the same fitting parameters for both the experimental and the simulation VDOS, although the two data sets exhibit noticeably different features. In a way, this result reassures us that the differences in the two VDOS did not simply “disappear" into the fitting parameters and genuinely implies that these differences do not play a substantial role in the mechanical response. Moreover, it suggests that the qualitative shape of the VDOS, i.e. the location of the peaks, especially on the low-frequency side, is of primary importance. In a broader perspective, this result implies that the origin of the JG β-relaxation in various types of glasses can be traced back to the generic shape of the VDOS and encourages the development of a universal theory based on the microscopic framework employed here.

Qualitative behaviour of intermediate scattering function from theoretical fitting

The square-root of $\nu(t)$ is shown in Fig. 5.8 following the relation $F(q,t) \sim \sqrt{\nu(t)}$. It can be seen the characteristic two-step decay of $F(q,t)$ presents in systems with well separated α- and β-relaxations, with the first decay occurring on the typical time scale of the β-relaxation, $\tau_\beta \sim 10^{-7}$s, followed by a much slower decay given by the time scale set by τ_1. While the

time scale τ_β closely matches the time scale τ_2 set by atomic dynamics dominated by Al, the typical α-relaxation time of glasses, $\tau_\alpha \sim 10^{-2}$s, is significantly different from the time scale τ_1 associated with Ni, as the α-process is more complex and the square-root mixing of the different time scales of the above relaxation reflects this fact. Moreover, the α-peak in G'', and the corresponding decay in $F(q,t)$, cannot be reduced to just τ_1, as the time scale range of the α-relaxation contains a strong contribution from soft modes (the boson peak) in the VDOS (Milkus and Zaccone, 2016). This is clear from Eq. (2.53) where the term ω_p^2 in the denominator gives a large weight to the low-ω_p part of the VDOS, which contains the boson peak proliferation of soft modes, as was shown in previous sections for the case of CuZr alloys which present α-relaxation only and also for dielectric relaxation of glycerol in Chapter 3.

Summary

I applied the theory of dissipative nonaffine lattice dynamics to MGs, to obtain dynamic viscoelastic moduli which are functions of the vibrational VDOS and of the emergent non-Markovian atomic-scale friction coefficient (memory kernel) that embodies the long-range coupling between atoms. Strong memory effects were found at the atomic level, possibly due to the non-local electronic component of interaction. The results of nonaffine lattice dynamics theory shed light onto the microscopic glassy-state dynamics over a temporal range of 12 orders of magnitude and reproduce the distinctive two-step decay of the intermediate scattering function that is a characteristic feature of systems exhibiting both α- and β-relaxations.

Chapter 6

Damping is related to disorder in elastic solids

The dynamical structure factor (DSF) conveys the information of phonon transport in crystalline solids, as well as in disordered systems. In particular, the width of the structural peaks in DSF is representative of the mechanical damping in the material. While anharmonic effects are believed to cause quadratic damping in low frequency regime for both longitudinal and transverse waves (Herring, 1954), the damping coefficient is instead found proportional to the frequency of the acoustic mode, and therefore is linear in low wavevectors, in a harmonic theory of quenched-averaging of the DSF.

To explain the origin of logarithmatic enhancement in Rayleigh scattering with the replica theory, I will mainly consider systems with similar elastic property as in (Gelin et al., 2016), in an athermal regime where scattering is purely harmonic (no viscous/anharmonic dissipation involved). However, such systems usually have coupled internal longitudinal and transverse propagators: the explicit form of damping is thus not as clearly defined (Lifshitz et al., 1986). Hence, the present work demonstrates that, contrary to claims in Caroli and Lemaître (2019), heterogeneous elasticity (HE) in the fully tensorial formulation developed here for the first time is indeed able to recover the anomalous Rayleigh scattering observed in simulations. I will work essentially within the linear acoustic dispersion relation regime

6.1 Damping in elastic waves

In the classical limit, the DSF derived in Section 2.8 and the Green's (wave) function are related by the fluctuation-dissipation theorem (FDT) (Kubo, 1957; Maurer and Schirmacher,

2004; Schirmacher, 2015; Schirmacher et al., 2015b):

$$S(\mathbf{q},\omega)=\frac{k_BTq^2}{\pi\omega}\mathrm{Im}[G(\mathbf{q},\omega)] \quad \text{with} \quad G(\mathbf{q},\omega)=\frac{1}{-\omega^2+q^2c^2(\omega)}, \tag{6.1}$$

where $c(\omega)$ is the (generalised, complex) sound velocity relating to the frequency-dependent linear elastic modulus $C(\omega)=\rho c^2(\omega)=C'(\omega)-iC''(\omega)$. The form of the Green's function in Eq. (6.1) essentially represents elastic waves propagating in the system where elasticity presents spatial correlations. Defining the sound attenuation (damping) coefficient $\Gamma(\omega)=\omega C''(\omega)/C'(\omega)$, and the resonance frequency $\Omega(q)=q\sqrt{C'(\omega)/\rho}$, it can be directly shown that the DSF becomes (Schirmacher et al., 2015b):

$$S(q,\omega)=\frac{k_BTq^2}{M\pi\omega}\frac{\Omega^2(q)\Gamma(\omega)/\omega}{(\Omega(q)^2-\omega^2)^2+(\Omega^2(q)\Gamma(\omega)/\omega)^2}. \tag{6.2}$$

Near the resonance frequency $\omega\sim\Omega(q)$, the form of DSF can be approximated in the form of DHO:

$$S(q,\omega)=\frac{k_BTq^2}{M\omega\pi}\frac{\omega\Gamma(q)}{(\Omega^2(q)-\omega^2)^2+\omega^2\Gamma(q)^2}. \tag{6.3}$$

Equation (6.3), for a fixed q, reaches a maximum value (peak) when $\omega_{max}^2=\Omega^2-\Gamma^2/2$. Assuming positive parameters Γ and Ω, the half width at half maximum (HWHF) takes the form

$$\left(\omega^2-\omega_{max}^2\right)=\Gamma\sqrt{\Omega^2-\Gamma^2/4}. \tag{6.4}$$

Thus, near the resonance frequency Ω and at low damping, Γ is roughly HWHM of the dynamic structure factor. I also note that, at $\Gamma\to 0$, $S(q,\omega)$ reduces to the sum of δ-functions:

$$\lim_{\Gamma\to 0}S(q,\omega)=\frac{k_BTq^2}{2M\omega^2}[\delta(\omega-\Omega)+\delta(\omega+\Omega)], \tag{6.5}$$

where the identity $2a\delta(x^2-a^2)=\delta(x+a)+\delta(x-a)$ was used. Expression (6.5) in the $\Gamma\to 0$ limit reflects the perfect crystal. Figure 6.1(a) shows the result of a 1D chain with the same springs (k_0) connecting nearest neighbours of equal mass M separated by equal distance a. The q dependent eigenvectors/eigenvalues are calculated numerically from the symmetric tridiagonal dynamical matrix of this simple system, before they are substituted into Eq. (2.133). To depict this, in Fig. 6.1, I provide plots of DSF for 1D linear chains connected with springs having some variations in spring constants (representing a realisation of disorder), which already shows broadening of δ-function peaks, indicating that the emergence of sound

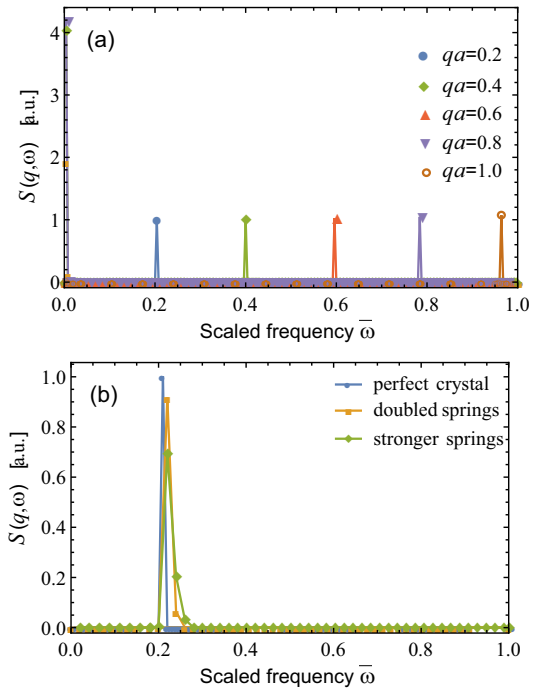

Fig. 6.1 The dynamical structure factor of 1D linear chains with and without damping, plotted against the non-dimensional frequency scaled by a factor $\sqrt{k_0/M}$. There are 3000 masses separated in equal distance in a unit cell. (a) DSF for several values of wavevector q, cf. Eq. (6.5). (b) DSF with added disorder in some springs. A hundred springs have their spring constants doubled, then further two hundred are replaced with three (100 out of 200) and four times (remaining 100) spring constants compared with the original one; the wavenumber $qa = 0.2$.

attenuation (damping) is linked to disorder in perfect harmonic crystals. It is clear in Fig. 6.1(a), no damping takes place at any q. The divergence of $S(q,\omega)$ as $\omega \to 0$ is due to the elastic $q = 0$ scattering.

When the interaction is harmonic, the occurrence of sound attenuation is due to defects, or generally structural disorder, which I will examine in the next section. In Fig. 6.1(b), I show a preliminary indication of main results, showing the computed DSF with a certain model disorder in springs: $3\% - 10\%$ (randomly chosen) springs were replaced with those of larger (twice or higher) spring constant. The more springs are replaced and the larger spring constants they have, the wider the curve becomes. I also find that, adding disorder does not change the position of the structural peak of DSF at the resonant frequency, which is expected given the form of $\Omega(q)$ used in Eqs. (6.2-6.3).

6.2 Quenched random disorder

When the local elastic modulus, or the spring constant k of a harmonic bond in a discrete lattice model, takes random values in the system, all quantities like DSF should be averaged over the distruibution of such random disorder. In general, quenched disorder could occur in three ways: by randomising masses, spring constants, or equilibrium positions. It is commonly accepted in scattering theories that the first two types of disorder are essentially equivalent (Gelin et al., 2016), so I let all particles have the same mass M. I note the disorder in the initial equilibrium positions might also cause the break of inversion symmetry, thus changing affine force fields (Cui and Terentjev, 2020; Lemaitre and Maloney, 2006; Milkus and Zaccone, 2016), which I am not considering here.

I consider the random distribution of values of the spring constant, assuming the spring constants satisfy a normal distribution, $k_i \sim \mathscr{P}(k_i) \equiv N(k_0, \sigma)$, where i is the index of the i-th spring, the mean value k_0 is the measure of material stiffness, and the variance σ serves as the measure of quenched disorder. In principle, the spring constant should always be non-negative. One can introduce the truncated Gaussian distribution to set a lower bound for spring constant (Schirmacher et al., 1998), namely $\mathscr{P}'(k) = \mathscr{P}(k)H(k-k_{min})$ for some $k_{min} > 0$. However, I found that the truncation does not change any (analytical and numerical) results. Using Eq. (2.133), the quenched averaging of DSF is easy due to δ-functions (which is why the truncation of the Gaussian range has no effect in this case).

$$\langle S(\mathbf{q},\omega)\rangle = \int \prod_i \mathscr{D}[k_i]\mathscr{P}(k_i)S(\mathbf{q},\omega) \propto \frac{f(q)}{\omega}\int \prod_i \mathscr{D}[k_i] e^{\sum_i -\frac{(k_i-k_0)^2}{2\sigma^2}} \delta(\omega^2 - \omega_{A,L}^2(\mathbf{q},k_i)),$$

where $f(q)$ represents the q-dependent part: the prefactor of δ-functions in Eq.(2.133). In the second equality I focus on the longitudinal acoustic mode, since only the acoustic branch $\Omega(q) = \omega_{A,L}(q)$ contributes to elastic waves (Born and Huang, 1954; Cui and Terentjev, 2020). That means, only one out of Nd modes survives, and is then subjected to quenched averaging. Although this still leaves us one set of δ-functions, which looks similar to Eq. (6.5), the physics is completely different. Here, the system with quenched random disorder is averaged over local realisations of the random variable (the spring constant), and I will shortly discover a non-zero damping coefficient, while in Eq. (6.5) I had a perfect crystal without damping in sound waves.

I also note that, unlike Eq. (6.1), this DSF relates to the lattice waves (or collective phonon modes). In general, the lattice wave and the elastic wave are different (Born and Huang, 1954; Trinkle, 2008), however, their difference is negligible when q is small. In principle, the acoustic branch $\omega_{A,L}(q)$ receives contributions from all springs satisfying

Gaussian distributions. For analytical clarity, I simplify this by using a single continuous variable k for the spring constant which is treated as a random variable. The quenched average becomes

$$\langle S(q,\omega)\rangle \propto \frac{f(q)}{\omega}\int e^{-\frac{(k-k_0)^2}{2\sigma^2}}\delta(\omega^2-\omega_{A,L}^2(\mathbf{q},k))dk. \tag{6.6}$$

Performing the integral over k gives

$$\langle S(q,\omega)\rangle \propto \frac{f(q)}{\omega}e^{-\frac{(\omega^2-\omega_{A,L}^2(\mathbf{q},k_0))^2}{2(\sigma/k_0)^2\omega_{A,L}^4(\mathbf{q},k_0)}}. \tag{6.7}$$

The acoustic phonon frequency normally would take a form $\omega_{A,L}^2 = 4(k/M)\sin^2(qa)$, where a is the lattice spacing along $\mathbf{q}$. I find that, in the averaged disordered system, the expression is changed very little. The maximum in Eq. (6.7) (the position of the acoustic resonance peak), is found at:

$$\omega_{max}^2 = \frac{1}{2}\omega_{A,L}^2(1-\sqrt{1-2\sigma^2/k_0^2}). \tag{6.8}$$

If I assume a relatively low disorder, $\sigma^2/k_0^2 \ll 1$, then $\omega_{max} \approx \omega_{A,L}(\mathbf{q},k_0)$ at the original resonant frequency. Also in this case, the disorder-averaged DSF roughly takes its half maximum when the exponent in Eq. (6.7) is of order 1. This gives the estimate of the half-width

$$\omega - \omega_{A,L} \approx \frac{\sqrt{2}}{2}\frac{\sigma}{k_0}\omega_{A,L}(\mathbf{q},k_0) \tag{6.9}$$

This means that at low disorder the damping coefficient, the width of the broadened DSF resonance peak as elucidated by Eq. (6.9), takes the explicit form: $\Gamma = \sqrt{2}\sigma\omega_{A,L}/k_0$. Notably, this scales linearly at low wavevectors. To verify this observation, I numerically compute the DSF of 1D linear chains, calculating the quenched-averaged DSF for 30 realisations of the random distribution of spring constants between the bonds, and average every point for a given ω, thus having an independent approximate numerical evaluation of $\langle S(q,\omega)\rangle$. This is plotted in Fig. 6.2(a), for an example case of $\sigma = 0.25k_0$, and several values of q on the same plot, with the numerical data fitted by Eq. (6.3) to determine $\Gamma(q)$ for each scattering peak.

Figure 6.2(a) shows the effect of quenched disorder is more pronounced with increasing q. This is because the bigger the space we average, the lower q is, and so the less average disorder is left in it. After fitting each peak of the averaged DSF, I obtain the relation between the wavenumber and the effective damping coefficient $\Gamma(q)$ defined in Eq. (6.3); this relationship is shown in Fig. 6.2(b), for several values of σ. The values of damping coefficient differ strongly for the cases of different disorder, but the logarithmic scale of the

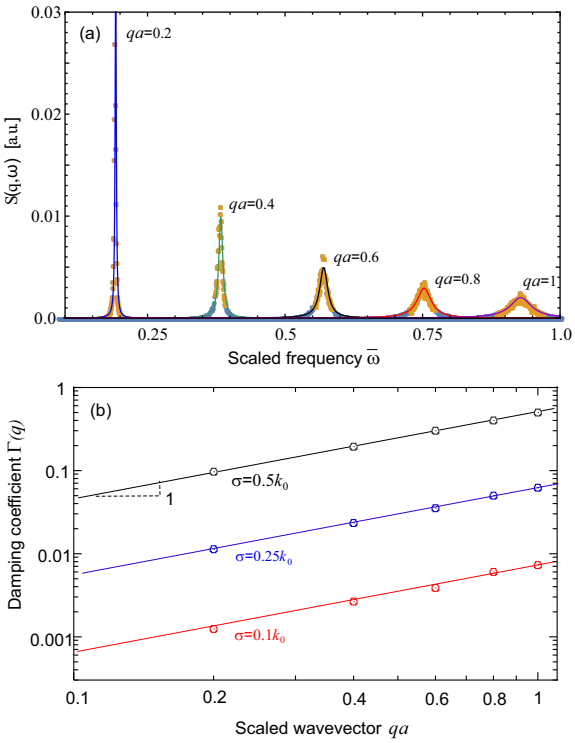

Fig. 6.2 (a) The numerical calculation showing the effect of Gaussian disorder in spring constants on damping, for $\sigma = 0.25k_0$. There are 20000 masses separated in equal distance in a unit cell. The averaged DSF $\langle S(q,\omega)\rangle$ for several values of q, numerically calculated using the Gaussian distribution in spring constants of 1D linear chain, plotted against the non-dimensional frequency scaled by a factor $\sqrt{k_0/M}$. The data for each q is fitted by DHO in Eq. (6.3) (solid line). (b) The log-log plot of the fitted damping constant Γ, obtained as the peak width (also scaled in units of frequency $\sqrt{k_0/M}$), plotted against the reduced wavenumber qa, shows the distinct linear scaling $\Gamma \sim q$ discussed in the text.

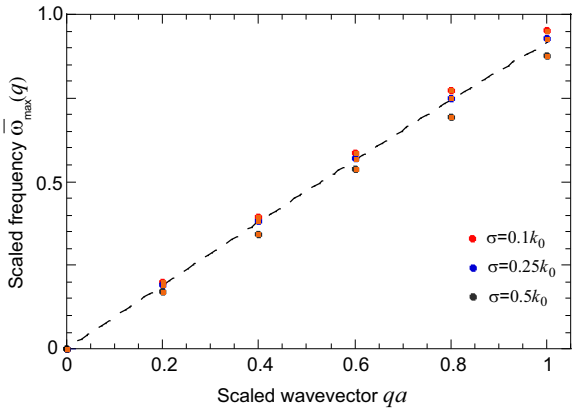

Fig. 6.3 The resonant frequency $\bar{\omega}_{max}(q)$, scaled by $\sqrt{k_0/M}$, obtained from numerical calculation with Gaussian disorder in spring constants, for several values of σ, see Fig. 6.2(a). The dashed line is the parameter-free curve $\bar{\omega} = 2\sin(qa/2)$, which fits the data well, and we can see that deviations from linearity are small, and the dependence on disorder strength σ is weak, see Eq. (6.8).

plot allows us to see the $\Gamma(q)$ dependence for all considered cases. Importantly, I rigorously confirm the linear dependence $\Gamma(q) \sim q$, which is an unexpected result never reported in the literature before.

The other fitting parameter for the numerically averaged DSF, illustrated in Fig. 6.2(a), is the resonance frequency $\Omega(q)$ in Eq. (6.3), which corresponds to the $\omega_{max}(q)$ in Eq. (6.8). The comparison of the model for the dispersion relation $\omega_{A,L} = \sqrt{4k_0/M}\sin(qa/2)$ supports its validity, especially when the wave vector q is not large. Here I find only a weak dependence on the strength of disorder σ, see Fig. 6.3. I have to add at this point that the estimated errors in the described procedure of averaging over several disorder realisations are very low, and I am not showing them in the plots.

6.3 Density of states and the "boson peak"

The density of states can be calculated from the (lattice) Green's function used in Eq. (6.1), which has been shown by Eq. (2.101) (by letting $z = \omega^2 + i\varepsilon, \varepsilon \to 0$):

$$D(\omega) = -\frac{2\omega}{\pi}\int \mathrm{Im}[\langle G(\mathbf{q},\omega)\rangle]d^d q. \tag{6.10}$$

Taking the quenched average of the Green's function (directly associated with the DSF considered above) does not change the result of the underlying FDT. Combining Eq. (6.1) and Eq. (6.7), and again benefiting from the use of δ-function under the integral over disorder, I can obtain the average (observable) VDOS of the longitudinal acoustic branch,

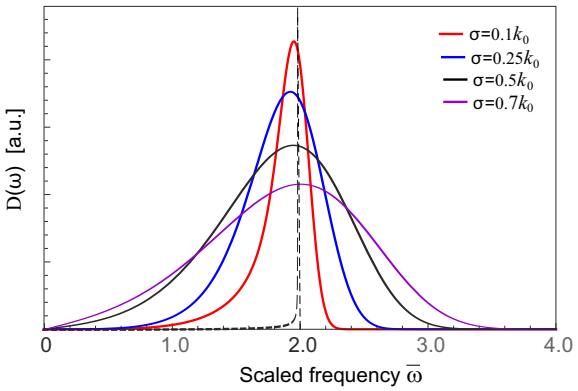

Fig. 6.4 VDOS calculated using Eq. (6.11) with several values of σ listed in the plot. Frequency is scaled in the same way as in Fig. 6.2. The cut-off q_D is chosen at π/a. In the limit of vanishing disorder, the "boson peak" transforms to a sharp resonance at a characteristic frequency of $2\sqrt{k_0/M}$ (in that similar to what one obtains from the analysis of an isolated effect (Kosevich, 2005)), obtained from the integration Eq. (6.11) shown by the dashed line.

which presents a characteristic feature of a peak at low frequency, in excess of the classical Debye law in the zero-disorder case:

$$D(\omega) \propto \omega \int \exp\left[\frac{-(\omega^2-\omega_{A,L}^2(\mathbf{q},k_0))^2}{2(\sigma/k_0)^2\omega_{A,L}^4(\mathbf{q},k_0)}\right] d^dq, \tag{6.11}$$

where I continue to use the approximation frequency $\omega_{A,L}^2 = (4k_0/M)\sin^2(qa/2)$.

The origin of this peak in this case is the Gaussian distribution of random constant k, which remains in the $D(\omega)$ even after the integration over wavevectors in Eq. (6.11). The position of this peak is in general not easy to find analytically. Figure 6.4 shows the VDOS predicted by Eq. (6.11)on 3d systems of varying strength of (Gaussian) random disorder in bond coefficients. Clearly, the characteristic peak position shifts with the increasing disorder strength. The weaker the disorder (smaller σ), the more narrow is the peak, ultimately blows up at a resonant frequency when $\sigma \to 0$. In other words, the characteristic peak disappears when it returns to the perfect crystalline solid. It might be tempting to associate this feature with the celebrated “boson peak”, which is a universal feature in amorphous and glassy solids (Schirmacher et al., 1998; Shintani and Tanaka, 2008), and in some non-centrosymmetric crystals (Cui et al., 2019b; Milkus and Zaccone, 2016), since the peak lies in the region where the boson peak is usually expected. Although the traditional "boson peak" is interpreted in a different way, it might be that some of the observed peaks at this range are of this origin. Same as the model of quenched random average of DSF, Eq. (6.11) applies to a general springs system with Gaussian distribution on spring constants. A similar instability in lattices

with disorder in spring constants has been recently observed in Shimada et al. (2020) as a result of proliferation of negative spring constants.

6.4 Toy model with spatially correlated elastic modulus

From now on, I focus on 2D systems. All results can be generalised to 3D case, upon letting $\alpha,\beta,\kappa,\chi = x,y,z$ go through full Cartesian components and specifying bond orientation through the pair of angles ϕ,θ: $\mathbf{n}_{ij} = (\cos\phi_{ij}\sin\theta_{ij}, \sin\phi_{ij}\sin\theta_{ij}, \cos\theta_{ij})$. Recall Eq. (2.111) the equation of elastic waves. With the pair interaction V_{IJ}, $C_{IJ}^{\mu\nu\kappa\chi} = h_{IJ} n_{IJ}^{\mu} n_{IJ}^{\nu} n_{IJ}^{\kappa} n_{IJ}^{\chi}$ where r_{IJ} is the interatomic distance, $\mathbf{n}_{IJ}$ is the unit vector pointing from I to J and $h_{IJ} = V''_{IJ}(r_{IJ}) r_{IJ}^2 - V'_{IJ}(r_{IJ}) r_{IJ}$ (Lemaitre and Maloney, 2006). Prime denotes the derivative with respect to distance. Here, I ignore the contribution of spatial correlations in stress tensors. The influence of long-range fluctuations in stress tensor on elastic waves will be discussed in Appendix D for the case where, instead, no fluctuations in the elastic moduli exist.

Writing $\mathbf{n}_{IJ} = (\cos\theta_{IJ}, \sin\theta_{IJ})$, the elastic constants appear to be of form $C_{IJ}^{\mu\nu\kappa\chi} = h_{IJ}\cos^i\theta_{IJ}\sin^{4-i}\theta_{IJ}, i = 0,...,4$. There are, hence, five local constants for each pair, they are (Gelin et al., 2016)

$$\begin{aligned} &C_{IJ}^1 = h_{IJ}; \quad C_{IJ}^2 = h_{IJ}\cos(2\theta_{IJ}); C_{IJ}^3 = h_{IJ}\sin(2\theta_{IJ}); \\ &C_{IJ}^4 = h_{IJ}\cos(4\theta_{IJ}); \quad C_{IJ}^5 = h_{IJ}\sin(4\theta_{IJ}). \end{aligned} \tag{6.12}$$

Contributions of each pair to the Lam*é* constants are $\mu_{IJ} = (1/8)(C_{IJ}^1 - C_{IJ}^4)$ and $\lambda_{IJ} = (1/8)(C_{IJ}^1 + C_{IJ}^4)$. I am able to express effective elastic constants $S^{\mu\nu\kappa\chi} \approx C^{\mu\nu\kappa\chi}$ in terms of these five local constants:

$$\begin{aligned} C_{IJ}^{xxxx} &= \frac{C_{IJ}^4}{8} + \frac{C_{IJ}^2}{2} + \frac{3C_{IJ}^1}{8}; \\ C_{IJ}^{xxxy} &= C_{IJ}^{xxyx} = C_{IJ}^{xyxx} = C_{IJ}^{yxxx} = \frac{C_{IJ}^5}{8} + \frac{C_{IJ}^3}{4}; \\ C_{IJ}^{xxyy} &= C_{IJ}^{xyxy} = C_{IJ}^{yxxy} = C_{IJ}^{xyyx} = C_{IJ}^{yxyx} = C_{IJ}^{yyxx} = \frac{C_{IJ}^1}{8} - \frac{C_{IJ}^4}{8}; \\ C_{IJ}^{yyyx} &= C_{IJ}^{yyxy} = C_{IJ}^{yxyy} = C_{IJ}^{xyyy} = -\frac{C_{IJ}^5}{8} + \frac{C_{IJ}^3}{4}; \\ C_{IJ}^{yyyy} &= \frac{C_{IJ}^4}{8} - \frac{C_{IJ}^2}{2} + \frac{3C_{IJ}^1}{8}. \end{aligned} \tag{6.13}$$

Then, the elastic wave function becomes

$$\begin{aligned}
\rho\frac{\partial^2 u^x(\mathring{\mathbf{r}})}{\partial t^2} &= \frac{\partial}{\partial \mathring{r}^x}\left[\left(\frac{C^4}{8}+\frac{C^2}{2}+\frac{3C^1}{8}\right)\frac{\partial u^x}{\partial \mathring{r}^x}+\left(\frac{C^5}{8}+\frac{C^3}{4}\right)\left(\frac{\partial u^x}{\partial \mathring{r}^y}+\frac{\partial u^y}{\partial \mathring{r}^x}\right)+\left(\frac{C^1}{8}-\frac{C^4}{8}\right)\frac{\partial u^y}{\partial \mathring{r}^y}\right] \\
&\quad+\frac{\partial}{\partial \mathring{r}^y}\left[\left(\frac{C^5}{8}+\frac{C^3}{4}\right)\frac{\partial u^x}{\partial \mathring{r}^x}+\left(\frac{C^1}{8}-\frac{C^4}{8}\right)\left(\frac{\partial u^x}{\partial \mathring{r}^y}+\frac{\partial u^y}{\partial \mathring{r}^x}\right)+\left(-\frac{C^5}{8}+\frac{C^3}{4}\right)\frac{\partial u^y}{\partial \mathring{r}^y}\right]; \\
\rho\frac{\partial^2 u^y(\mathring{\mathbf{r}})}{\partial t^2} &= \frac{\partial}{\partial \mathring{r}^x}\left[\left(\frac{C^5}{8}+\frac{C^3}{4}\right)\frac{\partial u^x}{\partial \mathring{r}^x}+\left(\frac{C^1}{8}-\frac{C^4}{8}\right)\left(\frac{\partial u^x}{\partial \mathring{r}^y}+\frac{\partial u^y}{\partial \mathring{r}^x}\right)+\left(-\frac{C^5}{8}+\frac{C^3}{4}\right)\frac{\partial u^y}{\partial \mathring{r}^y}\right] \\
&\quad+\frac{\partial}{\partial \mathring{r}^y}\left[\left(\frac{C^1}{8}-\frac{C^4}{8}\right)\frac{\partial u^x}{\partial \mathring{r}^x}+\left(-\frac{C^5}{8}+\frac{C^3}{4}\right)\left(\frac{\partial u^x}{\partial \mathring{r}^y}+\frac{\partial u^y}{\partial \mathring{r}^x}\right)+\left(\frac{C^4}{8}-\frac{C^2}{2}+\frac{3C^1}{8}\right)\frac{\partial u^y}{\partial \mathring{r}^y}\right].
\end{aligned} \tag{6.14}$$

To probe the simplest possible scenario of long-range correlations in the elastic constants, I assume $C^1(\mathbf{r}),C^2(\mathbf{r}),C^4(\mathbf{r}),C^5(\mathbf{r})=0$ while $C^3(\mathbf{r})\equiv C(\mathbf{r})=\rho C_0+\rho\Delta C(\mathbf{r})$ is expressed in terms of its mean value plus a random part, i.e. $\overline{\Delta C(\mathbf{r})}=0$ and $\overline{\Delta C(\mathbf{r}')\Delta C(\mathbf{r}'+\mathbf{r})}=B(\mathbf{r})=\gamma\cos(4\theta)/(r^2+a^2)\equiv\cos(4\theta)B(r)$ for some constants γ and a, where the final form is in polar coordinates. In principle, a might also depend on $\mathbf{r}$ as long as it decays faster than $\sim r^2$ when $r\to\infty$. Here, I just let it be a constant. In other words, only the effect of non-vanishing C^3 is considered, whose spatial autocorrelation scales as $1/r^2$. The power-law decay in the self-correlation of elasticity, $B(r)$, has been numerically investigated in simulations (Gelin et al., 2016). Similar behaviour in the spatial correlation of mass was analysed in detail within a scalar model of wave propagation (John and Stephen, 1983).

Equation (6.14) then reduces to

$$\begin{aligned}
&\rho\frac{\partial^2 u^x(\mathring{\mathbf{r}})}{\partial t^2} = \frac{1}{4}\left[\frac{\partial C(\mathring{\mathbf{r}})}{\partial \mathring{r}^x}\frac{\partial u^x}{\partial \mathring{r}^y}+\frac{\partial C(\mathring{\mathbf{r}})}{\partial \mathring{r}^y}\frac{\partial u^x}{\partial \mathring{r}^x}+2C(\mathring{\mathbf{r}})\frac{\partial^2 u^x}{\partial \mathring{r}^x\partial \mathring{r}^y}+\frac{\partial C(\mathring{\mathbf{r}})}{\partial \mathring{r}^x}\frac{\partial u^y}{\partial \mathring{r}^x}+\frac{\partial C(\mathring{\mathbf{r}})}{\partial \mathring{r}^y}\frac{\partial u^y}{\partial \mathring{r}^y}\right. \\
&\left.+C(\mathring{\mathbf{r}})\left(\frac{\partial^2 u^y}{\partial \mathring{r}^x\partial \mathring{r}^x}+\frac{\partial^2 u^y}{\partial \mathring{r}^y\partial \mathring{r}^y}\right)\right] \\
&=\frac{1}{4}\sum_{\mu\neq\nu}\left[\nabla_\mu(C\nabla_\nu)\right]u^x+\frac{1}{4}\sum_{\mu}\left[\nabla_\mu(C\nabla_\mu)\right]u^y; \\
&\rho\frac{\partial^2 u^y(\mathring{\mathbf{r}})}{\partial t^2} = \frac{1}{4}\left[\frac{\partial C(\mathring{\mathbf{r}})}{\partial \mathring{r}^x}\frac{\partial u^y}{\partial \mathring{r}^y}+\frac{\partial C(\mathring{\mathbf{r}})}{\partial \mathring{r}^y}\frac{\partial u^y}{\partial \mathring{r}^x}+2C(\mathring{\mathbf{r}})\frac{\partial^2 u^y}{\partial \mathring{r}^x\partial \mathring{r}^y}+\frac{\partial C(\mathring{\mathbf{r}})}{\partial \mathring{r}^x}\frac{\partial u^x}{\partial \mathring{r}^x}+\frac{\partial C(\mathring{\mathbf{r}})}{\partial \mathring{r}^y}\frac{\partial u^x}{\partial \mathring{r}^y}\right. \\
&\left.+C(\mathring{\mathbf{r}})\left(\frac{\partial^2 u^x}{\partial \mathring{r}^x\partial \mathring{r}^x}+\frac{\partial^2 u^x}{\partial \mathring{r}^y\partial \mathring{r}^y}\right)\right] \\
&=\frac{1}{4}\sum_{\mu}\left[\nabla_\mu(C\nabla_\mu)\right]u^x+\frac{1}{4}\sum_{\mu\neq\nu}\left[\nabla_\mu(C\nabla_\nu)\right]u^y.
\end{aligned} \tag{6.15}$$

In frequency space, the equation of motion of the frequency-dependent displacement vector $\mathbf{u}(\mathbf{r},z)$ is (I have dropped the ring)

$$\begin{aligned} & A(z)\mathbf{u}(\mathbf{r},z)=0, \\ \text{with} \qquad & A^{xx}=A^{yy}=-\rho z-\frac{1}{4}\sum_{\mu\neq\nu}\left[\nabla_\mu(C\nabla_\nu)\right], \\ & A^{xy}=A^{yx}=\frac{1}{4}\sum_{\mu}\left[\nabla_\mu(C\nabla_\mu)\right]. \end{aligned} \tag{6.16}$$

The spatial correlation of $C(\mathbf{r})$, which serves as the source of disorder, may be implemented by the probability distribution for its fluctuating part,

$$\mathscr{P}[\Delta C(\mathbf{r})]=P_0\exp\left[-\frac{1}{2}\int d^2r d^2r'\Delta C(\mathbf{r})B^{-1}(\mathbf{r}-\mathbf{r}')\Delta C(\mathbf{r}')\right], \tag{6.17}$$

where B^{-1} is the inverse of $B(\mathbf{r}-\mathbf{r}')$ such that

$$\int d^2pB(\mathbf{r}-\mathbf{p})B^{-1}(\mathbf{p}-\mathbf{q})=\delta(\mathbf{r}-\mathbf{q}), \tag{6.18}$$

while P_0 is a normalisation factor. The Lagrangian is expressed as (scaled by ρ),

$$\begin{aligned} &\mathscr{L}=\frac{1}{2}\int d^2r\mathbf{u}^TA\mathbf{u}=u^x(A_{xx}u^x+A_{xy}u^y)+u^y(A_{yx}u^x+A_{yy}u^y) \\ &=\frac{1}{2}\int d^2r\{-z\mathbf{u}\cdot\mathbf{u}-\frac{1}{4}\sum_{\mu\neq\nu}u^x\left[\nabla_\mu(C\nabla_\nu u^x)\right]-\frac{1}{4}\sum_{\mu}u^x\left[\nabla_\mu(C\nabla_\mu u^y)\right]-\frac{1}{4}\sum_{\mu\neq\nu}u^y\left[\nabla_\mu(C\nabla_\nu u^y)\right] \\ &-\frac{1}{4}\sum_{\mu}u^y\left[\nabla_\mu(C\nabla_\mu u^x)\right]\} \\ &=\frac{1}{2}\int d^2r\{-z\mathbf{u}\cdot\mathbf{u}-\frac{1}{4}\sum_{\mu\neq\nu}\left[\nabla_\mu[u^xC\nabla_\nu u^x]-(\nabla_\mu u^x)C(\nabla_\nu u^x)\right] \\ &-\frac{1}{4}\sum_{\mu}\left[\nabla_\mu[u^xC\nabla_\mu u^y]-C(\nabla_\mu u^x)(\nabla_\mu u^y)\right]-x\longleftrightarrow y\} \\ &=\frac{1}{2}\int d^2r\{-z\mathbf{u}\cdot\mathbf{u}-\frac{1}{4}\nabla_x[u^xC\nabla_yu^x+u^yC\nabla_yu^y+u^xC\nabla_xu^y+u^yC\nabla_xu^x]-\frac{1}{4}\nabla_y[x\longleftrightarrow y] \\ &+\frac{1}{2}C[(\nabla_xu^x)(\nabla_yu^x)+(\nabla_xu^y)(\nabla_yu^y)+(\nabla_xu^x)(\nabla_xu^y)+(\nabla_yu^x)(\nabla_yu^y)]\} \\ &=\frac{1}{2}\int d^2r\{-z\mathbf{u}\cdot\mathbf{u}-\frac{1}{4}\nabla_x[...]-\frac{1}{4}\nabla_y[...]+\frac{1}{2}C(\nabla\cdot\mathbf{u})(\nabla_xu^y+\nabla_yu^x)\} \\ &=\frac{1}{2}\int d^2r\{-z\mathbf{u}\cdot\mathbf{u}+\frac{1}{2}C(\nabla\cdot\mathbf{u})(\nabla_xu^y+\nabla_yu^x)\} \end{aligned} \tag{6.19}$$

where the object [...] vanishes on the boundary.

The formulation of the replica trick

I will give a short introduction about the replica method. The replica trick is a mathematical technique widely used in the statistical physics of spin glasses and systems with quenched disorder. It is based on the application of formula:

$$\ln Z = \lim_{n\to 0} \frac{Z^n - 1}{n}, \tag{6.20}$$

where Z is the partition function, or a similar thermodynamic function. The replica trick is a mean-field theory used to simplify the calculation of the configuration average $\langle \ln Z \rangle$, by reducing the problem to calculating the disorder average $\langle Z^n \rangle$ for an integer n. For a quenched random system, the (self-averaging) free energy is averaged over all random (pairwise) interactions J_{IJ} with a given distribution function $\mathscr{P}(J)$:

$$\langle F \rangle = -k_B T \langle \ln Z(J) \rangle = -k_B T \int \prod_{\{I,J\}} \mathscr{D} J_{IJ} \mathscr{P}(J) \ln Z(J). \tag{6.21}$$

Considering the partition function of the n non-interacting identical replicas of the original system, one has $Z^n(J) = \exp\left[-\beta \sum_{a=1}^{n} H(J)\right]$ where replicas are labeled in a. The original physical free energy could be taken as

$$\langle F \rangle = -k_B T \langle \ln Z(J) \rangle = -k_B T \lim_{n\to 0} \frac{\ln \langle Z^n(J) \rangle}{n} = -k_B T \lim_{n\to 0} \frac{\ln[\langle \exp(n \ln Z(J)) \rangle]}{n}. \tag{6.22}$$

The 2nd identity can be easily verified by writing $Z^n = \exp(n \ln Z)$. In general, the scheme of replica method consists of 3 steps: calculating Z^n; the analytic continuation of the obtained function of parameter n should be made for an arbitrary non-integer n; taking the limit $n \to 0$ (Dotsenko, 2000). With the source term J, the averaged Green's function might be calculated form the partition function (Maurer and Schirmacher, 2004):

$$G = \lim_{n\to 0} \frac{1}{n} \frac{\partial^2}{\partial J^2} Z^n(J) \bigg|_{J=0} = \lim_{n\to 0} Z^{n-1}(J=0) \frac{\partial^2}{\partial J^2} Z(J) \bigg|_{J=0}. \tag{6.23}$$

Return to the case of heterogeneous elasticity, using the replica-field representation, the generating functional for calculating the averaged Green's function takes the form

$$\begin{aligned}
&\langle Z^n(0)\rangle \equiv \int \mathscr{D}[\mathbf{u}_a(\mathbf{r})]\mathscr{D}[\Delta C(\mathbf{r})]P_0\cdot \\
&e^{\left[-\frac{1}{2}\sum_{a=1}^n \int d^2r\{-z\mathbf{u}_a(\mathbf{r})^2+\frac{C(\mathbf{r})}{2}(\nabla\cdot\mathbf{u}_a(\mathbf{r}))(\nabla_x u_a^y+\nabla_y u_a^x)\}-\frac{1}{2}\int d^2rd^2r'\Delta C(\mathbf{r})B^{-1}(\mathbf{r}-\mathbf{r}')\Delta C(\mathbf{r}')\right]} \\
&= \int \mathscr{D}[\mathbf{u}_a(\mathbf{r})]\mathscr{D}[\Delta C(\mathbf{r})]P_0 \exp\left[-\frac{1}{2}\sum_{a=1}^n \int d^2r\{-z\mathbf{u}_a(\mathbf{r})^2+\frac{1}{2}C_0(\nabla\cdot\mathbf{u}_a(\mathbf{r}))(\nabla_x u_a^y+\nabla_y u_a^x)\}\right. \\
&\qquad \left.+\frac{1}{2}\Delta C(\mathbf{r})(\nabla\cdot\mathbf{u}_a(\mathbf{r}))(\nabla_x u_a^y+\nabla_y u_a^x)-\frac{1}{2}\int d^2rd^2r'\Delta C(\mathbf{r})B^{-1}(\mathbf{r}-\mathbf{r}')\Delta C(\mathbf{r}')\right] \\
&\approx \int \mathscr{D}[\mathbf{u}_a(\mathbf{r})]\exp\left[-\frac{1}{2}\sum_{a=1}^n \int d^2r\left\{-z\mathbf{u}_a(\mathbf{r})^2+\frac{1}{2}C_0(\nabla\cdot\mathbf{u}_a(\mathbf{r}))(\nabla_x u_a^y+\nabla_y u_a^x)\right\}\right. \\
&\left.+\frac{1}{32}\sum_{a,b=1}^n \int d^2rd^2r'(\nabla\cdot\mathbf{u}_a(\mathbf{r}))(\nabla_x u_a^y(\mathbf{r})+\nabla_y u_a^x(\mathbf{r}))B(\mathbf{r}-\mathbf{r}')(\nabla\cdot\mathbf{u}_b(\mathbf{r}'))(\nabla_x u_b^y(\mathbf{r}')+\nabla_y u_b^x(\mathbf{r}'))\right].
\end{aligned} \tag{6.24}$$

By means of a Hubbard-Stratonovich transformation, I introduce the effective matrix fields $\Lambda_{ab}^{\mu\nu\kappa\chi}(\mathbf{r},\mathbf{r}',z)$ to replace the $\Delta C(\mathbf{r})$ in the harmonic part of the effective equation of motion. Then $\langle Z^n(0)\rangle$ becomes

$$\begin{aligned}
&\langle Z^n(0)\rangle \approx \int \mathscr{D}[\mathbf{u}_a(\mathbf{r})]\mathscr{D}[\Lambda_{ab}^{\mu\nu\kappa\chi}(\mathbf{r},\mathbf{r}',z)]\Lambda_0\cdot \\
&e^{\left\{-\frac{1}{2}\sum_{a=1}^n \int d^2r\left[-z\mathbf{u}_a(\mathbf{r})^2-\frac{C_0}{4}\left(\sum_{\mu\neq\nu}(u_a^x\nabla_\mu\nabla_\nu u_a^x+u_a^y\nabla_\mu\nabla_\nu u_a^y)+\sum_\mu(u_a^x\nabla_\mu\nabla_\mu u_a^y+u_a^y\nabla_\mu\nabla_\mu u_a^x)\right)\right]\right\}}\cdot \\
&e^{\left\{-\frac{1}{2}\sum_{a,b=1}^n\sum_{\mu\kappa\chi\nu=x,y}\int d^2rd^2r'\left[\Lambda_{ab}^{\mu\kappa\chi\nu}(\mathbf{r},\mathbf{r}',z)B^{-1}(\mathbf{r}-\mathbf{r}')\sum_{\kappa'\chi'}\Lambda_{ab}^{\mu\nu\kappa'\chi'}(\mathbf{r},\mathbf{r}',z)-\frac{1}{4}u_a^\mu(\mathbf{r})\nabla_\kappa\Lambda_{ab}^{\mu\nu\kappa\chi}(\mathbf{r},\mathbf{r}',z)\nabla_\chi u_b^\nu(\mathbf{r}')\right]\right\}}
\end{aligned} \tag{6.25}$$

where $\Lambda_{ab}^{\mu\nu\kappa\chi}=0$ if $\mu=\nu,\kappa=\chi$ or $\mu\neq\nu,\kappa\neq\chi$. The way $\Lambda_{ab}^{\mu\nu\kappa\chi}$ is introduced is to make Eq. (6.25) consistent with Eq. (6.15). We will see in the following calculations that, the way to index $\Lambda^{\mu\nu\kappa\chi}$ will be fulfilled by $\varepsilon^{\mu\nu\kappa\chi}$. The normalisation constant is represented as Λ_0.

The generating function including source $J_{ab}^{\mu\nu}(\mathbf{r},\mathbf{r}')$ is

$$\begin{aligned}
&\langle Z^n(J)\rangle = \int \mathscr{D}[\mathbf{u}_a(\mathbf{r})]\mathscr{D}[\Lambda_{ab}^{\mu\nu\kappa\chi}(\mathbf{r},\mathbf{r}',z)]\Lambda_0\cdot \\
&\exp\left\{-\frac{1}{2}\sum_{a=1}^{n}\int d^2r\left[-z\mathbf{u}_a(\mathbf{r})^2-\frac{C_0}{4}\left(\sum_{\mu\neq\nu}(u_a^x\nabla_\mu\nabla_\nu u_a^x+u_a^y\nabla_\mu\nabla_\nu u_a^y)+\sum_{\mu}(u_a^x\nabla_\mu\nabla_\mu u_a^y+u_a^y\nabla_\mu\nabla_\mu u_a^x)\right)\right]\right. \\
&\left.-\frac{1}{2}\sum_{a,b=1}^{n}\sum_{\mu\kappa\chi\nu=x,y}\int d^2rd^2r'\sum_{\kappa'\chi'}\Lambda_{ab}^{\mu\kappa\chi\nu}B^{-1}(\mathbf{r}-\mathbf{r}')\Lambda_{ab}^{\mu\kappa'\chi'\nu}-\frac{1}{4}u_a^\mu(\mathbf{r})\nabla_\kappa\Lambda_{ab}^{\mu\nu\kappa\chi}\nabla_\chi u_b^\nu(\mathbf{r}')+2J_{ab}^{\mu\nu}\Lambda_{ab}^{\mu\nu\kappa\chi}\right\} \\
&=\int \mathscr{D}[\mathbf{u}_a(\mathbf{r})]\mathscr{D}[\Lambda_{ab}^{\mu\nu\kappa\chi}(\mathbf{r},\mathbf{r}',z)]\Lambda_0\cdot \\
&e^{\left\{-\frac{1}{2}\sum_{a,b=1}^{n}\sum_{\mu\kappa\chi\nu=x,y}\int d^2rd^2r'\left[\mathbf{u}_a(\mathbf{r})A_{ab}(\Lambda_{ab}^{\mu\kappa\chi\nu})\mathbf{u}_b(\mathbf{r}')+\sum_{\kappa'\chi'}\Lambda_{ab}^{\mu\nu\kappa\chi}B^{-1}(\mathbf{r}-\mathbf{r}')\Lambda_{ab}^{\mu\nu\kappa'\chi'}+2J_{ab}^{\mu\nu}\Lambda_{ab}^{\mu\nu\kappa\chi}\right]\right\}}
\end{aligned} \tag{6.26a}$$

where

$$\begin{aligned}
A_{ab}(\Lambda)\equiv\delta(\mathbf{r}-\mathbf{r}')\delta^{ab}&\begin{pmatrix} -z-\frac{C_0}{4}\sum_{\mu\neq\nu}\nabla_\mu\nabla_\nu & -\frac{C_0}{4}\sum_{\mu}\nabla_\mu\nabla_\mu \\ -\frac{C_0}{4}\sum_{\mu}\nabla_\mu\nabla_\mu & -z-\frac{C_0}{4}\sum_{\mu\neq\nu}\nabla_\mu\nabla_\nu \end{pmatrix} \\
&-\frac{1}{4}\sum_{\kappa\chi}\begin{pmatrix} \nabla_\kappa\Lambda_{ab}^{xx\kappa\chi}(\mathbf{r},\mathbf{r}',z)\nabla_\chi & \nabla_\kappa\Lambda_{ab}^{xy\kappa\chi}(\mathbf{r},\mathbf{r}',z)\nabla_\chi \\ \nabla_\kappa\Lambda_{ab}^{yx\kappa\chi}(\mathbf{r},\mathbf{r}',z)\nabla_\chi & \nabla_\kappa\Lambda_{ab}^{yy\kappa\chi}(\mathbf{r},\mathbf{r}',z)\nabla_\chi \end{pmatrix}.
\end{aligned} \tag{6.26b}$$

By evaluating derivatives of $\langle Z^n(J)\rangle$ with respect to $J_{ab}^{\mu\nu}$ at $J_{ab}^{\mu\nu}=0$, I am able to find the averaged Green's function of $\Lambda_{ab}^{\mu\kappa\chi\nu}$. Integrating $\mathbf{u}_a$ out in Eq. (6.25), I obtain a field theory involving only the Λ field:

$$\langle Z^n(0)\rangle\propto\int\mathscr{D}[\Lambda]e^{\left\{-\frac{1}{2}\sum_{a,b=1}^{n}\sum_{\mu,\nu,\kappa,\chi}\left(\ln\det A(\Lambda_{ab}^{\mu\nu\kappa\chi})+\sum_{\kappa'\chi'}\int d^2rd^2r'\Lambda^{\mu\nu\kappa\chi}B^{-1}(\mathbf{r}-\mathbf{r}')\Lambda^{\mu\nu\kappa'\chi'}\right)\right\}}. \tag{6.27}$$

I seek for a saddle-point such that the exponential in Eq. (6.27) is stationary, which corresponds to the mean-field theory of spatially correlated disorder of the coherent-potential approximation (CPA) for the one-particle Green's function. A saddle point Λ' of the Λ field is a point such that the exponential in Eq. (6.27) contains no terms linear in a small fluctuation $\hat{\Lambda}\equiv\Lambda-\Lambda'$. On the other hand, if I expand the Lagrangian about Λ', keeping only quadratic displacement in $\hat{\Lambda}$, then the saddle-point value of Λ determines the averaged one-particle Green's function:

$$\Lambda'=\langle\Lambda\rangle. \tag{6.28}$$

Expanding in $\hat{\Lambda}$, $A_{ab}(\Lambda)$ is written as

$$A_{ab}(\Lambda) = A_{ab}(\Lambda') - \frac{1}{4}\sum_{\kappa\chi}\begin{pmatrix} \nabla_\kappa \hat{\Lambda}_{ab}^{xx\kappa\chi}(\mathbf{r},\mathbf{r}',z)\nabla_\chi & \nabla_\kappa \hat{\Lambda}_{ab}^{xy\kappa\chi}(\mathbf{r},\mathbf{r}',z)\nabla_\chi \\ \nabla_\kappa \hat{\Lambda}_{ab}^{yx\kappa\chi}(\mathbf{r},\mathbf{r}',z)\nabla_\chi & \nabla_\kappa \hat{\Lambda}_{ab}^{yy\kappa\chi}(\mathbf{r},\mathbf{r}',z)\nabla_\chi \end{pmatrix}$$
$$\equiv A_{ab}(\Lambda') + \hat{A}_{ab}(\hat{\Lambda}). \tag{6.29}$$

Making use of the identity

$$\ln\det(A(\Lambda') + \hat{A}(\hat{\Lambda})) = \ln\det(A(\Lambda')) + \sum_n^\infty \frac{(-1)^{n+1}}{n}\mathrm{Tr}(\underbrace{A^{-1}\hat{A}\ldots A^{-1}\hat{A}}_{2n}) \tag{6.30}$$

The corresponding saddle-point equations can be solved with a replica-diagonal field $\Lambda_{ab}^{\mu\nu\kappa\chi}(\mathbf{r},\mathbf{r}',z) = \Sigma^{\mu\nu}(\mathbf{r},\mathbf{r}',z)\delta^{ab}$, which is relevant to the evaluation of the averaged one-particle Green's function. Non-diagonal saddle points need only be taken into account at the stage of renormalisation (McKane and Stone, 1981). Then I have $\ln\det(A) = \mathrm{Tr}\ln(A)$. The self-energy $\langle\Sigma^{\mu\nu}\rangle$ measuring the average response of the μth component of the displacement field at $\mathbf{r}$ to an impulse in the νth component at $\mathbf{r}'$, can be determined by taking

$$\frac{\delta}{\delta\Sigma^{\mu\nu}}\left(\mathrm{Tr}\ln A(\Sigma^{\mu\nu}) + \int d^2r d^2r' \Sigma^{\mu\nu} B^{-1}(\mathbf{r}-\mathbf{r}')\Sigma^{\mu\nu}\right) = 0 \tag{6.31}$$

at $\Sigma_0^{\mu\nu}$, which yields

$$\langle\Sigma_0^{\mu\nu}\rangle = \frac{1}{8}\sum_{\kappa\chi}\nabla_\kappa B(\mathbf{r}-\mathbf{r}')\nabla_\chi\langle G_0(r^\mu, r'^\nu, z)\rangle\varepsilon^{\mu\nu\kappa\chi}; \tag{6.32a}$$

$$G_0(r^x, r'^x, z) = \left[-z - \frac{(C_0+\Sigma_0^{xx})}{4}(\nabla_x\nabla_y + \nabla_y\nabla_x)\right]^{-1}; \tag{6.32b}$$

$$G_0(r^y, r'^y, z) = \left[-z - \frac{(C_0+\Sigma_0^{yy})}{4}(\nabla_x\nabla_y + \nabla_y\nabla_x)\right]^{-1}; \tag{6.32c}$$

$$G_0(r^x, r'^y) = \left[-\frac{(C_0+\Sigma_0^{xy})}{4}(\nabla_x\nabla_x + \nabla_y\nabla_y)\right]^{-1}; \tag{6.32d}$$

$$G_0(r^y, r'^x) = \left[-\frac{(C_0+\Sigma_0^{yx})}{4}(\nabla_x\nabla_x + \nabla_y\nabla_y)\right]^{-1}, \tag{6.32e}$$

where $\varepsilon^{\mu\nu\kappa\chi} = 0$ if $\mu = \nu, \kappa = \chi$ or $\mu \neq \nu, \kappa \neq \chi$. Translation invariance holds after taking the ensemble average, hence the CPA Green's function G_0 depends only on the difference between two points in space.

In a nutshell, I start from full equations of elastic waves, namely Eq. (6.14), to write down the action in terms of replica fields, which is Eq. (6.25), with the fluctuating part in elasticity replaced with equivalent effective fields. The solution of the corresponding saddle-point equation, Eq. (6.27), gives rise to self-consistent equations in self-energy and the (elastic) Green's function, which is shown in Eq. (6.29).

Theory with non-zero C^1, C^2, C^4, C^5

I weaken the condition on the other elastic constants by letting C^1, C^2, C^4 and C^5 be all non-zero constants. The propagator A in $A(z)\mathbf{u}(\mathbf{r},z) = 0$ takes the form (scaled with ρ)

$$A^{\mu\nu} = -z\delta^{\mu\nu} - \sum_{\kappa\chi} \mathscr{C}^{\mu\nu\kappa\chi}\nabla_\kappa\nabla_\chi - \frac{1}{4}\sum_{\kappa\chi}[\nabla_\kappa(\Delta C\nabla_\chi)]\varepsilon^{\mu\nu\kappa\chi} \tag{6.33}$$

where $\mathscr{C}^{\mu\nu\kappa\chi}$ corresponds to the $\mathbf{r}$-independent part of elastic constants $C^i, i = 1,2,3,4,5$. The explicit form is not important and I do not provide it here. The Lagrangian becomes

$$\mathscr{L} = \frac{1}{2}\int d^2r\{-zu^2 + \frac{1}{2}\Delta C(\nabla\cdot\mathbf{u})(\nabla_x u^y + \nabla_y u^x) - \sum_{\mu\nu\kappa\chi} u^\mu \mathscr{C}^{\mu\nu\kappa\chi}\nabla_\kappa\nabla_\chi u^\nu)\} \tag{6.34}$$

and $\langle Z^n(J)\rangle$ is

$$\langle Z^n(J)\rangle = \int \mathscr{D}[\mathbf{u}^a(\mathbf{r})]\mathscr{D}[\Lambda_{ab}^{\mu\nu\kappa\chi}(\mathbf{r},\mathbf{r}',z)]\Lambda_0\cdot$$
$$e^{\left\{-\frac{1}{2}\sum_{a,b=1}^n\sum_{\mu\nu\kappa\chi=x,y}\int d^2rd^2r'\left[u_a^\mu(\mathbf{r})A_{ab}(\Lambda_{ab}^{\mu\nu\kappa\chi})u_b^\nu(\mathbf{r}')+\sum_{\kappa'\chi'}\Lambda_{ab}^{\mu\nu\kappa\chi}B^{-1}(\mathbf{r}-\mathbf{r}')\Lambda_{ab}^{\mu\nu\kappa'\chi'}+2J_{ab}^{\mu\nu}\Lambda_{ab}^{\mu\nu\kappa\chi}\right]\right\}} \tag{6.35a}$$

with

$$A_{ab}^{\mu\nu\kappa\chi}(\Lambda) \equiv \delta(\mathbf{r}-\mathbf{r}')\delta^{ab}\left(-z\delta^{\mu\nu} - \sum_{\kappa\chi}\mathscr{C}^{\mu\nu\kappa\chi}\nabla_\kappa\nabla_\chi\right) - \frac{1}{4}\sum_{\kappa\chi}\nabla_\kappa\Lambda_{ab}^{\mu\nu\kappa\chi}(\mathbf{r},\mathbf{r}',z)\nabla_\chi \tag{6.35b}$$

Again, letting $\Lambda_{ab}^{\mu\nu\kappa\chi} = \Sigma^{\mu\nu}\delta^{ab}$ and finding the saddle point of $\mathrm{Tr}\ln A(\Sigma^{\mu\nu}) + \int d^2r d^2r' \Sigma^{\mu\nu} B(\mathbf{r}-\mathbf{r}')\Sigma^{\mu\nu}$, I obtain the self-consistent equations for the self-energy and the Green's functions:

$$\langle \Sigma_0^{\mu\nu} \rangle = \frac{1}{8}\sum_{\kappa\chi} \nabla_\kappa B(\mathbf{r}-\mathbf{r}')\nabla_\chi \langle G_0(r^\mu, r'^\nu, z)\rangle \varepsilon^{\mu\nu\kappa\chi}; \tag{6.36a}$$

$$G_0(r^x, r'^x, z) = \Bigg[-z - \left(\frac{C^4}{8} + \frac{C^2}{2} + \frac{3C^1}{8}\right)\nabla_x\nabla_x - \left(\frac{C^1}{8} - \frac{C^4}{8}\right)\nabla_y\nabla_y - \left(\frac{C^5}{8} + \frac{(C_0 + \Sigma_0^{xx})}{4}\right)(\nabla_x\nabla_y + \nabla_y\nabla_x)\Bigg]^{-1}; \tag{6.36b}$$

$$G_0(r^y, r'^y, z) = \Bigg[-z - \left(\frac{C^4}{8} - \frac{C^2}{2} + \frac{3C^1}{8}\right)\nabla_y\nabla_y - \left(\frac{C^1}{8} - \frac{C^4}{8}\right)\nabla_x\nabla_x - \left(-\frac{C^5}{8} + \frac{(C_0 + \Sigma_0^{yy})}{4}\right)(\nabla_x\nabla_y + \nabla_y\nabla_x)\Bigg]^{-1}; \tag{6.36c}$$

$$G_0(r^x, r'^y) = \left[-\left(\frac{C^1}{8} - \frac{C^4}{8}\right)(\nabla_x\nabla_y + \nabla_y\nabla_x) - \frac{(C_0 + \Sigma_0^{xy})}{4}(\nabla_x\nabla_x + \nabla_y\nabla_y) - \frac{C^5}{8}(\nabla_x\nabla_x - \nabla_y\nabla_y)\right]^{-1}; \tag{6.36d}$$

$$G_0(r^y, r'^x) = \left[-\left(\frac{C^1}{8} - \frac{C^4}{8}\right)(\nabla_x\nabla_y + \nabla_y\nabla_x) - \frac{(C_0 + \Sigma_0^{yx})}{4}(\nabla_x\nabla_x + \nabla_y\nabla_y) - \frac{C^5}{8}(\nabla_x\nabla_x - \nabla_y\nabla_y)\right]^{-1}. \tag{6.36e}$$

Defining the Fourier transform as

$$\Sigma(\mathbf{q}, z) \equiv \int d^2(\mathbf{r}-\mathbf{r}') e^{i\mathbf{q}(\mathbf{r}-\mathbf{r}')}\Sigma(\mathbf{r}-\mathbf{r}', z), \tag{6.37}$$

the condition on the one-particle CPA Green's function may be written in momentum space:

$$\langle \Sigma_0^{\mu\nu} \rangle = -\frac{1}{4}\sum_{\kappa\chi} \varepsilon^{\mu\nu\kappa\chi} q_\kappa q_\chi \int d^2k \tilde{B}(\mathbf{q}-\mathbf{k}) \langle G_0(\mathbf{k}) \rangle; \tag{6.38a}$$

$$\tilde{B}(\mathbf{q}) \equiv \int d^2r e^{i\mathbf{q}\cdot\mathbf{r}} B(\mathbf{r}); \tag{6.38b}$$

$$G_0(q^x,q^x,z) = \left[-z + \left(\frac{C^4}{8} + \frac{C^2}{2} + \frac{3C^1}{8}\right) q^x q^x + \left(\frac{C^1}{8} - \frac{C^4}{8}\right) q^y q^y + \left(\frac{C^5}{4} + \frac{C_0 + \Sigma_0^{xx}}{2}\right) q^x q^y \right]^{-1}; \tag{6.38c}$$

$$G_0(q^y,q^y,z) = \left[-z + \left(\frac{C^4}{8} - \frac{C^2}{2} + \frac{3C^1}{8}\right) q^y q^y + \left(\frac{C^1}{8} - \frac{C^4}{8}\right) q^x q^x + \left(-\frac{C^5}{4} + \frac{C_0 + \Sigma_0^{yy}}{2}\right) q^x q^y \right]^{-1}; \tag{6.38d}$$

$$G_0(q^x,q^y) = \left[\left(\frac{C^1}{4} - \frac{C^4}{4}\right) q^x q^y + \frac{(C_0 + \Sigma_0^{xy})}{4} q^2 + \frac{C^5}{8}(q^x q^x - q^y q^y) \right]^{-1}; \tag{6.38e}$$

$$G_0(q^y,q^x) = \left[\left(\frac{C^1}{4} - \frac{C^4}{4}\right) q^x q^y + \frac{(C_0 + \Sigma_0^{yx})}{4} q^2 + \frac{C^5}{8}(q^x q^x - q^y q^y) \right]^{-1}, \tag{6.38f}$$

which must be solved self-consistently since the self-energy of the Green's function involves the full propagator itself. In the weak scattering limit, approximate solutions are possible because $\mathrm{Im}[\Sigma(\mathbf{q},z)]$ is small compared with C_0 and also the imaginary part of the propagator takes the form of a δ-function, $\mathrm{Im}[\langle G_0(\mathbf{k}) \rangle] \propto \delta(\omega^2 - k^2)$ upon averaging over all possible directions of dummy variable $\mathbf{k}$ and upon rescaling redundant constants (and $z = \omega^2 + i0$). Taking imaginary part, the correlation function in Eq. (6.35a) can be evaluated. Specifically, I want to calculate

$$\begin{aligned} &\int d^2k \tilde{B}(\mathbf{q}-\mathbf{k}) \langle G_0(\mathbf{q},z) \rangle \propto \int e^{i(\mathbf{q}-\mathbf{k})\cdot\mathbf{r}} \frac{\cos(4\theta)}{r^2+a^2} \langle G_0(\mathbf{k},z) \rangle d^2k d^2r \\ &= -\int e^{iqr\cos(\theta) - ikr\cos(\phi-\theta)} \frac{r\cos(4\theta)}{r^2+a^2} k\delta(\omega^2-k^2) dr dk d\theta d\phi \\ &\propto -\int e^{iqr\cos(\theta) - i\omega r\cos(\phi-\theta)} \frac{r\cos(4\theta)}{r^2+a^2} dr d\theta d\phi \end{aligned} \tag{6.39}$$

where $\hat{q}$ is aligned with the x-axis, forming an angle ϕ and an angle θ with $\hat{k}$ and with $\mathbf{r}$, respectively. On the second line, I have replaced $\langle G_0(\mathbf{k},z)\rangle$ with δ-function. Thus, I have

$$\begin{aligned}
&\int_{-\pi}^{\pi}\int_{-\pi}^{\pi}\cos(4\theta)e^{ir(q\cos\theta-\omega\cos(\phi-\theta))}d\theta d\phi \\
=&\int_{\theta=-\pi}^{\pi}\int_{\tau=-(\theta+\pi)}^{\tau=-(\theta-\pi)}\cos(4\theta)e^{ir(q\cos\theta-\omega\cos\tau)}d\theta d\tau \\
=&\int_{\theta=-\pi}^{\pi}\int_{\tau=-\pi}^{\pi}\cos(4\theta)e^{ir(q\cos\theta-\omega\cos\tau)}d\theta d\tau \\
=&\int_{\theta=-\pi}^{\pi}\cos(4\theta)e^{iqr\cos\theta}d\theta\int_{\tau=-\pi}^{\pi}e^{-i\omega r\cos\tau}d\tau \\
=&\int_{\theta=-\pi}^{\pi}\cos(4\theta)e^{iqr\cos\theta}d\theta\int_{\tau=-\pi}^{\pi}e^{i\omega r\cos\tau}d\tau \\
\propto&J_4(qr)J_0(\omega r)
\end{aligned} \tag{6.40}$$

where J_0 and J_4 are (modified) Bessel functions and I have used the periodicity of trigonometric functions in the last step. This gives

$$\langle\Sigma_0^{\mu\nu}\rangle\propto\sum_{\kappa\chi}\varepsilon^{\mu\nu\kappa\chi}q_\kappa q_\chi\int_0^\infty\frac{rJ_4(qr)J_0(\omega r)}{r^2+a^2}dr. \tag{6.41}$$

Making use of the linear dispersion relation, numerical computation reveals that the integral $f(q,\omega)=\int_0^\infty rJ_4(qr)J_0(\omega r)/(r^2+a^2)dr\sim-\ln q$ across a broad range, from low to intermediate values, of q. Figure 6.5 shows one plot for such fitting. In other words, the logarithmic dependence is caused by the integral of $r/(r^2+a^2)$, while the Bessel functions in the integrand are responsible for bending the overall shape of $f(q,\omega)$ away from the log asymptote, and thus for restricting the logarithmic dependence to an intermediate range of q. The Bessel functions are also responsible for the minus sign in front of the logarithm. This consideration is a further demonstration that the logarithmic correction stems from the power-law decay of correlations encoded in the integrand factor $r/(r^2+a^2)$. Thus, I have the averaged self-energy (susceptibility), in an intermediate range of q, as:

$$\mathrm{Im}\langle\Sigma_0^{\mu\nu}(q)\rangle\sim-q^2\ln q. \tag{6.42}$$

where the linear dispersion relation $q\propto\omega$ is assumed. A similar result was obtained by John and Stephen (1983) in a different context of Anderson localisation of electromagnetic waves where a scalar model with power-law correlation in the spatially varying mass parameter was considered. To my knowledge, the one presented here is the first derivation of this effect

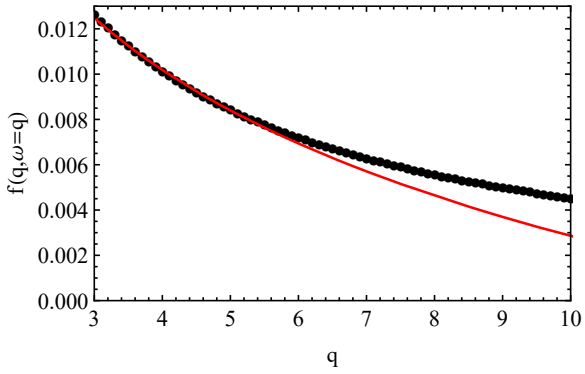

Fig. 6.5 Fitting of $f(q,\omega)$ (symbols), i.e. the numerical integral in Eq. (6.41), with logarithmic function $-p_0\ln(p_1 q)$ (solid line). Parameters are $a=10, c=1, p_0=0.008$ and $p_1=0.07$.

in the context of phonon propagation in elastic media, thus accounting for the full tensorial nature of the problem.

I note that there are no purely longitudinal and transverse waves with respect to the direction of $\mathbf{q}$. This is different from the cases considered in John et al. (1983); John and Stephen (1983); Maurer and Schirmacher (2004). However, cross terms in Eqs. (6.23e) and (6.23f) essentially contribute nothing to the density of states. One might define a more general relation between damping and self-energy over different directions. Hence Eq. (6.42) demonstrates that the self-energy of the phonon Green's function, which is closely related to the phonon damping coefficient, does indeed exhibit a logarithmic enhancement correction to the Rayleigh law as a result of power-law spatial correlations in at least the elastic constant C^3. Hence this result holds for materials that are described within the heterogeneous elasticity framework.

Theory with non-zero C^1, C^4, C^5 and long-range correlations in C^2 and C^3

In addition to letting $C^3(\mathbf{r}) \equiv \rho C_3 + \rho\Delta C_3(\mathbf{r})$, I further require $C^2(\mathbf{r}) \equiv \rho C_2 + \rho\Delta C_2(\mathbf{r})$ with $\overline{\Delta C}_{2,3}(\mathbf{r}) = 0$ and $\overline{\Delta C_{2,3}(\mathbf{r}')\Delta C_{2,3}(\mathbf{r}'+\mathbf{r})} = B_{2,3}(\mathbf{r}) = \gamma_{2,3}\cos(4\theta)/(r^2+a^2)$ for parameters $\gamma_{2,3}$, and parameter a. In this case, the configurational average is due to spatial fluctuations of both C^2 and C^3 and is given by

$$\mathscr{P}[\Delta C(\mathbf{r})] \propto \exp\left[-\frac{1}{2}\sum_{i=2,3}\int d^2r d^2r' \Delta C_i(\mathbf{r}) B_i^{-1}(\mathbf{r}-\mathbf{r}')\Delta C_i(\mathbf{r}')\right]. \tag{6.43}$$

To implement the same formalism as above, I now introduce two effective fields to get the CPA for the one-particle Green's function. The matrix operators (with effective fields) become

$$A^{\mu\nu} = -z\delta^{\mu\nu} - \sum_{\kappa\chi} \mathscr{C}^{\mu\nu\kappa\chi}\nabla_\kappa\nabla_\chi - \frac{1}{4}\sum_{\kappa\chi}[\nabla_\kappa(\Delta C_3\nabla_\chi)]\varepsilon^{\mu\nu\kappa\chi} + \frac{1}{2}\nabla_\mu\Delta C_2\nabla_\nu\delta^{\mu\nu}\eta^{\mu\nu}; \tag{6.44}$$

$$A^{\mu\kappa\chi\nu}_{ab}(\Lambda_2,\Lambda_3) \equiv \delta(\mathbf{r}-\mathbf{r}')\left(-z\delta^{\mu\nu} - \sum_{\kappa\chi}\mathscr{C}^{\mu\nu\kappa\chi}\nabla_\kappa\nabla_\chi\right) - \frac{1}{4}\sum_{\kappa\chi}\nabla_\kappa\Lambda^{\mu\nu\kappa\chi}_{ab,3}(\mathbf{r},\mathbf{r}',z)\nabla_\chi\varepsilon^{\mu\nu\kappa\chi} + \frac{1}{2}\nabla_\mu\Lambda^{\mu\nu}_{ab,2}\nabla_\nu\delta^{\mu\nu}\eta^{\mu\nu}, \tag{6.45}$$

where $\eta^{xx}=1$, $\eta^{yy}=-1$. Repeating similar steps, the self-consistent equations take the following form:

$$\langle\Sigma^{\mu\nu}_{0,2}\rangle = \frac{1}{4}\nabla_\mu B_2(\mathbf{r}-\mathbf{r}')\nabla_\nu\langle G_0(r^\mu,r^\nu,z)\rangle\eta^{\mu\nu}; \tag{6.46a}$$

$$\langle\Sigma^{\mu\nu}_{0,3}\rangle = \frac{1}{8}\sum_{\kappa\chi}\nabla_\kappa B_3(\mathbf{r}-\mathbf{r}')\nabla_\chi\langle G_0(r^\mu,r^\nu,z)\rangle\varepsilon^{\mu\nu\kappa\chi}; \tag{6.46b}$$

$$G_0(r^x,r'^x,z) = \left[-z - \left(\frac{C^4}{8} + \frac{C_2+\Sigma^{xx}_{0,2}}{2} + \frac{3C^1}{8}\right)\nabla_x\nabla_x - \left(\frac{C^1}{8}-\frac{C^4}{8}\right)\nabla_y\nabla_y - \left(\frac{C^5}{8} + \frac{(C_3+\Sigma^{xx}_{0,3})}{4}\right)(\nabla_x\nabla_y+\nabla_y\nabla_x)\right]^{-1}; \tag{6.46c}$$

$$G_0(r^y,r'^y,z) = \left[-z - \left(\frac{C^4}{8} - \frac{C_2-\Sigma^{yy}_{0,2}}{2} + \frac{3C^1}{8}\right)\nabla_y\nabla_y - \left(\frac{C^1}{8}-\frac{C^4}{8}\right)\nabla_x\nabla_x - \left(-\frac{C^5}{8} + \frac{(C_3+\Sigma^{yy}_{0,3})}{4}\right)(\nabla_x\nabla_y+\nabla_y\nabla_x)\right]^{-1}; \tag{6.46d}$$

$$G_0(r^x,r'^y) = \left[-\left(\frac{C^1}{8}-\frac{C^4}{8}\right)(\nabla_x\nabla_y+\nabla_y\nabla_x) - \frac{(C_3+\Sigma^{xy}_{0,3})}{4}(\nabla_x\nabla_x+\nabla_y\nabla_y) - \frac{C^5}{8}(\nabla_x\nabla_x-\nabla_y\nabla_y)\right]^{-1}; \tag{6.46e}$$

$$G_0(r^y,r'^x) = \left[-\left(\frac{C^1}{8}-\frac{C^4}{8}\right)(\nabla_x\nabla_y+\nabla_y\nabla_x) - \frac{(C_3+\Sigma^{yx}_{0,3})}{4}(\nabla_x\nabla_x+\nabla_y\nabla_y) - \frac{C^5}{8}(\nabla_x\nabla_x-\nabla_y\nabla_y)\right]^{-1}. \tag{6.46f}$$

I note that, even if B_2+B_3 has no long-range tail, the net effect of the imaginary part of $\langle\Sigma^{\mu\nu}_{0,2}\rangle + \langle\Sigma^{\mu\nu}_{0,3}\rangle$ still exhibits log-enhancement. To see this more clearly, I write down $\Sigma^{xx}_{0,2}$

and $\Sigma^{xx}_{0,3}$,

$$\begin{aligned}\langle\Sigma^{xx}_{0,2}\rangle &= \frac{1}{4}\nabla_x B_2(\mathbf{r}-\mathbf{r}')\nabla_x\langle G_0(r^x,r'^x,z)\rangle;\\ \langle\Sigma^{xx}_{0,3}\rangle &= \frac{1}{8}\nabla_x B_3(\mathbf{r}-\mathbf{r}')\nabla_y\langle G_0(r^x,r'^x,z)\rangle\\ &\quad+\frac{1}{8}\nabla_y B_3(\mathbf{r}-\mathbf{r}')\nabla_x\langle G_0(r^x,r'^x,z)\rangle.\end{aligned} \tag{6.47}$$

Using the same arguments as in the last section, namely transforming to $\mathbf{q}$ space, I can easily verify that $\mathrm{Im}\langle\Sigma_{0,2}\rangle \sim -q^2\ln q$ and $\mathrm{Im}\langle\Sigma_{0,3}\rangle \sim -q^2\ln q$. Hence, I also have that $\mathrm{Im}[\langle\Sigma^{xx}_{0,2}\rangle + \langle\Sigma^{xx}_{0,3}\rangle] \sim -q^2\ln q$ even if $B_2 = -B_3$. Since this works the same for all components μ,ν, I can conclude that

$$\mathrm{Im}[\langle\Sigma^{\mu\nu}_{0,2}\rangle + \langle\Sigma^{\mu\nu}_{0,3}\rangle] \sim -q^2\ln q, \tag{6.48}$$

which holds for all components μ,ν of the self energy.

Hence, the logarithmic enhancement to Rayleigh scattering law remains confirmed also in the case of power-law spatial correlations in two elastic constants, C^2 and C^3. I have rigorously proved that power-law correlations lead to the logarithmic enhancement of Rayleigh scattering in amorphous solids, under the same conditions studied in numerical simulations in Gelin et al. (2016) where this effect was observed. I note that, in Caroli and Lemaître (2019), it is reported that Rayleigh law without the logarithmic dependence is retrieved in the frame of fluctuating elasticity. The authors attribute this behavior to cancellation of the elastic correlations between spatial autocorrelations of non-diagonal part of local elastic coefficients. I emphasise that the imaginary part of self-energy obtained here in Eq. (6.48) does not split into purely transverse and longitudinal contributions, whereas that from their method vanishes because those authors assume fully isotropic elasticity splitting into uncoupled longitudinal and transverse contributions (see Eq. (34) in the ESI of Caroli and Lemaître (2019)), which does not correspond to the physical system in Gelin et al. (2016), nor to other simulated systems where the effect was observed.

Summary

Through explicitly calculating the quenched average of the longitudinal DSF with the representative Gaussian distribution of random bond constants in a perfect lattice, I obtained the expression for the effective damping coefficient, where its unexpected linear dependence on q was revealed. I have also developed a fully tensorial replica field theory of heterogeneous

elasticity, which predicts that long-range elastic correlations cause a logarithmic enhancement to Rayleigh scattering of phonons in amorphous systems without internal stresses.

Chapter 7

Conclusion and Outlook

In this thesis, I have firstly introduced a general version of the classical particle-bath Hamiltonian, which serves as a starting point to derive GLE, for systems subject to an external time-dependent (oscillating) field. Unlike previous models where the bath oscillators were always taken to be unaffected by the field, here I added the time-dependent force due to the field to both the Hamiltonian of the particle and the Hamiltonian of the bath oscillators. The resulting Hamiltonian has been solved analytically and the resulting GLE and FDT have been found. The formal structure of the GLE is still identical to that of standard GLE with external field acting on the particle only (and the memory function for the friction is the same), but the stochastic force is very different. Its ensemble average, remarkably, is non-zero and directly proportional to the AC field. The associated FDT has an additional term given by the time-correlation of the AC field, and is thus quadratic in the field amplitude.

An immediate application of the resulting GLE is to elucidate the dielectric spectroscopy or mechanical response of glasses. The Debye model treats each molecule as fully independent from all other molecules in the material and describes it with a Langevin equation for the orientation of the molecule in the field. The GLE derived here will open the possibility of describing both these effects at the same time, within the GLE picture that has been proposed recently to deal with the hierarchy of relaxation times in molecular glasses. In specific, the GLE makes it possible to directly link the VDOS measured experimentally with the macroscopic dielectric response and the underlying heterogeneous dynamics. Implementing the VDOS of a disordered elastic lattice near the T_g within the Lorentz sum rule, we are able to reproduce the dielectric response of glycerol in good agreement with state-of-the-art experimental data. The soft-mode model greatly improves over Kohlrausch (and MCT) fittings on the low-frequency side of the α peak, where I have shown that the response is controlled by extended modes. The high-ω side of the peak (α-wing) is instead dominated by the boson-peak soft mode excess in the VDOS, and, remarkably, it recovers stretched-

exponential relaxation. This result shows, for the first time, that the α-wing is caused by the boson peak contribution to the relaxation spectrum.

If there are more than one relaxation processes, say α- and β-peaks, we then require two stretched exponentials in the memory function, hence two relaxation times, to fit both α- and β-relaxations. The β-relaxation process cannot be recovered with only one stretched exponential (i.e. with only one term in the memory function). One of the stretched exponentials dominates the α- peak while the co-existing effect of two stretched exponential terms in the memory function gives rise to the secondary relaxation. In other words, the two terms of memory function both affect the secondary relaxation, whereas only one of them controls the α-relaxation. This implies that there is indeed a deep microscopic dynamical coupling between the two relaxation processes, which has not been unveiled so far.

The GLE derived in this thesis can be used as the starting point for a more microscopic description of nonlinear effects in dielectric relaxation of supercooled liquids under strong fields, for which a microscopic picture is currently lacking. Further applications of the proposed framework include quantum dissipative transport and Josephson tunnelling with dissipation, driven dynamics of colloids in soft matter systems, and molecular dynamics simulations of liquids and of amorphous solids in oscillatory shear. In future work this framework would be used to provide more microscopic insights into the dynamical nature of this coupling and in the context of the Ngai coupling model (Ngai, 1998).

Meanwhile, applying this analysis to mechanical response, the resultant framework (nonaffine lattice dynamics) also establishes that, in order to explain the mechanical α-relaxation and the α-wing asymmetry in metallic glass, an excess of soft vibrational modes, as well as strong memory effects in the dynamics due to non-local electronic coupling between many atoms, are necessary ingredients that cannot be neglected. A crucial input to the theory is the VDOS. Surprisingly, the qualitative features (i.e. peak positions) of the VDOS appear to play the main role in determining the viscoelastic response of the glass, implying a common behavior linking the JG β-relaxation to vibrational dynamics in glassy systems. These results should undoubtedly be useful for developing a universal theory of secondary relaxations in metallic glasses.

Applying the framework of nonaffine lattice dynamics to pre-stretched bonds might be a first step in the direction of a theory of granular matter and disordered solids where internal stresses are explicitly taken into account. The system of spring networks is rigid also below the Maxwell rigidity threshold, whereas for pre-compressed bonds the onset of rigidity is shifted to higher coordination number. Since this approach is directly applicable to a variety of glassy and partly-ordered systems that feature a boson peak, not only molecular glasses and metallic glasses but also polymer glasses (Hong et al., 2008), silica glasses (Ilg

and Barrat, 2007), by suitably extending the theory to include bond-bending interactions that are needed to describe covalent bonds. For non-centrosymmetic crystals such as the quartz (Chumakov et al., 2014), I have shown that employing an empirical potential for α-quartz, with long-range Coulombic effects explicitly considered, the elastic constants of α-quartz, consisting of the contribution of affine and nonaffine contributions, can be excellently recovered, where the nonaffine force field indeed plays a crucial role in the elastic constants.

These results are also relevant to studies of the boson peak (i.e. excess with respect to Debye's ω^2 law in the VDOS), which is typically observed in glasses but has recently also been measured in α-quartz (Chumakov et al., 2014). Recent works have highlighted the close connection between nonaffine elasticity and the boson peak anomaly (Milkus and Zaccone, 2016; Senguly and Sengupta, 2017), and it has been suggested that the root cause of both boson peak and nonaffine elasticity could be traced back to the inherent lack of centrosymmetry of both glasses and non-centrosymmetric crystals such as α-quartz (Milkus and Zaccone, 2016).

With the analytical formula for the estimated damping constant available, one can also work backwards and reveal the extent of disorder in a material using the scaling law of damping coefficient. In a continuum medium, the disorder reflects the variation of local elastic modulus C. For example, in α-quartz, the (largest) linewidth is measured around the resonance of 10meV along $(1,0,0)$ to have the width $\Gamma \sim 5$meV (Burkel, 2001). The Young's modulus C_{11} was computed to be 90GPa, therefore, this gives us an estimate for the disorder variance $\sigma \sim 30\text{GPa} = 0.3C_{11}$, a reasonable value of 'low disorder'. Very recently it has been reported the damping coefficient scales linearly with frequency in granular packings (Zhai et al., 2020), and hence $\Gamma \sim q$ as the acoustic branch has $\omega = cq$ at low q. This is in full agreement with my predicted damping law in Eq. (6.9). Importantly, the linear damping has been observed in packings with heterogeneous distributions of contact stiffness, whereas in packings with uniform contact stiffness the linear damping is less visible. When q becomes large, the lattice Green's function and the elastic Green's function are no longer equivalent (Trinkle, 2008). Considering the wave propagation with large wavevectors will be a possible future direction. Regarding to the controversial Rayleigh scattering, also note that many numerical simulations addressing this problem so far only extract affine elastic constants, while the nonaffine contribution to elasticity might be important in some systems and should be examined in detail in future work, although nonaffinity does not appear to be a necessary ingredient for the appearance of the anomalous scattering. Moreover, Moriel et al. (2019) argued on the basis of numerical data on computer glasses that Rayleigh scaling is expected at low wavenumbers, at which soft quasilocalised modes are scarce, while the logarithmically

enhanced Rayleigh scaling of the form $\Gamma(q) \sim q^{d+1} \ln q$ arises at higher q. In that case, the way to extract phononic and nonphononic excitations is different from Mizuno and Ikeda (2018), which might result in the different features of enhanced logarithmic dependence. I also note that the enhanced logarithmic Rayleigh scattering contributed by power-law elastic or stress correlations in my theory arises in a broad intermediate range of q. However, the discussion about this issue is beyond the scope of my current work, and will be studied in detail in future work.

My analysis with replica field is restricted to the athermal limit. At finite temperature, elastic correlators would receive additional effects from anharmonicity (Baggioli and Zaccone, 2019; Mizuno et al., 2020) and other thermal effects. I expect this problem to be important also for plasticity and yielding, which could be the object of future work.

References

Akhiezer, A. I., Akhiezer, I. A., and Pollvin, R. V. (1967). *Collective oscillations in a plasma*. Pergamon Press, Oxford.

Alexander, S. (1998). Amorphous solids: their structure, lattice dynamics and elasticity. *Physics Reports*, 296(2):65 – 236.

Allen, M. P. and Tildesley, D. J. (2017). *Computer Simulation of Liquids: Second Edition*. Oxford University Press, Oxford.

Andersen, H. C. (1980). Molecular dynamics simulations at constant pressure and/or temperature. *J. Chem. Phys.*, 72(4):2384–2393.

Angell, C. (1988). Structural instability and relaxation in liquid and glassy phases near the fragile liquid limit. *J. Non-Cryst. Solids*, 102(1):205 – 221.

Angell, C. A., Ngai, K. L., McKenna, G. B., McMillan, P. F., and Martin, S. W. (2000). Relaxation in glassforming liquids and amorphous solids. *J. Appl. Phys.*, 88(6):3113–3157.

Argon, A. S. (1979). Plastic deformation in metallic glasses. *Acta Mater.*, 27(1):47 – 58.

Ashcroft, N. W. and Mermin, N. D. (1976). *Solid State Physics*. Harcourt College Pbublishers.

Bagchi, B. (2012). *Molecular Relaxation in Liquids*. Oxford University Press, Oxford.

Baggioli, M. and Zaccone, A. (2019). Universal origin of boson peak vibrational anomalies in ordered crystals and in amorphous materials. *Phys. Rev. Lett.*, 122:145501.

Baldi, G., Giordano, V. M., and Monaco, G. (2011). Elastic anomalies at terahertz frequencies and excess density of vibrational states in silica glass. *Phys. Rev. B*, 83:174203.

Baldi, G., Giordano, V. M., Monaco, G., and Ruta, B. (2010). Sound attenuation at terahertz frequencies and the boson peak of vitreous silica. *Phys. Rev. Lett.*, 104:195501.

Baldi, G., Giordano, V. M., Ruta, B., Dal Maschio, R., Fontana, A., and Monaco, G. (2014). Anharmonic damping of terahertz acoustic waves in a network glass and its effect on the density of vibrational states. *Phys. Rev. Lett.*, 112:125502.

Baldi, G., Giordano, V. M., Ruta, B., and Monaco, G. (2016). On the nontrivial wave-vector dependence of the elastic modulus of glasses. *Phys. Rev. B*, 93:144204.

Ballauff, M., Brader, J. M., Egelhaaf, S. U., Fuchs, M., Horbach, J., Koumakis, N., Krüger, M., Laurati, M., Mutch, K. J., Petekidis, G., Siebenbürger, M., Voigtmann, T., and Zausch, J. (2013). Residual stresses in glasses. *Phys. Rev. Lett.*, 110:215701.

Balucani, U. and Zoppi, M. (1994). *Dynamics of liquid state*. Oxford University Press, Oxford.

Bernard, W. and Callen, H. B. (1959). Irreversible thermodynamics of nonlinear processes and noise in driven systems. *Rev. Mod. Phys.*, 31:1017–1044.

Binder, K. and Heermann, D. (2001). *The glass transition*. Springer-Verlag Berlin Heidelberg.

Birch, F. (1938). The effect of pressure upon the elastic parameters of isotropic solids, according to murnaghan's theory of finite strain. *Journal of Applied Physics*, 9(4):279–288.

Blickle, V., Speck, T., Helden, L., Seifert, U., and Bechinger, C. (2006). Thermodynamics of a colloidal particle in a time-dependent nonharmonic potential. *Phys. Rev. Lett.*, 96:070603.

Blochowicz, T. and Rössler, E. A. (2004). Beta relaxation versus high frequency wing in the dielectric spectra of a binary molecular glass former. *Phys. Rev. Lett.*, 92:225701.

Blumenfeld, R. (2004). Stresses in isostatic granular systems and emergence of force chains. *Phys. Rev. Lett.*, 93:108301.

Born, M. and Huang, K. (1954). *Dynamical Theory of Crystal Lattices*. Oxford University Press, Oxford.

Born, M. and Wolf, E. (1999). *Principles of Optics*. Cambridge University Press, Cambridge.

Bosak, A., Krisch, M., Chernyshov, D., and et al. (2012). New insights into the lattice dynamics of α-quartz. *Z. Kristallogr.*, 227:84.

Bragg, W. and Gibbs, R. E. (1925). The structure of α and β quartz. *Proc. Roy. Soc. Lond. A*, 109:405.

Brand, R., Lunkenheimer, P., and Loidl, A. (2002). Relaxation dynamics in plastic crystals. *J. Chem. Phys.*, 116(23):10386–10401.

Brink, T., Koch, L., and Albe, K. (2016). Structural origins of the boson peak in metals: From high-entropy alloys to metallic glasses. *Phys. Rev. B*, 94:224203.

Burkel, E. (2001). Determination of phonon dispersion curves by means of inelastic x-ray scattering. *Journal of Physics: Condensed Matter*, 13(34):7627–7644.

Böhmer, R., Ngai, K. L., Angell, C. A., and Plazek, D. J. (1993). Nonexponential relaxations in strong and fragile glass formers. *J. Chem. Phys.*, 99(5):4201–4209.

Caldeira, A. O. (2014). *An Introduction to Macroscopic Quantum Phenomena and Quantum Disspation*. Cambridge University Press, Cambridge.

Callen, H. B. and Welton, T. A. (1951). Irreversibility and generalized noise. *Phys. Rev.*, 83:34–40.

Cardona, M., Chamberlin, R. V., and Marx, W. (2007). The history of the stretched exponential function. *Ann. Phys. (Berl.)*, 16(12):842–845.

Carini, G., Federico, M., Fontana, A., and Saunders, G. A. (1993). Low-frequency light scattering and structural defects in samarium phosphate glasses. *Phys. Rev. B*, 47:3005–3010.

Caroli, C. and Lemaître, A. (2019). Fluctuating elasticity fails to capture anomalous sound scattering in amorphous solids. *Phys. Rev. Lett.*, 123:055501.

Carré, A., Berthier, L., Horbach, J., Ispas, S., and Kob, W. (2007). Amorphous silica modeled with truncated and screened coulomb interactions: A molecular dynamics simulation study. *J. Chem. Phys.*, 127:114512.

Carré, A., Horbach, J., Ispas, S., and Kob, W. (2008). New fitting scheme to obtain effective potential from car-parrinello molecular-dynamics simulations: Application to silica. *Europhys. Lett.*, 82:17001.

Cates, M. E., Wittmer, J. P., Bouchaud, J.-P., and Claudin, P. (1998). Jamming, force chains, and fragile matter. *Phys. Rev. Lett.*, 81:1841–1844.

Chumakov, A. I., Monaco, G., Fontana, A., Bosak, A., Hermann, R. P., Bessas, D., Wehinger, B., Crichton, W. A., Krisch, M., Rüffer, R., Baldi, G., Carini Jr., G., Carini, G., D'Angelo, G., Gilioli, E., Tripodo, G., Zanatta, M., Winkler, B., Milman, V., Refson, K., Dove, M. T., Dubrovinskaia, N., Dubrovinsky, L., Keding, R., and Yue, Y. Z. (2014). Role of disorder in the thermodynamics and atomic dynamics of glasses. *Phys. Rev. Lett.*, 112:025502.

Cicerone, M. T. and Tyagi, M. (2017). Metabasin transitions are johari-goldstein relaxation events. *J. Chem. Phys.*, 146(5):054502.

Cohen, Y.and Karmakar, S., Procaccia, I., and Samwer, K. (2012). The nature of the beta-peak in the loss modulus of amorphous solids. *Europhys. Lett.*, 100:36003.

Cui, B., Evenson, Z., Fan, B., Li, M.-Z., Wang, W.-H., and Zaccone, A. (2018a). Possible origin of β-relaxation in amorphous metal alloys from atomic-mass differences of the constituents. *Phys. Rev. B*, 98:144201.

Cui, B., Gebbia, J. F., Tamarit, J.-L., and Zaccone, A. (2018b). Disentangling α and β relaxation in orientationally disordered crystals with theory and experiments. *Phys. Rev. E*, 97:053001.

Cui, B., Milkus, R., and Zaccone, A. (2017a). Direct link between boson-peak modes and dielectric α-relaxation in glasses. *Phys. Rev. E*, 95:022603.

Cui, B., Ruocco, G., and Zaccone, A. (2019a). Theory of elastic constants of athermal amorphous solids with internal stresses. *Granul Matter.*, 21(3):69.

Cui, B. and Terentjev, E. M. (2020). Comparison of the helmholtz, gibbs, and collective-modes methods to obtain nonaffine elastic constants. *J. Mech. Phys. Sol.*, 140:103954.

Cui, B., Yang, J., Qiao, J. C., Jiang, M. Q., Dai, L. H., Wang, Y.-J., and Zaccone, A. (2017b). Atomic theory of viscoelastic response and memory effects in metallic glasses. *Phys. Rev. B*, 96:094203.

Cui, B., Zaccone, A., and Rodney, D. (2019b). Nonaffine lattice dynamics with the ewald method reveals strongly nonaffine elasticity of α-quartz. *J. Chem. Phys.*, 151(22):224509.

Damart, T., Tanguy, A., and Rodney, D. (2017). Theory of harmonic dissipation in disordered solids. *Phys. Rev. B*, 95:054203.

Davidson, D. W. and Cole, R. H. (1951). Dielectric relaxation in glycerol, propylene glycol, and n-propanol. *J. Chem. Phys.*, 19(12):1484–1490.

Dean, P. (1972). The vibrational properties of disordered systems: Numerical studies. *Rev. Mod. Phys.*, 44:127–168.

Debye, P. (1929). *Polar Molecules*. The Chemical Catalog, Inc., New York.

DeGiuli, E., Laversanne-Finot, A., Düring, G., Lerner, E., and Wyart, M. (2014). Effects of coordination and pressure on sound attenuation, boson peak and elasticity in amorphous solids. *Soft Matter*, 10:5628–5644.

Derlet, P., Maaß, R., and Löffler, J. (2012). The boson peak of model glass systems and its relation to atomic structure. *Eur. Phys. J. B*, 85(5):148.

Dixon, P. K., Wu, L., Nagel, S. R., Williams, B. D., and Carini, J. P. (1990). Scaling in the relaxation of supercooled liquids. *Phys. Rev. Lett.*, 65:1108–1111.

Donth, E. (2001). *The glass transition*. Springer-Verlag Berlin Heidelberg.

Döß, A., Paluch, M., Sillescu, H., and Hinze, G. (2002). From strong to fragile glass formers: Secondary relaxation in polyalcohols. *Phys. Rev. Lett.*, 88:095701.

Dotsenko, V. (2000). *Introduction to the Replica Theory of Disordered Statistical Systems*. Collection Alea-Saclay: Monographs and Texts in Statistical Physics. Cambridge University Press.

Economou, E. (2006). *Green's Functions in Quantum Physics*. Springer Series in Solid-State Sciences. Springer.

Ellenbroek, W. G., Zeravcic, Z., van Saarloos, W., and van Hecke, M. (2009). Non-affine response: Jammed packings vs. spring networks. *Europhys. Lett.*, 87(3):34004.

Evenson, Z., Naleway, S. E., Wei, S., Gross, O., Kruzic, J. J., Gallino, I., Possart, W., Stommel, M., and Busch, R. (2014). β relaxation and low-temperature aging in a au-based bulk metallic glass: From elastic properties to atomic-scale structure. *Phys. Rev. B*, 89:174204.

Ewald, P. P. (1921). The calculation of optical and electrostatic grid potential. *Ann. Phys. (Leipzig)*, 64:253.

Falk, M. L. and Langer, J. S. (1998). Dynamics of viscoplastic deformation in amorphous solids. *Phys. Rev. E*, 57:7192–7205.

Fennell, C. J. and Gezelter, J. D. (2006). Is the ewald summation still necessary? pairwise alternatives to the accepted standard for long-range electrostatics. *J. Chem. Phys.*, 124:234104.

Fisher, M. P. A. and Zwerger, W. (1985). Quantum brownian motion in a periodic potential. *Phys. Rev. B*, 32:6190–6206.

Folland, G. B. (1992). *Fourier Analysis and Its Applications*. Wadsworth, Belmont, CA.

Ford, G. W. (2017). The fluctuation–dissipation theorem. *Contemp. Phys.*, 58(3):244–252.

Froehlich, H. (1958). *Theory of Dielectrics*. Clarendon Press, Oxford.

Fuchs, M. and Cates, M. E. (2002). Theory of nonlinear rheology and yielding of dense colloidal suspensions. *Phys. Rev. Lett.*, 89:248304.

Fuchs, M., Gotze, W., Hofacker, I., and Latz, A. (1991). Comments on the alpha -peak shapes for relaxation in supercooled liquids. *J. Phys. Condens. Matter*, 3(26):5047–5071.

Gelin, S., Tanaka, H., and Lemaitre, A. (2016). Anomalous phonon scattering and elastic correlations in amorphous solids. *Nat. Mater.*, 15(4736):1177–1181.

Geng, J., Reydellet, G., Clément, E., and Behringer, R. (2003). Green's function measurements of force transmission in 2d granular materials. *Physica D: Nonlinear Phenomena*, 182(3):274 – 303.

Gilroy, K. S. and Phillips, W. A. (1981). An asymmetric double-well potential model for structural relaxation processes in amorphous materials. *Philos. Mag. B*, 43(5):735–746.

Goetze, W. (2008). *Complex Dynamics of Glass-Forming Liquids: A Mode-Coupling Theory*. Oxford University Press, Oxford.

Hansen, J.-P. and McDonald, I. (2008). *Theory of simple liquids*. Academic Press, London.

Harada, T. and Sasa, S. (2005). Equality connecting energy dissipation with a violation of the fluctuation-response relation. *Phys. Rev. Lett.*, 95:130602.

Harada, T. and Sasa, S. (2006). Energy dissipation and violation of the fluctuation-response relation in nonequilibrium langevin systems. *Phys. Rev. E*, 73:026131.

Herring, C. (1954). Role of low-energy phonons in thermal conduction. *Phys. Rev.*, 95:954–965.

Heyliger, P., Ledbetter, H., and Kim, S. (2003). Elastic constants of natural quartz. *J. Acous. Soc. Am.*, 114:644.

Hong, L., Begen, B., Kisliuk, A., Alba-Simionesco, C., Novikov, V. N., and Sokolov, A. P. (2008). Pressure and density dependence of the boson peak in polymers. *Phys. Rev. B*, 78:134201.

Hoover, W. G. (1985). Canonical dynamics: Equilibrium phase-space distributions. *Phys. Rev. A*, 31:1695–1697.

Hufnagel, T. C., Schuh, C. A., and Falk, M. L. (2016). Deformation of metallic glasses: Recent developments in theory, simulations, and experiments. *Acta Mater.*, 109:375 – 393.

Huisman, E. M. and Lubensky, T. C. (2011). Internal stresses, normal modes, and nonaffinity in three-dimensional biopolymer networks. *Phys. Rev. Lett.*, 106:088301.

Hänggi, P. and Ingold, G.-L. (2005). Fundamental aspects of quantum brownian motion. *Chaos*, 15(2):026105.

Ilg, P. and Barrat, J.-L. (2007). Driven activationvs.thermal activation. *Europhys. Lett.*, 79(2):26001.

Izvekov, S. (2017). Microscopic derivation of particle-based coarse-grained dynamics: Exact expression for memory function. *J. Chem. Phys.*, 146(12):124109.

Johari, G. P. and Goldstein, M. (1970). Viscous liquids and the glass transition. ii. secondary relaxations in glasses of rigid molecules. *J. Chem. Phys.*, 53(6):2372–2388.

John, S., Sompolinsky, H., and Stephen, M. J. (1983). Localization in a disordered elastic medium near two dimensions. *Phys. Rev. B*, 27:5592–5603.

John, S. and Stephen, M. J. (1983). Wave propagation and localization in a long-range correlated random potential. *Phys. Rev. B*, 28:6358–6368.

Jung, G., Hanke, M., and Schmid, F. (2017). Iterative reconstruction of memory kernels. *J. Chem. Theory Comput.*, 13(6):2481–2488.

Kalyan, D. and Richert, R. (2002). Dynamics of glass-forming liquids. vi. dielectric relaxation study of neat decahydro-naphthalene. *J. Chem. Phys.*, 117(9):4414–4418.

Kholkin, A., Pertsev, N., and Goltsev, A. (2008). Piezoelectricity and crystal symmetry. In *Piezoelectric and Acoustic Materials for Transducer Applications*, Boston. Springer.

Kihara, K. (1990). An x-ray study of the temperature dependence of the quartz structure. *Eur. J. Mineral.*, 2:63.

Kim, K. and Nelkin, M. (1973). Dynamic structure factor of a disordered harmonic solid. *Phys. Rev. B*, 7:2762–2771.

Kob, W. (2003). Course 5: Supercooled liquids, the glass transition, and computer simulations. In Barrat, J.-L., Feigelman, M., Kurchan, J., and Dalibard, J., editors, *Slow Relaxations and nonequilibrium dynamics in condensed matter*, pages 199–269. Springer, Berlin Heidelberg.

Köhler, S., Ruocco, G., and Schirmacher, W. (2013). Coherent potential approximation for diffusion and wave propagation in topologically disordered systems. *Phys. Rev. B*, 88:064203.

Kondic, L., Goullet, A., O'Hern, C. S., Kramar, M., Mischaikow, K., and Behringer, R. P. (2012). Topology of force networks in compressed granular media. *Europhys. Lett.*, 97(5):54001.

Kosevich, A. M. (2005). *The Crystal Lattice*. Wiley-VCH, Weinheim.

Kubo, R. (1957). Statistical-mechanical theory of irreversible processes. i. general theory and simple applications to magnetic and conduction problems. *J. Phys. Soc. Jpn.*, 12(6):570–586.

Kudlik, A., Benkhof, S., Lenk, R., and Rössler, E. (1995). Spectral shape of the α-process in supercooled liquids revisited. *Europhys. Lett.*, 32(6):511–516.

Landau, L. D. and Lifshitz, I. M. (1960). *Electrodynamics of Continuous Media*. Pergamon Press, Oxford.

Langer, J. S. (2008). Shear-transformation-zone theory of plastic deformation near the glass transition. *Phys. Rev. E*, 77:021502.

Lee, H. and Cai, W. (2009). Ewald summation for coulomb interactions in a periodic supercell. Lecture notes, Stanford University.

Lemaitre, A. and Maloney, C. (2006). Sum rules for the quasi-static and visco-elastic response of disordered solids at zero temperature. *J. Stat. Phys.*, 123:415.

Leontovich, M. A. and Rytov, S. M. (1952). On a differential law for the intensity of electric fluctuations and the influence of the skin-effect. *Zh. Eksp. Teor. Fiz.*, 23:246–252.

Lerner, E., Düring, G., and Bouchbinder, E. (2016). Statistics and properties of low-frequency vibrational modes in structural glasses. *Phys. Rev. Lett.*, 117:035501.

Levine, A. J. and Lubensky, T. C. (2000). One- and two-particle microrheology. *Phys. Rev. Lett.*, 85:1774–1777.

Li, Z., Bian, X., Yang, X., and Karniadakis, G. E. (2016). A comparative study of coarse-graining methods for polymeric fluids: Mori-zwanzig vs. iterative boltzmann inversion vs. stochastic parametric optimization. *J. Chem. Phys.*, 145(4):044102.

Li, Z., Lee, H. S., Darve, E., and Karniadakis, G. E. (2017). Computing the non-markovian coarse-grained interactions derived from the mori–zwanzig formalism in molecular systems: Application to polymer melts. *J. Chem. Phys.*, 146(1):014104.

Lifshitz, E., Kosevich, A., and Pitaevskii, L. (1986). Theory of elasticity. In Lifshitz, E., Kosevich, A., and Pitaevskii, L., editors, *Theory of Elasticity (Third Edition)*. Butterworth-Heinemann, Oxford, third edition edition.

Liu, C., Pineda, E., and Crespo, D. (2015). Mechanical relaxation of metallic glasses: An overview of experimental data and theoretical models. *Metals*, 5(2):1073–1111.

Liu, C. R., Pineda, E., Crespo, D., C., Q. J., Evenson, Z., and Ruta, B. (2017). Sub-tg relaxation times of the α process in metallic glasses. *J. Non-Cryst. Solids*, 471:322 – 327.

Liu, Y. H., Fujita, T., Aji, D. P. B., Matsuura, M., and Chen, M. W. (2014). Structural origins of johari-goldstein relaxation in a metallic glass. *Nat. Commun.*, 5:3238. Article.

Lunkenheimer, P., Pimenov, A., Schiener, B., Böhmer, R., and Loidl, A. (1996). High-frequency dielectric spectroscopy on glycerol. *Europhys. Lett.*, 33(8):611–616.

Lunkenheimer, P., Schneider, U., Brand, R., and Loidl, A. (2000). Glassy dynamics. *Contemp. Phys.*, 41(1):15–36.

Luo, P., Li, Y. Z., Bai, H. Y., Wen, P., and Wang, W. H. (2016). Memory effect manifested by a boson peak in metallic glass. *Phys. Rev. Lett.*, 116:175901.

Lutsko, J. F. (1988). Stress and elastic constants in anisotropic solids: Molecular dynamics techniques. *J. Appl. Phys.*, 64(3):1152–1154.

Maes, C. (2014). On the second fluctuation–dissipation theorem for nonequilibrium baths. *J. Stat. Phys.*, 154(3):705–722.

Maes, C.and Steffenoni, S. (2015). Friction and noise for a probe in a nonequilibrium fluid. *Phys. Rev. E*, 91:022128.

Maier, M., Zippelius, A., and Fuchs, M. (2018). Stress auto-correlation tensor in glass-forming isothermal fluids: From viscous to elastic response. *J. Chem. Phys.*, 149(8):084502.

Majmudar, T. S. and Behringer, R. P. (2005). Contact force measurements and stress-induced anisotropy in granular materials. *Nature*, 435(7045):1079–1082.

Mantisi, B., Tanguy, A., Kermouche, G., and Barthel, E. (2012). Atomistic response of a model silica glass under shear and pressure. *Eur. Phys. J. B*, 85:304.

Marruzzo, A., Köhler, S., Fratalocchi, A., Ruocco, G., and Schirmacher, W. (2013a). Vibrational anomalies and marginal stability of glasses. *Eur. Phys. J. Special Topics*, 216:83–93.

Marruzzo, A., Schirmacher, W., Fratalocchi, A., and Ruocco, G. (2013b). Heterogeneous shear elasticity of glasses: the origin of the boson peak. *Sci. Rep.*, 3(1):1407.

Martinez, L.-M. and Angell, C. A. (2001). A thermodynamic connection to the fragility of glass-forming liquids. *Nature*, 410(6829):663–667.

Masciovecchio, C., Baldi, G., Caponi, S., Comez, L., Di Fonzo, S., Fioretto, D., Fontana, A., Gessini, A., Santucci, S. C., Sette, F., Viliani, G., Vilmercati, P., and Ruocco, G. (2006). Evidence for a crossover in the frequency dependence of the acoustic attenuation in vitreous silica. *Phys. Rev. Lett.*, 97:035501.

Mattsson, J., Bergman, R., Jacobsson, P., and Börjesson, L. (2003). Chain-length-dependent relaxation scenarios in an oligomeric glass-forming system: From merged to well-separated α and β loss peaks. *Phys. Rev. Lett.*, 90:075702.

Maurer, E. and Schirmacher, W. (2004). Local oscillators vs. elastic disorder: A comparison of two models for the boson peak. *J. Low Temp. Phys.*, 137(3):453–470.

Mazzacurati, V., Ruocco, G., and Sampoli, M. (1996). Low-frequency atomic motion in a model glass. *Europhys. Lett.*, 34(9):681–686.

McKane, A. and Stone, M. (1981). Localization as an alternative to goldstone's theorem. *Ann. Phys. (N. Y.)*, 131(1):36 – 55.

Mendelev, M., Kramer, M., Ott, R., and Sordelet, D. (2009). Molecular dynamics simulation of diffusion in supercooled cu–zr alloys. *Philos. Mag.*, 89(2):109–126.

Meyer, A., Wuttke, J., Petry, W., Peker, A., Bormann, R., Coddens, G., Kranich, L., Randl, O. G., and Schober, H. (1996). Harmonic behavior of metallic glasses up to the metastable melt. *Phys. Rev. B*, 53:12107–12111.

Meyer, H., Voigtmann, T., and Schilling, T. (2017). On the non-stationary generalized langevin equation. *J. Chem. Phys.*, 147(21):214110.

Milkus, R. and Zaccone, A. (2016). Local inversion-symmetry breaking controls the boson peak in glasses and crystals. *Phys. Rev. B*, 93:094204.

Mizuno, H. and Ikeda, A. (2018). Phonon transport and vibrational excitations in amorphous solids. *Phys. Rev. E*, 98:062612.

Mizuno, H. and Mossa, S. (2019). Impact of elastic heterogeneity on the propagation of vibrations at finite temperatures in glasses. *Condens. Matter Phys.*, 22(4):43604.

Mizuno, H., Mossa, S., and Barrat, J.-L. (2013). Measuring spatial distribution of the local elastic modulus in glasses. *Phys. Rev. E*, 87:042306.

Mizuno, H., Mossa, S., and Barrat, J.-L. (2014). Acoustic excitations and elastic heterogeneities in disordered solids. *Proc. Natl. Acad. Sci. U.S.A*, 111(33):11949–11954.

Mizuno, H., Ruocco, G., and Mossa, S. (2020). Sound damping in glasses: Interplay between anharmonicities and elastic heterogeneities. *Phys. Rev. B*, 101:174206.

Mizuno, H., Saitoh, K., and Silbert, L. E. (2016). Elastic moduli and vibrational modes in jammed particulate packings. *Phys. Rev. E*, 93:062905.

Monaco, G. and Giordano, V. M. (2009). Breakdown of the debye approximation for the acoustic modes with nanometric wavelengths in glasses. *Proc. Natl. Acad. Sci. U.S.A*, 106(10):3659–3663.

Monaco, G. and Mossa, S. (2009). Anomalous properties of the acoustic excitations in glasses on the mesoscopic length scale. *Proc. Natl. Acad. Sci. U.S.A*, 106(40):16907–16912.

Montagna, M., Ruocco, G., Viliani, G., Dell'Anna, R., Di Leonardo, R., Dusi, R., Monaco, G., Sampoli, M., and Scopigno, T. (1999). Elastic constant inhomogeneity and the broadening of the dynamic structure factor in one-dimensional disordered systems. *Phys. Rev. Lett.*, 83:3450–3453.

Montroll, E. W. and Bendler, J. T. (1984). On lévy (or stable) distributions and the williams-watts model of dielectric relaxation. *J. Stat. Phys.*, 34(1):129–162.

Moriel, A., Kapteijns, G., Rainone, C., Zylberg, J., Lerner, E., and Bouchbinder, E. (2019). Wave attenuation in glasses: Rayleigh and generalized-rayleigh scattering scaling. *J. Chem. Phys.*, 151(10):104503.

Nabarro, F. R. N. and de Villiers, F. (1995). *Physics of Creep and Creep-Resistant Alloys*. Taylor and Francis, London.

Ngai, K. (2000). Dynamic and thermodynamic properties of glass-forming substances. *J. Non-Cryst. Solids*, 275(1):7 – 51.

Ngai, K. (2011). *Relaxation and Diffusion in Complex Systems*. Partially Ordered Systems. Springer New York.

Ngai, K. L. (1998). Relation between some secondary relaxations and the α relaxations in glass-forming materials according to the coupling model. *J. Chem. Phys.*, 109(16):6982–6994.

Nielsen, J. K. (1999). Linear response theory for thermodynamic properties. *Phys. Rev. E*, 60:471–481.

O'Hern, C. S., Silbert, L. E., Liu, A. J., and Nagel, S. R. (2003). Jamming at zero temperature and zero applied stress: The epitome of disorder. *Phys. Rev. E*, 68:011306.

Onsager, L. (1931). Reciprocal relations in irreversible processes. i. *Phys. Rev.*, 37:405–426.

Paluch, M., Ngai, K. L., and Hensel-Bielowka, S. (2001). Pressure and temperature dependences of the relaxation dynamics of cresolphthalein-dimethylether: Evidence of contributions from thermodynamics and molecular interactions. *J. Chem. Phys.*, 114(24):10872–10883.

Palyulin, V., Ness, C., Milkus, R., Elder, R., Sirk, T., and Zaccone, A. (2018). Parameter-free predictions of the viscoelastic response of glassy polymers from nonaffine lattice dynamics. *Soft Matter*, 14:8475.

Pardo, L. C., Lunkenheimer, P., and Loidl, A. (2006). Alpha and beta relaxation dynamics of a fragile plastic crystal. *J. Chem. Phys.*, 124(12):124911.

Parrinello, M. and Rahman, A. (1981). Polymorphic transitions in single crystals: A new molecular dynamics method. *J. Appl. Phys*, 52(12):7182–7190.

Plimpton, S. (1995). Fast parallel algorithms for short-range molecular dynamics. *J. Comput. Phys.*, 117(1):1 – 19.

Pérez-Madrid, A., Reguera, D., and Rubi, J. M. (2003). Origin of the violation of the fluctuation–dissipation theorem in systems with activated dynamics. *Physica A*, 329(3):357 – 364.

Qiao, J., Wang, Y.-J., Pelletier, J. M., Keer, L. M., Fine, M. E., and Yao, Y. (2015). Characteristics of stress relaxation kinetics of la60ni15al25 bulk metallic glass. *Acta Mater.*, 98:43 – 50.

Ramos, M. A., Vieira, S., Bermejo, F. J., Dawidowski, J., Fischer, H. E., Schober, H., González, M. A., Loong, C. K., and Price, D. L. (1997). Quantitative assessment of the effects of orientational and positional disorder on glassy dynamics. *Phys. Rev. Lett.*, 78:82–85.

Ray, J. R. (1983). Molecular dynamics equations of motion for systems varying in shape and size. *J. Chem. Phys.*, 79(10):5128–5130.

Ray, J. R., Moody, M. C., and Rahman, A. (1985). Molecular dynamics calculation of elastic constants for a crystalline system in equilibrium. *Phys. Rev. B*, 32:733–735.

Ray, J. R. and Rahman, A. (1984). Statistical ensembles and molecular dynamics studies of anisotropic solids. *J. Chem. Phys.*, 80(9):4423–4428.

Rufflé, B., Guimbretière, G., Courtens, E., Vacher, R., and Monaco, G. (2006). Glass-specific behavior in the damping of acousticlike vibrations. *Phys. Rev. Lett.*, 96:045502.

Ruta, B., Pineda, E., and Evenson, Z. (2017). Relaxation processes and physical aging in metallic glasses. *J. Phys. Condens. Matter*, 29(50):503002.

Rytov, S. M. (1953). *Theory of electrical fluctuations*. Academy of Sciences USSR, Moscow.

Scheidler, P., Kob, W., Latz, A., Horbach, J., and Binder, K. (2001). Frequency-dependent specific heat of viscous silica. *Phys. Rev. B*, 63:104204.

Schirmacher, W. (2015). *Theory of Liquids and Other Disordered Media*. Springer, Cham.

Schirmacher, W., Diezemann, G., and Ganter, C. (1998). Harmonic vibrational excitations in disordered solids and the "boson peak". *Phys. Rev. Lett.*, 81:136–139.

Schirmacher, W., Ruocco, G., and Mazzone, V. (2015a). Heterogeneous viscoelasticity: A combined theory of dynamic and elastic heterogeneity. *Phys. Rev. Lett.*, 115:015901.

Schirmacher, W., Ruocco, G., and Scopigno, T. (2007). Acoustic attenuation in glasses and its relation with the boson peak. *Phys. Rev. Lett.*, 98:025501.

Schirmacher, W., Scopigno, T., and Ruocco, G. (2015b). Theory of vibrational anomalies in glasses. *J. Non-Cryst. Solids*, 407:133 – 140.

Schlegel, M., Brujic, J., Terentjev, E. M., and Zaccone, A. (2016). Local structure controls the nonaffine shear and bulk moduli of disordered solids. *Sci. Rep.*, 6:18724–18724.

Schneider, U., Brand, R., Lunkenheimer, P., and Loidl, A. (2000). Excess wing in the dielectric loss of glass formers: A johari-goldstein β relaxation? *Phys. Rev. Lett.*, 84:5560–5563.

Schönhals, A., Kremer, F., and Stickel, F. (1993). Schönhals, kremer, and stickel reply. *Phys. Rev. Lett.*, 71:4096–4096.

Schwartzman-Nowik, Z., Lerner, E., and Bouchbinder, E. (2019). Anisotropic structural predictor in glassy materials. *Phys. Rev. E*, 99:060601.

Seifert, U. and Speck, T. (2010). Fluctuation-dissipation theorem in nonequilibrium steady states. *Europhys. Lett.*, 89(1):10007.

Senguly, S. and Sengupta, S. (2017). Excess vibrational modes of a crystal in an external non-affine field. *J. Chem. Sci.*, 129:891.

Sharapova, I. V., Krivchikov, A. I., Korolyuk, O. A., Jezowski, A., Rovira-Esteva, M., Tamarit, J. L., Pardo, L. C., Ruiz-Martin, M. D., and Bermejo, F. J. (2010). Disorder effects on heat transport properties of orientationally disordered crystals. *Phys. Rev. B*, 81:094205.

Sheng, H., Cheng, Y., Lee, P., Shastri, S., and Ma, E. (2008). Atomic packing in multicomponent aluminum-based metallic glasses. *Acta Mater.*, 56(20):6264 – 6272.

Shimada, M., Mizuno, H., and Ikeda, A. (2020). Vibrational spectrum derived from local mechanical response in disordered solids. *Soft Matter*, 16:7279–7288.

Shintani, H. and Tanaka, H. (2008). Universal link between the boson peak and transverse phonons in glass. *Nature Mater.*, 7(11):870–877.

Sjogren, L. and Sjolander, A. (1979). Kinetic theory of self-motion in monatomic liquids. *J. Phys. C: Solid State Phys.*, 12(21):4369.

Spaepen, F. and Turnbull, D. (1984). Metallic glasses. *Annu. Rev. Phys. Chem.*, 35(1):241–263.

Stillinger, F. H. (1988). Supercooled liquids, glass transitions, and the kauzmann paradox. *J. Chem. Phys.*, 88(12):7818–7825.

Strutt, J. W. (1871). Xv. on the light from the sky, its polarization and colour. *The London, Edinburgh, and Dublin Philosophical Magazine and Journal of Science*, 41(271):107–120.

Suga, H. and Seki, S. (1974). Thermodynamic investigation on glassy states of pure simple compounds. *J. Non-Cryst. Solids*, 16(2):171 – 194.

Sutter, J. P. and Yavas, H. (2017). Material properties of α-quartz that are relevant for its potential use in x-ray monochromators and analyzers. *arXiv:1612.07049*.

Sutton, A. P. and Chen, J. (1990). Long-range finnis–sinclair potentials. *Philos. Mag. Lett.*, 61(3):139–146.

Tadmor, E. and Miller, R. (2011). *Modeling materials: Continuum, atomistic and multiscale techniques*, volume 9780521856980. Cambridge University Press.

Tamarit, J. L., Pérez-Jubindo, M. A., and de la Fuente, M. R. (1997). Dielectric studies on orientationally disordered phases of neopentylglycol (andtris(hydroxymethyl aminomethane). *J. Phys. Condens. Matter*, 9(25):5469–5478.

Tielbürger, D., Merz, R., Ehrenfels, R., and Hunklinger, S. (1992). Thermally activated relaxation processes in vitreous silica: An investigation by brillouin scattering at high pressures. *Phys. Rev. B*, 45:2750–2760.

Toukmaji, A. Y. and Board, J. A. (1996). Ewald summation techniques in perspective: a survey. *Comput. Phys. Comm.*, 95:73.

Trinkle, D. R. (2008). Lattice green function for extended defect calculations: Computation and error estimation with long-range forces. *Phys. Rev. B*, 78:014110.

van Beest, B. W. H., Kramer, G. J., and van Santen, R. A. (1990). Force fields for silicas and aluminophosphates based on ab initio calculations. *Phys. Rev. Lett.*, 64:1955.

Van Hove, L. (1954). Correlations in space and time and born approximation scattering in systems of interacting particles. *Phys. Rev.*, 95:249–262.

Vdovichenko, G. A., Krivchikov, A. I., Korolyuk, O. A., Tamarit, J. L., Pardo, L. C., Rovira-Esteva, M., Bermejo, F. J., Hassaine, M., and Ramos, M. A. (2015). Thermal properties of halogen-ethane glassy crystals: Effects of orientational disorder and the role of internal molecular degrees of freedom. *J. Chem. Phys.*, 143(8):084510.

Vispa, A., Romanini, M., Ramos, M. A., Pardo, L. C., Bermejo, F. J., Hassaine, M., Krivchikov, A. I., Taylor, J. W., and Tamarit, J. L. (2017). Thermodynamic and kinetic fragility of freon 113: The most fragile plastic crystal. *Phys. Rev. Lett.*, 118:105701.

Wallace, D. C. (1970). Thermoelastic theory of stressed crystals and higher-order elastic constants. volume 25 of *Solid State Physics*, pages 301 – 404. Academic Press.

Wang, J., Mao, Z., Jiang, F., and Duffy, T. S. (2015a). Elasticity of single-crystal quartz to 10 GPa. *Phys. Chem. Min.*, 42:203.

Wang, L., Berthier, L., Flenner, E., Guan, P., and Szamel, G. (2019). Sound attenuation in stable glasses. *Soft Matter*, 15:7018–7025.

Wang, X. D., Ruta, B., Xiong, L., Zhang, D., Chushkin, Y., Sheng, H., Lou, H., Cao, Q., and Jiang, J. (2015b). Free-volume dependent atomic dynamics in beta relaxation pronounced la-based metallic glasses. *Acta Mater.*, 99:290 – 296.

Wang, Y., Wang, Y., and Zhang, J. (2020). Connecting shear localization with the long-range correlated polarized stress fields in granular materials. *Nat. Commun.*, 11(1):4349.

Wang, Z., Sun, B. A., Bai, H. Y., and Wang, W. H. (2014). Evolution of hidden localized flow during glass-to-liquid transition in metallic glass. *Nat. Commun.*, 5:5823.

Weiss, U. (2012). *Quantum Dissipative Systems*. World Scientific, Singapore.

Widmer-Cooper, A., Perry, H., Harrowell, P., and Reichman, D. R. (2008). Irreversible reorganization in a supercooled liquid originates from localized soft modes. *Nat. Phys.*, 4:711.

Wiedersich, J., Blochowicz, T., Benkhof, S., Kudlik, A., Surovtsev, N. V., Tschirwitz, C., Novikov, V. N., and Rössler, E. (1999). Fast and slow relaxation processes in glasses. *J. Phys. Condens. Matter*, 11(10A):A147–A156.

Will, G., Bellotto, M., Parrish, W., and Hart, M. (1988). Crystal structures of quartz and magnesium germanate by profile analysis of synchroton-radiation high resolution power data. *J. Appl. Cryst.*, 21:182.

Williams, G. and Watts, D. C. (1970). Non-symmetrical dielectric relaxation behaviour arising from a simple empirical decay function. *Trans. Faraday Soc.*, 66:80–85.

Wittmer, J., Xu, H., Benzerara, O., and Baschnagel, J. (2015). Fluctuation-dissipation relation between shear stress relaxation modulus and shear stress autocorrelation function revisited. *Molecular Physics*, 113(17-18):2881–2893.

Wittmer, J. P., Xu, H., Polińska, P., Gillig, C., Helfferich, J., Weysser, F., and Baschnagel, J. (2013). Compressibility and pressure correlations in isotropic solids and fluids. *Eur. Phys. J. E*, 36(11):131.

Wolf, D., Keblinski, P., Phillpot, S. R., and Eggebrecht, J. (1999). Exact method for the simulation of coulombic systems by spherically truncated, pairwise r-1 summation. *J. Chem. Phys.*, 110:8254.

Wolfgardt, M., Baschnagel, J., Paul, W., and Binder, K. (1996). Entropy of glassy polymer melts: Comparison between gibbs-dimarzio theory and simulation. *Phys. Rev. E*, 54:1535–1543.

Wuttke, J. (2013). Frida data analysis. http://sourceforge.net/projects/frida/.

Wuttke, J., Kiebel, M., Bartsch, E., Fujara, F., Petry, W., and Sillescu, H. (1993). Relaxation and phonons in viscous and glassy orthoterphenyl by neutron scattering. *Z. Phys. B*, 91(3):357–365.

Wyart, M. (2010). Scaling of phononic transport with connectivity in amorphous solids. *EPL (Europhysics Letters)*, 89(6):64001.

Wyckoff, R. W. G. (1963). *Crystal Structures*, volume 1. John Wiley & Sons, New York.

Yoshino, H. (2012). Replica theory of the rigidity of structural glasses. *J. Chem. Phys.*, 136(21):214108.

Yoshino, H. and Mézard, M. (2010). Emergence of rigidity at the structural glass transition: A first-principles computation. *Phys. Rev. Lett.*, 105:015504.

Yoshino, H. and Zamponi, F. (2014). Shear modulus of glasses: Results from the full replica-symmetry-breaking solution. *Phys. Rev. E*, 90:022302.

Yu, H. B., Richert, R., and Samwer, K. (2017). Structural rearrangements governing johari-goldstein relaxations in metallic glasses. *Sci. Adv.*, 3(11).

Yu, H. B., Wang, W. H., Bai, H. Y., and Samwer, K. (2014). The β-relaxation in metallic glasses. *Natl. Sci. Rev.*, 1(3):429–461.

Zaccone, A. (2020). Relaxation and vibrational properties in metal alloys and other disordered systems. *Journal of Physics: Condensed Matter*, 32(20):203001.

Zaccone, A. and Del Gado, E. (2010). On mean coordination and structural heterogeneity in model amorphous solids. *J. Chem. Phys.*, 132(2):024906.

Zaccone, A. and Scossa-Romano, E. (2011). Approximate analytical description of the nonaffine response of amorphous solids. *Phys. Rev. B*, 83:184205.

Zaccone, A. and Terentjev, E. M. (2013). Disorder-assisted melting and the glass transition in amorphous solids. *Phys. Rev. Lett.*, 110:178002.

Zaccone, A. and Terentjev, E. M. (2014). Short-range correlations control the g/k and poisson ratios of amorphous solids and metallic glasses. *J. Appl. Phys.*, 115(3):033510.

Zhai, C., Herbold, E., and Hurley, R. (2020). The influence of packing structure and interparticle forces on ultrasound transmission in granular media. *Proc. Natl. Acad. Sci. U.S.A.*

Zhu, Z. G., Li, Y. Z., Wang, Z., Gao, X. Q., Wen, P., Bai, H. Y., Ngai, K. L., and Wang, W. H. (2014). Compositional origin of unusual β-relaxation properties in la-ni-al metallic glasses. *J. Chem. Phys.*, 141(8):084506.

Zwanzig, R. (1973). Nonlinear generalized langevin equations. *J. Stat. Phys.*, 9(3):215–220.

Zwanzig, R. (2002). *Nonequilibrium Statistical Mechanics*. Oxford University Press, Oxford.

Appendix A

Binary metallic glasses with the EAM potential

It would be more convenient to work in unrescaled coordinates firstly and the results would be manifest via $\partial f(X)/\partial X = (\partial f(X(x))/\partial x)(dx/dX)$ for functions f and X depending on x only. Thus, in this section, I write R_I as unscaled tagged-particle positions. In order to calculate the dynamics and the viscoelastic response, I need to evaluate the interaction energy between atoms in the material. In particular, I need to find expressions for the Hessian matrix and for the affine force field $\Xi^{\mu}_{I,\kappa\chi}$, as a function of the interatomic interaction potential, given under the EAM. Upon considering the various contributions to the interaction potential between atoms in the CuZr- based MGs, the total potential energy acting on a tagged atom I is given by

$$\mathscr{U}_I = F_A\left(\sum_{J\neq I}\rho_{AB}(R_{IJ})\right) + \frac{1}{2}\sum_{J\neq I}\psi_{AB}(R_{IJ}). \tag{A.1}$$

Recall R_{IJ} represents the radial distance between I and J, ρ_{AB} is the contribution to the electronic charge density from particle J of type B at the location of particle I of type A; ψ_{AB} is a pairwise potential between an atom of type A and an atom of type B, and F_A is the embedding function that gives the energy required to place the tagged particle I of type A into the electron cloud. Hence, the total potential is the sum over all particles, $\mathscr{U} = \sum_I \mathscr{U}_I$.

The many-body nature of the EAM potential is a result of the embedding energy term. Both summations in the formula are over all neighbors J of particle I within the cutoff distance (Sutton and Chen, 1990). Then I can get the net force acting on a tagged atom using

the following set of relations:

$$\mathbf{n}_{IJ} = \frac{\mathbf{R}_{IJ}}{R_{IJ}}; \quad \bar{\rho}_I = \sum_{J \neq I} \rho_{AB}(R_{IJ}) \tag{A.2}$$

$$Z_{IJ} = \frac{\partial \mathscr{U}_I}{\partial R_{IJ}} = \frac{1}{2}\frac{\partial \psi_{AB}(R_{IJ})}{\partial R_{IJ}} + \frac{\partial F_A}{\partial \bar{\rho}_I}\frac{\partial \rho_{AB}(R_{IJ})}{\partial R_{IJ}} \tag{A.3}$$

$$\begin{aligned}
\mathbf{f}_I &= -\frac{\partial \mathscr{U}}{\partial \mathbf{R}_I} = -\frac{\partial \mathscr{U}_I}{\partial \mathbf{R}_I} - \frac{\partial \sum_{K \neq I} \mathscr{U}_K}{\partial \mathbf{R}_I} \\
&= -\frac{\partial \mathscr{U}_I}{\partial \mathbf{R}_I} - \frac{\partial \sum_{K \neq I} \mathscr{U}_K}{\partial R_{JK}}\frac{\partial R_{IK}}{\partial \mathbf{R}_I} \\
&= -\frac{\partial \mathscr{U}_I}{\partial \mathbf{R}_I} + \frac{\partial \sum_{K \neq I} \mathscr{U}_K}{\partial R_{JK}}\frac{\mathbf{R}_{IK}}{R_{IK}} \\
&= -\frac{\partial \mathscr{U}_I}{\partial \mathbf{R}_I} + \sum_{K \neq I} Z_{KI}\frac{\mathbf{R}_{IK}}{R_{IK}}.
\end{aligned} \tag{A.4}$$

The Hessian is then written for $I \neq J$ as:

$$\begin{aligned}
\underline{\underline{H}}_{IJ}|_{I \neq J} &= \frac{\partial^2 \mathscr{U}}{\partial \mathbf{R}_I \mathbf{R}_J} = \frac{\partial \frac{\partial \mathscr{U}_I}{\partial \mathbf{R}_I}}{\partial \mathbf{R}_J} - \frac{\partial \sum_{K \neq I} Z_{KI}\frac{\mathbf{R}_{IK}}{R_{IK}}}{\partial \mathbf{R}_J} \\
&= \frac{\partial^2 \mathscr{U}_I}{\partial \mathbf{R}_I \partial \mathbf{R}_J} - \frac{\partial Z_{JI}}{\partial \mathbf{R}_J}\frac{\mathbf{R}_{JI}}{R_{JI}} - Z_{JI}\frac{\partial \frac{\mathbf{R}_{IJ}}{R_{IJ}}}{\partial \mathbf{R}_J} - \frac{\partial \sum_{K \neq I, K \neq J} Z_{KJ}\frac{\mathbf{R}_{IK}}{R_{IK}}}{\partial \mathbf{R}_J} \\
&= \frac{\partial^2 \mathscr{U}_I}{\partial \mathbf{R}_I \partial \mathbf{R}_J} - \frac{\partial Z_{JI}}{\partial R_{IJ}}\frac{\partial R_{IJ}}{\partial \mathbf{R}_J} \otimes \frac{\mathbf{R}_{IJ}}{R_{IJ}} - Z_{JI}\frac{\partial \frac{\mathbf{R}_{IJ}}{R_{IJ}}}{\mathbf{R}_J} - \sum_{K \neq I, K \neq J} \frac{\partial Z_{KI}}{\partial \mathbf{R}_J} \otimes \frac{\mathbf{R}_{IK}}{R_{IK}}
\end{aligned} \tag{A.5}$$

with $d = 3$:

$$\frac{\partial \frac{\mathbf{R}_{IJ}}{R_{IJ}}}{\partial \mathbf{R}_J} = \frac{I_{3\times 3}}{R_{IJ}} - \frac{\mathbf{R}_{IJ} \otimes \mathbf{R}_{IJ}}{R_{IJ}^3}, \tag{A.6}$$

and:

$$\begin{aligned}
\mathbf{H}_{II} &= \frac{\partial^2 \mathscr{U}}{\partial \mathbf{R}_I \mathbf{R}_I} = \frac{\partial^2 \mathscr{U}_I}{\partial \mathbf{R}_I^2} - \frac{\partial \sum_{K \neq I} Z_{KI}}{\partial \mathbf{R}_J}\frac{\mathbf{R}_{IK}}{R_{IK}} - \sum_{K \neq I} Z_{KI}\frac{\partial \frac{\mathbf{R}_{IK}}{R_{IK}}}{\partial \mathbf{R}_I} \\
&= \frac{\partial^2 \mathscr{U}_I}{\partial \mathbf{R}_I^2} + \frac{\partial \sum_{K \neq I} Z_{JI}}{\partial \mathbf{R}_J}\frac{\mathbf{R}_{IK}}{R_{IK}} \otimes \frac{\mathbf{R}_{IK}}{R_{IK}} - \sum_{K \neq I} Z_{KI}\frac{\partial \frac{\mathbf{R}_{IK}}{R_{IK}}}{\partial \mathbf{R}_I} \\
&= \frac{\partial^2 \mathscr{U}_I}{\partial \mathbf{R}_I^2} + \frac{\partial \sum_{K \neq I} Z_{JI}}{\partial \mathbf{R}_J}\frac{\mathbf{R}_{IK}}{R_{IK}} \otimes \frac{\mathbf{R}_{IK}}{R_{IK}} + \sum_{K \neq I} Z_{KI}\left(\frac{I_{3\times 3}}{R_{IK}} - \frac{\mathbf{R}_{IK} \otimes \mathbf{R}_{IK}}{R_{IK}^3}\right)
\end{aligned} \tag{A.7}$$

for the diagonal $I = J$ elements. To find $\boldsymbol{\Xi}_{I,\kappa\chi} = \sum_J \boldsymbol{\Xi}_{IJ,\kappa\chi}$, I write

$$\Xi^{\mu}_{IJ,\kappa\chi} = -S_{IJ,\mu\nu}\frac{\partial R^{\nu}_{IJ}}{\partial \eta_{\kappa\chi}} = -\frac{1}{2}S_{IJ,\mu\nu}(\delta_{\nu\kappa}R^{\chi}_{IJ} + \delta_{\nu\chi}R^{\kappa}_{IJ}) \tag{A.8}$$

with:

$$\begin{aligned}
\underline{\underline{S}}_{IJ} &= \frac{\partial^2 \mathscr{U}_I}{\partial \mathbf{R}_{IJ}\partial \mathbf{R}_{IJ}} = \frac{\partial}{\partial \mathbf{R}_{IJ}}\left(\frac{\partial \mathscr{U}}{\partial \mathbf{R}_{IJ}}\right) = \frac{\partial}{\partial \mathbf{R}_{IJ}}\left(\sum_K \frac{\partial \mathscr{U}_K}{\partial \mathbf{R}_{IJ}}\right) \\
&= \frac{\partial}{\partial \mathbf{R}_{IJ}}\left(\sum_{K,L\neq K}\frac{\partial \mathscr{U}_K}{\partial R_{LK}}\frac{\partial R_{LK}}{\partial \mathbf{R}_{IJ}}\right) \\
&= \frac{\partial}{\partial \mathbf{R}_{IJ}}\left(\frac{\partial \mathscr{U}_I}{\partial R_{JI}}\frac{\partial R_{JI}}{\partial \mathbf{R}_{JI}} + \frac{\partial \mathscr{U}_J}{\partial R_{JI}}\frac{\partial R_{JI}}{\partial \mathbf{R}_{JI}}\right)\frac{\partial \mathscr{U}_I}{\partial R_{JI}}\frac{\partial R_{JI}}{\partial \mathbf{R}_{JI}} \\
&= \frac{\partial}{\partial \mathbf{R}_{IJ}}\left(Z_{IJ}\frac{\mathbf{R}_{IJ}}{R_{IJ}} + Z_{JI}\frac{\mathbf{R}_{IJ}}{R_{IJ}}\right) \\
&= \frac{\partial}{\partial \mathbf{R}_{IJ}}(Z_{IJ}\mathbf{n}_{IJ} + Z_{JI}\mathbf{n}_{IJ}) \\
&= \frac{\partial Z_{IJ}}{\partial \mathbf{R}_{IJ}}\mathbf{n}_{IJ} + Z_{IJ}\frac{\partial \mathbf{n}_{IJ}}{\partial \mathbf{R}_{IJ}} + \frac{\partial Z_{JI}}{\partial \mathbf{R}_{IJ}}\mathbf{n}_{IJ} + Z_{JI}\frac{\partial \mathbf{n}_{IJ}}{\partial \mathbf{R}_{JI}} \\
&= \frac{\partial}{\partial \mathbf{R}_{IJ}}\left(\frac{\partial \mathscr{U}_I}{\partial \mathbf{R}_{IJ}}\right)\mathbf{n}_{IJ} + Z_{IJ}\frac{\partial}{\partial \mathbf{R}_{IJ}}\left(\frac{\mathbf{R}_{IJ}}{R_{IJ}}\right) \\
&+ \frac{\partial}{\partial \mathbf{R}_{IJ}}\left(\frac{\partial \mathscr{U}_J}{\partial \mathbf{R}_{IJ}}\right)\mathbf{n}_{IJ} + Z_{JI}\frac{\partial}{\partial \mathbf{R}_{IJ}}\left(\frac{\mathbf{R}_{IJ}}{R_{IJ}}\right) \\
&= \sum_K \frac{\partial\left(\frac{\partial \mathscr{U}_I}{\partial R_{IJ}}\right)}{\partial R_{IK}}\frac{\partial R_{IK}}{\partial \mathbf{R}_{IJ}}\mathbf{n}_{IJ} + Z_{IJ}\frac{R_{IJ} - \mathbf{R}_{IJ}\frac{\partial R_{IJ}}{\partial \mathbf{R}_{IJ}}}{R^2_{IJ}} \\
&+ \sum_K \frac{\partial\left(\frac{\partial \mathscr{U}_J}{\partial R_{IJ}}\right)}{\partial R_{JK}}\frac{\partial R_{JK}}{\partial \mathbf{R}_{IJ}}\mathbf{n}_{IJ} + Z_{JI}\frac{R_{IJ} - \mathbf{R}_{IJ}\frac{\partial R_{IJ}}{\partial \mathbf{R}_{IJ}}}{R^2_{IJ}} \\
&= \frac{\partial^2 \mathscr{U}_I}{\partial^2 R_{IJ}}\mathbf{n}_{IJ}\mathbf{n}_{IJ} + Z_{IJ}\frac{(1 - \mathbf{n}_{IJ}\mathbf{n}_{IJ})}{R_{IJ}} + \frac{\partial^2 \mathscr{U}_J}{\partial^2 R_{IJ}}\mathbf{n}_{IJ}\mathbf{n}_{IJ} \\
&+ Z_{JI}\frac{(1 - \mathbf{n}_{IJ}\mathbf{n}_{IJ})}{R_{IJ}}.
\end{aligned} \tag{A.9}$$

To distinguish **S** from **H**, one can rewrite $\mathbf{H}(I \neq J)$ as

$$
\begin{aligned}
\mathbf{H}_{IJ} &= \frac{\partial^2 \mathscr{U}}{\partial \mathbf{R}_I \partial \mathbf{R}_J} = \frac{\partial}{\partial \mathbf{R}_I}\left(\sum_K \frac{\partial \mathscr{U}_K}{\partial \mathbf{R}_J}\right) = \frac{\partial}{\partial \mathbf{R}_I}\left(\sum_{K,L\neq K} \frac{\partial \mathscr{U}_K}{\partial R_{KL}}\frac{\partial R_{KL}}{\partial \mathbf{R}_J}\right) \\
&= \frac{\partial}{\partial \mathbf{R}_I}\left(\sum_{L\neq J} \frac{\partial \mathscr{U}_J}{\partial R_{JL}}\frac{\partial R_{JL}}{\partial \mathbf{R}_J} + \sum_{K\neq J, L\neq K} \frac{\partial \mathscr{U}_K}{\partial R_{KL}}\frac{\partial R_{KL}}{\partial \mathbf{q}_j}\right) \\
&= \frac{\partial}{\partial \mathbf{R}_I}\left(\sum_{L\neq J} \frac{\partial \mathscr{U}_J}{\partial R_{JL}}\frac{\partial R_{JL}}{\partial \mathbf{R}_J} + \sum_{K\neq J} \frac{\partial \mathscr{U}_K}{\partial R_{KJ}}\frac{\partial R_{KJ}}{\partial \mathbf{R}_J}\right) \\
&= \frac{\partial}{\partial \mathbf{R}_I}\left(\sum_{L\neq J} \frac{\partial \mathscr{U}_J}{\partial R_{JL}}\frac{\mathbf{R}_{JL}}{\partial R_{JL}} + \sum_{K\neq J} \frac{\partial \mathscr{U}_K}{\partial R_{KJ}}\frac{\mathbf{R}_{JK}}{\partial R_{JK}}\right) \\
&= \sum_{K\neq J} \frac{\partial}{\partial \mathbf{R}_I}\left(\frac{\partial \mathscr{U}_J}{\partial R_{JK}}\frac{\mathbf{R}_{JK}}{R_{JK}} + \frac{\partial \mathscr{U}_K}{\partial R_{KJ}}\frac{\mathbf{R}_{JK}}{R_{JK}}\right) \\
&= \sum_{K\neq J}\left(\sum_{L\neq J} \frac{\partial}{\partial R_{JL}}\left(\frac{\partial \mathscr{U}_J}{\partial R_{JK}}\right)\frac{\partial R_{JL}}{\partial \mathbf{R}_I}\frac{\mathbf{R}_{JK}}{R_{JK}}\right) + \frac{\partial \mathscr{U}_J}{\partial R_{JI}}\frac{\partial}{\partial \mathbf{R}_I}\left(\frac{\mathbf{R}_{JI}}{R_{JI}}\right) \\
&+ \sum_{K\neq J}\left(\sum_{L\neq J} \frac{\partial}{\partial R_{KL}}\left(\frac{\partial \mathscr{U}_K}{\partial R_{JK}}\right)\frac{\partial R_{KL}}{\partial \mathbf{R}_I}\frac{\mathbf{R}_{JK}}{R_{JK}}\right) + \frac{\partial \mathscr{U}_I}{\partial R_{JI}}\frac{\partial}{\partial \mathbf{R}_I}\left(\frac{\mathbf{R}_{JI}}{R_{JI}}\right) \\
&= \sum_{K\neq J}\left(\frac{\partial}{\partial R_{JI}}\left(\frac{\partial \mathscr{U}_J}{\partial R_{JK}}\right)\frac{\partial R_{JI}}{\partial \mathbf{R}_I}\frac{\mathbf{R}_{JK}}{R_{JK}}\right) + Z_{JI}\frac{(-1+\mathbf{n}_{IJ}\mathbf{n}_{IJ})}{R_{IJ}} \\
&+ \sum_{K\neq J}\left(\sum_{L\neq K} \frac{\partial}{\partial R_{KL}}\left(\frac{\partial \mathscr{U}_K}{\partial R_{KJ}}\right)\frac{\partial R_{KL}}{\partial \mathbf{R}_I}\frac{\mathbf{R}_{JK}}{R_{JK}}\right) + Z_{IJ}\frac{(-1+\mathbf{n}_{IJ}\mathbf{n}_{IJ})}{R_{IJ}} \\
&= \sum_{K\neq J}\left(\frac{\partial}{\partial R_{JI}}\left(\frac{\partial \mathscr{U}_J}{\partial R_{JK}}\right)\mathbf{n}_{IJ}\mathbf{n}_{JK}\right) + Z_{JI}\frac{(-1+\mathbf{n}_{IJ}\mathbf{n}_{IJ})}{R_{IJ}} \\
&+ \sum_{K\neq J,I} \frac{\partial}{\partial q_{KI}}\left(\frac{\partial \mathscr{U}_K}{\partial R_{KJ}}\right)\mathbf{n}_{IK}\mathbf{n}_{JK} + \sum_{K\neq I} \frac{\partial^2 \mathscr{U}_I}{\partial R_{IK}\partial R_{IJ}}\mathbf{n}_{IK}\mathbf{n}_{JI} \\
&+ Z_{IJ}\frac{(-1+\mathbf{n}_{IJ}\mathbf{n}_{IJ})}{R_{IJ}}.
\end{aligned}
\tag{A.10}
$$

Appendix B

From particle-particle to particle-bath oscillator interactions

Performing Taylor expansion up to the 2nd order around the minimum surface $\mathbf{R}_I^\circ$, the Hamiltonian can be written as

$$\mathscr{H} = \sum_I^N \sum_\mu^d \frac{(M_I \dot{s}_I^\mu)^2}{2} + \mathscr{U}(\mathbf{R}_I^\circ) + \frac{1}{2} \sum_{IJ}^N \sum_{\mu,\nu}^d s_I^\mu s_J^\nu \left[\frac{\partial^2 \mathscr{U}(\mathbf{R}_I)}{\partial R_I^\mu \partial R_J^\nu} \right]_{\mathbf{R}_I^\circ}. \tag{B.1}$$

The full solution of the displacement of particle I can be written as

$$\mathbf{s}_I(t) = \sum_m^{Nd} \frac{\mathbf{e}_I^m}{\sqrt{M_I}} (A_m e^{-i\omega_m t} + B_m e^{i\omega_m t}), \tag{B.2}$$

where $\mathbf{e}_I^m$ is the elements of I-th particle in eigenvector of the dynamical matrix corresponding to the m-th mode and A_m, B_m are coefficients subject to initial conditions. I can write the expression more generally:

$$\mathbf{s}_I(t) = \sum_m^{Nd} \frac{1}{\sqrt{M_I}} \boldsymbol{\varepsilon}_I^m Q_m(t). \tag{B.3}$$

The $\boldsymbol{\varepsilon}_I^m$ are distinguished from $\mathbf{e}_I^m$ only in normalisation. For particle I, from mechanical equilibrium position $\mathbf{R}_I = \mathbf{R}_I^\circ$, its position is $r_I^\mu(t) = R_I^\mu + s_I^\mu(t)$. Substituting this back to Eq. (B.1), I have

$$\mathscr{H} = \frac{1}{2} \sum_m^{Nd} \left| \dot{Q}_m \right|^2 + \frac{1}{2} \sum_m^{Nd} \omega_m^2 \left| Q_m \right|^2 + \mathscr{U}(\mathbf{R}_I), \tag{B.4}$$

where the first two terms on the RHS are kinetic and potential energies in terms of canonical coordinates $Q_m(t)$, respectively. I can also define the canonical momenta as $P_m =$

$\partial\mathscr{H}/\partial Q_m = \dot{Q}_m$. Clearly, there are Nd independent harmonic oscillators.
Next consider the Hamiltonian including one tagged particle (position R_0^μ, mass M_0):

$$\mathscr{H}' = \sum_\mu \frac{M_0(\dot{s}_0^\mu)^2}{2} + \mathscr{U}(\mathbf{R}_0) + \frac{1}{2}\sum_m^{Nd} |\dot{Q}_m|^2 + \frac{1}{2}\sum_m^{Nd} \omega_m^2 |Q_m|^2 + \mathscr{U}(\mathbf{R}_I^\circ) + \mathscr{U}(\mathbf{R}_0, \mathbf{R}_I). \quad \text{(B.5)}$$

The last term is the potential due to interaction between the tagged particle and remaining oscillators. I assume the linear coupling, which is $\mathscr{U}(\mathbf{R}_0^\mu, \mathbf{R}_I) = \mathscr{U}(\mathbf{R}_0^\mu, Q_m) = \sum_m c_m R_0^\mu Q_m$ where c_m reflects the coupling strength between the tagged particle and m-th oscillator, which are different.

In oscillatory electric field, there is an additional electric potential contributing to Hamiltonian,

$$\begin{aligned}
\mathscr{H}_E &= -\sum_{I\mu} z_I E^\mu(t)(R_I^\mu + s_I^\mu(t)) \\
&= -\sum_{I\mu} z_I E^\mu(t) R_I^\mu - \sum_{I\mu m} \frac{z_I E^\mu(t)}{\sqrt{M_I}} Q_m(t)(\varepsilon_I^\mu)^m \\
&= -\sum_{I\mu} z_I E^\mu(t) R_I^\mu - \sum_m \left(\sum_{I\mu} \frac{z_I E^\mu(t)}{\sqrt{M_I}} (\varepsilon_I^\mu)^m \right) Q_m(t),
\end{aligned} \quad \text{(B.6)}$$

where z_I label the charge. The first term depending on $\mathbf{R}_I$ can be absorbed into $\mathscr{U}(\mathbf{R}_I)$ and one could repeat above steps to obtain the Hamiltonian of harmonic oscillators in external dielectric field. Let the electric field be along one direction (say x). From Eq (B.6), it is clear that the "charge" is carried by each oscillator, which is $\sum_I z_I(\varepsilon_I^x)^m/\sqrt{M_I}$.

Appendix C

Time-frequency conversion and derivation of Eqs. (5.1)- (5.2)

I present the conversion from viscoelastic response in the time-domain (in which experimental data have been taken) to viscoelastic response in the frequency domain. The converted data have been used for comparison with the theoretical predictions in the main text.

The stress response to a strain $\eta(t)$ in the time domain is given by the Boltzmann causality principle as

$$\sigma(t) = \int_{-\infty}^{t} C(t-t')\dot{\eta}(t')dt' \tag{C.1}$$

where $C(t)$ is the time-dependent elastic modulus and $\dot{\eta}$ is the strain rate. I take the Fourier transform of Eq. (C.1):

$$\begin{aligned}\tilde{\sigma}(\omega) &= \int_{-\infty}^{\infty}\int_{-\infty}^{\infty} C(t-t')H(t-t')\dot{\eta}(t)e^{-i\omega t}dt'dt \\ &= \int_{-\infty}^{\infty} C(u)H(u)e^{-i\omega u}du \int_{-\infty}^{\infty}\dot{\eta}(t')e^{-i\omega t}dt\end{aligned} \tag{C.2}$$

where $u = t - t'$. Note that, the domain of $\sigma(t)$ is generally the whole real line, while the domain of $C(t)$ is defined only for $t > 0$. If the Fourier transform exists, then we can denote it by $\tilde{\sigma}(\omega)$, which is given by

$$\tilde{\sigma}(\omega) = \mathscr{F}[C(t)]\mathscr{F}[\dot{\eta}(t)] = \tilde{C}(\omega)\tilde{\eta}(\omega). \tag{C.3}$$

Note that the second equation is the usual expression of linear stress-strain relation in the frequency domain (Lemaitre and Maloney, 2006).

In the stress-relaxation experiments, one starts by applying to the (initially relaxed) sample a sudden deformation η_0:

$$\eta(t<0)=0; \qquad \eta(t>0)=\eta_0=const. \tag{C.4}$$

"Sudden" means that the deformation is applied over a time much shorter than the shortest time-scale of the Maxwell distribution τ_{min}, and can thus be modelled as a Heaviside step function. Under these conditions, I can write

$$\dot{\eta}_0(t)=\eta_0\delta(t). \tag{C.5}$$

From Eq.(C.1) and Eq.(C.5), I have:

$$\sigma(t)=\int_{-\infty}^{t}\eta_0 C(t-t')\delta(t')dt', \tag{C.6}$$

$$\Rightarrow \quad \sigma(t<0)=0; \qquad \sigma(t>0)=\eta_0 C(t). \tag{C.7}$$

The experimental data in the time-domain might be fitted with the Kohlrausch empirical function in order to obtain a smooth function for the Fourier transformation. Also, this allows us to enucleate the α-relaxation from the data. I therefore take the Fourier transform of the empirical Kohlrausch function $\sigma(t)=\sigma_\infty+\sigma_0 e^{-(t/\tau)^\beta}$ used for the fitting of the experimental data:

$$\int_0^\infty[\sigma_\infty+\sigma_0 e^{-(t/\tau)^\beta}]e^{-i\omega t}dt=\tilde{C}(\omega)\int_0^\infty\eta_0 e^{-i\omega t}dt. \tag{C.8}$$

Upon rearranging terms, I thus obtain:

$$\frac{\sigma_\infty}{\sigma_0}+i\omega\int_0^\infty e^{-(t/\tau)^\beta}(\cos\omega t-i\sin\omega t)dt=\tilde{C}(\omega)\frac{\eta_0}{\sigma_0}. \tag{C.9}$$

This simplifies to the real and imaginary part of $\tilde{C}(\omega)=C'(\omega)+iC''(\omega)$, which corresponds to Eq. (5.1) and Eq. (5.2), respectively.

Appendix D

The long-range autocorrelation of the stress tensor

Here I assume $C^{\mu\nu\kappa\chi}$ has no fluctuations, while fluctuations exist in the internal stress, a situation encountered in glasses (Maier et al., 2018). Writing $p_{IJ} = -(1/2)V'_{IJ}(r_{IJ})r_{IJ}$, the local stress tensor can be decomposed at the pair level as:

$$\begin{aligned}
\sigma^1_{IJ} &= p_{IJ}, \\
\sigma^2_{IJ} &= -p_{IJ}\cos(2\theta_{IJ}), \\
\sigma^3_{IJ} &= -p_{IJ}\sin(2\theta_{IJ}).
\end{aligned} \tag{D.1}$$

In this representation, σ^1_{IJ} is the pair-level pressure, while σ^2_{IJ} and $\sigma^3_{IJ} = \sigma^{xy}_{IJ}$ represent two shear stresses. I am able to express effective elastic constants $S^{\mu\nu\kappa\chi}$ in this new representation.

Given $\sigma^1, \sigma^2, \sigma^3$, I obtain

$$
\begin{aligned}
S^{xxxx}(\mathbf{r}) &= C^{xxxx} + \sigma^2(\mathbf{r}) - \sigma^1(\mathbf{r}) \\
S^{xxxy}(\mathbf{r}) &= C^{xxxy} + \sigma^3(\mathbf{r}) \\
S^{xxyx}(\mathbf{r}) &= C^{xxyx} \\
S^{xxyy}(\mathbf{r}) &= C^{xxyy} \\
S^{xyxx}(\mathbf{r}) &= C^{xyxx} + \sigma^3(\mathbf{r}) \\
S^{xyxy}(\mathbf{r}) &= C^{xyxy} - \sigma^1(\mathbf{r}) - \sigma^2(\mathbf{r}) \\
S^{xyyx}(\mathbf{r}) &= C^{xyyx} \\
S^{xyyy}(\mathbf{r}) &= C^{xyyy} \\
S^{yxxx}(\mathbf{r}) &= C^{yxxx} \\
S^{yxxy}(\mathbf{r}) &= C^{yxxy} \\
S^{yxyx}(\mathbf{r}) &= C^{yxyx} + \sigma^2(\mathbf{r}) - \sigma^1(\mathbf{r}) \\
S^{yxyy}(\mathbf{r}) &= C^{yxyy} + \sigma^3(\mathbf{r}) \\
S^{yyxx}(\mathbf{r}) &= C^{yyxx} \\
S^{yyxy}(\mathbf{r}) &= C^{yyxy} \\
S^{yyyx}(\mathbf{r}) &= C^{yxyy} + \sigma^3(\mathbf{r}) \\
S^{yyyy}(\mathbf{r}) &= C^{yyyy} - \sigma^1(\mathbf{r}) - \sigma^2(\mathbf{r}).
\end{aligned}
\tag{D.2}
$$

Substituting Eq. (D.2) back to Eq. (2.111) gives (I drop the ring on $\mathbf{r}$):

$$
\begin{aligned}
\rho \frac{\partial^2 u^x}{\partial t^2} &= \frac{\partial}{\partial r^x}\left[\left(C^{xxxx} + \sigma^2(\mathbf{r}) - \sigma^1(\mathbf{r})\right)\frac{\partial u^x}{\partial r^x} + \left(C^{xxxy} + \sigma^3(\mathbf{r})\right)\frac{\partial u^x}{\partial r^y} + C^{xxyx}\frac{\partial u^y}{\partial r^x} + C^{xxyy}\frac{\partial u^y}{\partial r^y}\right] \\
&\quad + \frac{\partial}{\partial r^y}\left[\left(C^{xyxx} + \sigma^3(\mathbf{r})\right)\frac{\partial u^x}{\partial r^x} + \left(C^{xyxy} - \sigma^1(\mathbf{r}) - \sigma^2(\mathbf{r})\right)\frac{\partial u^x}{\partial r^y} + C^{xyyx}\frac{\partial u^y}{\partial r^x} + C^{xyyy}\frac{\partial u^y}{\partial r^y}\right]; \\
\rho \frac{\partial^2 u^y}{\partial t^2} &= \frac{\partial}{\partial r^x}\left[C^{yxxx}\frac{\partial u^x}{\partial r^x} + C^{yxxy}\frac{\partial u^x}{\partial r^y} + \left(C^{yxyx} + \sigma^2(\mathbf{r}) - \sigma^1(\mathbf{r})\right)\frac{\partial u^y}{\partial r^x} + \left(C^{yxyy} + \sigma^3(\mathbf{r})\right)\frac{\partial u^y}{\partial r^y}\right] \\
&\quad + \frac{\partial}{\partial r^y}\left[C^{yyxx}\frac{\partial u^x}{\partial r^x} + C^{yyxy}\frac{\partial u^x}{\partial r^y} + \left(C^{yyyx} + \sigma^3(\mathbf{r})\right)\frac{\partial u^y}{\partial r^x} + \left(C^{yyyy} - \sigma^1(\mathbf{r}) - \sigma^2(\mathbf{r})\right)\frac{\partial u^y}{\partial r^y}\right].
\end{aligned}
\tag{D.3}
$$

I assume only σ^3 exhibits long-range behavior, i.e. $\sigma^3(\mathbf{r}) = \rho\sigma_0 + \rho\Delta\sigma(\mathbf{r})$ is expressed in terms of its mean value plus a random part, i.e. $\overline{\Delta\sigma(\mathbf{r})} = 0$ and $\overline{\Delta\sigma(\mathbf{r}')\Delta\sigma(\mathbf{r}'+\mathbf{r})} = B(\mathbf{r}) = \gamma\cos(4\theta)/(r^2+a^2) \equiv \cos(4\theta)B(r)$ for some constants γ and a again. All other elastic constants like $C^{\mu\nu\kappa\chi}$ or σ^1, σ^2 are short-ranged and hence can be regarded as constants

when r is large. The long-range decay in shear stress correlations has been derived using generalised hydrodynamic theory in (Maier et al., 2018). Then the elastic wave equation becomes

$$\begin{aligned}\rho\frac{\partial^2 u^x(\mathbf{r})}{\partial t^2} &= \mathscr{S}^{x\nu\kappa\chi}\frac{\partial^2 u^\nu}{\partial r^\kappa \partial r^\chi} + \frac{\partial\Delta\sigma(\mathbf{r})}{\partial r^x}\frac{\partial u^x}{\partial r^y} + \frac{\partial\Delta\sigma(\mathbf{r})}{\partial r^y}\frac{\partial u^x}{\partial r^x};\\ \rho\frac{\partial^2 u^y(\mathbf{r})}{\partial t^2} &= \mathscr{S}^{y\nu\kappa\chi}\frac{\partial^2 u^\nu}{\partial r^\kappa \partial r^\chi} + \frac{\partial\Delta\sigma(\mathbf{r})}{\partial r^x}\frac{\partial u^y}{\partial r^y} + \frac{\partial\Delta\sigma(\mathbf{r})}{\partial r^y}\frac{\partial u^y}{\partial r^x},\end{aligned} \tag{D.4}$$

where $\mathscr{S}^{\mu\nu\kappa\chi}$ corresponds to the $\mathbf{r}$-independent part of elastic or stress tensors. In frequency space, the equation of motion of the frequency-dependent displacement vector $\mathbf{u}(\mathbf{r},z)$ is

$$\begin{aligned}&A(z)\mathbf{u}(\mathbf{r},z) = 0,\\ \text{with}\quad &A^{\mu\nu} = -z\delta^{\mu\nu} - \sum_{\kappa\chi}\mathscr{S}^{\mu\nu\kappa\chi}\nabla_\kappa\nabla_\chi - \sum_{\kappa\neq\chi}(\nabla_\kappa[\Delta\sigma\nabla_\chi])\delta^{\mu\nu}.\end{aligned} \tag{D.5}$$

The fluctuation of $\sigma(\mathbf{r})$ is implemented by the probability distribution for its fluctuating part,

$$\mathscr{P}[\Delta\sigma(\mathbf{r})] = P_0\exp\left[-\frac{1}{2}\int d^2r d^2r'\Delta\sigma(\mathbf{r})B^{-1}(\mathbf{r}-\mathbf{r}')\Delta\sigma(\mathbf{r}')\right]. \tag{D.6}$$

The Lagrangian is expressed as (scaled by ρ),

$$\begin{aligned}&\mathscr{L} = \frac{1}{2}\int d^2r\mathbf{u}^T A\mathbf{u} = u^x(A_{xx}u^x + A_{xy}u^y) + u^y(A_{yx}u^x + A_{yy}u^y)\\
&= \frac{1}{2}\int d^2r\Bigg\{-z\mathbf{u}\cdot\mathbf{u} - \sum_{\mu\nu\kappa\chi}u^\mu\mathscr{S}^{\mu\nu\kappa\chi}\nabla_\kappa\nabla_\chi u^\nu - u^x\nabla_x(\Delta\sigma\nabla_y u^x) - u^x\nabla_y(\Delta\sigma\nabla_x u^x) - u^y\nabla_x(\Delta\sigma\nabla_y u^y)\\
&-u^y\nabla_y(\Delta\sigma\nabla_x u^y)\Big\}\\
&= \frac{1}{2}\int d^2r\Bigg\{-z\mathbf{u}\cdot\mathbf{u} - \sum_{\mu\nu\kappa\chi}u^\mu\mathscr{S}^{\mu\nu\kappa\chi}\nabla_\kappa\nabla_\chi u^\nu - [\nabla_x(u^x\Delta\sigma\nabla_y u^x) + \nabla_y(u^x\Delta\sigma\nabla_x u^x) - 2\Delta\sigma(\nabla_y u^x)(\nabla_x u^x)]\\
&-[x\leftrightarrow y]\Big\}\\
&= \frac{1}{2}\int d^2r\Bigg\{-z\mathbf{u}\cdot\mathbf{u} - \sum_{\mu\nu\kappa\chi}u^\mu\mathscr{S}^{\mu\nu\kappa\chi}\nabla_\kappa\nabla_\chi u^\nu + 2\Delta\sigma[(\nabla_y u^y)(\nabla_x u^y) + (\nabla_x u^x)(\nabla_y u^x)]\Bigg\},\end{aligned} \tag{D.7}$$

where the last equality holds because objects like $\nabla_x(u^x\Delta\sigma\nabla_y u^x)$ vanish on the boundary.

Using the replica-field representation, the generating functional for calculating the averaged Green's function takes the form

$$\langle Z^n(0)\rangle \equiv \int \mathscr{D}[\mathbf{u}_a(\mathbf{r})]\mathscr{D}[\Delta\sigma(\mathbf{r})]P_0 \exp\left[-\frac{1}{2}\sum_{a=1}^{n}\int d^2r\{-zu_a(\mathbf{r})^2+2\Delta\sigma[(\nabla_y u^y)(\nabla_x u^y)+(\nabla_x u^x)(\nabla_y u^x)]\}\right.$$
$$\left.-\sum_{\mu\nu\kappa\chi} u^\mu \mathscr{S}^{\mu\nu\kappa\chi}\nabla_\kappa\nabla_\chi u^\nu - \frac{1}{2}\int d^2r d^2r' \Delta\sigma(\mathbf{r})B^{-1}(\mathbf{r}-\mathbf{r}')\Delta\sigma(\mathbf{r}')\right]$$
$$\approx \int \mathscr{D}[\mathbf{u}_a(\mathbf{r})]\exp\left[-\frac{1}{2}\sum_{a=1}^{n}\int d^2r\left\{-zu_a(\mathbf{r})^2-\sum_{\mu\nu\kappa\chi}u^\mu\mathscr{S}^{\mu\nu\kappa\chi}\nabla_\kappa\nabla_\chi u^\nu\right\}\right.$$
$$+\frac{1}{2}\sum_{a,b=1}^{n}\int d^2r d^2r'[(\nabla_y u_a^y(\mathbf{r}))(\nabla_x u_a^y(\mathbf{r}))+(\nabla_x u_a^x(\mathbf{r}))(\nabla_y u_a^x(\mathbf{r}))]B(\mathbf{r}-\mathbf{r}')[(\nabla_y u_b^y(\mathbf{r}'))(\nabla_x u_b^y(\mathbf{r}'))$$
$$\left.+(\nabla_x u_b^x(\mathbf{r}'))(\nabla_y u_b^x(\mathbf{r}'))]\right], \tag{D.8}$$

where again $a,b=1,...,n$. I introduce effective matrix fields $\Lambda_{ab}^{\mu\nu\kappa\chi}(\mathbf{r},\mathbf{r}',z)$ to replace the $\Delta\sigma(\mathbf{r})$ in the harmonic part of the effective equation of motion:

$$\langle Z^n(0)\rangle \approx \int \mathscr{D}[\mathbf{u}_a(\mathbf{r})]\mathscr{D}[\Lambda_{ab}^{\mu\nu\kappa\chi}(\mathbf{r},\mathbf{r}',z)]\Lambda_0\cdot$$
$$\exp\left\{-\frac{1}{2}\sum_{a=1}^{n}\int d^2r\left[-zu_a(\mathbf{r})^2-\sum_{\mu\nu\kappa\chi}u^\mu\mathscr{S}^{\mu\nu\kappa\chi}\nabla_\kappa\nabla_\chi u^\nu\right]-\frac{1}{2}\sum_{a,b=1}^{n}\sum_{\mu\nu,\kappa\neq\chi}\int d^2r d^2r'\cdot\right.$$
$$\left.\left[\Lambda_{ab}^{\mu\nu\kappa\chi}(\mathbf{r},\mathbf{r}',z)B^{-1}(\mathbf{r}-\mathbf{r}')\sum_{\kappa'\neq\chi'}\Lambda_{ab}^{\mu\nu\kappa'\chi'}(\mathbf{r},\mathbf{r}',z)-u_a^\mu(\mathbf{r})\nabla_\kappa\Lambda_{ab}^{\mu\nu\kappa\chi}(\mathbf{r},\mathbf{r}',z)\nabla_\chi u_b^\nu(\mathbf{r}')\delta^{\mu\nu}\right]\right\}. \tag{D.9}$$

The way $\Lambda_{ab}^{\mu\nu\kappa\chi}$ introduced is to make Eq. (D.9) consistent with Eq. (D.5) and Λ_0 is a normalisation constant. The generating function including source $J_{ab}^{\mu\nu}(\mathbf{r},\mathbf{r}')$ is then:

$$\langle Z^n(J)\rangle = \int \mathscr{D}[\mathbf{u}_a(\mathbf{r})]\mathscr{D}[\Lambda_{ab}^{\mu\nu\kappa\chi}(\mathbf{r},\mathbf{r}',z)]\Lambda_0 \exp\left\{-\frac{1}{2}\sum_{a,b=1}^{n}\sum_{\mu\nu,\kappa\neq\chi}\int d^2r d^2r' \cdot \right.$$
$$\left.\left[\mathbf{u}_a(\mathbf{r})A_{ab}(\Lambda_{ab}^{\mu\nu\kappa\chi})\mathbf{u}_b(\mathbf{r}') + \sum_{\kappa'\neq\chi'}\Lambda_{ab}^{\mu\nu\kappa\chi}B^{-1}(\mathbf{r}-\mathbf{r}')\Lambda_{ab}^{\mu\nu\kappa'\chi'} + 2J_{ab}^{\mu\nu}\Lambda_{ab}^{\mu\nu\kappa\chi}\right]\right\}, \tag{D.10}$$

where

$$A_{ab}(\Lambda_{ab}^{\mu\nu\kappa\chi}) \equiv \delta^{ab}\delta(\mathbf{r}-\mathbf{r}')(-z\delta^{\mu\nu} - \sum_{\mu\nu\kappa\chi}\mathscr{S}^{\mu\nu\kappa\chi}\nabla_\kappa\nabla_\chi) - \sum_{\kappa\neq\chi}\nabla_\kappa\Lambda_{ab}^{\mu\nu\kappa\chi}\nabla_\chi\delta^{\mu\nu}. \tag{D.11}$$

By evaluating derivatives of $\langle Z^n(J)\rangle$ with respect to $J_{ab}^{\mu\nu}$ at $J_{ab}^{\mu\nu}=0$, we are able to find the averaged Green's function of $\Lambda_{ab}^{\mu\nu\kappa\chi}$. Integrating $\mathbf{u}_a$ out in Eq. (D.9), I obtain a field theory involving only the Λ field:

$$\langle Z^n(0)\rangle \propto \int \mathscr{D}[\Lambda] e^{\left\{-\frac{1}{2}\cdot\sum_{ab=1}^{n}\sum_{\mu\nu,\kappa\neq\chi}\left(\ln\det A(\Lambda_{ab}^{\mu\nu\kappa\chi}) + \sum_{\kappa'\neq\chi'}\int d^2r d^2r' \Lambda^{\mu\kappa\chi\nu}B^{-1}(\mathbf{r}-\mathbf{r}')\Lambda^{\mu\nu\kappa'\chi'}\right)\right\}}. \tag{D.12}$$

To solve the saddle-point problem, I take

$$\frac{\delta}{\delta\Sigma^{\mu\nu}}\left(\mathrm{Tr}\ln A(\Sigma^{\mu\nu}) + \int d^2r d^2r' \Sigma^{\mu\nu}B^{-1}(\mathbf{r}-\mathbf{r}')\Sigma^{\mu\nu}\right) = 0 \tag{D.13}$$

at $\Sigma_0^{\mu\nu}$, yielding

$$\langle\Sigma_0^{\mu\nu}\rangle = \frac{1}{2}\sum_{\kappa\neq\chi}\nabla_\kappa B(\mathbf{r}-\mathbf{r}')\nabla_\chi\langle G_0(r^\mu, r'^\nu, z)\rangle\delta^{\mu\nu}; \tag{D.14a}$$

$$G_0(r^x, r'^x, z) = \left[-z - (C^{xxxx}+\sigma^2-\sigma^1)\nabla_x\nabla_x - (C^{xxxy}+\Sigma_0^{xx})\nabla_x\nabla_y - (C^{xyxx}+\Sigma_0^{xx})\nabla_y\nabla_x \right.$$
$$\left. -(C^{xyxy}-\sigma^1-\sigma^2)\nabla_y\nabla_y\right]^{-1}; \tag{D.14b}$$

$$G_0(r^y, r'^y, z) = \left[-z - (C^{yxyy}+\Sigma_0^{yy})\nabla_x\nabla_y - (C^{yxyy}+\Sigma_0^{yy})\nabla_y\nabla_x - (C^{yxyx}+\sigma^2-\sigma^1)\nabla_x\nabla_x \right.$$
$$\left. -(C^{yyyy}-\sigma^1-\sigma^2)\nabla_y\nabla_y\right]^{-1}; \tag{D.14c}$$

$$G_0(r^x, r'^y) = [-C^{xxyx}\nabla_x\nabla_x - C^{xxyy}\nabla_x\nabla_y - C^{xyyx}\nabla_y\nabla_x - C^{xyyy}\nabla_y\nabla_y]^{-1}; \tag{D.14d}$$

$$G_0(r^y, r'^x) = [-C^{yxxx}\nabla_x\nabla_x - C^{yxxy}\nabla_x\nabla_y - C^{yyxx}\nabla_y\nabla_x - C^{yyxy}\nabla_y\nabla_y]^{-1}. \tag{D.14e}$$

In $\mathbf{q}$ space, the condition on the one-particle CPA Green's function may be rewritten as:

$$\langle \Sigma_0^{\mu\nu} \rangle = -\frac{1}{2} \sum_{\kappa \neq \chi} \delta^{\mu\nu} q_\kappa q_\chi \int d^2k \tilde{B}(\mathbf{q}-\mathbf{k}) \langle G_0(\mathbf{k}) \rangle; \qquad \tilde{B}(\mathbf{q}) \equiv \int d^2r e^{i\mathbf{q}\cdot\mathbf{r}} B(\mathbf{r}) \tag{D.15a}$$

$$G_0(q^x, q^x, z) = \big[-z + (C^{xxxx} + \sigma^2 - \sigma^1) q_x q_x + (C^{xxxy} + \Sigma_0^{xx}) q_x q_y + (C^{xyxx} + \Sigma_0^{xx}) q_y q_x + (C^{xyxy} - \sigma^1 - \sigma^2) q_y q_y \big]^{-1} \tag{D.15b}$$

$$G_0(q^y, q^y, z) = \big[-z + (C^{yxyy} + \Sigma_0^{yy}) q_x q_y - (C^{yxyy} + \Sigma_0^{yy}) q_y q_x + (C^{yxyx} + \sigma^2 - \sigma^1) q_x q_x + (C^{yyyy} - \sigma^1 - \sigma^2) q_y q_y \big]^{-1} \tag{D.15c}$$

$$G_0(q^x, q^y) = [C^{xxyx} q_x q_x + C^{xxyy} q_x q_y + C^{xyyx} q_y q_x + C^{xyyy} q_y q_y]^{-1} \tag{D.15d}$$

$$G_0(q^y, q^x) = [C^{yxxx} q_x q_x + C^{yxxy} q_x q_y + C^{yyxx} q_y q_x + C^{yyxy} q_y q_y]^{-1} \tag{D.15e}$$

Applying similar manipulations as for disorder in elastic constants in Chapter 6, one can find that the self-energy scales as,

$$\mathrm{Im} \langle \Sigma_0^{\mu\nu}(q) \rangle \sim -q^2 \ln q. \tag{D.16}$$